

Andrey Yurkov

Refractories for Aluminium

Electrolysis and the Cast House

 Springer

Refractories for Aluminium

Andrey Yurkov

Refractories for Aluminium

Electrolysis and the Cast House

 Springer

Andrey Yurkov
Moscow, Russia

ISBN 978-3-319-11441-5 ISBN 978-3-319-11442-2 (eBook)
DOI 10.1007/978-3-319-11442-2
Springer Cham Heidelberg New York Dordrecht London

Library of Congress Control Number: 2014951216

© Springer International Publishing Switzerland 2015

This work is subject to copyright. All rights are reserved by the Publisher, whether the whole or part of the material is concerned, specifically the rights of translation, reprinting, reuse of illustrations, recitation, broadcasting, reproduction on microfilms or in any other physical way, and transmission or information storage and retrieval, electronic adaptation, computer software, or by similar or dissimilar methodology now known or hereafter developed. Exempted from this legal reservation are brief excerpts in connection with reviews or scholarly analysis or material supplied specifically for the purpose of being entered and executed on a computer system, for exclusive use by the purchaser of the work. Duplication of this publication or parts thereof is permitted only under the provisions of the Copyright Law of the Publisher's location, in its current version, and permission for use must always be obtained from Springer. Permissions for use may be obtained through RightsLink at the Copyright Clearance Center. Violations are liable to prosecution under the respective Copyright Law.

The use of general descriptive names, registered names, trademarks, service marks, etc. in this publication does not imply, even in the absence of a specific statement, that such names are exempt from the relevant protective laws and regulations and therefore free for general use.

While the advice and information in this book are believed to be true and accurate at the date of publication, neither the authors nor the editors nor the publisher can accept any legal responsibility for any errors or omissions that may be made. The publisher makes no warranty, express or implied, with respect to the material contained herein.

Printed on acid-free paper

Springer is part of Springer Science+Business Media (www.springer.com)

Preface

The idea of this book came during the organization of the seminars “Refractories and Carbon Cathode Materials for Aluminium Industry” that were held in 2001, 2002, 2003, and 2004 in Samara, Sayanogorsk, Novokuznetsk, and Bratsk (Russia). The hosts of these seminars were smelters and secondary aluminium plants, and that enabled people directly involved in refractories and carbon cathode materials and the service life of metallurgical devices to be invited.

We tried to plan the seminar programs so that the invited lectures from academic science were followed by the applied science papers, which in turn were followed by the papers and presentations of leading producers of materials used in the aluminium industry. It seems to me it helped to speak one language among the people involved in R&D of materials science, in reduction and casting of aluminium, in problems of service life, sometimes in connection with procurement issues.

At that time, in the course of preparatory work for these seminars and the invitation of the key lectures, from one side, and in preparation for the proceedings, from another, the understanding was growing that the theme “Refractories and Carbon Cathode Materials for Aluminium Industry” is a multidisciplinary sphere, where one meets people with different educations and different understandings of the processes.

Probably the key issue there is that the reduction of aluminium (as a part of the metallurgy of aluminium) is actually high-temperature electrochemistry, which is a sufficiently more peculiar sphere than ferrous metallurgy. Peculiarity number one is that the reduction of aluminium is an electrochemical reaction giving heat, and this heat should dissipate, while the temperature range of the processing of this reaction is very narrow — only 25–30°. Both freezing of electrolyte and overheating of electrolyte will stop the reduction process. Peculiarity number two is that the main constituent of electrolyte for the reduction of aluminium is cryolite, which is a substance that dissolves alumina in the best possible way. Certainly, it will dissolve all other oxides, and not only oxides. Peculiarity number three is that the producers of carbon materials (and carbon cathode refractory materials as well) try to set themselves a little bit apart from refractory society, speak a slightly different

language, and use special terminology and testing methods. Probably peculiarity number four is that in contrast with traditional metallurgy (where also something may be improved anytime), the construction of reduction cells for the electrolysis of aluminium is still under development, and at least for some 20 years this process will continue.

Probably one more peculiarity is that “refractories for aluminium” is a rather young branch, because initially aluminium producers used refractories that were made for ferrous metallurgy. It was only in the 1980s and 1990s that special research and development together with industrial trials outlined “refractories for aluminium” as a special branch.

The main materials for the lining of the reduction cells:

- carbon cathode blocks and carbon ramming pastes;
- carbon and silicon carbide side lining materials and ramming pastes, concretes and mortars for the installation of them;
- refractory barrier layer bricks and dry barrier mixtures;
- heat insulation materials

are described in the following sequence:

- the purpose of the material and its basic properties, grades of materials;
- raw materials for processing;
- installation in the reduction cell;
- elements of technology and processing, processing equipment, structure of the materials;
- the typical defects of materials;
- testing and characterization.
- the behavior in reduction cell during the service in connection with physical changes and chemical interactions.

Critical pore sizes for the penetration of corrosive liquids in refractory materials are discussed for every specific material.

The casting of aluminium is a traditional process, but the interesting point in the cast house is how the materials that cannot be considered optimal refractory materials from the viewpoint of physical chemistry were worked out and adjusted in the course of R&D in a way that can be considered quite satisfactory for service life and economics of processing.

Currently, it is possible to say that for the existing Hall–Heroult process of aluminium reduction, the service life of the metallurgical equipment has reached a certain satisfactory level, and significant investments in R&D of refractory materials for aluminium are not likely. The exception is the materials science of carbon cathode materials, where certain efforts could be made.

Yet to implement the technology of inert anode for the reduction of aluminium (and most probably in combination with drained cathode design), profound materials science R&D will be required.

The book is addressed to the people working at aluminium smelters and at the secondary aluminium plants and to the people producing refractories and heat

insulation materials. The designers and specialists in construction of metallurgical devices may also find something useful by looking through the material. I tried to compose the book's material in such a way that it may cover the interests of people from R&D and to the persons in charge of service life. Even procurement people might look through selected pages. I hope that both undergraduate and postgraduate students will also find something interesting by reading this text in the course of specialization.

The figures and illustrations for this book were made by Dr. Dmitry Ivanov, to whom I'm very grateful. Special words of gratitude go to Prof. Vasily Kryukovsky for his consultations in reduction technology and to Prof. Dick Bradt for his permanent warm words of encouragement toward the project; the consultations of Prof. Peter Polyakov and the team of "Light Metals" from Krasnoyarsk are also appreciated. Special thanks to Vasily Borisov for his consultations on constructions of reduction cells and dry autopsies and for his assistance in our joint investigations, and special thanks to Dr. Sergey Hramenko, with whom we tried to find answers to many questions that are in our joint publications. Thanks and words of gratitude to all participants and co-organizers of the seminars of "Refractories for Aluminium" in Samara, Novokuznetsk, Sayanogorsk, and Bratsk.

Moscow, Russia

Andrey Yurkov

Contents

1 The Properties of Refractory and Heat Insulation	
Materials	1
1.1 Classifications and Some Words About Quality Control	1
1.2 Density, Porosity, and Related Characteristics	5
1.3 Mechanical Characteristics	11
1.3.1 Compressive and Bending Strength	15
1.3.2 Modulus of Elastic, Hardness and Weibull Modulus	18
1.3.3 Elements of Fracture Mechanics	19
1.4 Thermomechanical Properties	23
1.4.1 Refractoriness	24
1.4.2 Hot Modulus of Rupture	25
1.4.3 Reheat Change. Permanent Linear Change on Reheating	26
1.4.4 High-Temperature Deformation. Characteristic Points and Softening Point	26
1.4.5 Creep	28
1.5 Thermal Conductivity, Heat Capacity, and Temperature Conductivity (Heat Diffusivity)	29
1.5.1 Elements of Theory	29
1.5.2 The Measurement of Thermal Conductivity	35
1.5.3 Methods of Thermal Conductivity Measurements Based on the Principle of Stationary Heat Flow	36
1.5.4 Methods of Thermal Conductivity Measurements Based on the Principle of Nonstationary Heat Flow (Dynamic Methods)	37
1.6 Thermal Coefficient of Linear Expansion, Thermal Strains, and Thermal Shock Resistance	39
1.6.1 Thermal Coefficient of Linear Expansion	39
1.6.2 Thermal Expansion of Refractory and Heat Insulation Materials: Elements of Theory	40

1.6.3	Measurement of Linear Coefficients of Thermal Expansion	42
1.6.4	Thermal Strains	43
1.6.5	Thermal Shock	43
1.6.6	Thermal Shock Factors	46
1.6.7	Thermal Shock Resistance Measurements	47
1.7	Corrosion Resistance	48
1.7.1	Elements of Theory	50
1.7.2	Tests	56
	References	58
2	Refractories and Carbon Cathode Materials for Aluminium Reduction Cells	65
2.1	Reduction of Aluminium. Elements of Reduction Technology. The Main Controlled Parameters of Reduction (Electrolysis). Elements of Energy Balance and Heat Balance of Reduction Cell. Reduction Shop. Types of Reduction Cells	65
2.2	Lining of Reduction Cells. Preheating, Startup, and Operation. Retrofit of Cells and Tendencies. The Main Causes of Failures. Dry Autopsies	75
2.2.1	Brief Information on the Lining of Reduction Cells	75
2.2.2	Preheating and the Startup of Reduction Cells	81
2.2.3	Some Words About Service Life and the Main Reasons for Shutdowns	84
2.2.4	Dry Autopsies	87
2.3	Carbon Cathode Bottom Blocks	90
2.3.1	Types and Properties	90
2.3.2	Elements of Technology, Raw Materials, and Processing	92
2.3.3	Defects in Carbon Cathode Blocks	108
2.3.4	Testing and Characterization	112
2.3.5	Some Words on Grades of Carbon Cathode Blocks	118
2.3.6	Some Words on the Structure of Carbon Cathode Blocks in Connection with Grain Size Composition, Sintering, and Pore Size Structure	120
2.3.7	Interaction of Carbon Cathode Blocks with the Steel Shell and the Collector Bars. Cracks Induced by Thermal Strains and Thermal Shock	125
2.3.8	Interaction of Carbon Cathode Blocks with Electrolyte During Startup and in Service: Wear. Infiltration	130
2.3.9	Carbon Ramming Paste	140

2.4	Coatings of Carbon Cathode Blocks and New Cathode Materials. Drained Cathode	146
2.5	Side Lining	152
2.5.1	Side Lining Materials	152
2.5.2	Carbon Side Lining; Causes for Decay	154
2.5.3	Silicon Carbide Side Lining	156
2.5.4	Variants of Silicon Carbide Materials (and Others) as a Side Lining	158
2.5.5	Silicon Carbide Mortars, Ramming Mixes and Castables for Installation of SiC Side Lining	172
2.6	Refractory Barrier Materials of the Cell Lining. Dry Barrier Mixes and Bricks. Properties and Chemical Resistance. The Processes During Service. Interactions with Infiltrated Electrolyte. Change of Properties. Lenses	178
2.6.1	Bricks and Dry Barrier Mixtures	178
2.6.2	Corrosion Resistance Testing	181
2.6.3	Chemical Interaction of Sodium Fluoride Salts with Alumina Silica Refractories	182
2.6.4	The Influence of Porosity and Permeability on Corrosion Resistance of Refractories	187
2.6.5	Some More Words on Barriers for Electrolyte Penetration	189
2.7	Heat Refractory Insulation Materials for the Lining of Reduction Cells	190
2.7.1	Diatomaceous (Moler) Heat Insulation Materials	190
2.7.2	Perlite-Based Heat Insulation Materials	191
2.7.3	Vermiculite-Based Heat Insulation Materials	192
2.7.4	Calcium Silicate Heat Insulation Materials	193
2.7.5	Thermal Aging of Heat Insulation Materials at Service and Thermal Conductivity of Infiltrated Heat Insulation Materials	195
	References	199
3	Refractories and Heat Insulation Materials for the Cast House	209
3.1	Cast House	209
3.2	Physical and Chemical Interaction of Refractories with Aluminium and Aluminium Alloys	211
3.2.1	Chemical Interaction of Aluminium and Aluminium-Based Alloys with Components of Refractories	211
3.2.2	Antiwetting Admixtures to Alumina Silica Refractories	215
3.2.3	Wetting of Alumina Silica Refractories by Molten Aluminium and Aluminium Alloys	217

- 3.2.4 Some Words on Corrosion Mechanism 218
- 3.2.5 Tests for Corrosion Resistance 222
- 3.3 Refractory Materials 223
- 3.4 Elements of Lining Design 228
 - 3.4.1 Some Words on Drying and Preheating
of Furnaces 230
- 3.5 Melting and Holding Furnaces 232
- 3.6 Induction Furnaces, Ladles 235
 - 3.6.1 Ladles 238
- 3.7 Launderers (Runners), Casting Equipment. Elimination
of Asbestos-Containing Materials 238
 - 3.7.1 Casting Equipment (Tooling) 240
 - 3.7.2 Ceramic Foam Filters 241
- References 241
- 4 Refractories for Anode Baking Furnaces 245**
 - 4.1 Lining 245
 - References 249
- Glossary 251**

About the Author

Andrey Yurkov, graduated from Moscow Mendeleev University of Chemical Technology, Department of Ceramics and Refractories. He earned a Ph.D. in structural ceramics and a Dr. Sci. degree in materials science of refractory materials, and he has published more than 100 publications.

His areas of expertise include materials science and processing of non-oxygen- and oxygen-containing ceramics and refractories as well as their applications in the aluminium industry, including service life of metallurgical devices (reduction cells and melting and holding furnaces) and their design and construction.

While working for Russian Aluminium (RUSAL), Dr. Yurkov has been organizer and chairperson of the seminars (conferences) “Refractories and Carbon Cathode Materials for Aluminium Industry.”

Chapter 1

The Properties of Refractory and Heat Insulation Materials

1.1 Classifications and Some Words About Quality Control

Refractories are the construction materials used for the lining of furnaces or some parts of furnaces in ferrous and nonferrous metallurgy, in the metallurgy of aluminium, in particular, in the glass and concrete industry, in chemistry, and in power generation. The selection of refractories is determined by specific conditions of the service of the furnace – the temperature, working cycle, interaction with aggressive melts and gases, mechanical interaction of the material in the furnace, and so forth. Nonoptimal selection of refractories leads to a decrease in the furnace's service life, to an increased consumption of the refractories, to an increased time of furnace repairs, to a deterioration in the production quality, and poor economical characteristics of the industrial process. Sometimes poor-quality refractories may lead to emergency breakdowns of furnaces and accidents.

There are small differences in different classifications of refractory materials among ISO, DIN, and ASTM standards [1–4]. The most common definition is that refractories are shaped and unshaped materials that are durable at high temperature ($>1,500\text{ }^{\circ}\text{C}$). Usually, heat refractory insulation materials have a service temperature of $800\text{--}1,100\text{ }^{\circ}\text{C}$.

The melting point of aluminium (Al) is $660\text{ }^{\circ}\text{C}$, the smelting of Al-based alloys takes place at $700\text{--}800\text{ }^{\circ}\text{C}$, and the temperature in an Al reduction cell is about $950\text{--}970\text{ }^{\circ}\text{C}$. The linings in the coke calcining furnaces, alumina calcining furnaces, and anode baking furnaces really require a relatively high refractoriness of materials. We shall use the term “refractories” for all high-temperature construction materials used in the Al industry that meet the classifications of the standards [1–4], but we'll take into account high-temperature heat insulation materials with a service temperature above $800\text{ }^{\circ}\text{C}$.

The term “refractories for Al industry” is relatively young. Initially, Al producers didn't pay much attention to special requirements of refractories. The exceptions were carbon cathode materials, which should be electroconductive.

But in all other applications, Al producers used the refractories for ferrous metallurgy. The first attempts to increase the service life of high-temperature devices for the production of Al and additional requirements appeared in the 1970s. The first refractories, specially designed for the applications in the metallurgy of Al, appeared in the 1980s. Since then, there has been a small applied segment of R&D, design, and production, known as “refractories for the aluminium industry.”

One characteristic of a refractory is the mineral composition. In the Al industry, the most common are alumina silica refractories, carbon, and silicon carbide refractories.

Some words about carbon materials. Historically, the production of carbon materials has stood apart from the refractory industry, having many commonalities. The producers and researchers of carbon materials introduced several characteristics specific for the refractory industry and do not like the use of term “carbon refractories” when one refers to carbon cathode materials. Yet we will use the term “carbon refractories,” taking into account the peculiarities of carbon materials, because it is a material for refractory application, as it can withstand the corrosive interaction of liquid media at high temperatures over a long period.

Refractories can be classified according to porosity. The influence of pores is sufficient on any property of refractories.

The classification of refractory heat-insulating materials is based on the density and temperature interval within which the maximum shrinkage does not exceed 2 % [5, 6]. It is necessary to keep in mind that the classification temperature according to ASTM 155 [5] and ISO-2245 [6] does not correspond to the safe temperature of refractory application, which we will discuss later.

Refractories may be shaped or unshaped (monolithics, castables). Unshaped refractories have appeared in the Al industry although they are not gaining popularity as quickly as in ferrous metallurgy. Dry barrier mixtures are commonly used now in reduction cells, and monolithic refractories have found their place in holding and melting furnaces of the cast house, ladles, and launders. In a limited amount, monolithics are used for coke calcining furnaces and for anode baking furnaces.

Depending on technology, refractories may be fired, unfired, and heat-treated (fused refractories are not used in the Al industry). Fired refractories go through high-temperature long-term firing (with temperatures up to 1,900 °C), which gives stability during service. Unfired refractories are subjected to heat treating at temperatures not exceeding 250 °C. These materials get their properties in high-temperature service. Their properties change during this heat treatment, which should be taken into account. Usually, the temperature of firing for heat-treated refractories is above 860 °C.

This classification is rather tentative, as the final heat treatment of calcium silicate heat insulation refractory materials is about 180 °C, while the service temperature is above 800 °C. The exfoliation of vermiculite grains takes place at 650–800 °C, but the heat treatment of vermiculite heat insulation slabs takes place at 250–280 °C, with a service temperature above 800 °C.

The properties of refractory materials are determined by the refractory producer– the refractory maker – and the refractory user – the metallurgist. Rather

frequently, between those two is the engineering company that makes the furnace or reduction cell. The producer of raw materials for the production of refractories controls the process and finished products and gives certificates of quality for the refractory producer. The refractory producer controls the quality of raw materials for refractory fabrication, the refractory fabrication itself, and the finished refractory products and gives quality certificates for the metallurgist. Still, metallurgists often take control of the refractory materials that they receive. The regulations about sampling of raw materials and unshaped refractory products and the acceptance of refractories are according to standards [7, 8], and they are valid for cathode carbon blocks [9–11]. Sometimes the customer makes only an outer external inspection (the condition of edges, corners, and cracks, if any). However, sometimes the customer performs a random selected check of the quality in an independent laboratory or in the customer’s laboratory.

Some time ago, certain refractory producers started making statistical measurements of quality control. The idea of statistical quality control was developed in the automobile industry [12–15]. At present, it is not very common for the refractory producer to give the customer the quality control data in the form of Shewhart charts [15], yet this trend looks promising for customers (Figs. 1.1 and 1.2).

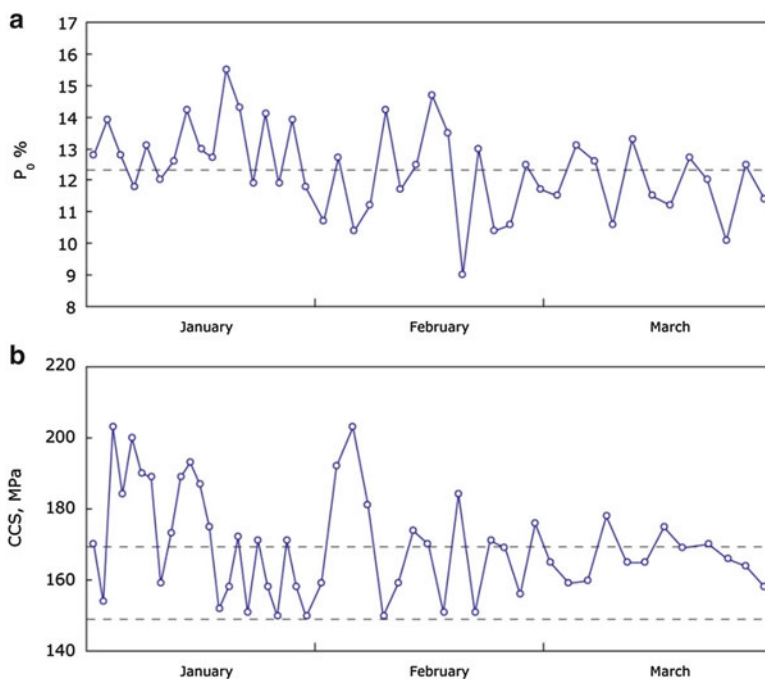


Fig. 1.1 The records of (a) open porosity of nitride-bonded silicon carbide side lining refractories (in the customer’s specification, the open porosity should be below 18 %); (b) the cold crushing strength of nitride-bonded silicon carbide side lining refractories (in the customer’s specification, the cold crushing strength should be above 150 Mpa)

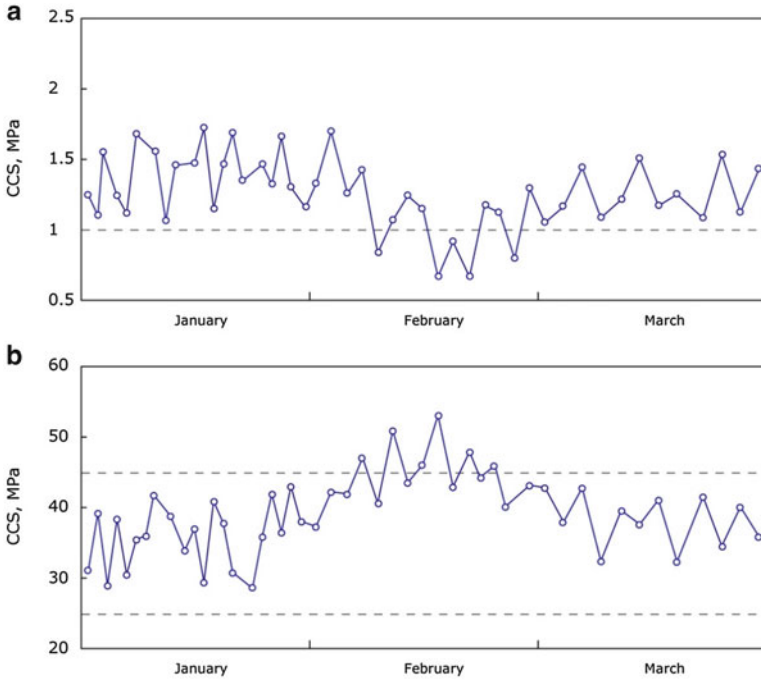


Fig. 1.2 The records of the cold crushing strength of (a) vermiculite heat insulation materials (in the customer's specification, the CCS should be above 1 MPa); (b) carbon (30 % graphite) cathode materials (in the customer's specification, the CCS should be in the range 25–50 MPa)

If the customer requires the lowest or highest acceptable limit of a property (e.g., bending strength above 150 MPa or porosity below 15 %), then the C_{pk} index is calculated:

$$C_{pk} = (x_{\max(\min)} - x_{av.}) / 3\sigma \quad (1.1)$$

where $x_{av.}$ is the average value of the quality.

If the customer requires the property to be in an interval of values (e.g., cold crushing strength not lower than 45 MPa and not higher than 80 MPa), then the C_p index is calculated:

$$C_p = (x_{\max} - x_{\min}) / 6\sigma \quad (1.2)$$

where x_{\max} , and x_{\min} are the maximum and minimum values of the quality, respectively, and σ is the root-mean-square deviation.

C_p or C_{pk} values < 1 reflect a poor fabrication control (e.g., C_p or $C_{pk} = 0.33$ suggest that 32.2 % of the products do not meet the specification's requirements), C_p or C_{pk} values > 1 reflect a normal level of quality control (fewer than 0.27 % of products do not meet the requirements), C_p or $C_{pk} > 1.33$ suggests a very good fabrication control (fewer than 0.0066 % of products do not meet the requirements).

Even if the refractory product is not subjected to critical applications, a quality record in the form of Shewhart charts will give the customer a sense of confidence, but it may tell the producer about the tendency for quality to diminish (probably due to some minor changes in raw materials or the occasional lack of temperature control, etc.).

Without a doubt, cathode carbon blocks in the reduction cell have a critical application. One crack in the cathode carbon block may shut down the reduction cell within 10 days of startup. Of course, it is impossible to “measure” a crack (at least if one isn’t using nondestructive quality control, which we will briefly discuss in Sect. 2.3, devoted to carbon cathode blocks). However, it is possible to keep a continuous record on strength, and excessive strength may push you to start thinking about possible tensions (and a consequent crack) due to an unexpected increase in the strength (in comparison with regular values; see Fig. 1.2b).

Another example is the strength of vermiculite slabs (Fig. 1.2a). Certainly, the probability of a shutdown of the reduction cell due to low strength of vermiculite heat insulation slabs in the bottom part of the reduction cell is very low (and probably close to zero). However, this graph may give the producer of these slabs initial information in order to understand of the following issues:

- What’s wrong with the processing, and where are the problems?
- Is the problem in the decay of the quality of vermiculite ore?
- Is the problem with the temperature of exfoliation of the vermiculite?
- Is the problem with the quality of the sodium/potassium silicate for the binder, supplied by another company?
- Or is the problem simply with the quality of water during the spring overflow of the local river?

With critical applications of refractories, statistical quality control might become the link for long-term relationships between the customer and the producer of refractory materials.

In the ferrous industry, the characteristic “specific consumption of refractory per ton of the metal” is now being replaced by the characteristic “refractory consumption in money equivalent.” However, in Al production, neither the first nor the second characteristic attracts big attention. Aluminium producers usually calculate the cost of production for the high-temperature device itself, not differentiating to construction or refractories. It is probably a question to be addressed in the future.

1.2 Density, Porosity, and Related Characteristics

Porosity and density are very important characteristics of refractory materials. Almost all refractory materials are porous. The pores may occupy 1–80 % of the material. The majority of the mechanical, thermal, and other characteristics of refractories depends on the density and porosity.

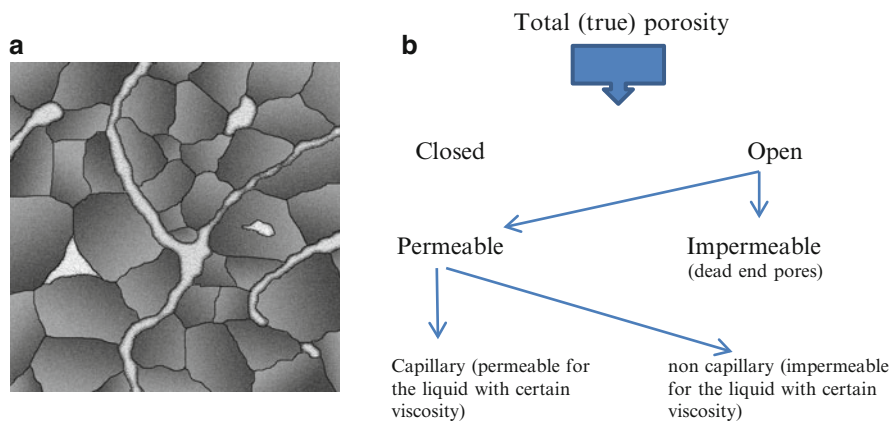


Fig. 1.3 (a) Schematic illustration and (b) diagram of types of porosity

In refractory materials, the pores may be open (having a connection with the atmosphere and each other) or closed (separated from the atmosphere and each other). Most pores are open and may be filled with water or another liquid. Closed pores cannot be filled with liquid. The schematic diagram of pores and an illustration of pores and porosity appear in Fig. 1.3(a, b). There are three main kinds of porosity: open porosity P_o , closed porosity P_c , and total porosity P_t .

The total porosity is a sum of the open and closed porosity:

$$P_t = P_o + P_c \quad (1.3)$$

where

Total porosity, % (P_t – sometimes written simply as P) – is the ratio of the total volume of open and closed pores to the total volume of the material, including the volume of the pores and the solid matter;

Open porosity, P_o , % – is the ratio of the volume of open pores to the volume of the material, including the volume of the pores and the solid matter;

Closed porosity, P_c % – is the ratio of the volume of closed pores to the volume of the material, including the volume of the pores and the solid matter.

The pore structure of refractories has many variations (Fig. 1.3a, b).

In carbon materials, almost all the porosity is open. The number of closed pores is small, especially in graphitic materials. The exception is the closed porosity in anthracite grains, which are used for the production of semigraphitic carbon cathode materials. In semigraphitic carbon blocks, there is a certain portion (<5 %) of closed pores.

Refractory materials always contain some number of closed pores. Usually, closed pores inside grains have small dimensions; on the contrary, closed pores at the joints of three- to five grains may be big.

The ratio of open and closed porosity to some extent is a characterization of the sintering process in ceramics and refractories. According to the theory of sintering, the porosity of the ceramic body, consisting of nonporous starting grains, remains open until the relative density won't reach 83–85 %. During the sintering process, if a relative density of 85 % is reached, the closed porosity will appear in the course of the sintering. At a relative density of 95 %, almost all the porosity is closed.

Open pores have connections with each other and form the channels of complicated shapes with dead-end branches, widened and narrowed parts. Open pores also may be at the joints of three or more grains, but open pores may exist inside the grains as well. Inside the grains, the pores have small dimensions. Some of the open pores are dead-end pores, but some of them (called tunnel pores) may be permeable.

Water absorption, %, is the ratio of the weight of the water that occupies the volume of open pores to the weight of the dry material:

$$B = [(a_2 - a_1) / a_1] 100, \quad (1.4)$$

where a_1 is the weight of the dry sample, and a_2 is the weight of the sample with absorbed water.

There are two methods to determine the water absorption of the refractories: the boiling method and the vacuum method. The boiling method is used to classify the ceramic tiles and involves drying the tiles out and then boiling them in water for 2 h, followed by cooling to room temperature over a 4-h period. The tiles are weighed both before and after the water immersion to determine the percentage of water absorption. The vacuum method evacuates the air from a chamber with the tiles inside and then immerses the tiles in water. Once again, the tiles are weighed before and after water immersion to determine the apparent porosity, apparent relative density, and bulk density.

The open porosity is determined by the volume of the liquid (water) that entered the pores upon boiling or after vacuum:

$$P_o = [(a_2 - a_1) / V] \cdot 100, \quad (1.5)$$

where V is the volume of the sample, and a_1 and a_2 are the respective weights of the dry sample and the sample with saturated water (liquid).

The determination of porosity by the hydrostatic method comprises a determination of the weight and saturation of it by boiling in water or saturation in vacuum by another liquid that does not interact with the refractory (in the case of materials that can react with water) [16, 17]. Then the saturated sample is weighed in the liquid (water) and in air. If the tested sample may react with water, the determination of apparent, real, and open porosities is performed in vacuum and then absorbed by kerosene, xylol, and ethyl or butyl alcohol according to ASTM C830-00 [18]. The application of melted paraffin or wax for the determination of the apparent, real, and open porosities is made according to ASTM C914-95 (1999) [19].

The true density is the ratio of the mass of material to its volume without pores (true volume); it is measured in g/sm^3 or kg/m^3 . The true density is a constant for every specific substance and depends on the crystal structure and the packing density of atoms. It is determined according to ISO 5018 and DIN EN 993-2/A1, and 215 ASTM C135 [16, 17,20, 29]. The true (real) density of cathode carbon blocks and the carbon ramming paste is determined according to ISO 9088 and BS ISO 21687 [21, 22]. All methods use a pycnometric technique, when the tested material is finely ground, so that almost all closed pores are crushed, and thus the liquid may penetrate open and closed pores as well. It is possible to calculate the true density of crystalline materials using the data of X-ray crystallography. Usually, the X-ray density is higher (within a level of 1 %) because in the pycnometric technique, it is impossible to crush submicron pores.

The apparent (bulk) density is the ratio of the mass of material to its volume, which takes into account the volume of the pores. The terms “bulk density” and “apparent density” are very close; the dimension is g/sm^3 or kg/m^3 . The apparent density is calculated as

$$\rho = m/v \quad (1.6)$$

where m is mass and v is volume.

In industrial practice, it is widely accepted to determine the bulk density by the dimension method – dividing the weight of a rectangular brick by its volume. The length, width, and height are measured by a ruler in several places and the average value is taken [23–26]. Of course, this determination is less accurate due to the possible warpage of the bricks and blocks (Fig. 1.5) but quite effective for the technological control of production. The bulk (apparent density) of cathode carbon materials is determined according to ISO 12985-1:2000 [27].

More precisely, the apparent density is determined by the hydrostatic (buoyancy) method according to standards ASTM-C-20-00, DIN EN 993-1, and ISO 5017 [16, 25, 26]. The apparent density is calculated according to

$$\rho = m_1/(m_3 - m_2) \quad (1.7)$$

where m_1 is the dry mass, m_3 is the immersed mass after saturation by boiling or another method, and m_2 is an immersed mass.

The determination of the apparent density and open porosity of carbon cathode materials is made according to ISO 12985-2:2000 [28].

In industrial practice, the structure of refractories is characterized by the apparent density and open porosity, and, usually, the real density and closed porosity and not used. The exception is the quality of carbon cathode blocks, where the real (true) density is taken into account not only in research, but in industrial practice as well (because it characterizes the ratio of graphitization). Water absorption is not used frequently. In research, the real density and closed porosity are important. In several cases, it is important to know the gas permeability of the material and the

ratio of permeable and dead-end pores. For research practice, it is very useful to know the sizes of open pores (pore size distribution), determined by porometry.

Permeability is the ability of the refractory material to transmit the gas or liquid. The permeable porosity is a part of the capillary porosity. The permeability of the material may aid in understanding the corrosion resistance, the resistance to infiltration of metal, slag, or electrolyte, although there is no direct consequence.

According to ASTM C-577-99 [30] and ISO 8841-1991 [31], the gas permeability is determined in samples 50 mm high and 50 mm in diameter at the pressure of compressed air or nitrogen by comparing the pressure difference at least at three different rates of flow. One perm is a unit of gas permeability, when within 1 s the gas flow of 1 cm³ with viscosity 1 Pz takes place through the cross section of a square centimeter at the pressure drop 1 din/cm². ASTM C-577-99 [30] uses the unit of permeability darcy or senty darcy, while the SI system recommends μm²; 1 nanoperm = 0.1 μm² = 0.1013 darcy.

The values of gas permeability usually differ, depending on the measurement in the direction of pressing and perpendicular to the direction of pressing. The value of the gas permeability may differ two times and even more at room temperature and at a temperature of 1,000–1,200 °C. Sometimes for research needs, in order to describe the pore structure, researchers use the labyrinth factor or coefficient of tortuosity for tunnel pores.

The tortuosity coefficient [33] is the ratio of open porosity to permeable porosity:

$$B = (P_o/P_{per.})^{0.5} \quad (1.8)$$

According to data of (Table 1.1) [32, 33], the ratio of permeable porosity to general porosity is usually 15 % in shamotte alumina silica refractories, about 40 % in silica refractories, and about 30 % in magnesia refractories.

Generally speaking, the pore size characteristics are close within one type of refractory and differ for different types of refractories.

The dimensions of pores may differ from millimeters to nanometers. The most universal method for the determination of pore dimensions is a mercury porosimetry ASTM C-493-98 [34]. It gives the pore size distribution. Sample one-mode, bi-mode, and nonmode pore sizes appear in Fig. 1.4. Forty to fifty years ago, limited attention was paid to the sizes of pores. The main criterion for the optimization of refractory properties was low porosity. Now people from research and industry have come to the conclusion that in many applications, the pore size should be taken into account. Of course, the Andreasen equation [35] for the optimization of grain size composition, with the aim to diminish the porosity of the material, as well as variants of the Andreasen equation [36] are valid in R&D practice, yet the pore size distribution (Fig. 1.5) is being taken into account more and more frequently.

The specific inner surface of refractories can be calculated from the open porosity and gas permeability [31]. It can be determined by the low-temperature

Table 1.1 Types of porosity and inner specific surface area of different traditional refractories [17, 18]

Refractory	Fireclay (shamotte)			Silica			Magnesia		
Real (true) density, g/sm ³	2.71	2.69	2.73	2.35	2.42	2.34	3.63	3.72	3.72
Apparent density, %	2.02	1.69	2.04	1.9	1.95	1.85	3.09	2.81	2.79
Total porosity, %	25.3	37.2	33.6	19.3	19.3	21.8	15.0	24.5	25.0
Open porosity, %	22.4	33.6	21.2	18.4	19.0	21.2	14.8	23.0	24.3
Permeable porosity, %	3.9	6.5	3.2	11.6	7.0	8.2	2.9	8.4	9.3
Permeability, μm ²	0.42	1.05	0.27	0.44	0.36	0.50	1.22	0.71	0.78
Specific surface area, sm ² /sm ³									
Calculated from permeability	1,220	1,530	1,210	7,710	3,790	4,000	550	3,380	4,160
Calculated from mercury porometry	10,800	10,810	15,070	10,870	3,950	12,610	510	5,480	5,580

Fig. 1.4 Possible shapes of rectangular samples

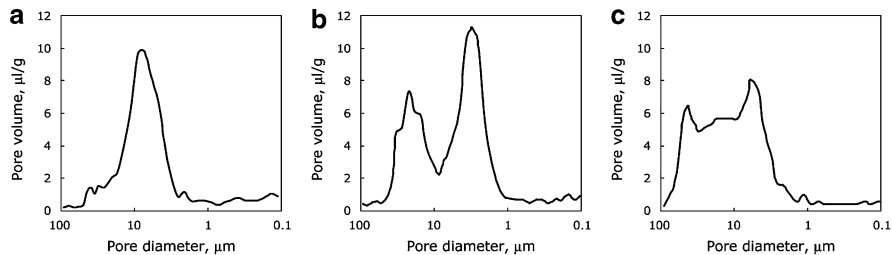


Fig. 1.5 The types of pore size distribution: (a) monomodal; (b) bimodal; (c) disordered (chaotic)

absorption of nitrogen (BET method) and according to the integral curve of mercury porosimetry.

Different refractory materials may have approximately equal values of porosity but an absolutely different ratio of permeable pores, a different pore size distribution, and a different pore structure.

In general, the porosity of traditional fireclay refractories (Table 1.2) is 22–25 %, while modern alumina silica materials reach 13–15 %, silicon carbide refractories have porosity 12–18 %, cathode carbon refractories have porosity 15–22 %, while almost all the pores are open and permeable. The porosity of low-cement and ultralow-cement castables is 12–15 %, while the ratio of permeable pores is very low (the permeability is 0.1–0.4 μm^2).

1.3 Mechanical Characteristics

Mechanical characteristics should be taken into account in the selection of the refractory material for specific conditions of the service or for the construction design of the furnace or part of the furnace. Mechanical characteristics are also used for production quality control.

Usually for the estimation of the mechanical properties of the refractories, specialists use cold crushing strength (CCS; or compressive strength), (flexural) bending strength (modulus of rupture, MOR), and elastic modulus (or Young's modulus). In the specification of refractory materials that will be subjected to abrasion, erosion, and wear, usually the characteristics of wear resistance are included. In research practice, the hardness, fracture toughness, and some other characteristics may be taken into account.

The compressive strength is a maximum compression tension that the material can withstand without breaking down:

Table 1.2 Porosity of refractory and heat insulation materials, used in aluminium industry

Material		Porosity, %	
		Open	Total
Fireclay	Traditional brick	18–20	22–28
	Medium-cement castable with fire-clay filler	16–20	22–28
	Low-cement castable with fireclay filler	10–13	13–15
Nitride-bonded silicon carbide		10–16	12–19
Carbon cathode materials	Semigraphitic	14–19	18–23
	Graphitic	22–25	18–22
	Graphitized	26–28	21–23
	Graphitized impregnated	13–17	20–22
Diatomaceous (moler)		50–60	60–70
Vermiculite		60–70	60–70
Calcium silicate heat insulation		70–80	70–80
Calcium silicate (vollastonite) for launders		25–35	45–55

$$\sigma = P/S, \quad (1.9)$$

where P is the load of the failure, and S is a surface of the cross section of the tested sample.

The CCS of refractories can be determined on cubic or cylindrical shapes (Fig. 1.6) having equal height and diameter (length) 50 mm [37, 38] or on half-bricks 114 mm × 114 mm × 68 mm or 114 mm × 114 mm × 76 mm. The compressive strength of carbon materials is determined according to ISO 18515 [39] and ASTM C695-91(2010) [40]. The ISO standard recommends isometric cylinders (the height is equal to the diameter), while the ASTM standard recommends the ratio of length to diameter $L/D = 2$. This should be at least remembered, because usually uniaxial samples demonstrate a bigger compressive strength comparing with samples having $L/D = 2$.

On the one hand, compressive strength is a simple and convenient method of estimating the mechanical strength of refractories, and to some extent it reveals the degree of the sintering process in refractories. On the other hand, the level of compressive strength may be critical for refractory shapes if they are layered in the bottom of a 50-m-tall furnace.

The level of smoothness of the surfaces and the degree of parallelism may considerably influence the results. Refractories are brittle, and even in case of small deviations in the flatness of the surface, the applied local pressure may increase several times, giving conelike cracking. For semigraphitic carbon materials, according to ASTM C 695 [40], there is a limitation on the number of grains on the surface; it should be below 10 (however, in semigraphitic materials, the coarse anthracite fraction of grains may be above 10 mm).

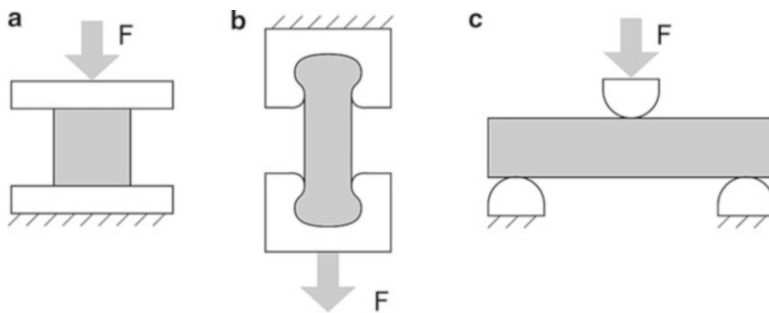


Fig. 1.6 Types of strength testing: compression, tensile, and three-point bending strength

For easily deformed heat insulation materials, according to standards [41–43], the compressive strength is determined on the samples with flat surfaces, and the load, corresponding to 10 % of compression, is taken for the calculation.

The tensile strength is the maximum tensile force applied to the square of the cross section. Due to the difficulties of making the shapes for the testing (Fig. 1.6b), the tensile strength is rarely determined. These shapes may be made by a monolithic technique for ceramic materials or by machining of the shapes for carbon materials, which is done sometimes. There is no special standard for refractory testing; for research needs, it is possible to use the standard for the testing of tensile strength for structural monolithic ceramics [44].

The bending strength, also known as the flexural strength or modulus of rupture (MOR), is also a characteristic that is determined on refractories very frequently, probably as frequently as the compression strength.

The determination of the bending strength combines the compressive and tensile stresses, which probably gives a more advanced picture of the material's properties.

Bending strength may be determined at rods or at rectangular bars by three- and four-point bending (Fig. 1.6c) [45–50]. The bending strength at three-point bending is calculated according to the formula

$$\sigma = 3PL/2bd^2 \quad (1.10)$$

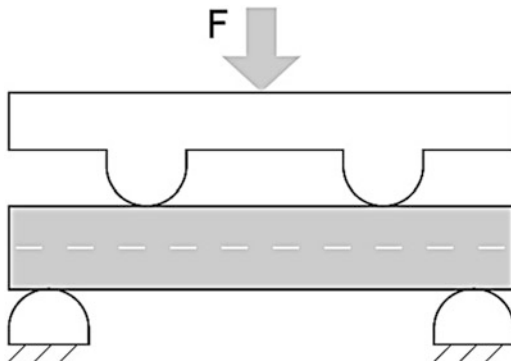
and at four-point bending (Fig. 1.7) by

$$\sigma = 3P(L - 1)/2bd^2 \quad (1.11)$$

where P is a maximum load at rupture of the test piece, d is a thickness of the test piece, b is the width of the test piece, L is the distance between the outer supporting points, and l is the distance between the inner supporting points.

Usually, a three-point measurement gives 20–25 % values compared with four-point bending. It is determined in accordance with standards [38, 46]. For carbon cathode materials, it is also possible to measure flexural strength using three- and

Fig. 1.7 Types of strength testing: four-point bending strength



four-point bending techniques according to standards [47–50]. Also, it is necessary to remember that the lower flat surface of the tested piece is subjected to tensile stress, and the smoothness of the surface may play a certain role. The grinding and polishing of this surface might remove the surface cracks; thus, the value of the flexural strength may increase by 10–30 %.

As mentioned in Sect. 1.2, porosity influences all properties of refractories. Usually, there is a rule: “The bigger the porosity, the lower the strength.” In textbooks and in technical literature, there are at least 50 formulas giving a link between the strength and the porosity. Probably the most well-known was given by D. P. H. Hasselman [51]:

$$\sigma_p = \sigma_o(1 - \kappa P) \quad (1.12)$$

Also, there is an expression by Ryshkevitch [52]:

$$\sigma_p = \sigma_o \exp(-\kappa P) \quad (1.13)$$

where in both formulas κ is a coefficient, P is the total porosity, and σ_o is the strength of nonporous material.

There is an approximate ratio for the values of tensile strength, bending strength, and compression strength for refractory and carbon materials:

$$\sigma_{\text{compression.}} = 2 - 5 \sigma_{\text{flexural.}} = 6 - 10 \sigma_{\text{tensile}} \quad (1.14)$$

The strength of refractory materials is a statistical characteristic. It should be determined on a group of samples. Sometimes the strength is not critical for the evaluation of the probable service life, but sometimes it is (e.g., for carbon cathode blocks). For correct evaluation of the strength of a material, it is probably good to give not only the strength with the average deviation, but also the dispersion. In some cases, material with a strength of 20 ± 2 MPa might be better compared with a

Table 1.3 Average values of bending strength and compression strength at room temperature for materials, used in Al industry

Material	Compression strength, MPa	Bending strength, MPa
Diatomaceous brick (moler) (density 0.4 g/sm ³)	0.8–1.2	0.1–0.2
Fireclay (density 0.4 g/sm ³)	1.0	0.3
Calcium silicate heat insulation ($P = 80\%$)	2.0–2.5	0.8
Fireclay brick	20	5–9
Alumina brick	35–50	10–15
High-alumina brick	200	30–50
Calcium silicate (vollastonite) for launders $P = 45\text{--}55\%$	10–15	7–8
Medium-cement castable	30–50	3–5
Low-cement castable	90–160	8–10
Nitride-bonded silicon carbide	150–200	30–40
Carbon cathode semigraphitic material (30 % graphite, GCA)	35–50	8–12
Carbon cathode semigraphitic material (30 % graphite, ECA)	25–45	7–9
Graphitized carbone cathode material	20–25	9–11

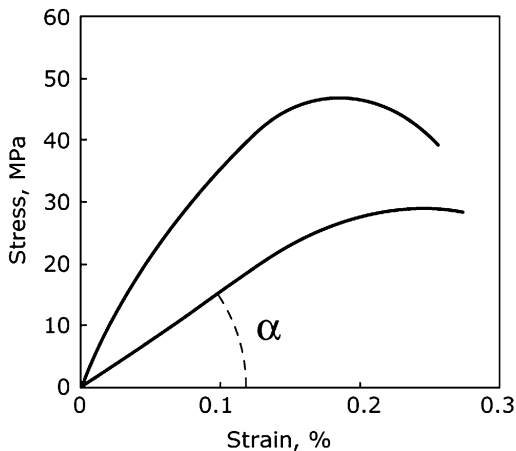
material having a strength of 25 ± 7 MPa, because a bigger variation gives evidence on the micro-cracked structure and inhomogeneity. Table 1.3 contains the values of the strength of several materials used in the Al industry.

1.3.1 Compressive and Bending Strength

The elastic modulus, or Young's modulus, is a coefficient of proportionality (elastic strain constant) between the stress and deformation below the elastic limit of the material (Fig. 1.8). The elastic modulus is an important mechanical characteristic of structural materials; it is closely related to strength, hardness, and abrasion resistance. Materials with a high elastic modulus value have high values of strength and hardness.

The static (mechanical) elastic modulus is determined in the linear part of the elastic deformation at the "strain-deformation" diagram of the sample at static load. The difficulty in determining the static elastic modulus is in the fact that the deformation before the fracture is only microns and a precise apparatus is required. The static elastic modulus may be measured at strength tests (compression, bending, tensile), and, of course, the sample will be broken. In reality, the measurement of the dynamic elastic modulus is more popular.

Fig. 1.8 Stress–strain dependencies for brittle and semibrittle material



The dynamic elastic modulus is determined by measuring the wave propagation velocity of ultrasonic pulses in the material. It is a nondestructive method, based on the dependence between the elastic modulus and the velocity of the propagation of the sonic or ultrasonic waves (mechanical vibrations). The method is very precise. The apparatus is not complicated, and it is possible to measure the dynamic elastic modulus at high temperatures. It is measured according to the standards ASTM C 1198-01 [53] and ISO 3312:1987 [54], and the elastic modulus of carbon materials is measured according to ASTM standard C747 [55].

It is necessary to remember that at dynamic elastic modulus determination, only separate grains (and the defects inside grains) are subjected to deformation, while at static elastic modulus determination, the whole sample deforms. For structural ceramics, the difference in the values of the elastic modulus, determined by static and dynamic methods, is within several percent. For refractory materials, the values of the dynamic elastic modulus are always bigger than those of static elastic modulus values, and for carbon materials the difference is big. The static elastic modulus better reflects the mechanical behavior at service for refractories. Measuring the dynamic elastic modulus is rather simple and is good for quality control. For structural design of the components, the static elastic modulus is preferable. For carbon materials, a certain level of the elastic modulus (determined by the dynamic method) may be considered upper level in order to avoid a strained brittle structure of the material (due to the chilling tensions because of the rapid cooling). Some values of the elastic modulus appear in Table 1.4.

As the material is elongated upon extension (during the mechanical loading), its width diminishes. The ratio of the relative diminishing of the width at deformation to the $\Delta d/d$ to the relative elongation $\Delta l/l$ is a Poisson ratio μ :

$$\mu = \Delta d/d / \Delta l/l, \quad (1.15)$$

which is in connection with elastic modulus:

Table 1.4 Values of elastic modulus for materials

Material	Elastic modulus, GPa	
	Static	Dynamic
Fireclay brick	60–100	
Alumina brick	150–200	
High-alumina brick	200–250	
Medium-cement castable	100–150	150–200
Nitride-bonded silicon carbide	250–350	230–250
Carbon cathode anthracitic graphitic material (30 % graphite, GCA)	10–15	20–30
Carbon cathode anthracitic graphitic material (30 % graphite, ECA)	3–9	8–12
Graphitized carbon cathode material	3–7	10–14

$$\mu = E/2G - l \quad (1.16)$$

where G is a shear modulus.

For the majority of refractory materials, the value of Poisson's ratio is 0.25–0.3.

The elastic modulus depends on the porosity of the materials [51]:

$$E = E_o(1 - 1.95 P - 0.9 P^2) \quad (1.17)$$

where E_o is the elastic modulus on nonporous material.

Wear resistance (including abrasion resistance) sometimes is included in the specification to refractory materials. Wear resistance depends on the hardness, but also it depends on the grain dimensions, the porosity, the binders, and so on.

In the Al industry, wear resistance should be taken into account in sidewall lining of the cells, in the launders for liquid Al, in ladles, in the feeding holes of the melting furnaces, in coke calcining furnaces, and in anode baking furnaces. In some cases, it might be the key characteristic of the material. The wear resistance of carbon cathode blocks is described in Sect. 2.3.

The wear resistance of refractories is determined according to ASTM C-704-01 [56]. This test method measures the relative abrasion resistance of various refractory samples under standard conditions at room temperature. The abrasion resistance of a refractory material provides an indication of its suitability for service in abrasion or erosive environments.

One kilogram of the size-graded silicon carbide grain is blasted by air to a flat surface of the refractory material through a nozzle. The tested sample is weighed before and after the abrasion test; the relative abrasion is a ratio of the weight loss of the material to its bulk density (the amount of refractory lost from the specimen by abrasion). This method is valid for shaped and for the monolithic (castable) refractories. The results of wear resistance according to ASTM C-704-01 [56] are in Table 1.5.

For structural ceramics, there is a big number of the tribological wear resistance tests, where the tested sample may contact the moving flat surface, while the tested

Table 1.5 Abrasion resistance of materials (ASTM C-704-01 [49])

Material	Abrasion resistance (average volume loss, cm ³)
Silica brick	22
Alumina brick	4
Glass	9
Medium-cement castable	9–10
Low-cement castable	5–8
Andalusite low-cement castable	4–6
N-SiC	1–1.5

sample might be a ball (JIS R1613-1993 [57]) or a pin (ASTM G99-04 [58]). Also, a big number of nonstandard tests, using sand-blasting apparatus, using a rotating iron wheel, sometimes instead of silicon carbide grain silica grain are used.

1.3.2 Modulus of Elastic, Hardness and Weibull Modulus

For structural materials, the hardness is connected with the wear and abrasion resistance, which is why it might be useful for research and lab testing. Rockwell and Brinell hardness values are not used for the characterization of ceramics. The hardness values, determined by Vickers (square pyramid), Knoop (rhombic pyramid), and Berkovich (triangle pyramid) indenters, which have physical values, have a dimension of gigapascals (GPa) and may be used for the characterization of ceramics and refractories.

The hardness determination of refractories is limited by its heterogeneous coarse-grained structure. The hardness values characterize small volumes of the material. There is no standard for the determination of the hardness for refractories; for research purposes, it is possible to use ASTM C1327-08 [59] and ASTM C1326-13 [60] for structural ceramics. Many publications describe the determination of the fracture toughness of ceramics by measurement of cracks around the indented areas during hardness testing [61–63].

Micro-hardness measurement of ceramics may also be used for research purposes and the laboratory estimation of phases in refractory material, because usually the grain size of refractory materials is bigger than the indented area.

Hardness testing of the refractories is not an everyday procedure, yet it is very useful to remember that the hardness of self-bonded silicon carbide ceramics is in the range of 20–25 GPa, the hardness of nitride-bonded silicon carbide refractories is 16–20 GPa, and the hardness of alumina ceramics is 12–16 GPa, which is three to four times higher than with dense alumina silica dense refractories.

The Weibull statistical theory of brittle materials is applied for structural ceramics [64], but sometimes the strength distribution is measured on refractory materials and the Weibull distribution graph is plotted. According to the Weibull

statistical theory of brittle materials, the probability of cracks in the material depends on its volume. The failure probability of a stressed material depends on the volume and the “coefficient of homogeneity” – which is the Weibull modulus:

$$m = \log(V_1/V_2)/\log(\sigma_1/\sigma_2), \quad (1.18)$$

where m is the Weibull modulus, and V_1 , V_2 , σ_1 , and σ_2 are the volumes and strengths of the samples, respectively, made from one material. Usually, the samples are tested for compression strength or flexural strength. Generally speaking, the larger the Weibull modulus is, the less variable the strength of the material.

For different classes of materials, the values of Weibull modulus fluctuate: For structural ceramics, the material is considered to be homogeneous if the Weibull modulus is above 15–20; for nitride-bonded silicon carbide, it is 15; for alumina brick, it is 6; for porcelain tableware, it is in the range 4–11; baked carbon anodes are considered to be homogeneous if the Weibull modulus is 6–9. We haven’t found the values of the Weibull modulus for cathode carbon blocks.

1.3.3 Elements of Fracture Mechanics

Cracklike defects always exist in refractory and carbon cathode materials. They may be technological and structural defects, but they may also appear during service. As refractories are coarse-grained materials, every grain boundary of relatively coarse grain may be considered a crack. On cooling, the small grains of a binder contacting the coarse grain shrink, causing a cracklike defect to appear. In stressed materials, these cracks are the defects causing the material failure. The strength of the material depends on a defect dimension. The stress intensity factor K_{1c} is proportional to the square root of the critical crack length [65]:

$$K_{1c} = \sigma Y a^{0.5}, \quad (1.19)$$

where σ is the critical stress, Y is a coefficient, a is the critical crack length, and K_{1c} is the stress intensity factor.

For refractories, there is no standard for determining the stress intensity factor; for research needs, it is possible to use the standards for determining the stress intensity factor for ceramics. In ceramics, the stress intensity factor is determined by testing the bending strength (Fig. 1.10) of a sample with a notch (which imitates the crack) or by testing the compression strength of a cylinder with a notch. According to ASTM C1421-10 [66], for structural ceramics it is possible to test the samples with a previously introduced crack, with a surface crack, or with a notch. For research purposes, stress intensity factor can be determined by measuring the crack length around the indenter at hardness testing [61–63].

The characteristic of the materials known as the *stress intensity factor* comes from Griffith’s theory of preexisting cracks in brittle solids, demonstrating a fully

Fig. 1.9 Fracture toughness testing

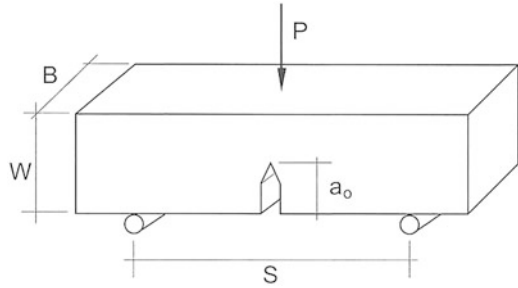
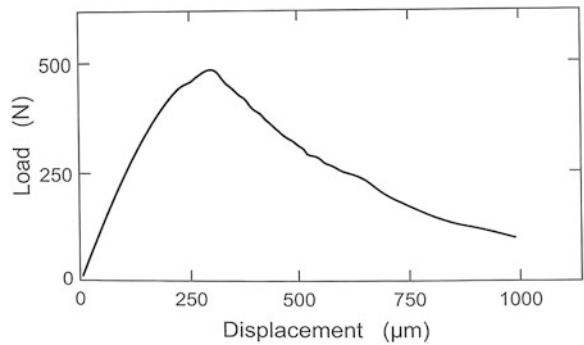


Fig. 1.10 Load–displacement curve of graphite material, redrawn from Allard [68]



elastic type of failure (curve 1 in Fig. 1.9). In reality, elastic behavior is more typical of structural ceramics with a high elastic modulus, less typical of refractories (curve 2, Fig. 1.8), and not typical of composites and carbon materials (Fig. 1.10). Still, it is very useful to keep in mind the values of the stress intensity factor. The stress intensity factor for structural alumina ceramics is $4\text{--}7 \text{ MPa}\cdot\text{m}^{0.5}$; for structural silicon carbide ceramics, it is $4\text{--}5 \text{ MPa}\cdot\text{m}^{0.5}$; for nitride-bonded silicon carbide, it is about $2 \text{ MPa}\cdot\text{m}^{0.5}$; and for shamoto brick and medium-cement concrete, it is below $1 \text{ MPa}\cdot\text{m}^{0.5}$. According to Panov et al. [67], the fracture toughness of carbon cathode blocks is only $0.15 \text{ MPa}\cdot\text{m}^{1.5}$. Allard et al. [68–70] give values of $0.3\text{--}1 \text{ MPa}\cdot\text{m}^{1.5}$ for anthracitic graphitic blocks, with a tendency to decrease in the case of graphitic materials.

Practical considerations and experience tell us that in the metallurgy of Al, refractories are subjected to chemical wear, abrasion, and chemical attack, but they rarely go out of service because of cracking due to overloading. From a scientific point of view, the investigation of refractory brittleness is interesting [71], yet in industrial practice, people are usually satisfied with characteristics such as compression, flexural strength, elastic modulus, and abrasion resistance. The exception is carbon cathode blocks.

The mechanical behavior of carbon cathode blocks is extremely critical for the service life of the reduction cell, especially in the beginning of service. A single crack in a carbon cathode block leads to shutdown of the cell. The knowledge of mechanical characteristics such as compression, flexural strength, and elastic



Fig. 1.11 Crack through the carbon cathode blocks

modulus is insufficient to forecast the cracking of a cathode and consequent shutdown of the cell.

The cracking of a carbon cathode block may take place even 1 or 2 weeks from the startup of the cell. A crack in a carbon cathode block may open within 12 months or 60 months. A crack may go through two or three carbon cathode blocks (Fig. 1.11), and possibly more, and currently there is no dependencies from fracture mechanics that could forecast a crack's appearance. It is likely that the dependencies describing crack propagation will be useful for predicting cracking due to thermal shock in correlation with preheating regimes of the cells. Additionally, the theory of slow crack growth may help our understanding of crack openings in the blocks with a service life over 24–60 months. Yet the existing problems in the behavior of carbon cathode blocks await research scientists who specialize in fracture mechanics.



Fig. 1.12 Cathode bottom of reduction cell before the dry autopsy

The difficulty with implementing fracture mechanics mechanisms to address the problems of crack openings in carbon cathode blocks arises because the mechanical behavior of carbon cathode blocks is not fully elastic. Even at room temperature, carbon cathode blocks demonstrate elastoplastic or “pseudo-plastic” behavior (Figs. 1.10, 1.12, and 1.13) [69].

It is well known that sometimes cathode heaving during heating and startup may exceed 100 mm in the center of the cell (Fig. 1.13); this deformation is sufficiently higher than the brittle material can withstand without cracking. The temperature of the preheating rarely exceeds 800 °C, which is not quite sufficient for the transformation from elastic to plastic behavior of a high-temperature material such as carbon.

An additional circumstance that is necessary to take into account upon application of the fracture mechanics mechanism to the fracture of cathode blocks (especially for estimating the probability of crack opening after 24 months) is that we measure all mechanical characteristics of porous carbon materials (even at elevated temperatures), whereas in service, the pores of carbon cathode blocks are filled with cryolite and the material is intercalated with sodium. Figure 1.12 gives the evidence of the plastic behavior of carbon cathode materials in service in reduction cells.



Fig. 1.13 Bottom heaving of the cell with lens under the cathode bottom blocks

1.4 Thermomechanical Properties

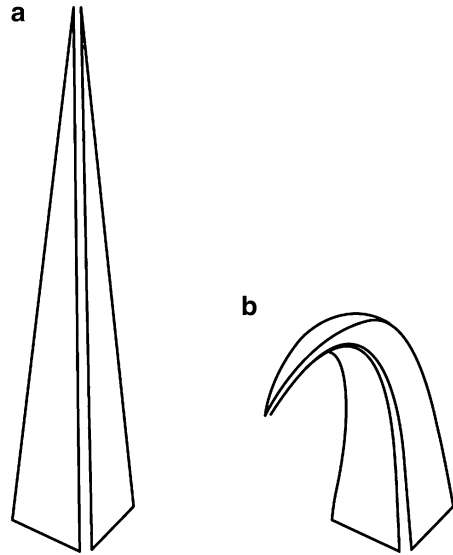
The thermomechanical properties of refractories are refractoriness, hot modulus of rupture (hot bending strength), reheat change of dimensions, deformation at high temperatures, and creep (sometimes other characteristics of mechanical behavior are used for research purposes). The main purpose of refractory materials is to withstand certain mechanical characteristics at high temperatures. In order to have a full picture of the mechanical behavior of refractories at high temperatures, it is better to have all of the abovementioned characteristics, which is a rather time-consuming process. In industrial practice, usually one or two of these characteristics are measured. Yet for laboratory investigations, it is worth having all of these characteristics.

The refractoriness is a rather rarely used characteristic, yet nobody has declared that it is not useful.

Finally, consumers of refractory and high-temperature heat insulation products need to know the safe service temperature of the material. There is no need to use materials with a softening point above 1,600 °C for smelting of Al with a melting point of 660 °C. On the contrary, it is risky to install a vermiculite slab with a softening point of 750 °C under the refractory layer in the reduction cell, whereas the temperature at the bottom of this layer might be in the range of 750–850 °C.

However, in the specifications for the materials, producers do not indicate such a characteristic. In order to have an idea of the safe temperature of service, it is necessary to have the full range of thermomechanical characteristics, but once the application engineer has all these characteristics for every high-temperature process, the estimation of the safe service temperature is at last state of the art, now based on this application engineer's experience.

Fig. 1.14 Cones for the determination of refractoriness



1.4.1 Refractoriness

Refractoriness is a property to withstand high temperatures without melting. Sometimes people confuse refractoriness with the safe service temperature. In reality, the safe service temperature might be 200–600 °C lower than the temperature of refractoriness. The refractoriness is a temperature of the deformation of a cone (pyramid), shaped from the powdered refractory. Refractoriness is expressed in degrees Centigrade and indicates the temperature at which the cone (Fig. 1.14a), a pyramid of a certain shape, having melted (Fig. 1.14b), will touch the flat surface of the pad.

Refractoriness is not a physical constant. It has almost nothing in common with the melting point. Refractory materials are usually polymineral; they consist of crystalline matter and also some glass as a secondary phase. The temperature of refractoriness characterizes a certain level of softening of the material of the cone-to viscous state with the level of viscosity 10^4 – 10^5 Pa*s). Only for very pure materials does the temperature of refractoriness correlate with the melting point.

The standards for refractoriness were developed in different countries: In Germany, the Seger cone was developed, and the DIN standard for refractoriness uses the Seger cone [72], while in the United States, the Orton cone was developed, and the ASTM standard [73] uses the Orton cone. Japanese standards for refractoriness and the Russian standard are close to the ISO 1146-1988 [74]. In different standards, the rate of heating differs; there are the tables of approximate correspondence of refractoriness, determined according to different standards. Generally speaking, there is probably no need to have uniformity in standards having historical

inheritance, because the term “refractoriness” gives a general understanding of the characterization of the refractory property.

The method of refractory determination comprises crushing and milling of the refractory shape to -0.2 mm (the castables are simply additionally milled). The powdered material is shaped in the form of a pyramid and the samples are placed in the furnace together with standard cones. The temperature of refractoriness is the temperature of the drop of the tested cone (compared with the drop of the standard cones).

Because of the heterogeneity of their composition and structure, ceramic refractories do not exhibit a uniform melting point. The refractoriness is characterized by the optical determination of the pyrometric cone equivalent (according to Seger), that is, the temperature at which the tip of a cone made of the sample material softens to the point that it touches the base plate. Reference cones with well-established pyrometric cone equivalents at temperature intervals of 10 °C and above, along with the test cones made from the sample material, are heated in the same furnace so that it is possible to make an accurate comparative temperature determination for the softening point of the refractory material to within approximately 20 °C.

1.4.2 Hot Modulus of Rupture

The high-temperature strength of the refractories is measured using the measurement of bending (flexural) strength (Fig. 1.8), and it is a question of convenience (it is more difficult to measure the crushing strength at elevated temperatures). For different classes of materials, the dependences of the hot modulus of rupture (HMOR) from temperature differ. For magnesia refractories, the modulus of rupture (MOR) doesn't change until $1,200$ °C, and for silica refractories, the HMOR at $1,200$ °C is about 85 % of the value at ambient temperature. For nitride-bonded silicon carbide, the MOR values increase with temperature at $1,000$ – $1,300$ °C but remain almost the same even at $1,500$ °C. Generally, the MOR decreases with temperature due to increased viscosity of the glassy phases, but for refractory materials without a glassy phase, it may increase due to the absence of brittle behavior at high temperature.

There are some apparatus and methodical limitations in the HMOR measurement. The MOR is defined as the maximum stress a rectangular test piece of specific dimensions can withstand in a three-point bending test until it breaks, expressed in N/mm^2 or MPa. Test piece dimensions are 150 mm \times 25 mm \times 25 mm.

According to ASTM C-583-00 [75] and ISO 5013-85 [76], the three-point bending apparatus is used, and the rate of heating below 980 °C should be below 330 °C/h and not exceed 110 °/h after 980 °C with exposure at least for 3 h. For castables and chemically bonded materials, the exposure at the temperature of testing should be above 12 h. The HMOR values are calculated according to the equation for the three-point bending test [Eq. (1.11)].

The MOR is an important variable in the characterization of refractory materials. Along with other thermophysical properties, the maximum load at high temperatures is an important parameter for the quality control and development of furnace linings.

1.4.3 Reheat Change. Permanent Linear Change on Reheating

Reheat change of dimensions is irreversible change of dimensions of refractory shape at heating. It may be negative (shrinkage) and positive (expansion). The shrinkage may occur not only to decrease in porosity at sintering, but also due to the phase transformations. Examples are the decrease in dimensions at the transformation of $\gamma\text{-Al}_2\text{O}_3$ to $\alpha\text{-Al}_2\text{O}_3$ and at the synthesis of mullite from alumina and silica. The shrinkage may take place due to the sintering process, while the sintering process may occur due to the presence of the glassy phase (liquid-phase sintering) and to solid-state sintering. The shrinkage takes place with all clay materials (shamotte) and with aluminous, magnesia, and other materials. The expansion is common for silica and spinel refractories. The main cause for the absence of the constant shape and volume for refractories is the insufficient temperature of heat treatment or insufficient time of exposure at required temperature. This characteristic is very important for unfired refractories and heat insulation materials.

The standard method for the reheat change is ASTM C113-14 [77]. For heat insulation material, the volume is calculated by directly measuring dimensions, and the time of exposure may be 2 and/or 5 h (it should be noted in the specifications).

Some producers indicate in the specifications that the time of exposure at max temperature is 6 or 12 h (because the reheat change may not take place within 2 h or may take place but not through the end). Unfired refractory or heat insulation materials may sinter at service, and their dimensions may diminish. An example is unfired vermiculite materials on a sodium silicate binder. For such materials, exposure at the service temperature should be 50 h or even 100 h during testing. Usually, the value for the reheat change according to the procedure just described is like the value obtained in a dilatometer, but sometimes the values might differ a little.

1.4.4 High-Temperature Deformation. Characteristic Points and Softening Point

The characteristic points on a high-temperature deformation curve are probably the most significant information for the estimation of the safe service temperature of refractories.

Nonoxygen compounds (carbides, nitrides, and borides) have the highest softening points and deformation temperatures (above 2,000 °C), pure oxide refractories (magnesia, zirconia, and alumina) have softening points in the range 1,800–2,000 °C, mullite refractories have a softening point of 1,500 °C, and shamotte-fired clay refractories with a high silica content have a softening point of 1,200–1,300 °C.

In reduction cells, the high-temperature deformation behavior of refractory materials has limited significance, because the softening points of carbon and silicon carbide materials are sufficiently higher than the temperatures in reduction cells. The same may be said about fireclay bricks; however, the high-temperature deformation behavior of heat-insulating materials (moler diatomaceous, vermiculite, perlite, calcium silicate) might be quite significant.

In the furnaces of the Al foundry, the temperatures are also rather low, so even fireclay-based refractories usually demonstrate softening points 400–500° lower than the temperature of Al melt, which is sufficient.

In anode baking furnaces, the high-temperature deformation behavior of refractory materials is sufficient. The flue walls deform in a plastic way.

According to ISO 1893-1989 [78], DIN 51064 [79], and DIN EN 993-8 [80], the temperature is increased continuously for the refractory sample, compressed at a pressure of 0.2 MPa (0.05 MPa), and a certain level of deformation is fixed. The samples are cylinders either with or without inner holes.

In diagrams of “linear change temperature,” different characteristic points are fixed (Fig. 1.15). In samples of cylinders without an inner hole, the characteristic

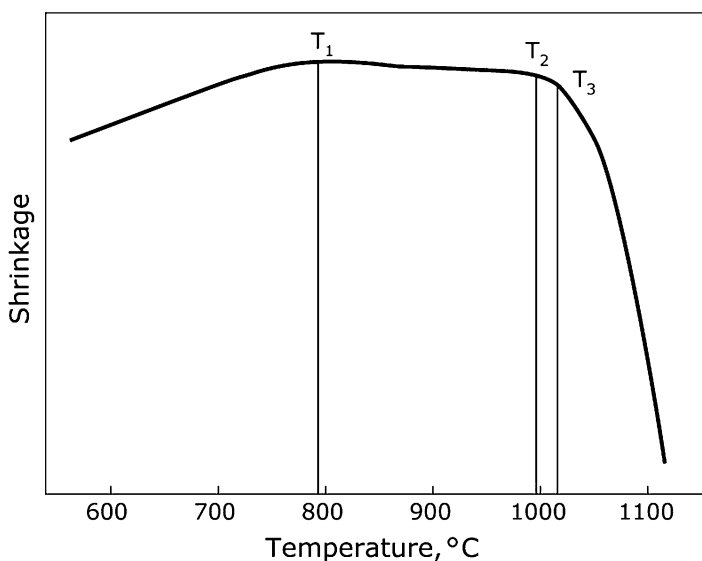
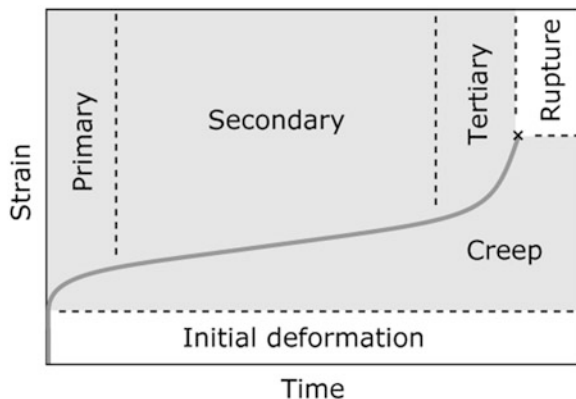


Fig. 1.15 Temperature deformation curve for vermiculite heat insulation material. Note long temperature interval between T_1 (maximum expansion) and T_2 (softening point – 0.5 % deformation) and short temperature interval between T_2 (0.5 % deformation) and T_3 (2 % deformation)

Fig. 1.16 Creep of refractory materials – the stages



points are the temperature of the maximum height, which corresponds to the temperature when the expansion of the sample is compensated by the shrinkage; the temperature corresponding to shrinkage of 0.6 % (0.3 mm); the temperature corresponding to shrinkage of 4 % (2 mm); and the temperature of failure. In samples of cylinders with an inner hole (differential method), the characteristic points are the temperature of the maximum height and the temperatures corresponding to deformation of 0.5, 1, 2, and 5 %.

The temperatures of deformation, determined according to different standards, differ. According to ASTM C16-81 [81], for a certain temperature, the degree of deformation is fixed for a certain compression. For heat insulation materials, the specific pressure on samples is 0.05 MPa [12].

1.4.5 Creep

Creep is the plastic deformation of refractories at high temperatures (below the melting point) under mechanical stress (below the crushing strength). Creep in compression (CIC, according to ISO 3187 [82, 83]) refers to the percent of shrinkage of a refractory test piece under a constant load and exposed to a constant high temperature over a long period of time.

Generally speaking, creep may be measured at tension, flexure, and compression. Compression of cylindrical samples is the easiest way to estimate creep. Creep has three stages (Fig. 1.16): first, nonpermanent; second, permanent; and third, nonpermanent (breakage). The typical time for creep measurement is 4 h, but within 4 h the permanent stage of deformation may not be achieved. So the time of creep testing may vary from 4–10 h, but sometimes it may be extended up to 50 h.

According to ISO 1983-1989 [12], the shape of the samples is the same, as for high temperature deformation – it is cylinders 50 × 50 mm with inner diameter of 12.5 mm. Testing is performed at a pressure 0.2 MPa within 50 h.

According to ASTM C-832-00 [84], the samples of heat insulation are parts of a 38-mm × 38-mm × 114-mm brick that is tested at a pressure of 0.18 MPa. Deformation is measured optically, the time is 20–50 h, and the testing temperature depends on the type of refractory and the sphere of application.

In the Al industry, the creep values are interesting for heat insulation materials in reduction cells, because their service is in permanent relatively high pressure and permanent pressure (due the weight of carbon blocks with busbars and the weight of Al melt and the bath). It's likely that 50-h tests are essential.

The flue wall of anode baking furnaces deforms due to creep in service, but this takes place due to the appearance of the glassy phase in refractories due to evaporation of sodium from anodes. Usually, the temperature of high-temperature deformation of the refractories before service is sufficiently higher compared with the service temperature.

1.5 Thermal Conductivity, Heat Capacity, and Temperature Conductivity (Heat Diffusivity)

Thermal conductivity is characterized by the coefficient of thermal conductivity λ , which has unit W/m·K. It characterizes the amount of heat being transferred through the unit of the surface layer of the material within the unit of time, while the difference in the temperature between the surfaces of the layer is 1°.

Temperature conductivity (heat diffusivity) characterizes how fast the temperature in the material is spreading.

Heat capacity is the amount of heat that is necessary in order to increase the temperature of the unit of material 1° (Kelvin).

Thermal conductivity is probably the most important parameter for all thermal calculations in the design of all furnaces, reduction cells, ladles, runners, and so forth in any temperature process.

Heat capacity and temperature conductivity (heat diffusivity) should be taken into account at the service of any furnaces having cycles of heating and cooling down. In the Al industry, heat capacity and temperature are sufficient in the runners (launders) for molten Al and in anode baking furnaces. Also, they are useful in all thermal calculations.

1.5.1 Elements of Theory

The heat transfer in refractory materials takes place due to conductive heat transfer and radiation. Refractories are heterogeneous and consist of condensed matter (grains), contacts between the grains, and the pores (filled with gas). The heat transfer through the refractory material is a sum of the processes that take place

simultaneously: heat transfer through condensed matter (conductive heat transfer and radiation), heat transfer through pores (radiation, convection, and conductive heat transfer due to the thermal conductivity of the gas), and heat transfer through the contacts between the grains.

Conductive heat transfer has a phononic nature, which means that the heat is transferred due to the oscillation of the atoms in the crystal lattice. Crystals with a simple lattice, such as silicon carbide or carbon, have a lower dissipation of heat waves and a higher thermal conductivity compared to crystals with a more complex lattice. For example, the conductive thermal conductivity of aluminium nitride or silicon carbide (binary compounds with approximately equal atomic weights) is higher than alumina, magnesia, and zirconia. And the conductive thermal conductivity of said alumina, magnesia, and zirconia is higher than that of spinel, mullite, and zircon.

The temperature dependencies of the thermal conductivity for different materials are not the same. Some materials (BeO, CaO, MgO, SiC) have a high thermal conductivity at low temperatures (up to 10–20 W/m·K), but it diminishes with a temperature increase. Other materials (silica, zirconia) have a low conductive thermal conductivity at low temperatures (1–2 W/m·K), but it increases with as the temperature increases.

Radiation transfer through the grains becomes sufficient after 800–1,000 °C.

The thermal conductivity of the pores is a sum of the gas's thermal conductivity, radiation, and convection. The thermal convection should be taken into account only if the pores are larger than 5 mm, which is not typical for modern refractories. The thermal conductivities of air, nitrogen, oxygen, and argon are approximately the same, so the value of this factor should be taken into account only if helium or hydrogen is in the pores. The main factor for thermal conductivity in the pores beginning from 800 to 1,000 °C is radiation.

Pores and the contacts between grains are barriers for thermal conductivity. The thermal conductivity of materials (having equal total porosity) with continuous condensed matter (big closed porosity) is 2–2.5 times higher compared with materials with continuous contacts. The thermal conductivity of fireclay brick at 600 °C is 0.25 W/m·K, while the thermal conductivity of fireclay fiber material is 0.11–0.12 W/m·K (Table 1.6). The thermal conductivity of diatomaceous brick with a different porosity may differ at 200 °C, but it becomes very close at 600–700 °C (Fig. 1.17).

The thermal conductivity for a material may be high at low temperatures and low at high temperatures, but the picture may be absolutely different for other materials (Fig. 1.18). Many materials have a temperature dependence of thermal conductivity temperature, demonstrating a high thermal conductivity at low and high temperatures. There are many equations describing the temperature dependencies of thermal conductivity for specific materials. There are equations describing the thermal conductivity behavior depending on porosity. All these dependencies are more or less approximate and are good for estimations of the thermal conductivity. The engineering calculations of the thermal balance of the furnaces and reduction cells require the exact values of thermal conductivity, obtained at precise measurements.

Table 1.6 Thermal conductivity of traditional refractory and heat insulation materials (data from the reference handbooks [85–87])

Material	Thermal conductivity at °C, W/m·K							Comment	
	20	200	400	500	600	800	1,000		1,200
Fireclay	1.16	–	–	1.34	–	1.47	1.51	1.55	Stationary heat flow
Silica	1.16	–	–	1.40	–	1.50	1.63	–	Stationary heat flow
Magnesia (90 % MgO)	5.82	–	–	4.66	–	3.6	3.5	2.8	Stationary heat flow
High alumina (85 % Al ₂ O ₃)	–	2.33	–	2.2	2.1	2.1	2.1	2.1	Stationary heat flow
Alumina (99 % Al ₂ O ₃)	15.0	5.8	4.3	3.8	3.2	2.8	2.8	2.8	Stationary heat flow
Zircon alumina	–	–	–	–	–	1	–	1.2	Stationary heat flow
Zircon	4.3	3.5	2.8	2.6	2.5	2.4	2.3	2.3	Stationary heat flow
Nitride-bonded silicon carbide	–	–	–	–	–	–	–	–	Stationary heat flow
Reaction-bonded silicon carbide (SiSiC)	81	7.8	8.4	–	9	14–18	–	–	Stationary heat flow
<i>Heat insulation materials</i>									
<i>Fireclay</i>									
Fireclay ($\rho = 1.0 \text{ g/sm}^3$)			0.50		0.60				Stationary heat flow
Fireclay ($\rho = 0.6 \text{ g/sm}^3$)			0.25		0.30				Stationary heat flow
Fireclay ($\rho = 0.4 \text{ g/sm}^3$)			0.20		0.25				Stationary heat flow
<i>Alumina silica</i>									
Alumina silica ($\rho = 1.0 \text{ g/sm}^3$)			0.65		0.60				Stationary heat flow
Alumina silica ($\rho = 0.8 \text{ g/sm}^3$)			0.35		0.40				Stationary heat flow
Alumina silica ($\rho = 0.5 \text{ g/sm}^3$)			0.25		0.30				Stationary heat flow
<i>Alumina</i>									
Alumina ($\rho = 1.8 \text{ g/sm}^3$)			0.90		0.90				Stationary heat flow
Alumina ($\rho = 1.3 \text{ g/sm}^3$)			0.80		0.80				Stationary heat flow
Alumina ($\rho = 1.1 \text{ g/sm}^3$)			0.55		0.55				Stationary heat flow

(continued)

Table 1.6 (continued)

Material	Thermal conductivity at °C, W/m·K								Comment
	20	200	400	500	600	800	1,000	1,200	
<i>Moler (diatomaceous), vermiculite, and calcium silicate</i>									
Moler ($\rho = 0.4 \text{ g/sm}^3$)		0.110	0.130	0.137	0.140				Stationary heat flow
Moler ($\rho = 0.5 \text{ g/sm}^3$)		0.120	0.133	0.138	0.140				Stationary heat flow
Moler ($\rho = 0.6 \text{ g/sm}^3$)		0.130	0.137	0.145	0.155				Stationary heat flow
Moler ($\rho = 0.55 \text{ g/sm}^3$)		0.090	0.110	0.145	0.160				Stationary heat flow
Moler ($\rho = 0.55 \text{ g/sm}^3$)		0.15	0.22	0.23	0.24				Non stationary heat flow
Vermiculite ($\rho = 0.4 \text{ g/sm}^3$)		0.10	0.13	0.14	0.15				Stationary heat flow
Vermiculite ($\rho = 0.4 \text{ g/sm}^3$)		0.22	0.28	0.30	0.32				Non stationary heat flow
Calcium silicate ($\rho = 0.22 \text{ g/sm}^3$)		0.05	0.08	0.90	0.10				Stationary heat flow
Calcium silicate ($\rho = 0.22 \text{ g/sm}^3$)		0.11	0.15	0.16	0.18				Non stationary heat flow
<i>Fiber</i>									
Fireclay blanket		0.080	0.105		0.120		0.230		Stationary heat flow
High-alumina blanket		0.06	0.09		0.13		0.19	0.28	0.41
Alumina blanket		0.06	0.10		0.16		0.25	0.39	0.62

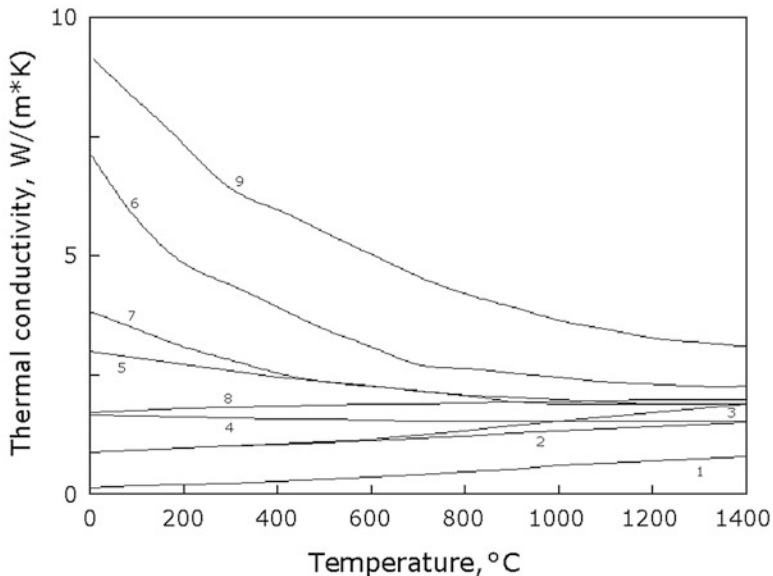


Fig. 1.17 Thermal conductivity of lightweight fireclay brick (1), fireclay brick (2), silica brick (3), mullite brick (4), alumina brick (5), zircon (6), cromite (8), magnesia (9) according to [85–87]

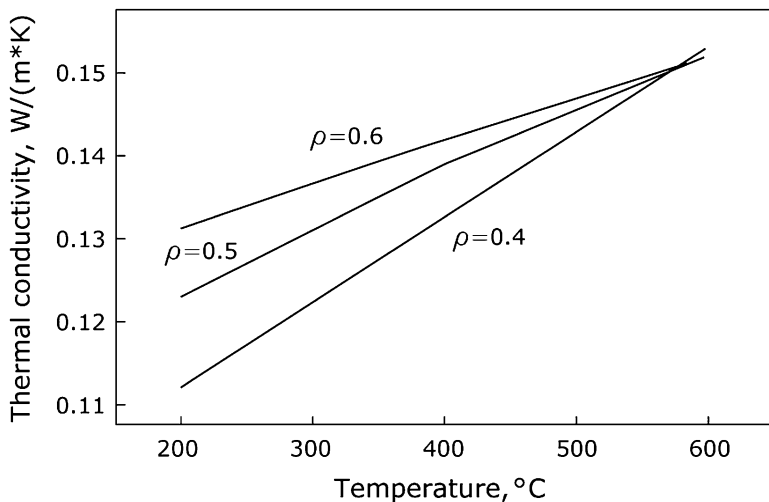


Fig. 1.18 Thermal conductivity of diatomaceous bricks with different densities

Currently, there is no theory to forecast the thermal conductivity of the refractory material and its temperature dependence. For heat insulation materials, the value of the thermal conductivity may increase two to five times as the temperature increases from 200 to 1,200 °C.

Table 1.7 Values of coefficient b for the calculation of the thermal conductivity of porous refractory materials [86]

Porosity, %	<10	10–15	15–20	20–25
b	1.5	2.0	2.4	2.6

Usually, the thermal conductivity for dense refractory materials diminishes several times with the temperature increase. Reference data are available [85–87], yet it is necessary to take into account the chemical composition and porosity (Table 1.6).

The following equation describes the dependence of the thermal conductivity on the porosity:

$$\lambda = \lambda_0 (1 - bP_t), \quad (1.20)$$

where λ_0 is the heat conductivity for the material with zero porosity, P_t is the total porosity, and the values for the coefficient b are given in Table 1.7.

Below 500 °C, fireclay refractories with small pores are more temperature-conductive compared with fireclay refractories with big pores (at equal total porosity). Above 500 °C, fireclay refractories with big pores are more conductive (compared with fireclay refractories with small pores) due to value of the radiation. For silica refractories, the thermal conductivity of materials with big pores becomes higher compared with the thermal conductivity of materials with small pores beginning at 1,200 °C.

In order to choose a refractory or heat insulation material for a specific purpose, it is necessary to have at least two or three values of the thermal conductivity at different temperatures (e.g., at 300 and 800 °C) and to know the measurement method. The thermal conductivity measurements of the lining materials for one furnace or thermal unit preferably should be made in one laboratory by the same method.

Also, it is necessary to take into account that there exists so-called thermal aging, which is deterioration of the properties with the service lifetime. Due to thermal aging, the thermal conductivity may increase by 10–20 %. Due to the impregnation of heat-insulating materials with salts (by infiltration of the bath), the values of the thermal conductivity may increase 20–75 times (this is described in Sects. 2.6 and 2.7).

The heat capacity is the amount of heat necessary to increase the temperature of the unit of material by 1°. In practice, it is necessary to define the molar heat capacity (J/mol·K), which is determined for pure substances, and the specific heat capacity (J/kg·K).

The values of heat capacity can be calculated according to the formula

$$c_v = \sum c_i m_i \quad (1.21)$$

where m_i is a concentration and c_i is a heat capacity of the constituent (e.g., alumina). Table 1.7 contains the heat capacity values for pure oxides.

A material's heat capacity cannot be calculated if certain processes occur during the heating of the material (evaporation, decomposition, or other reactions). The values of heat capacity are measured in calorimeters.

Heat capacity values are required for nonstationary calculations of refractory linings and for the recalculation of thermal conductivity characteristics, obtained by stationary and nonstationary methods.

Although the heat capacity doesn't depend on the structure of the materials, the value of the heat capacity depends on the porosity, because the weight of the material diminishes as the porosity increases. That is why porous heat insulation material requires less heat in order to be heated to a certain temperature compared to nonporous refractory material, which is taken into account in the design of the Al launders (runners) and in anode baking furnaces.

Thermal diffusivity (m^2/s) characterizes the velocity of spreading of the temperature in the material and is calculated as

$$a(t)\rho = \lambda(t)/c_v(t), \quad (1.22)$$

where $\lambda(t)$ is the thermal conductivity, ρ is the density, and $c_v(t)$ is the specific heat capacity. The thermal conductivity and thermal diffusivity are linked with each other via the heat capacity.

1.5.2 The Measurement of Thermal Conductivity

In general, thermal conductivity measurements comprise the measurement of the heat flow passing through the sample of certain dimensions and the temperatures on isothermal surfaces, while the distance between these surfaces is known.

There are many methods of taking thermal conductivity measurements, and all of them have certain inaccuracies and discrepancies (the main uncertainty is the impossibility to eliminate the heat drain).

The methods of obtaining thermal conductivity measurements are divided into two main groups:

1. Based on the principle of stationary heat flow;
2. Based on the principle of nonstationary heat flow (dynamic methods).

Very generally speaking, it is possible to say that the methods based on the principle of stationary heat flow are better for measurements of materials with medium and low thermal conductivity, while the methods based on the principle of

nonstationary heat flow are better for highly conductive materials. Sometimes it is simply impossible to make measurements of highly conductive materials at a relatively high temperature. Measurement of thermal conductivity by dynamic methods takes less time.

Unfortunately, for the same material, the thermal conductivity value measured by the method of stationary heat flow always differs from the thermal conductivity measured by the method of nonstationary heat flow.

The values in Table 1.6 and Fig. 1.18 give a general idea of the thermal conductivity values. For project designs of furnaces (while working with the thermal balances of the furnaces and with the equations of the heat flow), it is better to have thermal conductivity values obtained by several methods. After the construction of the newly designed furnace, the trials and the energy balance may give an idea of what thermal conductivity values are preferred for this specific design of the furnace. A comparison of thermal conductivity values for heat-insulating vermiculite material [88] obtained by stationary and dynamic methods (Table 1.6) give good evidence of this.

When considering the relining of the furnace during the course of repair, here it is better to make measurements of the materials using one method of thermal conductivity measurements. Thermal conductivity values, measured even by a consistent method of nonstationary heat flow but according to different standards, may differ considerably. The performance of the reduction cell is extremely sensitive to a change in the heat balance. The rather common decision to change the supplier of the heat insulation materials for the relining of the reduction cells may cause changes in the performance of the reduction cells if the thermal conductivity value of the newly installed heat insulation materials differs from the thermal conductivity value of the previously used materials.

1.5.3 Methods of Thermal Conductivity Measurements Based on the Principle of Stationary Heat Flow

The advantage of thermal conductivity measurement methods based on stationary heat flow is their relatively high accuracy and the fact that the measurement conditions are close to the conditions of refractory service. The disadvantage is the fact that it is very difficult to make measurements at 200, 300, and 400 °C, and the real measurement will be performed at a medium temperature of the sample, such as 315, 345 °C, and so forth. This occurs because the measurement is performed, fixing the temperature between the cold and hot surfaces, and then make the temperature dependence of the thermal conductivity, and having this dependence, people determine the values at 200, 300, 400, 600, and 800 °C.

According to ASTM C201, ASTM C202 [89, 90], the sample (usually half of a brick with flat, parallel surfaces) is placed in the furnace so that one surface (with a

thermocouple) is subjected to temperature (due to SiC heaters), while the other (also with a thermocouple) is with the copper calorimeter, so that the calorimeter measures the amount of heat (due to the change in the temperature of the water in the calorimeter). The temperature on the hot surface may be between 300–1,350 °C. In order to achieve stability of thermal characteristics during measurements, one should heat-treat the sample before the measurements at a temperature at least 50° higher than the temperature of the measurement. The measurements may be fulfilled parallel and normally to the direction of pressing. The accuracy of the method is within 10 %.

The thermal conductivity of shaped heat insulation materials is determined according to ASTM C182-88 (1998) [91], and the thermal conductivity of unfired materials is determined according to ASTM C417-93 (1998) [92]. Both standards employ the stationary heat flow method. To determine the thermal conductivity of monolithics, the sample should be dried at 120 °C for 24 h before measurement. In the test unit, the sample should be heat-treated at 260 °C for 16 h to remove moisture. However, the measurement is considered to be correct only if the following measurement gives no more than a 2 % difference in value; otherwise, it is necessary to make the next measurement.

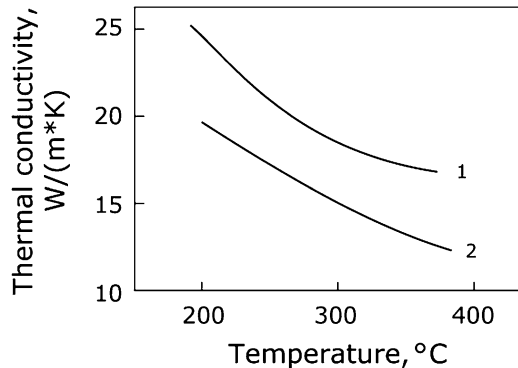
The thermal conductivity of the carbon cathode blocks is measured according to ASTM C767 [93] and ISO 12987 [94] in the range of 20–60 °C by comparative methods. It is obvious that the values of the thermal conductivity of carbon cathode blocks are essential at preheating and at service, where the temperature is above 900 °C. The implementation of a good dynamic method of measuring the thermal conductivity of carbon cathode blocks is required.

Although plant repair managers are rather conservative in everything that concerns the use of lining materials for the relining of reduction cells, sometimes they have to change the type and the producer of cathode blocks, and here the exact directly measured values of the thermal conductivity of cathode blocks at high temperatures might be very useful – at least to keep the preheating and startup period unchanged. Next, the startup period will be more influenced by impregnation of the carbon blocks by the cryolite, because the thermal conductivity will be increased several times (to be discussed in Sect. 2.3).

1.5.4 Methods of Thermal Conductivity Measurements Based on the Principle of Nonstationary Heat Flow (Dynamic Methods)

Many methods of thermal conductivity measurements are based on the principle of nonstationary heat flow. The methods of hot wire measurement, double-hot wire measurement, hot disc measurement, hot strip, and laser flash measurement are widely used for different materials.

Fig. 1.19 The values of thermal conductivity for nitride-bonded silicon carbide materials, measured by hot-wire and laser flash methods



According to ASTM C1113 [95], the hot wire method is an absolute method for direct determination of the thermal conductivity based on the measurement of the temperature increase of a linear heat source/hot wire (cross-wire technique, according to ISO 8894-1 [96]) or at a specific distance from a linear heat source (parallel-wire technique, according to ISO 8894-2).

The laser flash method [97, 98] is often used for measuring the thermal conductivity of structural ceramics. The sample is heated by laser pulse and the temperature increase on the back side of the sample is measured. The thermal conductivity is calculated from Eq. (1.10). This method has no limitations on the temperature and is good for measuring materials with a high thermal conductivity, but it gives values 20–30 % higher than the values given by the hot wire (Table 1.6, Fig. 1.19). Also, it is necessary to take into account that the test samples for measurements according to the laser flash method are small (the thickness of the plate to be tested is about 2 mm, and there may be difficulty in cutting the required sample from the coarse-grained material). The thermal diffusivity and thermal conductivity of carbon materials can be measured by the flash method according to ASTM C714-05 [99].

Figure 1.19 demonstrates the thermal conductivity dependencies for N-SiC side lining, determined by the hot wire [96] and laser flash methods [99, 13, 14]. The difference in the values is easily seen and is within 15–25 %. In [85] it is stressed that for the project designs of the furnaces, the values of thermal conductivity obtained by stationary heat flow methods are preferable to those calculated by dynamic methods. The coefficients of 0.7–0.8 used for the project designs are used for the calculations if the values of the thermal conductivity by hot wire methods are taken. The repeatability is about 15 %, while the reproducibility is 20–25 %.

1.6 Thermal Coefficient of Linear Expansion, Thermal Strains, and Thermal Shock Resistance

1.6.1 Thermal Coefficient of Linear Expansion

The thermal coefficient of linear expansion is the relative increase in the linear dimension of the material as its temperature increases 1° . Usually, the average thermal coefficient of linear expansion is used in practice: It is the relative increase in the linear dimension, divided by the temperature interval at which this increase in dimension took place:

$$\alpha = \Delta L/L_0/(t - t_0) \quad (1.23)$$

where α is the thermal coefficient of linear expansion (dimension: K^{-1}), ΔL is the linear dimension change of a material, having dimension L_0 , after heating from temperature t_0 to temperature t . The thermal coefficient of linear expansion is a tangent of the slope of the graph $\Delta L/L = f(t)$ (Fig. 1.20).

In engineering practice of Al metallurgy, in order to make the design of the device workable at increased temperatures, usually the average thermal coefficient of linear expansion is used. The values of the average thermal coefficient of linear expansion are contained in reference books [100, 101]. The expansion is calculated according to

$$\Delta L = L_0 \cdot \alpha \cdot (t - t_0) \quad (1.24)$$

The expansion of a refractory plate having length 1 m and $\alpha = 5 \times 10^{-6} K^{-1}$ at the temperature increase from 0 to $1,000^\circ C$ will be 5 mm.

In R&D practice, it is useful to use not only the value of the average thermal coefficient of linear expansion, but the dependence of $\Delta L/L = f(t)$ itself. This will give much more information on the processes that take place upon heating of the

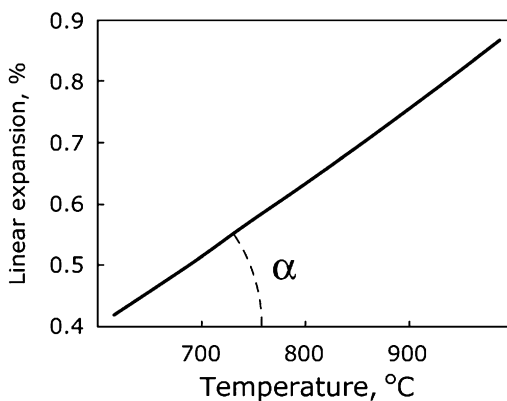


Fig. 1.20 Thermal expansion

Table 1.8 Thermal linear coefficient of expansion for anisotropic crystals [100–102]

	$\times 10^6 \text{ K}^{-1}$	
	Normal to <i>c</i> -axis	Parallel to <i>c</i> -axis
Al ₂ O ₃	8.3	9.0
TiO ₂	6.8	8.3
SiO ₂ (quartz)	14	9
Al ₂ O ₃ ·TiO ₂	−2.6	11.5
3Al ₂ O ₃ ·2SiO ₂	4.5	5.7
ZrSiO ₄	3.7	6.2
CaCO ₃	−6	25
α-SiC	4.3	2.7
β-SiC	2.77	—
Graphite	1	27

material. This is necessary to understand the temperature of the phase transformations or to estimate the sintering process or the protective coatings that won't exfoliate in high-temperature service.

1.6.2 Thermal Expansion of Refractory and Heat Insulation Materials: Elements of Theory

Tables 1.8 and 1.9 and Fig. 1.21 give some reference data on the values of the thermal coefficient of linear expansion for oxides, refractory, and ceramic materials [100–102]. Crystals with a cubic lattice (CaO, MgO) have equal values of linear coefficients of expansion along all axes. The typical linear coefficients of thermal expansion for such materials are $6\text{--}8 \times 10^{-6} \text{ K}^{-1}$ and increase with the temperature up to $10\text{--}15 \times 10^{-6} \text{ K}^{-1}$. Anisotropic crystals with low symmetry have different values of linear coefficients of thermal expansion along different axes, but with a temperature increase, this difference becomes smaller. Materials with strong chemical bonds (silicon carbide, titanium diboride, diamond) have low values of linear coefficients of thermal expansion. However, these materials have high values of Debye characteristic temperature (values of the linear coefficients of thermal expansion grow below the Debye temperature and are almost constant above it).

Pores do not affect the values of linear coefficients of thermal expansion if the continuous media are solid particles. If the material consists of particles that are not bonded together and the continuous media are pores (as in vermiculite-based heat insulation materials), linear coefficients of thermal expansion depend on the structure of pores, the dimension of the particles, and so forth.

Some anisotropic crystals have negative linear coefficients of thermal expansion in one direction, and the volume expansion of such materials is low. The low expansion of cordierite, aluminium titanates, and lithium aluminosilicates is explained by the strong crystal lattice anisotropy. The material made from these substances may have a very high thermal shock resistance. Yet in the process of

Table 1.9 Thermal linear coefficient of expansion for refractory and heat insulation materials ($\times 10^6 \text{ K}^{-1}$) [100–102]

Material	$\times 10^6 \text{ K}^{-1}$ (0–1,000°)
Magnesia	13–15
Silica	11–13
Silica glass	0.5
Zirconia (stabilized)	10
Zircon (ZrSiO_4)	4.2
Chromite	9–11
Mullite	5.5–5.8
Mullite-alumina	7.0–7.5
Alumina	8.0–8.8
Kaolin	4.5–5.5
Fireclay (15 % Al_2O_3)	7–9
Fireclay (30 % Al_2O_3)	4.5–6.0
Moler (diatomaceous)	2–3
Silicon carbide	4.5
Anthracitic graphitic carbon cathode block	2.9–3.5
Graphitized carbon cathode block	2.9–3.0
TiB_2	8.1
Vermiculite	11
Calcium silicate	5.5

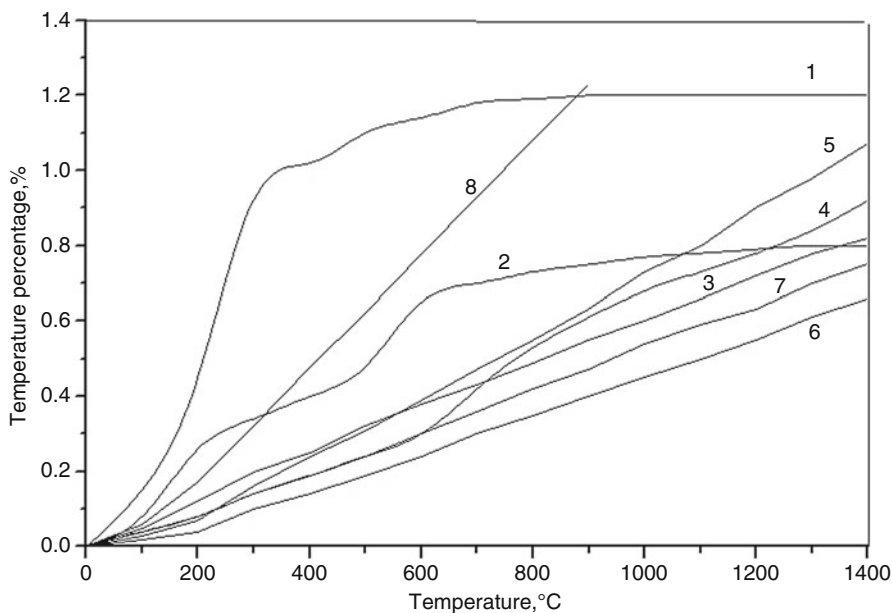


Fig. 1.21 Temperature dependencies of linear expansion according to [100–102]

making strong structural ceramics from these substances, it is necessary to be very careful, because sizable strains may occur between the grains.

For unheated heat insulation and refractory materials, the temperature dependence of thermal expansion is essential. Figure 2.90 in Sect. 2.7 shows the temperature dependencies of linear coefficients of thermal expansion for several vermiculite-based materials. The materials cannot be recommended for use in the high-temperature devices due to high-volume increases upon heating. The exceptions are materials 2 and 3, which have uniform temperature dependencies of linear coefficients of thermal expansion.

1.6.3 Measurement of Linear Coefficients of Thermal Expansion

The measurement of linear coefficients of thermal expansion is made by dilatometers. There are differential and absolute dilatometers. A differential dilatometer measures the difference between the linear thermal expansion of a well-known, high-temperature material and the tested samples. The standard materials are silica glass, polycrystalline alumina, sapphire, and graphite. The temperature is measured in the middle of the sample by a thermocouple. The differential measurement of the linear coefficient of thermal expansion is made according to ASTM E831-14 [103] and ISO 2478:1987 [104]. The measurement of the thermal expansion of heat insulation materials is made according to ISO 2477:1987 [105].

ISO 14420:2005 [106] specifies a method to determine the coefficient of linear thermal expansion of carbonaceous or graphite materials (solid materials) for the production of Al between 20 and 300 °C. It applies to baked anodes and shaped carbon products.

The absolute measurement of thermal expansion provides the ability to fix direct change dimensions of the sample upon heating by optical or photo devices. According to Japanese standard JIS 2207-1976 [107], it is possible to fix the thermal expansion of the samples by cathetometers or comparators (including fixing the photo images). Another method is the interferometry method according to ASTM E 289-99 [108]. It gives an accuracy of $4 \times 10^{-8} \text{ K}^{-1}$, which is one order of magnitude more precise compared to measurement by dilatometer according to ASTM E831-93 [103].

In the Al industry, it is necessary to take into account the thermal expansion of refractories in the bottom part of holding and melting furnaces in the cast house and in anode baking furnaces. The thermal expansion of carbon cathode is relatively small; however, it might be sufficient to take it into account. Yet the sodium expansion of cathode blocks is several times higher compared to the values of thermal expansion. In the design of the reduction cells, the value of the thermal expansion of carbon cathode blocks is only the reference data.

1.6.4 Thermal Strains

If the material is isotropic and can expand without limitations, there are no inner strains in such material upon heating. If something prevents the expansion, the thermal stresses appear in the material. If the constrained refractory block is heated, the stress will be compressive. If the refractory block is cooled down, it will withstand tensile stress because the outer part of the block attempts to shrink (to contract) due to the temperature decrease, but the hot interior part prevents the contraction:

$$\sigma = E\varepsilon = E(t - t_0)\alpha \quad (1.25)$$

where E is the elastic modulus, and ε is the strain.

During calculations, the heat flow from the middle to the center is taken to be very small; in such a case, the thermal stress is

$$\sigma = (E(t - t_0)\alpha)/(1 - \mu) \quad (1.26)$$

where μ is Poisson's ratio.

Such stresses on cooling may occur if the reduction cell is switched off in order to make a dry autopsy. Figures 1.22 and 1.23 show the cracks that appeared upon cooling in cathode carbon blocks (Fig. 1.22) and silicon carbide side lining (Fig. 1.23). Although the thermal conductivity of carbon cathode blocks and silicon carbide is high, their dimensions are big enough as well as their absolute values of shrinkage. The outer parts of the blocks shrink, while the inner parts are still hot enough to prevent them from shrinking, and tensile stresses may have values exceeding the strength. This is normal (when cooling the cell for dry autopsy), and there is no need to pay attention to such cracks upon examination of the materials during dry autopsies.

The thermal expansion of refractory constructions should be calculated and taken into account during design of the furnaces in order to avoid excessive thermal strains and consequent chippings and spallings. The thermal expansion of a 6-m-long roof of a furnace at a temperature of 800–900 °C will be 28–30 mm if the thermal expansion coefficient of the refractory is $5\text{--}6 \times 10^{-6} \text{ K}^{-1}$.

1.6.5 Thermal Shock

According to Eq. (1.26), the rapid cooling of a cathode carbon block from 900 to 100 °C gives thermal stress that is sufficiently higher than the bending strength. The same is true for silicon carbide material.

Thermal stresses in materials can introduce cracks. The critical temperature drop — after which the thermal stresses in the material will equal or exceed the

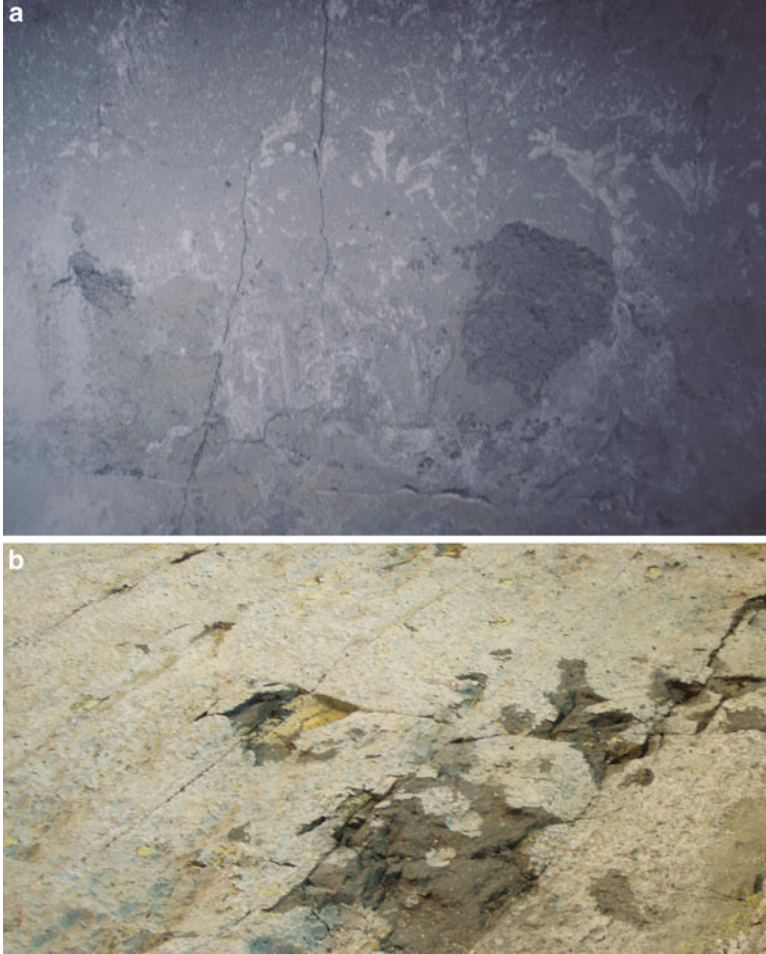


Fig. 1.22 (a, b) Cracks due to cooling in carbon cathode blocks

strength — may be considered the critical quench temperature and may be used for the ranking of the material to withstand the rapid change of the temperature, or thermal shock:

$$\Delta T_{\text{crit}} = \sigma(1 - \mu)/E\alpha \quad (1.27)$$

This equation was introduced by Hasselman [109, 110], who was the first to give the quantitative criteria for thermal shock resistance, or *R* factor.

Thermal shock resistance is the ability of the material to withstand temperature drops and increases, that is, to withstand thermal shock. Thermal shock resistance is one of the most important characteristics of refractory materials. According to rough estimations, approximately one third of refractories are damaged due to

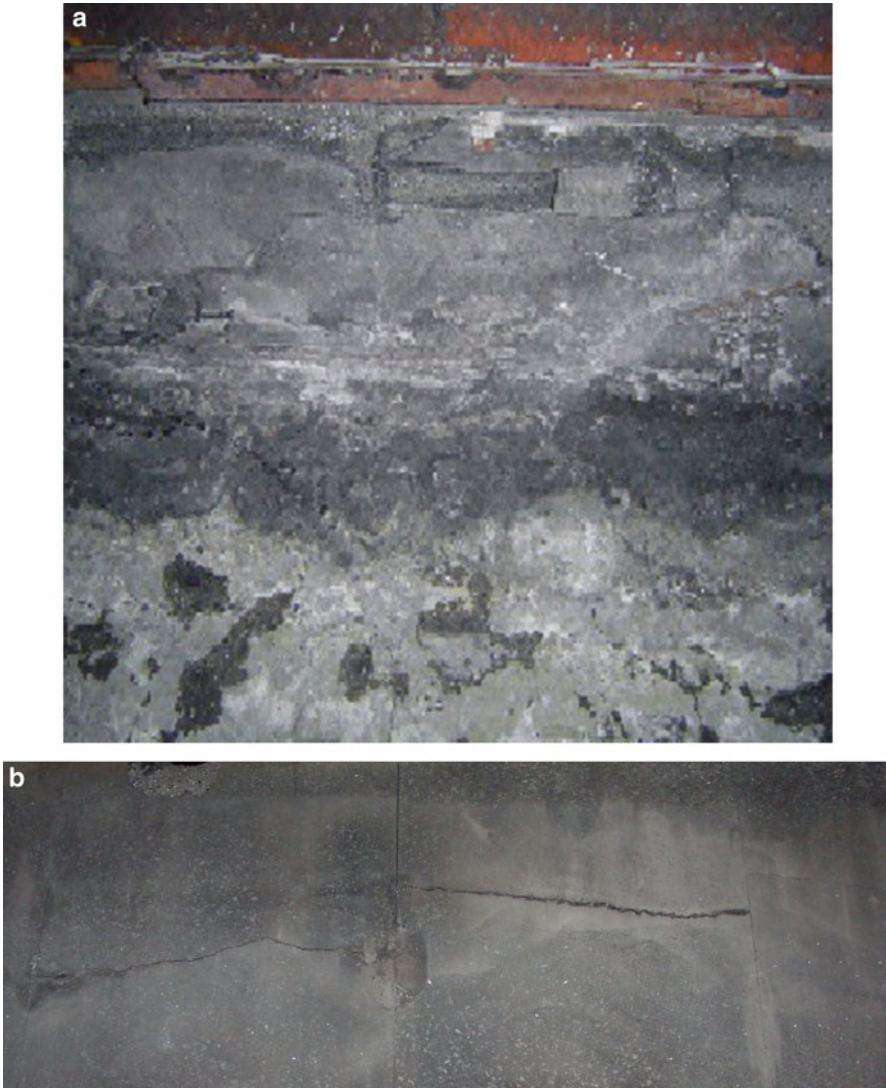


Fig. 1.23 (a, b) Cracks due cooling in SiC lining

poor thermal shock resistance at temperatures sufficiently lower than refractoriness. Thermal stresses may be tensile, compressive, and shear; due to thermal stresses, refractory materials may chip and split off the linings in feeding cavities (holes) and charging doors of the furnaces, doors, and lids. This kind of deterioration was simulated in the old version of the ASTM standard [112]. Another variant of deterioration of the material due to the thermal shock takes place when cracks occur in the material due to the thermal stresses, and the strength of the material diminishes severely (Fig. 1.24). This mechanism (strength deterioration at thermal cycling) is in the new ASTM standard [115].

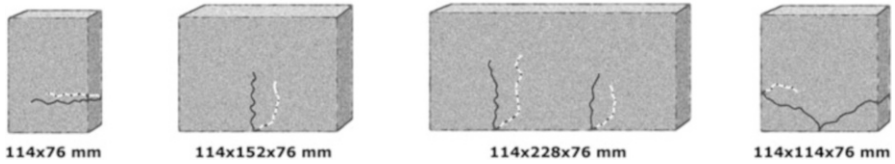


Fig. 1.24 Samples of bricks after thermal shock testing

In the Al industry, thermal shock-resistant materials should be used in loading openings (holes) of coke calcining furnaces, anode baking furnaces, ladles, and runners. The possibility of applying thermal shock resistance factors to cathode carbon blocks is discussed later.

There are three main cases when thermal stresses appear:

- If the refractory material is multiphase and consists of phases with different thermal expansion: Heating and cooling will promote the appearance of microcracking, which leads to a deterioration in strength. In such cases, materials usually do not crack. Porosity diminishes the probability of microcracking.
- If the material has no ability to expand.
- If, during thermal cycling, a big temperature gradient takes place in the material: The expansion of one zone of the material will not coincide with the expansion in another zone, and that may lead to cracking. The higher the value of thermal conductivity and the lower the value of thermal expansion, the better thermal shock resistance such a material will have.

Thermal shock resistance is not a physical property of the material; it depends on many physical characteristics of the material, but also on the shape of the refractory article, its dimensions, the cooling and heating conditions, among other factors. Because of this, there is neither a single criterion or factor, nor is there a single method of its determination. However, people usually use the thermal shock factor (criterion) R , and, additionally, there are many methods of determining the thermal shock, both standard and nonstandard.

The thermal shock factors (criteria) are used in R&D practice and during the R&D of materials design. Methods of estimating the thermal shock resistance are required in order to estimate the ability of the material to be used in thermal devices and in furnaces and for production quality control. There are no strict dependencies between thermal shock resistance factors and the values of the thermal shock resistance; however, sometimes correlations can be made.

1.6.6 Thermal Shock Factors

The classical research on the thermal shock resistance of refractories and brittle solids was made by D. P. H. Hasselman [109, 110]. For samples of a simple shape (thin plate, hollow cylinder, sphere), which are cooled in a liquid medium, the

difference of the temperatures at which the stress reaches the value of strength is calculated in Eq. (1.27); usually, this critical temperature drop ΔT_{crit} is called R . This is the first thermal shock resistance factor. According to this factor, the material should have a high thermal shock resistance if it has a low elastic modulus, a low value of the thermal coefficient of linear expansion, and high strength.

Equation (1.27) has a dimension of degrees and reveals the maximum temperature drop in the samples. The first thermal shock factor R reflects the tendency of the thermal shock resistance from strength, thermal expansion, and elastic modulus, but it is impossible to use this factor in order to make a forecast on the service life of the refractory.

Next, factor R' is more applicable when the cooling conditions are not severe (as it takes place at cooling of the sample at air):

$$R' = R\lambda, \quad (1.28)$$

where λ is the thermal conductivity. This factor has dimension degree \cdot m/s. There are many factors of thermal shock resistance, which are supposed to be applied for specific conditions. The research of Harmuth and Bradt [111] opens the way to new approaches to the estimation of thermal shock resistance. However, currently, refractory materials are compared in terms of thermal shock resistance on the basis of experimental data.

1.6.7 Thermal Shock Resistance Measurements

There are many methods to measure thermal shock resistance. The most convenient are quenching “heated material – water” and “heated material – air.” In order to simulate the specific service conditions of refractories, several other methods of thermal shock testing have been investigated.

Initially, the thermal shock resistance according to ASTM 38-89 [112] was measured by quenching the bricks in water, while the appearance of the cracks and the cracking of the material were fixed. The technique of quenching in water is described in DIN 51068-1 [113]. Quenching in air (compressed air) is described in standard DIN 993-11 [114].

A new standard ASTM C-1171-05 [115] estimates the appearance of cracks in refractory material on thermal cycling by the decrease in strength and change in the sound velocity in the samples.

Usually, the strength is measured after one thermal shock, though it is possible to make several cycles and measure the strength degradation after each cycle. Rectangular bars or rods are tested for bending strength.

According to ASTM C-1171-05 [115], the recommended furnace temperature is 1,200 °C (for specific material and service conditions, it may be changed), the time in the furnace is 10–30 min, and the cooling regime may vary – from quenching in the water to quenching in the air on fireclay or on a metallic surface. The values of

the strength are fixed after each cycle. The degradation of the strength after the first water cycle may be 70–90 %, and the degradation of the strength after the first air cycle may be 20–70 %.

According to the withdrawn standard ASTM C-1100 [115], the determination of the relative resistance of refractories to thermal shock conditions resulting from changing heating and cooling cycles was induced by gas burner and compressed air, while the observation of cracks due to the thermal cycles was visual.

Japanese standard JIS 2657-1995 testing method for spalling of refractory bricks and insulating firebricks. The brick is placed into the furnace at a distance equal to two thirds the brick's length, and after 15 min in the furnace, it is cooled down at room temperature or in water. The appearance of cracks and spalling and chipping is fixed.

The question of a good method for estimating the thermal shock resistance of carbon materials is still open. Due to high thermal conductivity and semibrittle mode of deformation, carbon cathode materials are more thermal shock-resistant compared to refractories. Yet it doesn't mean that there is no problem with thermal shock resistance in carbon cathode materials. We discuss it in Sect. 2.3.

The values of thermal shock cycles “temperature – water” for fireclay and mullite refractories are within 5–7, and up to 30–50 cycles for silicon carbide refractories. The values of thermal shock cycles “temperature – air” for fireclay and mullite refractories are within 25–30 cycles, and up to 50–100 cycles for silicon carbide refractories.

1.7 Corrosion Resistance

Refractories are considered to be corrosion-resistant to melts and gases in furnaces and high-temperature devices. As mentioned in Sect. 1.6, approximately one third of refractories are damaged because of poor thermal shock resistance at temperatures sufficiently lower than refractoriness. Most likely, this ratio for the refractories in the Al industry and the decay of the refractories due to corrosion are even higher.

Corrosion phenomena are very complex, and it is necessary to take into account different processes and mechanisms of degradation and deterioration. Corrosion of refractories at high temperatures may take place by gases, but, of course, it may take place (Fig. 1.25) by liquids (liquid aluminium, liquid electrolyte). In reality, these processes are very difficult to separate. In the investigation of the side-wall corrosion of the side lining in a reduction pot, it is necessary to take into account the erosion of side walls by the particles of alumina and flowing bath. The erosion to be taken into account is degradation of the flue walls in anode baking furnaces, though it is not the main mechanism of degradation.

The corrosion includes the process of chemical corrosion itself, but it is also necessary to take into account the penetration of the aggressive liquid in open permeable pores, the diffusion of the aggressive melt (or constituents of the aggressive melts) into the structure of refractory materials, and others.

The reactions of gases and liquids with refractories may cause stresses, resulting in cracking and spalling, and open the door to the penetration of aggressive liquids.

Of course, it is very useful to know the general theoretical principles of chemical corrosion and apply it to new designs of high-temperature aggregates and furnaces. Knowledge of thermodynamics can give a good estimation of the forecast of future chemical interactions, but it doesn't guarantee the exact forecast of the future service life of refractory in the furnace. Tests for chemical corrosion of refractories are common in the ferrous industry, but they are quite popular in the metallurgy of Al.

In ferrous metallurgy, the corrosion resistance of refractories has been investigated for more than 100 years. The general principles of refractory corrosion approaches have been described by Brosnan, Rigaud, and several other authors [116–118].

Yet the Al industry has several peculiarities. Relatively low temperatures in reduction cells and in the cast house are compensated by the high corrosion ability of molten aluminium and the bath. The main constituent of the bath for the electrolysis process, N_3AlF_6 , has a unique ability to dissolve alumina – the constituent of the major part of the refractories. However, it also dissolves other oxides very quickly. Refractories for Al came from refractories for the ferrous industry.

In the ferrous industry, the characteristic “specific consumption of refractory per tonne of the metal” is now being replaced by the characteristic “refractory consumption in money equivalent.” However, in Al production, neither the first nor the second characteristic has received much attention.

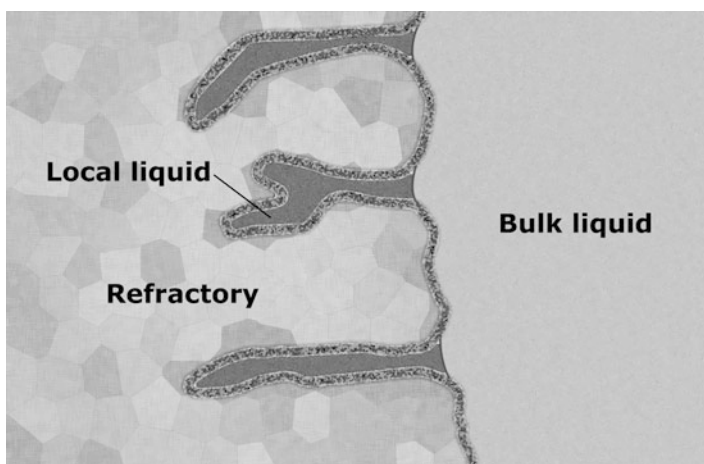


Fig. 1.25 General view of chemical corrosion of refractories by liquid phase

Table 1.10 Volume effects of silicon carbide and silicon nitride oxidation

Reaction	$\Delta V/V, \%$
$\text{SiC} + 2 \text{O}_2 = \text{SiO}_2 + \text{CO}_{2(\text{g})}$	+112
$\text{SiC} + 3 \text{CO}_2 = \text{SiO}_2 + 4 \text{CO}_{(\text{g})}$	+112
$\text{Si}_3\text{N}_4 + 7 \text{O}_2 = 3 \text{SiO}_2 + 4 \text{NO}_{2(\text{g})}$	+80
$\text{Si}_3\text{N}_4 + 6 \text{CO}_2 = 3 \text{SiO}_2 + 6 \text{CO}_{(\text{g})} + 4 \text{N}_{2(\text{g})}$	+80

Table 1.11 Change of porosity and density of N-SiC side lining in the reduction cell during service

No.	Apparent density (initial), g/cm^3	Apparent density (after 180 days), g/cm^3	Open porosity (initial), %	Open porosity (after 180 days), %
1	2.68	2.75	15.8	10.4
2	2.72	2.92	14.7	3.8
3	2.68	2.77	15.6	7.5

1.7.1 Elements of Theory

Corrosion by Gases

Although usually the main corrosion agent of refractories is liquid, corrosion by gases should also be taken into account. Refractories are porous, and so gases may interact with the surface of refractories but may also penetrate in the open permeable pores of refractories and interact with the inner surface of refractories. In practice, the gas corrosion of refractories in an Al foundry is not big. The gas corrosion in an electrolysis shop should be taken into account in side lining. Both carbon and silicon carbide side linings withstand oxidation in the presence of vapors of sodium and fluorine salts, which enhance the oxidation. The flue wall of anode baking furnaces is corroded by gases in two ways. First, the refractory contacting the carbon anodes (and the carbon filling and covering) is in a reduction atmosphere, and some part of the silicon oxide may interact with CO/CO₂ gases and volatile, which increases the porosity and brittle structure. Second, the vapors of sodium compounds (which are always in green anodes because of the utilization of anode butts) may interact with alumina silicate refractories and penetrate the pores of the refractories, changing the chemical composition and decreasing the high-temperature deformation and refractoriness.

Volume effects of the reactions should also be taken into account (not only in gas corrosion of refractories). The reactions of oxidation of nitride-bonded silicon carbide side lining are positive. The positive volume effect of the reaction may play a positive role, diminishing the open porosity (Table 1.11). However, on the other hand, it may cause tensile strains, which may result in either spalling or cracking of the refractory (Fig. 1.26).



Fig. 1.26 Cracking in side lining due to strains, caused by oxidation

Corrosion by Melts

Corrosion of refractories by melts takes place in reduction pots and the cast house. The melt of liquid metal or the bath contacts the surface of the refractory wall, made from bricks or from castables. The chemical interaction between the constituents of the melt and the constituents of the refractory takes place, and all chemical principles of interaction between liquid and solid reactants should be taken into account. The chemical nature of reactants (acid–base) may also be a factor.

If there is no movement of the melt (Fig. 1.25), the thermodynamic equilibrium should sooner or later be established, and phase diagrams may give information on possible interactions between the constituents of refractories and the constituents of the melt. However, as a rule, there are no thermodynamic equilibria in real processing, so the knowledge of the phase diagrams may only show directions.

If the refractory interacts with the melt and the reactants are dissolved in the melt, the slow process of dissolution of refractory should take place. If this process is not accompanied by constant movement of the melt (as it takes place in the reduction cell due to magnetic forces) or by erosion by solid particles in the moving melt, it is very slow and in practice shouldn't be taken into account.

Another process is a penetration of the melt in the refractory's permeable pores. The process of physical penetration without dissolution is governed by capillary forces (surface tension), hydrostatic pressure, viscosity of the melt, and gravity. An illustration of such a process appears in Fig. 1.27, which shows the probability of the penetration of the Al melt in the pores of the carbon block with and without the application of the current.

Carbon is not wetted by liquid Al and is poorly wetted by bath (in the absence of electric current).

The hydrostatic pressure of the bath and the metal in the reduction cell is

$$P_h = \rho_{Al} \cdot g \cdot h_{Al} + \rho_{El} \cdot g \cdot h_{El} \quad (1.29)$$

where P_h is the hydrostatic pressure,

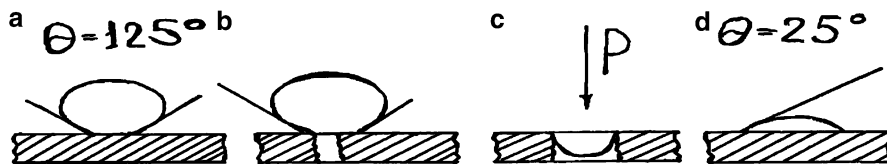


Fig. 1.27 Wetting of carbon by bath without current (a) and with application of (d) current and the infiltration of the bath in the pores, having diameter below 15 μm (b) and above 15 μm (c), while the height of the liquid bath is 0.3 m

ρ_{Al} is the density of Al,
 ρ_{El} is the density of the bath,
 h_{Al} is the height of Al,
 h_{El} is the height of the bath,
 and g is the gravity factor.

At startup, usually the reduction cell is filled with the molten bath; its height is 0.25–0.3 m, and the molten Al is poured in the cell after one day. The density of the bath is about 2,200 kg/m^3 , so the bath pressure is 5.4–6.5 kPa.

The capillary pressure without current (at startup) for different pore radii will be

$r, \mu\text{m}$	1	5	10	15	20	25	30	40
$P \times 10^3 \text{ (Pa)}$	-79.8	-16	-8	-5.3	-4	-3.2	-2.7	-2

The molten bath (cryolite) should not enter the pores of the carbon cathode block without polarization (application of current) due to capillary forces. Yet pores above 15–20 μm will be permeable to molten bath, because the negative capillary pressure in the pores is compensated by the hydrostatic pressure of the bath layer.

The contact wetting angle of carbon by bath at cryolite ratio (CR) is 125° [120] without current and diminishes to 20° at cathode density 0.8 A/sm^2 , and then the capillary pressure will be

$r, \mu\text{m}$	1	5	10	15	20	25	30	40
$P \times 10^3, \text{ (Pa)}$	131.6	26.3	13.2	8.8	6.6	5.3	4.4	3.3

If the pores are small and uniform in size and there is no interaction between the refractory and the melt, it might be possible to make a refractory, nonpermeable by the melt.

For the physical penetration (without chemical interaction), the rate of penetration dl/dt depends on the pore radius r , surface tension of the melt γ , and viscosity of the melt η :

$$dl/dt = r\gamma \cos \theta / 4\eta l \quad (1.30)$$

where $\cos \theta$ is the wetting angle.

This expression is valid only for a constant temperature, because the surface tension, the wetting angle, and the viscosity are functions of the temperature. In



Fig. 1.28 Carbon side lining in “out-of-service” reduction cell

reality, a constant temperature in the furnace wall is never achieved due to the temperature gradients. Also, the chemical interaction between the melt and the constituents of the refractory usually takes place, and the viscosity changes. Although in reality it may not be achieved, this principle suggests that the pores in the refractory should be small and uniform.

While discussing the pore size dimensions in a refractory, it is necessary to mention the surface tension of the melt. The penetration of the melt in the refractory depends not only on the pore radii, but also on the surface tension of the melt and the contact angle of wetting. Some time ago in the ferrous metallurgy it was considered, the critical pore diameter of the refractory for the pig iron melt is 30 μm , while the critical pore diameter of the refractory for the steel is 5–10 μm . The melt of Al has extra-low viscosity and a low contact angle of wetting, so it can penetrate even pores 1 μm in diameter. The same may be said about the molten electrolyte.

Upon moving along the pores in the depth of the refractory, due to interactions with refractory the melt changes the composition and its viscosity may increase. This may lead to self-stoppage of the penetration of the melt in the depth of the refractory. On the other hand, the melt may dissolve the contacts between the grains, and the grain may flow out of the refractory wall in the melt. In practice, this takes place in the side lining of the reduction cell on the border of the molten bath and the air. It is quite common in the carbon side lining (Fig. 1.28) but may take place for silicon carbide lining as well.

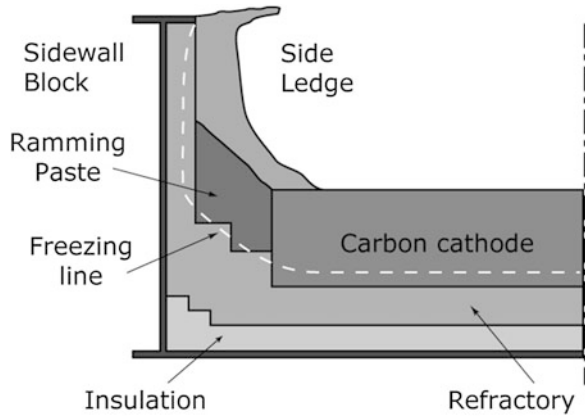
Aluminium is a rather reactive metal, and it can react with oxygen at temperatures of 700–800 °C (which are common for an Al foundry) to form alumina. In the melting and holding furnaces of an Al foundry, an atypical process takes place in ferrous metallurgy: oxidation of Al melt on the triple border “refractory–melt–air.” Oxidation takes place with the positive volume effect, and the resulting alumina takes more space, so the thickness of the refractory wall increases (Fig. 1.29).

Another facet to protection from chemical corrosion is the question of the temperature gradients in the walls and in the bottom of high-temperature metallurgical aggregate in connection with the melt’s freezing point. This is discussed in more detail in the chapters devoted to the reduction pots and to the furnaces of the foundry. Yet here we shall discuss the general principle of protection from corrosion by heat balance in the walls.

Fig. 1.29 Corrosion of the refractory by Al melt at the bellyband of the holding furnace



Fig. 1.30 Cross section of the reduction cell with freezing line of electrolyte



The temperature on the border of the melt and refractory is considered to be close to the temperature of the melt. The temperature on the outer side of refractory wall and the shell should be close to ambient temperature near the furnace. Different combinations of dense refractories and porous and fibrous heat insulation materials help to achieve the required result.

In the classical design of reduction cells, it is recommended that the freezing point of electrolyte should be within the level of carbon cathode blocks – near the lower surface (Fig. 1.30). This should protect the refractory barrier layer of the reduction cell from interaction with molten electrolyte.

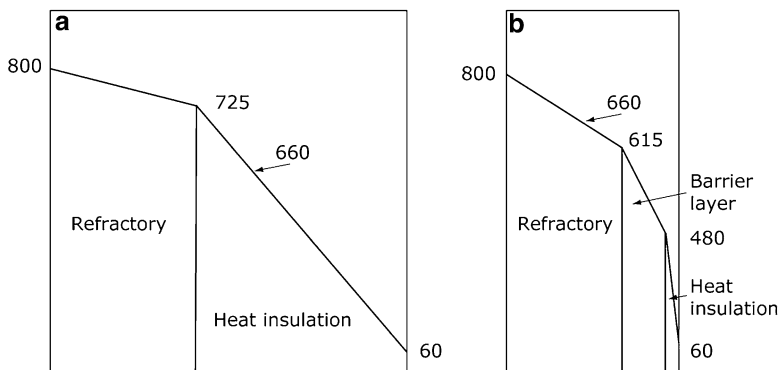


Fig. 1.31 Temperature gradients in the side lining of Al holding furnace

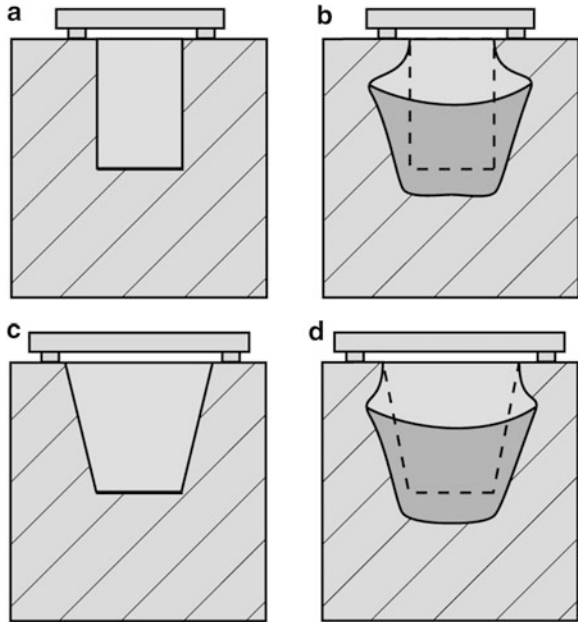
Figure 1.31 contains two variants of heat insulation of the holding furnace side wall. Both variants give the required result – a temperature of 30–40 °C on the outer side of the wall in the beginning of the service. However, the location of the freezing point in these variants of the lining has different positions – in variant “a,” it is in the insulation layer, while in variant “b,” it is in the “working” layer of dense refractory.

In lining construction “a,” nothing will prevent molten Al from entering the permeable pores, cracks, and shafts between the bricks. In lining construction “b,” the melt will stop in the working layer of the dense refractory because of the solidification. In both cases, the path of the Al melt in the lining is a conductor for extra heat: The thermal conductivity of the infiltrated lining will increase. However, this increase in the thermal conductivity in variant “b” will be relatively small. With good construction, the linings of holding furnaces should work for many years, and the temperature on the shell should be low.

In the case of variant “a,” the melt reaches the layer of the thermal insulation and the thermal balance will change considerably. The increase in the thermal conductivity of the heat insulation layer relatively soon will shift the location of the freezing point more closely to the outer side of the lining. This will give an extra increase in thermal conductivity of the heat insulation layer, and so on the process will go.

This is an illustration of the general principles to decrease the corrosion by a correctly chosen thermal balance of the lining. These issues are even more important in the design of reduction cells, where the thermal balance helps to have a frozen side ledge on the side lining, protecting the refractory from the chemical interaction by reactive melt. The issues of the thermal balance in connection with the freezing point of the liquid bath in the cathode blocks, formation of the side ledge, overheating of the cell, and the energy savings are discussed in Chap. 2.

Fig. 1.32 Scheme of cup corrosion test for bricks and concretes (a, b) and dry barrier mixtures (c, d)



1.7.2 Tests

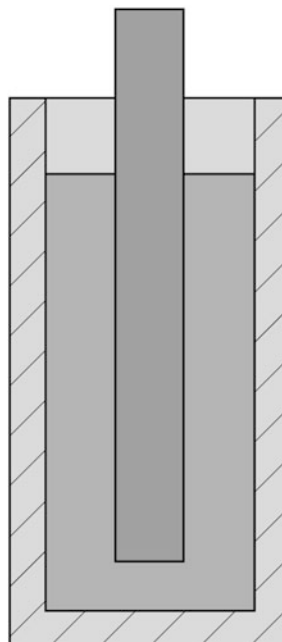
Laboratory corrosion testing has been in existence for many years, and yet there is no uniformity in these attempts to evaluate the corrosion resistance of specific refractory for specific conditions. Roughly, corrosion tests may be divided into “static” and “dynamic” tests. The term “static” usually means that the corrosive liquid is stationary, it doesn’t move against the tested refractory, and the system “corrosive liquid–refractory” will tend to reach equilibrium. During a “dynamic” test, the corrosive liquid moves against the refractory surface and the thermodynamic and chemical equilibria won’t be reached.

Another division is the cup of immersion testing. With the cup test, the conditions are stationary. If the tested refractory rods are immersed in the corrosive melt, the conditions are close to stationary. If the immersed tested rods are rotating in the corrosive melt (or probably are moving up and down), the conditions are dynamic.

Finally, the aim of the applied research on corrosion testing is to find suitable and relatively inexpensive and simple procedures to evaluate whether a refractory will have a long service life in a specific metallurgical process. In real metallurgical processes, too many factors affect the corrosion; that’s the reason for the lack of uniformity in corrosion testing. The same may be said about standardization: Only a few corrosion tests are standard.

For the cup test, usually a hole about 35–58 mm in diameter and about 40 mm deep is drilled in a brick (Fig. 1.32a, b), and either the corrosive liquid is poured in the hole or the corrosive agent is placed in this hole in a dry state before testing. The

Fig. 1.33 Scheme of rod corrosion test



brick with the corrosive agent in a “cup” and with a lid above is placed in a furnace for 8–24 h. The hole in a castable may be introduced without drilling, and for dry barrier mixtures, a cup with sloped sides is formed. After cooling, the sample is cut diagonally and the infiltrated area is measured in square centimeters. The standards ASTM C768-99 [120] and DIN 51069-2-1972 [121] were withdrawn, but the method of testing fireclay brick for corrosion resistance to cryolite is in ISO 20292 [121].

The immersed tests are usually produced in big crucibles, filled with at least one corrosive agent. The dimension of the tested rods (usually rectangular bars) is 25 mm × 25 mm × 100 mm or 10 mm × 10 mm × 150 mm (Fig. 1.33). The bars may rotate or be dipped and pulled out or may be tested without rotation. The corrosion resistance tests for silicon carbide side lining materials are discussed in detail in Chap. 2. The corrosion resistance tests for Al melt are discussed in Chap. 3. The tests for sodium swelling of carbon materials are discussed in Chap. 2, devoted to the lining materials for electrolysis, rather than in the chapter devoted to corrosion resistance.

Depending on the type of corrosion process, the corrosion resistance may be measured in the increase/decrease of the weight of the tested materials or in the increase/decrease of the volume. Usually, static, dynamic, cup, and immersion tests are isothermal. Microscopic investigation is highly recommended after all corrosion tests.

References

1. ISO 8656-1-1988. Refractory products – sampling of raw materials and unshaped products.
2. ISO 5022-79. Shaped refractory products – sampling and acceptance testing.
3. ISO 1927-1:2012. Monolithic (unshaped) refractory products – Part 1: Introduction and classification.
4. DIN 51061-1973 (2,3). Testing of ceramic raw and finished materials; sampling, refractory bricks.
5. ASTM C-155-97 (2002). Standard classification of insulating firebrick.
6. ISO 2245-1990. Shaped insulating refractory products: Classification.
7. DIN 51061–3. Testing of ceramic raw and finished materials; sampling, refractory bricks.
8. ISO 1927–2:2012. Monolithic (unshaped) refractory products – Part 2: Sampling for testing.
9. ASTM D6354 – 12. Standard guide for sampling plan and core sampling of carbon cathode blocks used in aluminum production.
10. ISO 8007:1985. Carbonaceous materials used in the production of aluminium – sampling from cathodic blocks and prebaked anodes – General.
11. Sorlie M, Oye H. Cathodes in aluminium electrolysis. 3rd ed. Aluminium, Verlag; 2010.
12. ISO 2477-1987. Shaped insulating refractory products – determination of permanent change in dimensions on heating.
13. Total Quality Management. QI story: tools and techniques. A guidebook for teams; 1991, 147 p.
14. Statistical Process Control (SPC). Reference Manual, 1995, Chrysler Corporation, Ford Motor Company, and General Motors Corporation.
15. ISO 7870–2:2013. Control charts – Part 2: Shewhart control charts

Density, Porosity and Related Characteristics: The Types of Porosity

16. ASTM C-20-00. Standard test method for apparent porosity, water absorption, apparent specific gravity, and bulk density of burned refractory brick and shapes by boiling water.
17. ISO 5016:1986. Shaped insulating refractory products – determination of bulk density and true porosity.
18. ASTM C 830–00. Standard test method for apparent porosity, liquid absorption, apparent specific gravity, and bulk density of refractory shapes by vacuum pressure.
19. ASTM C914-95 (1999). Standard test method for bulk density and volume of solid refractories by wax immersion. ISO 5018:1983 Refractory materials – determination of true density.
20. ASTM C 135-96. Standard test method for true specific gravity of refractory materials by water immersion.
21. ISO 9088:1997. Carbonaceous materials used for the production of aluminium – cathode blocks and prebaked anodes – determination of the density in xylene by a pycnometric method.
22. BS ISO 21687:2007. Carbonaceous materials used in the production of aluminium. determination of density by gas pycnometry (volumetric) using helium as the analysis gas. Solid materials.
23. ASTM C-134-99. Standard test methods for size, dimensional measurements, and bulk density of refractory brick and insulating firebrick.
24. ISO 5016:1997. Shaped insulating refractory products – determination of bulk density and true porosity.

25. ISO 5017:2013–01. (E). Dense shaped refractory products – determination of bulk density, apparent porosity and true porosity.
26. DIN EN 993–1. Methods of tests for dense shaped refractory products – determination of bulk density, apparent porosity and true porosity.
27. ISO 12985–1:2000. Carbonaceous materials used in the production of aluminium – baked anodes and cathode blocks – Part 1: determination of apparent density using a dimensions method.
28. ISO 12985–2:2000. Carbonaceous materials used in the production of aluminium – baked anodes and cathode blocks – Part 2: determination of apparent density and of open porosity using a hydrostatic method.
29. DIN EN 993-2/A1. EN-Methods of test for dense shaped refractory products – Part 2: determination of true density.
30. ASTM C-577-99. Standard test method for the permeability of refractories.
31. ISO 8841:1991. Dense shaped refractory products – determination of permeability to gas.
32. Strelov KK. The structure and the properties of refractories (in Russian). Moscow: Metallurgia; 1982. 207 p.
33. Strelov KK, Kashev ID. Theoretical aspects of refractories materials technology (in - Russian). Moscow: Metallurgy; 1996. 608 p.
34. ASTM D4284-12. Standard test method for determining pore volume distribution of catalysts and catalyst carriers by mercury intrusion porosimetry
35. Andreasen AM, Anderesen J. Ueber die Beziehung zwischen Kornabstufung und Zwischenraum in Produkten aus losen Koernern (mit einigen Experimenten). Kolloid Zeitschrift. 1930;50:S. 217–28.
36. Dinger DR, Funk JE. Particle size control for high-solids castable refractories. Am Ceram Soc Bull. 1994;73(N10):66–9.

Mechanical Characteristics

37. ISO 10059–1:1992. Dense, shaped refractory products – determination of cold compressive strength – Part 1: referee test without packing. ISO 10059–2:2003. Dense, shaped refractory products – determination of cold compressive strength – Part 2: test with packing.
38. ASTM C133-97. Standard test methods for cold crushing strength and modulus of rupture of refractories.
39. ISO 18515:2007. Carbonaceous materials for the production of aluminium – cathode blocks and baked anodes – determination of compressive strength.
40. ASTM C 695-91(2010). Standard test method for compressive strength of carbon and graphite; 1981.
41. ISO 8895:2004. Shaped insulating refractory products – determination of cold crushing strength.
42. DIN EN 1094–5. Insulating refractory products – Part 5: determination of cold crushing strength of shaped products.
43. ASTM C 165. Standard test method for measuring compressive properties of thermal insulations.
44. ASTM C-1273-95a. Standard test method for tensile strength of monolithic advanced ceramics at ambient temperature, 2000.
45. ISO 5014–86. Refractory products – determination of modulus of rupture at ambient temperature.
46. DIN EN 993–6. EN-Methods of test for dense shaped refractory products – determination of modulus of rupture at ambient temperature.

47. ISO/DIS 12986–1,2. Carbonaceous materials used in the production of aluminium – prebaked anodes and cathode blocks – Part 1: determination of bending/shear strength by a three-point method.
48. ISO 12986–2:2009. Carbonaceous materials used in the production of aluminium – prebaked anodes and cathode blocks – Part 2: determination of flexural strength by the four-point method.
49. ASTM C1025. Test method for modulus of rupture in bending of electrode graphite.
50. ASTM C651. Test method for flexural strength of manufactured carbon and graphite articles using four-point loading at room temperature.
51. Hasselman DPH. Relation between the effects of porosity on strength and Young's modulus of elasticity of polycrystalline materials. *J Am Ceram Soc.* 1963;46:564–5.
52. Ryshevitch E. Compression strength of porous sintered alumina and Zirconia. *J Am Ceram Soc.* 1953;36:65–8.
53. ASTM C 1198–01. Standard test method for dynamic Young's modulus, shear modulus and Poisson's ratio for advanced ceramics by sonic resonance
54. ISO 3312:1987. Sintered metal materials and hard metals – determination of Young modulus.
55. ASTM C747. Test method for moduli of elasticity and fundamental frequencies of carbon and graphite materials by sonic resonance.
56. ASTM C 704–01. Standard test method for abrasion resistance of refractory materials at room temperature.
57. JIS R 1613–1993. Ball-on-disk test method for abrasion resistance.
58. ASTM G99-04. Standard test method for wear testing with a pin-on-disk apparatus.
59. ASTM C1327–08. Standard test method for Vickers indentation hardness of advanced ceramics.
60. ASTM C1326–13. Standard test method for Knoop indentation hardness of advanced ceramics.
61. ASTM C 1421-01a. Standard test methods for determination of fracture toughness of advanced ceramics at ambient temperature.
62. Evans AG, Charles EA. Fracture toughness determination by indentation. *J Am Ceram Soc.* 1979;62:428–62.
63. Chantikul P, Lawn BR, Marshall DB. A critical evaluation of indentation techniques for measuring fracture toughness. *J Am Ceram Soc.* 1981;64:539–43.
64. ASTM C 1239–00. Standard practice for reporting uniaxial strength data and estimating Weibull distribution parameters for advanced ceramics.
65. *Refractories Handbook*. The technical association of refractories of Japan. 1988. 578 p.
66. ASTM C1421–10. Standard test methods for determination of fracture toughness of advanced ceramics at ambient temperature.
67. Panov E, Diachenko S, Danilenko S. Heat processes in reduction cells and holding furnaces of aluminium production (in Russian). Moscow: Ruda i Metally; 1998. 256 p.
68. Allard B, Roughby D, Fantozzi G, Dumas D, Lacroix P. Fracture behavior of carbon materials. *Carbon.* 1991;29(3):457–98.
69. Sato S, Sato K, Inamura Y. A rationalization of the graphitizing heat treatment process of carbon. *Carbon.* 1975;13:309–16.
70. Allard B. et al. Fracture behavior of carbon materials for aluminium smelters. *Light Met.* 1991;120:749–758
71. Harmuth H, Bradt RC. Investigation of refractories brittleness by fracture mechanical and Fractographic methods. *Interceram Ref Refractories Man.* 2010.

Thermo Mechanical Properties

72. DIN 51063. Testing of ceramic raw and finished materials. Pyrometric Seger cone, Part 1 determination of the bending point (pyrometric cone equivalent), Part 2 testing of Seger cones. ISO 1146:1988 Pyrometric reference cones for laboratory use – specification.
73. ASTM 24–01. Standard test method for Pyrometric cone equivalent (PCE) of fireclay and high alumina refractory materials.
74. ISO 1146–1988. Pyrometric reference cones for laboratory use.
75. ASTM C-583-00. Standard test method for modulus of rupture of refractory materials at elevated temperatures.
76. ISO 5013–85. Refractory products – determination of rupture at elevated temperatures.
77. ASTM C113-14. Standard test method for reheat change of refractory brick.
78. ISO 1893-1989. Refractory products. Determination of refractoriness-under-load (differential – with rising temperature).
79. DIN 51064. Testing of ceramic raw and semi-finished materials; determination of fire resistance of refractory bricks under load.
80. DIN EN 993-8. Methods of testing dense shaped refractory products – Part 8: Determination of refractoriness-under-load.
81. ASTM C16-96. Standard test method for load testing refractory brick at high temperatures.
82. ISO 3187 1989. Refractory products – determination of creep in compression.
83. ISO 2477-1987. Shaped insulating refractory products – determination of permanent change in dimensions on heating.
84. ASTM 832-00. Standard test method of measuring the thermal expansion and creep of refractories under load.

Thermal Conductivity, Heat Capacity, and Temperature Conductivity (Heat Diffusivity)

85. Routschka G, Wuthnow H. Handbook of refractory materials: design, properties, testings. Essen: Vulkan Verlag; 2012. 355 p.
86. Strelou KK. Structure and properties of refractories (in Russian). Metallurgia; Moscow; 1982. 207 p.
87. Litovsky EY, Puchkelevitch NA. Thermo physical properties of materials (in Russian). Moscow: Metallurgia; 1982. 150 p.
88. Andresen FB, Mikkelsen J. Thermal conductivity measurements of cathode insulation materials. Light Met. 2000:429–437.
89. ASTM C201-93 (1998). Standard test method for thermal conductivity of refractories.
90. ASTM C202-93(2013). Standard test method for thermal conductivity of refractory brick.
91. ASTM C182-88 (1998). Standard test method for thermal conductivity of insulating firebrick.
92. ASTM C417-93 (1998). Standard test method for thermal conductivity of unfired monolithic refractories.
93. ASTM C767-93(2013). Standard test method for thermal conductivity of carbon refractories.
94. ISO 12987:2004. Carbonaceous materials for the production of aluminium – anodes, cathodes blocks, sidewall blocks and baked ramming pastes – determination of the thermal conductivity using a comparative method.
95. ASTM C1113/C1113M-09(2013). Standard test method for thermal conductivity of refractories by hot wire (platinum resistance thermometer technique).
96. ISO 8894-1:2 (1990). Refractory materials – determination of thermal conductivity – Part 1 (cross-array), Part 2 (parallel).

97. DIN EN 821-2. Monolithic ceramics – thermo-physical properties – Part 2: Determination of thermal diffusivity by the laser flash (or heat pulse) method.
98. ISO 18755:2005. Fine ceramics (advanced ceramics, advanced technical ceramics) – determination of thermal diffusivity of monolithic ceramics by laser flash method.
99. ASTM C714-05(2010). Standard test method for thermal diffusivity of carbon and graphite by thermal pulse method.

The Thermal Coefficient of the Linear Expansion, Thermal Strains and Thermal Shock Resistance

100. Routschka G, Wuthnow H. Handbook of refractory materials: design, properties, testings. Essen: Vulkan Verlag; 2012. 355 p.
101. Refractories Handbook. The technical association of refractories of Japan. 1998. 587 p.
102. Strelov KK. Structure and properties of refractories (in Russian). Metallurgia: Moscow; 1982. 207 p.
103. ASTM E831-14. Standard test method for linear thermal expansion of solid materials by thermomechanical analysis.
104. ISO 2478:1987. Dense shaped refractory products – determination of permanent change in dimensions on heating.
105. ISO 2477:1987. Shaped insulating refractory products – Determination of permanent change in dimensions on heating.
106. ISO 14420:2005. Carbonaceous products for the production of aluminium – baked anodes and shaped carbon products – determination of the coefficient of linear thermal expansion.
107. JIS 2207-1976. Test method for the rate of linear change of refractory brick on heating.
108. ASTM E 289-99. Standard test method for linear thermal expansion of rigid solids with interferometry.
109. Hasselman DPH. Unified theory of thermal shock fracture initiation and crack propagation in brittle ceramics. J Am Ceram Soc. 1969;52:600–4.
110. Hasselman DPH. Thermal stress resistance parameters for brittle refractory ceramics. A compendium. Am Ceram Soc Bull. 1970;49:1033–7.
111. Harmuth H, Bradt RC. Investigation of refractory brittleness by fracture mechanical and fractographic methods. Interceram Ref Refractories Man. 2010.
112. ASTM 38-89. Standard test method for the thermal shock resistance of refractory brick (withdrawn).
113. DIN 51068-1-1976. Testing of ceramic materials; determination of resistance to thermal shock; water quenching method for refractory bricks.
114. DIN EN 993-11. Methods of test for dense shaped refractory products – Part 11: Determination of resistance to thermal shock.
115. ASTM C1171-05(2011). Standard test method for quantitatively measuring the effect of thermal shock and thermal cycling on refractories.

Corrosion Resistance

116. Brosnan D. Corrosion of refractories. In: Charles S, editor. Refractories handbook. New York: CRC Press; 2004. p. 39–77.
117. Rigaud M. Corrosion of refractories and ceramics. In: Winson R, editor. Uhlig's corrosion handbook. New York: Wiley; 2011.

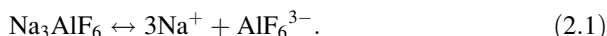
118. Lee WE, Zhang S. Melt corrosion of oxide and oxide–carbon refractories. *Int Mat Rev.* 1999;44(3):77–104.
119. ASTM C768-99. Withdrawn standard; ASTM C768-99 standard practice for drip slag testing refractory materials at high temperature (withdrawn 2004).
120. DIN 51069-2-1972. Testing of ceramic materials; comparing test of the resistance of refractory bricks to the attack of solid and liquid materials at high temperature, crucible method (withdrawn).
121. ISO 20292:2009. Materials for the production of primary aluminium – dense refractory bricks – determination of cryolite resistance.

Chapter 2

Refractories and Carbon Cathode Materials for Aluminium Reduction Cells

2.1 Reduction of Aluminium. Elements of Reduction Technology. The Main Controlled Parameters of Reduction (Electrolysis). Elements of Energy Balance and Heat Balance of Reduction Cell. Reduction Shop. Types of Reduction Cells

During the industrial reduction process, molten cryolite dissociates:



The AlF_6^{3-} ion is also partly dissociated:



Alumina dissolves in cryolite and dissociates:



or



and the ions of aluminium discharge on the cathode:



The oxygen ions discharge on the carbon anode and interact with carbon:



Finally, the composition of anode gases is 20–40 % CO and 60–80 % CO₂.

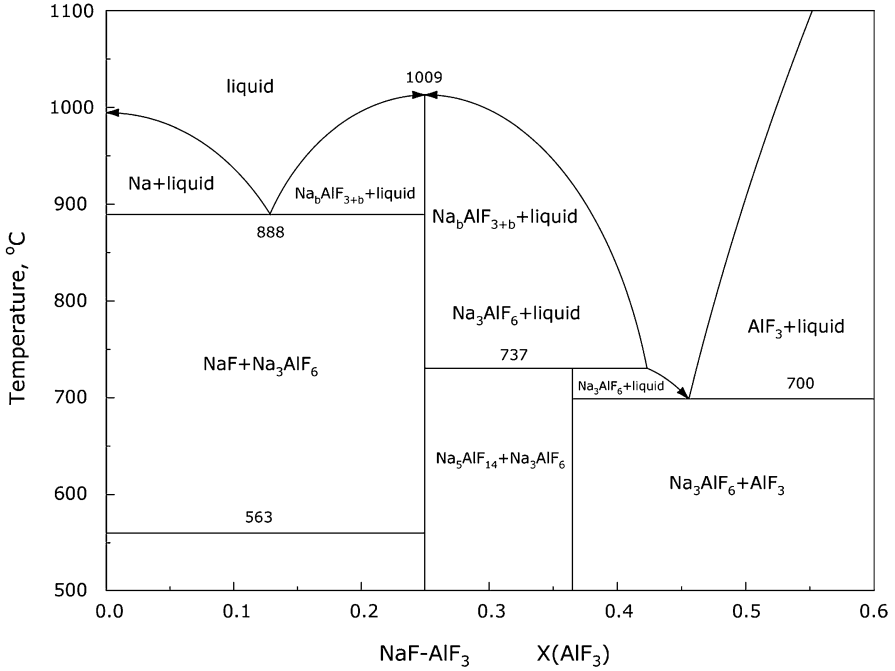
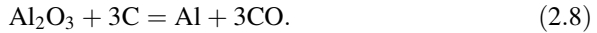
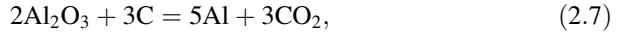


Fig. 2.1 NaF-AlF₃ diagram [1–4]

In a simplified view, all cathode and anode reactions may be shown as



The melts of aluminium and of electrolyte are nonmiscible liquids. The density of liquid Al is 2.3 g/sm³, while the density of liquid bath is kept around 2.1 g/sm³, so in a reduction cell, the melt of electrolyte is above the molten Al. Actually, the surface of molten Al on the bottom of a reduction pot appears to be the cathode in the reduction process. Usually, the depth of molten Al is 15–40 sm, and the depth of electrolyte is 15–25 sm.

In an industrial process, the electrolyte (the bath) has three main functions:

1. It conducts the electrical current between the anode and the cathode.
2. It dissolves alumina.
3. It gives a physical barrier between the Al forming on the cathode and the carbon dioxide/oxide that appears on the anode.

In a Hall–Heroult process, the electrolyte is cryolite, Na₃AlF₆ (3NaF · AlF₃), with dissolved alumina and additives (up to 16–18 %) of aluminium fluorite, calcium fluorite, magnesium fluorite, and sometimes other fluorites [1–4]. The melting point of pure cryolite is 1,010 °C (Fig. 2.1), but the temperature of electrolyte may be

reduced either by adding fluorides or by varying the ratio between sodium fluoride (NaF) to aluminium fluoride (AlF₃). In pure cryolite, Na₃AlF₆ (3NaF · AlF₃), the cryolite ratio (CR) is 3. Both variants—additives or variation of the cryolite ratio—decrease the melting point of the bath to 930–960 °C. The temperature of the process is 950–965 °C, and the freezing point is about 950 °C.

Different cryolite ratios and additives in different ways influence the basic technical and economic characteristics of the reduction process, improving one characteristic and decreasing another. Currently, it is impossible to describe the optimal composition of electrolyte, and the situation with smelters depends on various local circumstances, including raw materials, energy costs, and design of cells, among other factors.

The anodes are in the molten electrolyte; the interpolar space between the anode and cathode is 4–6 sm. Normally, the depth of the level of Al at the bottom of the reduction cell (after tapping) is 25–35 sm, and the depth of the level of electrolyte is 15–25 sm. Above the melt of electrolyte on the border with air is crusted frozen electrolyte, covered with alumina. Some frozen electrolyte forms the ledge on the side lining.

The tapping of Al is done once a day (we discuss the lining of the ladle in Chap. 3); the amount of Al on the bottom of the cell should be sufficient for the normal operation of the cell. The ladle with Al, tapped from the cells, is moved to the cast house. Usually, the dross is taken from the surface of liquid Al before weighing and pouring in the holding furnace for making alloys. An important issue for the refractory specialist is that the level of molten Al (and consequently the level of the electrolyte above the level of molten Al) in the reduction cell varies throughout the day—after tapping, it is low, and it slowly increases throughout the day.

The amount of Al during the reduction process is calculated according to Faraday's law:

$$M = 0.3354It, \quad (2.9)$$

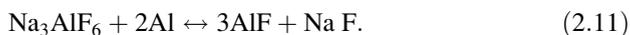
where M is the amount of Al, 0.3354 is the electrochemical coefficient for Al (g/A-h), I is the current (A), and t is the time.

In practice, the amount of Al is lower. There are reverse reactions (which also take place and take energy), and there are current leakages in the cell itself and in the bus bar system and shell.

Here are some examples of “reversed” reactions, which result in the appearance of unstable transient nonstoichiometric substances:



or



Aluminium sub-fluoride (AlF_2) is not stable and transforms into aluminium fluoride and highly dispersed aluminium, which easily oxidizes:



Aluminium subfluoride may also oxidize by oxygen:



and by carbon dioxide under anodes:



In the course of these reactions, the received aluminium may transform back into alumina. Also, reverse electrochemical reactions consume energy.

Current efficiency is a productivity of the cell.

The reduction process is controlled according to several parameters:

- energy consumption: 13,000–14,000 kW per ton of Al;
- alumina consumption: about 1,920 kg per ton of Al;
- carbon consumption: up to 425–550 kg per ton of Al [the theoretical consumption according to reaction (2.7) is 338 kg per ton and 667 kg per ton according to reaction (2.8)];
- current efficiency: up to 95 % for reduction cells with baked anodes and up to 90 % for reduction cells with a Soderberg anode.

As a rule, the parameters on the cells with 60 months' service and longer are lower.

One more very important parameter that is not directly included in the parameters of reduction is the service life of reduction cells.

The best-known parameters as of this publication are

- energy consumption: around 12,000–13,200 kW per ton of Al;
- current efficiency: up to 96 %.

Currently, the tendency is to decrease the current in order to reach lower energy consumption.

This book is addressed to refractory producers as well as to specialists in cell lining and design and in the reduction process. Carbon consumption and alumina consumption in a reduction are in no way influenced by the quality of refractory materials or design of the cells. The quality of refractory materials and the design of the cells influence the service life directly. If we are speaking about energy consumption and current efficiency, there is no direct link between the quality of refractory and the carbon cathode materials on current efficiency, but indirectly the design of cells (which takes into account the materials) may have some influence on energy consumption.

In terms of each part of the reduction cell and the materials for these parts, we will comment on possible links between material quality and design on energy consumption, current efficiency, and service life.

Also, we list some instabilities of the reduction technology that usually are not connected with the quality of the cathode materials but may seriously influence the service life of the cell:

- poor quality of alumina, which leads to the formation of sludge on the cathode surface;
- poor quality of anodes (due to poor quality of coke or pitch or deviations in anode technology), which may lead to overheating of the cell;
- overheating of the electrolyte;
- freezing of electrolyte as a sludge, operating cells with insufficient electrolyte; and others.

The cathode current density is 0.7–1,05 A/sm². The voltage in the reduction pot is 4.1–4.5 V [25], and the tendency is to decrease the voltage to 3.7–4 V.

The reduction pots may be divided into small, with current 100–200 kA; medium, with current 200–300 kA; and super powerful, with current 300–500 kA. The reduction shops are long buildings, usually with a width of about 25–28 m, while the length may be up to 1.6 km. Usually, reduction pots with cells below 200 kA are placed lengthwise in two rows, while cells of 200 kA or higher are normally placed in one row. Between the cells should be sufficient space to move industrial vehicles.

The reduction cell (electrolytic cell, reduction pot) is a high-temperature device to produce Al by electrolysis (reduction). It is a shallow bath tank (depth 0.6–0.8 m), filled with melts of Al and electrolyte (bath). The length of the reduction cell is 10–15 m, and the width is 3–5 m.

The reduction cell is lined with carbon cathode bottom blocks and side lining. The voltage on cathode blocks is supplied by steel collector bars and a system of bus bars. Below the cathode blocks are the refractory layer and the heat insulation layer.

Figure 2.2 contains a schematic of the reduction cell with baked anodes. Although reduction cells with a Soderberg anode are still in operation, their characteristics (technical and ecological) are lower compared to reduction cells with baked anodes. There is no principal difference in the construction of a cathode, a refractory lining, and a steel cradle between reduction cells with baked anodes and those with a Soderberg anode.

The service life of the reduction cell is one of the main technical and economical characteristics. The reduction cell is a rather cost-consuming device, and the cost of the produced Al depends on the service life of reduction cells. The service life of the modern reduction cell should be about 10 years, or 120 months. Some reduction cells are operated up to 120 months and even longer. However, the average service life of the reduction pot currently is 60–72 months. Sudden shutdowns during startup in the first year of service are a headache for the plant managers yet rarely happen.

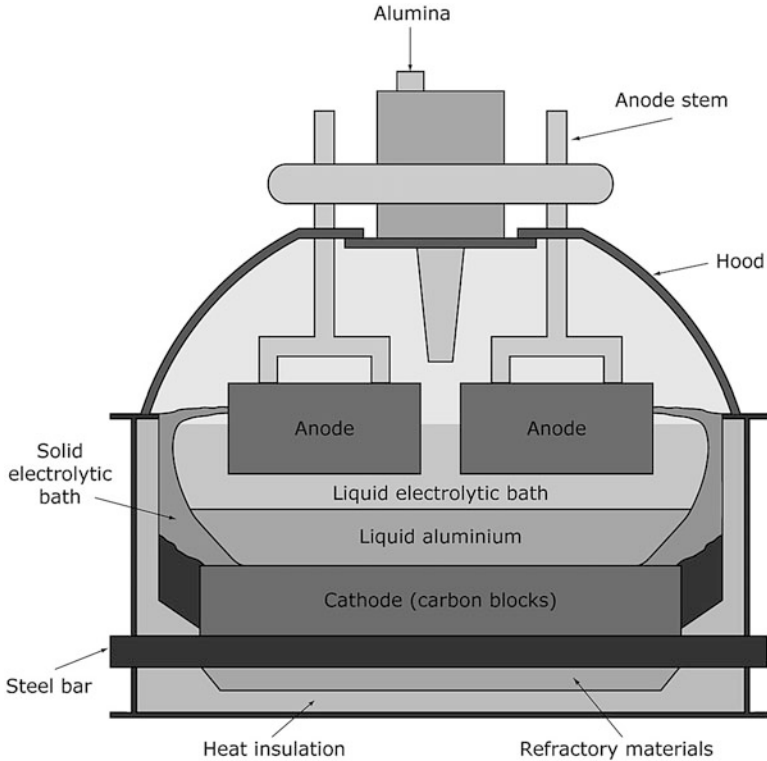


Fig. 2.2 Reduction cell (cross section)

There are about 30 typical constructions of reduction cells (not including variants and subvariants of typical constructions). Generally speaking, these constructions are not optimal, and producers have spent money for the modernization of existing constructions and R&D of new constructions. If we consider that the new constructions of reduction cells are accepted for installation after 6–7 years of trial service, the problem of functional depreciation of reduction cell constructions (obsolescence) will exist for at least 20 years. We consider the target for the service life of Hall–Heroult reduction cells to be 10–12 years (120–144 months).

One more issue that should be kept in mind by the refractory producer is the permanent movement of the molten Al and electrolyte in the cell. As we already stated, the depth of molten metal in the cell is 24–35 sm and the level of electrolyte is 18–22 sm. A reduction cell of $15\text{ m} \times 4\text{ m}$ with direct current of 440,000 Amp may be considered a big rod with direct current. Inside this “rod” one will always find fluctuations of the magnetic field, which result in permanent movement of the melt with speed of 1.5–9 sm/s up to 15–30 sm/s. Figure 2.3 shows examples of velocity fields in reduction cells.

The history of cell designs for reduction cells is more than 100 years old, but the features of all designs that remain are that a considerable amount of heat is

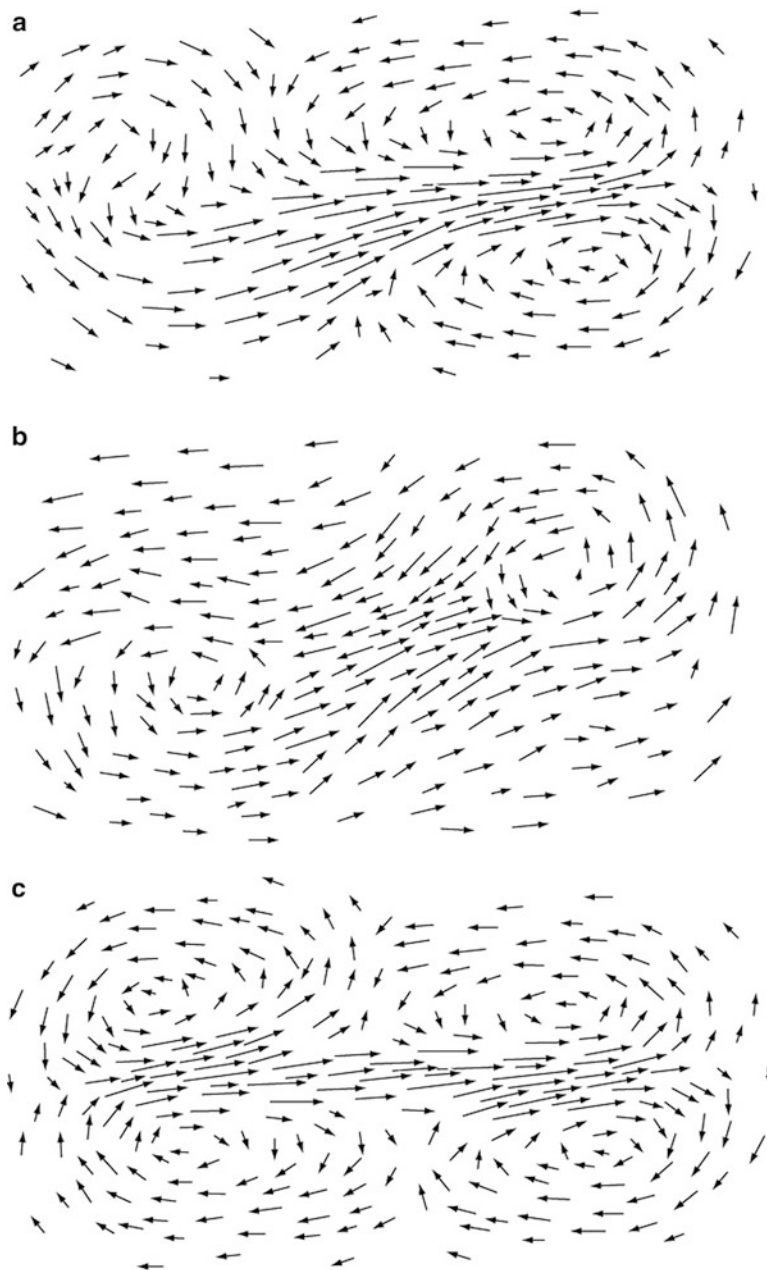


Fig. 2.3 Examples of velocity fields of molten aluminium and electrolyte in reduction cells

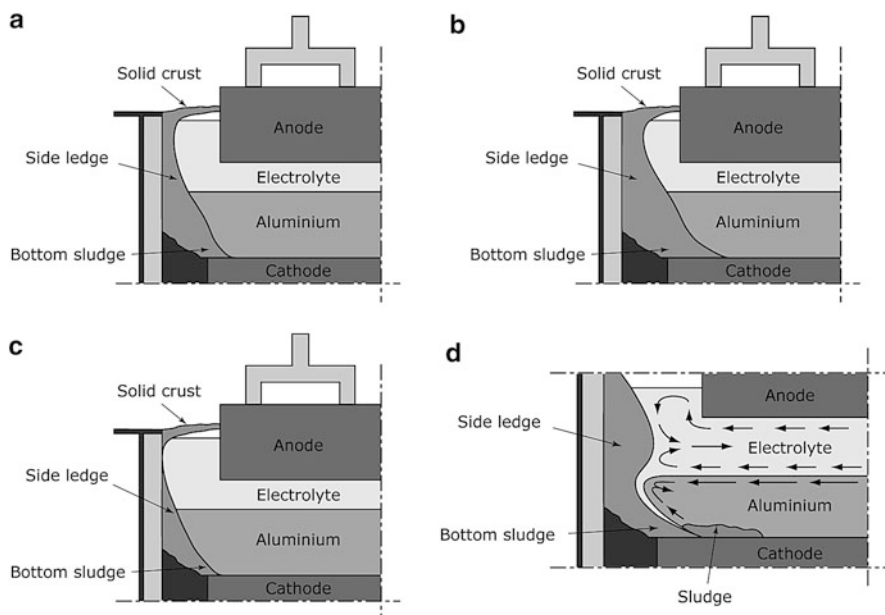


Fig. 2.4 Cross section of the side lining, showing the frozen electrolyte in the form of side ledge and sludge: (a) in normal operation; (b) side ledge is increased, low energy supply; the *bottom* sludge is excessive; (c) the cell is overheated, a part of the side ledge is dissolved; (d) normal operation; the *arrows* show the movement of aluminium and electrolyte in the cell

dissipated through the side wall of the cell, and electrolyte freezes on the side lining, protecting the lining materials (Fig. 2.4). The normal thickness of the side ledge is 3–5 sm, but it varies along the height to 8–12 sm. This frozen electrolyte plays a positive role, protecting the materials. It dissolves upon overheating of the cell, or this protective layer may be destroyed by the movement of the molten Al and the electrolyte circulating in the cell (Fig. 2.3) under the influence of magnetic forces. Electrolyte frozen on the bottom (it is called sludge) plays a negative role, because it decreases the surface of the cathode.

Probably the main issue that refractory producers with a significant experience in production and supply of refractories for ferrous metallurgy and other industries do not understand is that the reduction cell is a high-temperature metallurgical device that is heated up due to the electrochemical reaction of the reduction of Al. This processing of this reaction requires very strict temperature conditions, and consequently, the heat balance of the reduction cell is sufficiently more complex compared to conventional high-temperature metallurgical devices. A 10–15° temperature increase above the required temperature will increase the probability of deviations in reduction processing (anode effect, etc.), while freezing the electrolyte on the edges of the blocks will decrease the surface of the cathode, where the said electrochemical reaction takes place, and hence the productivity of the cell, while the difference between the freezing point of electrolyte and the working

temperature is only 15–20°. *Probably this note may be a help for producers of refractories for their activity in the Al industry.*

The current energy is used for the electrochemical reaction of Al reduction, and this is the key issue of the reduction process. But the current energy is also spent in the carbon cathode block, in the collector bar, in the contact between collector bar and carbon cathode block. It is spent in the electrolyte, in the layer of Al, due to the carbon oxide bubbles under the anode, and in various contacts in the anode system. Hence, not all energy from the current is used for direct purposes. The value of energy is received by multiplying the current by the voltage. Below is a diagram of the energy and voltage balance of a reduction cell. In pale yellow are the cells of the table depicting the factors of the voltage balance, subject to change with time. In green are the cells of the table, depicting the factors of voltage balance that to some extent may be improved by the quality of cathode materials and cell design.

The aging of cathode materials leads to an increased cathode voltage drop and consequently to increased energy consumption. The persons in charge of the reduction process have some maintenance devices to keep the process going, yet this set of devices is not big. They are dependent on many process factors, including the quality of alumina and of the anodes (and the coke for the anodes), but they are very dependent on the quality of the cathode lining materials.

Probably the perfect heat balance of the cell is a key factor for a proper reduction process as well as for a long service life of the cell (Fig. 2.5).

The classical heat balance of the reduction cell has not significantly changed for 100 years (Fig. 2.6a). The side lining has no or almost no heat insulation, while the bottom has good thermal insulation. The infiltration of electrolyte through the carbon cathode blocks to the refractory layer increases the thermal conductivity of refractories, but the infiltration increases the thermal conductivity of the heat insulation layer dramatically. The heat flow through the bottom increases.

Approximately 50 % of the heat is dissipated through the side wall (including the bus bar and flange), and approximately 50 % is dissipated through the bottom and the upper part. Previously, it was believed that the more heat that goes through the side part of the reduction cell, the better. For instance, the heat flow through the side wall forms a side ledge, which prevents the side lining materials from deteriorating; additionally, the increased energy dissipation promotes extra amperage [4]. However, considerations of energy economy led to a search for variants to decrease thermal losses (Fig. 2.6b). Not much has been achieved, but as of this publication, in 2015, energy consumption below 13,000 kWh/t of Al is a reality, and there are the plans to diminish it to 12,000 kWh/t Al, and even further, to 10,000 kWh/t.

As we will discuss later, there is currently no known material that would be resistant to the following:

- molten aluminium;
- molten cryolite;
- gaseous vapors of sodium and fluoride compounds in the presence of oxygen, carbon monoxide, and carbon dioxide.

external voltage drop	0,15 v	Heat losses 6,375 kWh/1 kgAl, voltage drop 2,032 v
cathode voltage drop (including the voltage drop in cathode block, the voltage drop on the contact of carbon block with busbar and the voltage drop in the busbar)	0,2-0,37 v	
anode voltage drop (including the voltage drop in anode, the voltage drop on the contact of anode with rod and the voltage drop in the rod and clamp)	0,35-0,5 v	
bubble induced voltage drop under anode	0,17-0,25 v	
electrolyte voltage drop	1,34 - 1,5 v	
alumina decomposition voltage	1,756 v	The energy to produce Al 6,331 kWh/1 kgAl (taking into account overvoltage), voltage 2,018 v

Fig. 2.5 Simplified diagram of voltage balance for a reduction cell. The data are generalized from [1–4]

Even if such an idea (sort of an adiabatic reduction cell) is realized, the Hall–Heroult reduction process will likely require a sufficiently greater surface of electrochemical reaction (to be discussed in Sect. 2.5).

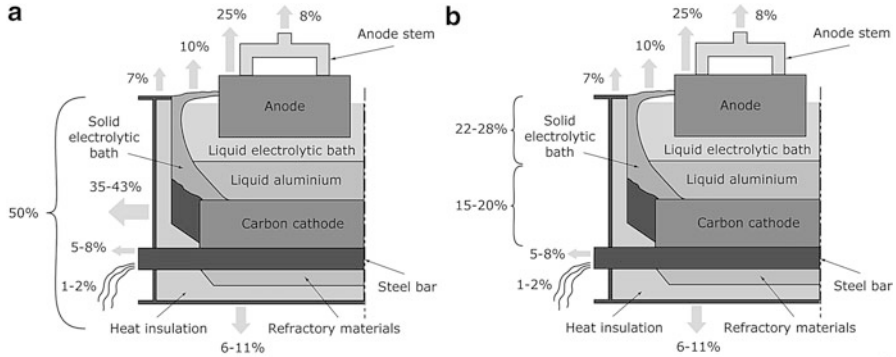


Fig. 2.6 (a, b) The heat balance of a Hall-Heroult cell. (a) Classical according to [1, 2]; (b) Updated (Generalized from [3–9])

2.2 Lining of Reduction Cells. Preheating, Startup, and Operation. Retrofit of Cells and Tendencies. The Main Causes of Failures. Dry Autopsies

2.2.1 Brief Information on the Lining of Reduction Cells

The reduction cell is lined with carbon cathode blocks and a side lining. The voltage to the cathode is supplied by steel collector bars and collector bars. Below the carbon blocks are the layer of refractories and the heat insulation layers (Fig. 2.7).

The carbon cathode blocks may be full-length or split. They may be up to 3,500–3,900 mm in length, 750 mm in width, and 550 mm in height.

Carbon cathode blocks are installed (Fig. 2.8) on the refractory barrier layer.

The gaps between the blocks are 30–40 mm, while the peripheral seams between the end of the cathode blocks and the peripheral side lining are up to 150 mm. They are filled with carbon ramming paste. Today there are alternatives to the manual ramming of gaps with hand rammers and the machined ramming with special devices; they are more convenient because of the elimination of the “human” factor.

The side lining is made from silicon carbide blocks or from carbon side-wall blocks.

The current is applied to the cathode blocks by steel collector bars.

Steel collector bars are implemented (“rodded”) into the slots of cathode blocks by cast pig iron by carbonaceous glue, or by contact paste. Today the thermal expansion fit of the steel collector bar into the slot is no longer used.

All methods have advantages and disadvantages. Gluing of ramming is simpler, the labor costs are low, and it doesn’t introduce cracks. However, the voltage drop is higher than in cast contact, and the increase in the voltage drop will be relatively quick (which promotes additional energy consumption of the reduction cell process).

The slots in the carbon cathode blocks for gluing, ramming, and casting the steel bar differ. Typical shapes of the slots appear in Fig. 2.8.

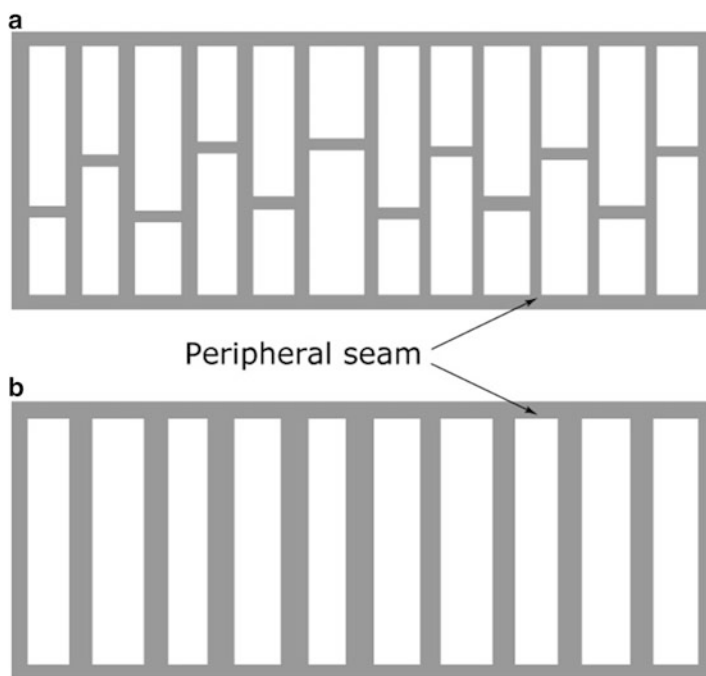


Fig. 2.7 The scheme of the cell with (a) slit cathode carbon blocks and with full-length (b) carbon cathode blocks

Casting with cast iron may introduce cracks (Fig. 2.9, 2.10). To avoid this potential issue, carbon blocks should be preheated in special furnaces before sealing by cast iron, which is rather costly. However, the electrical resistivity with a cast seal is an order of magnitude lower than that with ramming and gluing [10, 11] and the increase in the voltage drop at service is rather steady (which makes the reduction process more effective from the energy consumption point of view). Labor costs for cast-iron sealing are approximately 50 % higher than with ramming and gluing, but all methods are used at smelters (Fig. 2.9).

If the refractory layer is made from bricks, it is impossible to avoid point contacts between the carbon block and the supporting refractory brick layer. Usually, a thin (30–40-mm) powdered bedding refractory layer is used over this layer of brick material in order to avoid gaps between the brick layer and the bottom blocks and to distribute the load more effectively. In the past, this bedding material was granular alumina; later, there were many variants, such as carbon ramming paste and castables (fireclay-based and SiC-based), among others. Perhaps the most typical material of granular bedding is a dry fireclay (alumina silicate) mixture. It may be used as thin pad materials, but it may also be used as the refractory barrier layer itself.

Typically, the refractory layer is made from alumina silicate (most frequently fireclay) bricks or unshaped dry barrier mixtures. The main purpose of the



Fig. 2.8 Installation of carbon cathode block with sealed steel collector bar in the shell

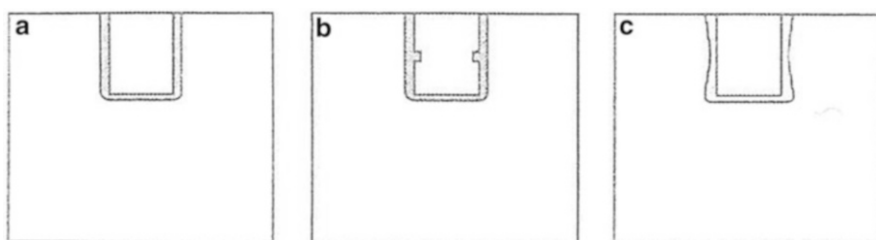


Fig. 2.9 Examples of slot shapes for (a) ramming paste, (b) glue sealing, (c) cast iron sealing

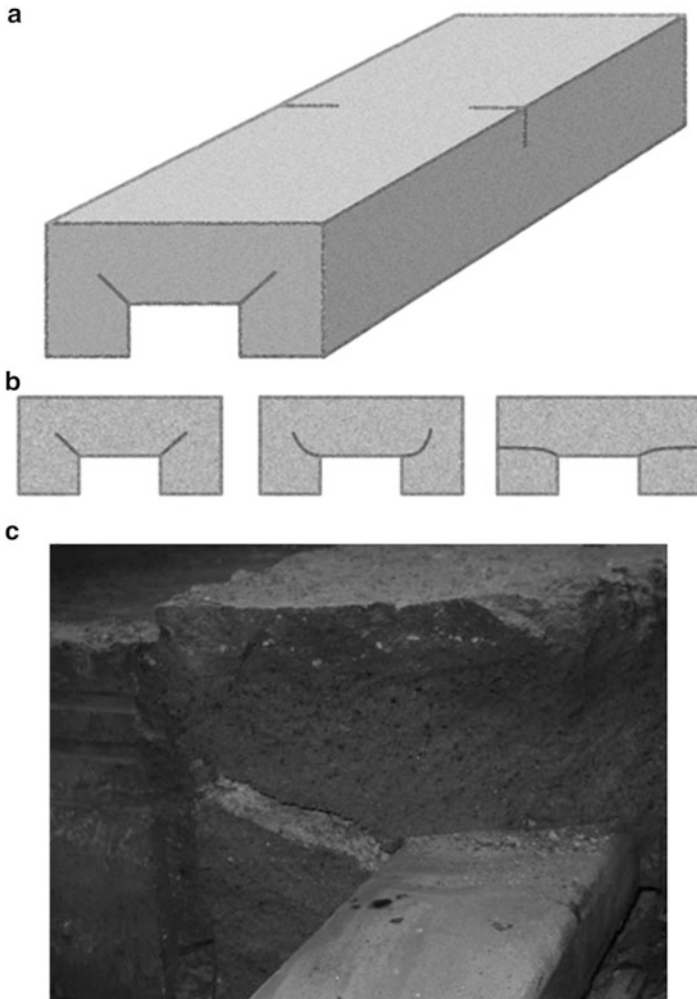


Fig. 2.10 (a, b) Shapes of cracks in carbon cathode block due to thermal tensions at casting; (c) picture of cracks in block at dry autopsy

refractory layer is to withstand the temperature and to be a barrier for the penetration of liquid fluorides, which reach the refractory layer rather easily through the permeable pores of carbon cathode materials to the refractory layer and then to the heat insulation layers.

The question of joints between the bricks is a question of high visibility. Liquid bath can easily penetrate between the gaps of bricks. Some producers prefer to use bricks with dimensional tolerances that can be achieved only by mechanical grinding. This is not done regularly, but the question of dimensional tolerances in this application is serious, and only highly qualified brick layers perform the lining.

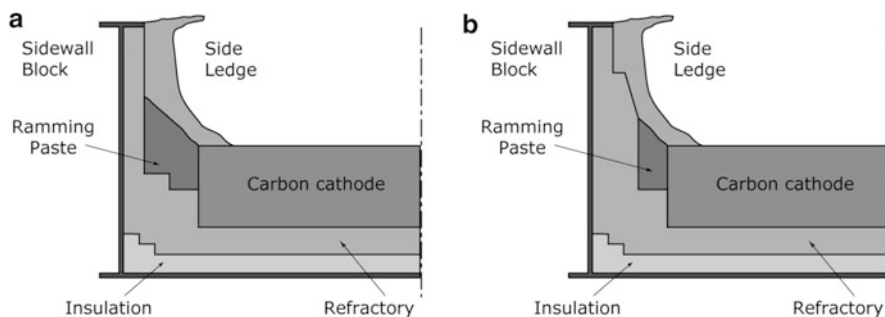


Fig. 2.11 (a, b) Cross section of typical lining

The bottom heat insulation layer of reduction cells is composed of diatomaceous (moler) bricks, vermiculite slabs, perlite bricks, and calcium silicate boards. To smooth the surface of the bottom of the steel cradles, sometimes people use fireclay grit (grain).

The side-wall blocks are protected from the bath and aluminium carbon ramming mix. In modern constructions, this cover is made from a separate baked piece of anthracitic graphitic or graphitic refractory. The construction is called a “combiblock” (Fig. 2.11b). Depending on the construction and design, the height of the cover varies from 0.3 to 0.5 m.

The side-wall blocks from carbon or silicon carbide are placed on a refractory shoulder side line. This side line is above the refractory layers under the cathode bottom blocks. It may be made of bricks or from castables, usually together with heat insulation boards. This sideline has two purposes. First, side lining is installed in the refractory side line, and, second, it helps to compensate for the mechanical tensions due to the sodium swelling (and thermal expansion) in carbon bottom blocks. Heat insulation materials are easily deformed due to tension, but the construction of the refractory lining remains undamaged.

After the installation of the side lining, the deck top is welded to the steel shell. The gap between the upper part of the side-wall block and the deck top is filled with a ramming mix with a high thermal conductivity. Earlier ramming mixes used included carbon and fireclay-based concrete, but the contemporary variant is SiC-based concrete.

The temperature of the process is 950–965 °C, and the temperature on the upper edge of the carbon bottom block may be considered the same at least in the center. Near the edges of the cell and in the corners the temperature is usually below the freezing point of electrolyte, which explains why the edges of the carbon cathode blocks are covered with bottom sludge. A temperature of 910–920 °C is close to optimal during a normal reduction process on the border of the bottom edge of the carbon cathode block and the upper part of the refractory barrier layer. Of course, in the side edges of the carbon cathode block, the isotherm 910–920 °C goes in the block (Fig. 2.12). The temperature between the bottom of the refractory layer and the upper layer of the thermal insulation is within 700–750 °C but sometimes may

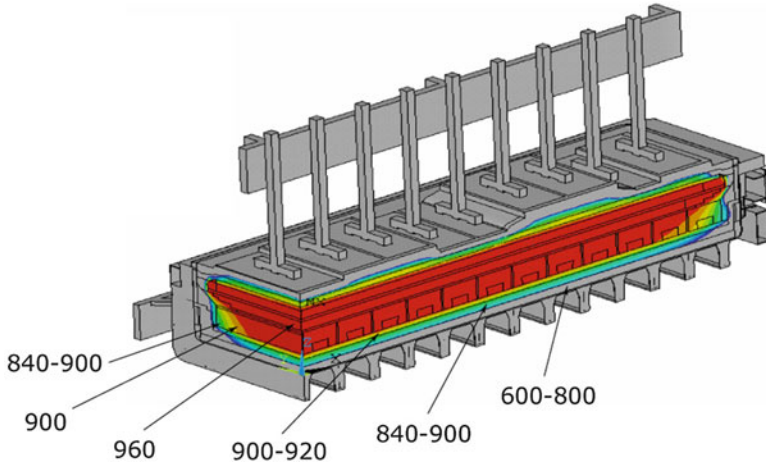


Fig. 2.12 Approximate temperatures in different layers of the lining in a reduction cell during normal processing

reach 800–850 °C. Usually during a normal operation, the side lining is covered with a side ledge, so the temperature on the side lining that contacts the bath may be considered to be 900–930 °C, while the temperature of the side wall of the steel cradle is below 200 °C.

The temperature of the steel shell in the bottom in normal operation is 80–120 °C, while the temperature of the steel cradle in the bottom before shutdown may be up to 150 °C, and even 200–300 °C.

Hence, the service temperatures of refractories are not very high, especially in comparison with the service temperatures of refractories in ferrous metallurgy.

Usually, the lining (repair) of a reduction cell is performed in a specialized repair shop; rarely, it is made right in the reduction shop. Typically, a thin layer leveling the granulated fireclay grit is placed in the new steel cradle or in the cradle after repair, and then the heat insulation slabs are lined. On the layers of heat insulation the refractory barrier layer is lined (bricks or dry barrier mixtures), the side line is made near the edges, and the cathode bottom blocks are installed. There are no mortars between the insulation layers. Bricklayers try to avoid using mortars because excessive water requires evaporation, which is not an easy process. Sometimes mortars are used to line the upper layer of bricks (if the refractory layer is made from bricks). The carbon ore SiC side-wall blocks are installed on the side line after the cathode bottom blocks have been installed.

Probably the most important operation in lining is the ramming of the gaps with a carbon ramming mix. It is usually performed right in the reduction shop, when the new reduction cell is installed in the line, but it may also be performed in the repair shop. This definition is essential in countries with temperatures that are sometimes below zero degrees Celsius; usually, the reduction shop building is not heated,

while the repair shop building is heated. In such cases, a special tent is usually installed above the cell and hot air is supplied inside the tent.

As mentioned, the construction and design principles of Hall–Heroult reduction cells are a work in progress. Cells that were new 20–30 years ago may require modernization because their efficiency characteristics are not as good as those of newly designed cells. Still, though, from an investment point of view, the modernization (retrofit) may be more attractive than the construction of a new smelter or a change in the cell design (which may lead to a multitude of technical problems, such as energy supply, change of rectifiers, internal logistics of transportation of aluminium at the smelter, etc.).

The conventional procedure to increase the productivity and efficiency is to retrofit the cell in order to increase the current. This retrofit, whose purpose is to increase the current and efficiency, is a complex engineering problem. The standard decision to change the grade of the carbon cathode block for a block with increased electrical conductivity is accompanied by an increase in thermal conductivity. An increased quantity of aluminium means an increased heat of the electrochemical reaction, which should dissipate. As a rule, a retrofit made to increase the production comprises not only a change in the grade of the block, but also the redesign of the lining of the cell, sometimes including even a change in the length of carbon cathode blocks.

The concept of drained anode will be discussed in the next chapter, together with the question of coatings on carbon cathode blocks. When a drained anode is implemented, the thickness of the level of aluminium and electrolyte will be close to zero; hence, the voltage drop in the cathode will decrease and the energy consumption of the reduction process will dramatically decrease. It is expected that the current efficiency of the drained anode will also increase.

2.2.2 Preheating and the Startup of Reduction Cells

It is necessary to preheat the newly lined reduction cell, that is, to heat the lining to the temperature of the service and to prepare the cell for pouring the molten bath without dangerous thermal tensions. During the preheating, the ramming paste in the gaps carbonizes. The bottom lining becomes monolithic, and the water from mortars, vermiculite, or calcium silicate slabs is evaporated.

The preheating and startup of reduction cells are described in [10–12]. There are several methods of preheating, some of which are interesting from a retrospective point of view. The main methods are preheating with burners and electric resistance preheating (Table 2.1):

1. preheating during anode bake (for Soderberg anode);
2. electric resistance preheating (coke bed, shunted, with full current);
3. liquid metal preheating.
4. thermal preheating (with oil burners, with gas burners, with electrical panels);
5. liquid bath (cold start).

Table 2.1 Advantages and disadvantages of preheating methods (Based on [10–12])

Method	Advantages	Disadvantages
Liquid metal preheating	Rapid heating of the surface, relatively rapid settling of vertical gradients, low-temperature gradients on the surface, low oxidation of carbon cathode materials, ecologically friendly	Rapid temperature increase of carbon cathode blocks and in ramming paste. Risk of thermal cracking in carbon blocks, risk of shrinkage of the ramming paste and leakages
Resistance electrical preheating	Short time	High-temperature gradients during preheating, uneven temperature distribution at the surface of cathode
Thermal preheating	Low-temperature difference along the surface and uniformity of the temperature gradient, easily programmed	Require more time. Oxidation of carbon materials from the surface. More complex from the point of operation

At this time, the two main methods of preheating are electric resistance preheating and thermal preheating (Fig. 2.13). All other methods just listed are interesting from a historical point of view.

Depending on the method, the preheating lasts from 24 to 72 h. During preheating the carbonization of the ramming paste in the gaps takes place, and the cathode becomes monolithic.

Ideally, the surface temperature of the cathode bottom should be similar to the temperature of the bath (950–970 °C) that is poured in the cell, and there should not be local overheatings (above 1,000 °C).

The surface of the cell is large, and it is almost impossible to achieve uniform heating. It is considered normal if only 10 % of the whole surface is lower than required [10–12].

The recommended rate of heating is 30° per hour within the first 11 h of preheating and 10° per hour within the following 60 h, while the temperature step at the highest point (950–970°) should be at least 1 h.

The cathode should become monolithic after preheating. In reality, it becomes monolithic only sometime after preheating and startup, while changes in the cathode continue to occur within the whole service life cycle.

During preheating, it is necessary to avoid thermal shock cracks and to form the structure of the ramming paste in the gaps and in the peripheral seams (Fig. 2.13).

During startup, the liquid bath (electrolite), specially prepared and taken from other cells, is poured into the cell and the current is switched into the cell. After one day, the liquid Al (taken from other cells) is poured into the cell, and the process of Al reduction begins. The main issue of startup is to avoid overheating or freezing, which may ruin the cathode, and so the cell should be operated in a normal regime.

When the required temperature is obtained and a sufficient temperature exposure took place, the gas/oil burners are switched off and removed, the anodes are

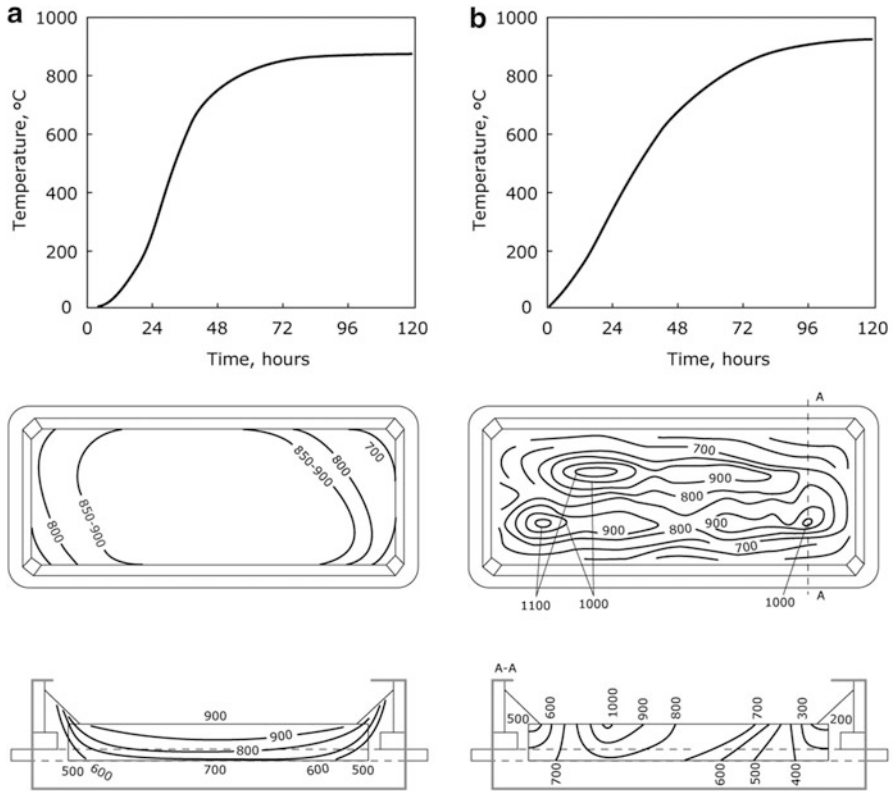


Fig. 2.13 Comparison of (a) resistance electrical preheating and (b) thermal preheating: temperature regimes; temperature gradients at the *bottom*—front view, side view redrawn from [10]

positioned, and the bath (tapped in advance from other cells) is poured into the cell. With electric resistance heating, the anodes are raised so that coke may be removed and then they are lowered again and the liquid bath is poured. As the liquid bath is poured into the cell (usually three launders, or 10–14 t), the current is switched in with a voltage of 6–8 V. Within a week, the voltage is slowly decreased to 4–4.5 V. The metal (previously tapped from the other cells) is poured in the cell after the so-called soaking period (12–36 h). After this, the alumina is added to the bath and the reduction process begins. The early operation process lasts up to 3 months, after which the normal operation begins.

Probably the most important facts the producers of refractories and carbon cathode materials should know about preheating, startup, and the early operation are the following:

1. Startup specialists begin the reduction process with a bath that has a CR of about 3, and then steadily reduce it to 2.6–2.8. The consequences are that

- At the beginning of the process, the temperature of the bath in the cell may be 1,000–1,020 °C (see diagram in Fig. 2.1), while in normal operation, it is 950–965 °C.
 - The viscosity of the bath changes; the same may be said about the freezing point and the chemical activity of the bath to refractories.
2. There are data on the bath's viscosity depending on the CR and the temperature [13–15], but for simplicity, refractory producers may keep in mind that the viscosity of the bath in the reduction cell is close to the viscosity of water.
 3. During startup and the early operation period, the planned losses of cryolite (and aluminium fluoride) are up to 12–18 t/cell. This amount of the bath (electrolyte) should be refilled at the start-up period and it is planned at the smelter. Aluminium and these fluorine salts (bath) appear at first in the cathode block and then reach the refractory barrier layer. In a pessimistic scenario, the molten fluorine salts reach the heat insulation layer.

2.2.3 Some Words About Service Life and the Main Reasons for Shutdowns

The modern reduction cell is a rather costly high-temperature device. The cost of reduction cell repairs has a sufficient effect on the production cost of Al and smelter operation. Another reason for the special attention plant managers give to the service life of the cells is that sudden shutdowns means unreceived Al and problems with operation.

There are many ways to record the data on service life and sudden shutdowns, some of which are very sophisticated. Weibull distribution analysis of failures is well accepted on smelters [10]. Probably the most convenient record on any smelter is the record of the service life and the plotting of the number of pots against age (Fig. 2.14). Another record may be the percentage of sudden shutdowns. If there are problems with the service life, such maxima may reveal the specific reasons for the failure.

As of this writing, a service life within 2,100–2,500 days is considered normal.

There are many reasons for reduction cell shutdowns, and it usually is very difficult to distinguish only one reason. Professor H. Øye [10] has listed the following factors as influence the service life:

- materials;
- cell design;
- construction;
- preheat;
- startup;
- operation.

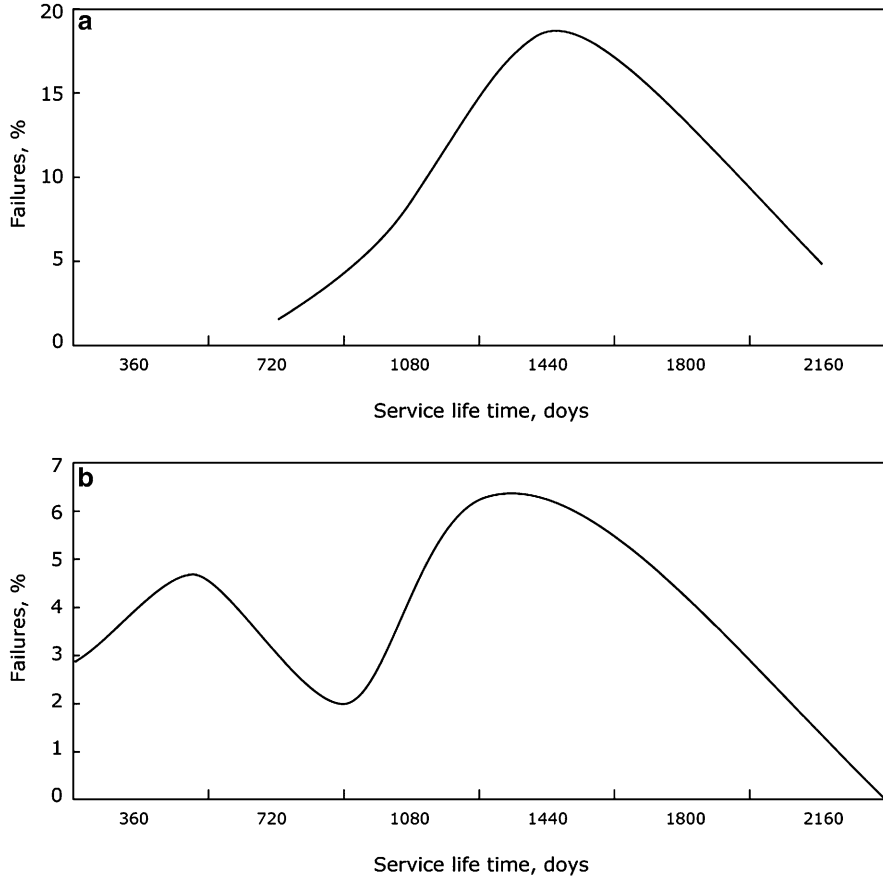


Fig. 2.14 Distribution of cell failures on smelters A and B

The value of these factors varies from one smelter to another, and even at only one smelter, the value of these factors may be discussed for a long time. The undisputable facts [10] are that a poorly designed and constructed cathode cannot work for a long time even if the preheating, startup, and operation were fairly good; and there is no need to expect a good service life from a cell with a good construction if it is made from ambiguous materials and without proper care.

At smelters with a good service life, the reduction cells are switched off according to schedule. The main reason for this is economics: The production characteristics of a cell with a considerable service life are low compared to a “young” cell, and it is more economically attractable to change it for a new, “young” cell. However, there is a certain percent of sudden shutdowns due to damage to the bottom or side lining (to be discussed later), due to damage to the shell (deformation due to sodium swelling, damage to the deck top), the melt penetrations, and so forth.

As we may recall, after the preheating, the bottom lining (including cathode bottom block gaps and seams) is a single unit, the cathode bottom. Reasons for damage to the cathode bottom and metal leakage may be any of the following:

- thermal shock due to nonuniform heating and the appearance of cracks;
- nonuniform shrinkage of the ramming paste in the gaps and poor bonding (gaps) between the blocks and the ramming mix due to the lack of adhesion;
- stratification of the ramming mix and sodium-induced exfoliation of cathode blocks;
- local overheatings and cracking;
- mechanical strains in cathode bottom blocks caused by interactions with bus bars and cracks;
- mechanical strains in cathode blocks caused by interactions with the shell and lining in the course of sodium swelling;
- problems with the design (freezing point of electrolyte in the heat insulation layer);
- exfoliation of the upper part of carbon cathode blocks;
- overheating because of problems in reduction technology;
- bottom heaving;
- bottom wear;
- metal penetration in the cathode;
- undetected defects (cracks or holes) in carbon cathode blocks during fabrication or during the casting of the steel bars;
- quality of the ramming paste;
- human factor during the lining process (especially during ramming);
- side lining degradation from oxidation;
- side lining degradation due to the lack of a side ledge (either from overheating or from too high a speed of electrolyte in the cell).
-

Readers may choose to attribute the above-mentioned factors affecting the service life (materials, cell design, construction, preheat, startup, operation) as the reasons for the specific failures, that they meet with.

Once molten Al leaks in the bottom lining, in the best case, the future service life is months, but sometimes it may be hours. The iron content in Al increases, there may be local overheatings, and the metal may leak in the steel collector bar windows.

The cathode bottom failure may be caused by any of the following factors:

- leakage of the bath or infiltration of the bath under the carbon blocks and the appearance of the “lens,” formed due to the interaction of the electrolyte and the refractory, with the subsequent rise of the bottom blocks (sometimes followed by cracking of the blocks); in turn, it may be caused by overheating of the bottom lining;
- cathode wear (up to 10–20 mm/year);
- holes in the blocks;

- leakage of the bath and the metal in the crack;
- leakage of the bath in the holes and nonuniformities in the gaps with the subsequent appearance of the “lens” with cracking, and so on.

It is not easy to detect the appearance of cracks in the carbon cathode blocks in the cell under operation. It is difficult to fix the leakage of the bath and aluminium in the bottom lining. Thus, the reasons for switch off of the cell are as follows:

- high iron content in aluminium;
- temperature of the cradle bottom (above 300 °C);
- high temperature of one or several bus bars (above 300 °C).

The exfoliation of the surface layers of the carbon cathode blocks in early operation is usually not the reason for switch off (to be discussed later). This process takes place because of (1) the interaction of the carbon and the bath and (2) the poor quality of the carbon cathode blocks.

The reasons for cathode damage may be the inner cracks and undetectable holes in the carbon blocks and the poor-quality construction of the cathode lining.

Sometimes sudden shutdowns of “young” cells with 1 or 2 years of service life take place. Such shutdowns diminish the service life on the smelter and are extremely undesirable. According to various estimates, this takes place due to the poor quality of cathode materials, poor construction, or poor startup.

2.2.4 Dry Autopsies

Dry autopsies came into practice relatively recently, in the 1990s. Professor Øye implemented them in the analysis of failure modes [10]. Although rather costly, dry autopsies are a good instrument for understanding cathode failure reasons in order to make corrective actions in the construction of the cell, to pay special attention to the quality of lining materials, or to make corrective actions to the preheating and startup procedures. In our days a series of dry autopsies (with different service time of the cell) is a standard procedure in the process of the design and implementation of the new cell type.

Usually, the analysis of the reasons for shutdown of the cell, based on the dry autopsy results, is state-of-the-art, but a very brief description (mainly from Prof. Øye [10]) may help to remember the necessary actions during the process.

Make a dry autopsy plan (the full process is time-consuming and may take up to 2–3 weeks), which includes the collection of all initial information on the cell, the dry autopsy process itself (which may take a long time), analysis of the lining materials received in the course of the dry autopsy, the preliminary report and the final report of results of the autopsy, and the causes of the failure (if there’s a failure) (Fig. 2.15).

Collect all preliminary information (cell design, lining design, lining material specifications, information on producers, information on shell, type of preheating

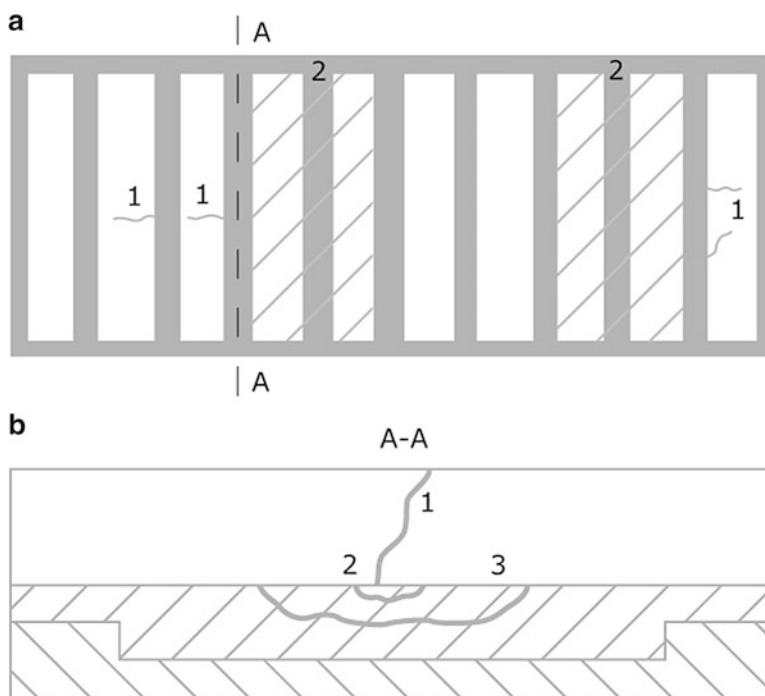


Fig. 2.15 Plan view (a) of reduction cell, cleaned from electrolyte and aluminium for dry autopsy. 1—visual cracks in cathode blocks, 2—planned places for trenches; (b) cross section of the lining from the trench: 1—crack in cathode block with traces of aluminium; 2—aluminium under the crack; 3—corroded by electrolyte refractory; (c) photo of dry autopsy

and the record, type of startup and the record, operational data during the reduction process, the direct cause of shutdown if one occurred, history of Fe and Si content in Al, information on side ledge and bottom sludge, the records of temperature, the records on cathode voltage drop, information on specific problems if any occurred).

Measure the geometry of the shell (length, width, diagonals) and compare it with the drawing (deformations of the sides, of the bottom) and inspect possible cracks and local deformations of the shell, steel bars, and steel bar windows.

Clean the cell of electrolyte, visually inspect the bottom (cracks, holes, heaving, exfoliation, state of joints), and if in perfect condition, decide whether to do the cutting and drilling. If visual defects are seen, it is necessary to decide where to drill and cut the bottom. A sketch of the preliminary inspection with a drawing of the surface of the cell that marks the visual defects may be a good help in deciding where to make a trench (groove). It is necessary to be cautious and careful here, because the removed cathode block may be the entire cause of the failure. Usually, it is better to make a groove (trench) in the lining near the place(s) of possible damage (cracks or holes) (Fig. 2.16).



Fig. 2.15 (continued)



Fig. 2.16 Exfoliated carbon cathode blocks after startup

After the groove (trench) in the lining is made, careful inspection and recording are done to inspect the trace of liquid metal in the crack in the carbon block and in the refractory, the trace of electrolyte leakage in the carbon block (or in the joints) and in the refractory, the condition of the collector bars (interactions and deformations), and the condition of the refractory layer and the heat insulation layers (chemical interaction and deformations).

Usually, the groove (trench) in the lining is at least 1 m in width, so it is possible to inspect the carbon blocks, collector bars, refractory and insulation layers on the side opposite where the damage occurred. This is also important information.

Laboratory analysis of carbon cathode blocks, refractory, and heat insulation layers sometimes may be a considerable help in considering a more serious failure.

The dry autopsy report should include the drawings, photos, results of laboratory analysis, conclusions on the direct cause of failure, and the causes that indirectly might influence the failure (e.g., the temporary overheating of electrolyte was not the direct cause of the leakage of electrolyte, but it might be the reason for the melting of electrolyte in the existing thin crack in the cathode bottom block), and the recommendations on improving the lining, design, construction, and operation.

2.3 Carbon Cathode Bottom Blocks

In this section, we discuss the following characteristics of carbon cathode bottom blocks:

- types and properties;
- elements of technology (raw materials, processing);
- analysis and testing;
- defects;
- service (chemical interaction—reactions, mechanical interaction + thermal shock), infiltration.

2.3.1 *Types and Properties*

The bottom of the reduction cell has two roles: to be the bottom of the high-temperature metallurgical device, with a certain level of molten aluminium and bath, and to be the cathode, on the surface of which the electrochemical reaction of Al reduction takes place. The upper level of the bottom is made out of electroconductive carbon blocks (Fig. 2.17a). The shape of the steel collector bar may vary (Fig. 2.17b). The full-length blocks may be 3–3.8 m in length. The slit blocks may be 1–2.5 m in length. The width of the blocks may vary from 0.3 to 0.7 m (the latter is with two slots), and the height varies in the range 0.4–0.55 m.



Fig. 2.17 (a) Carbon cathode bottom block; (b) shapes of the slots

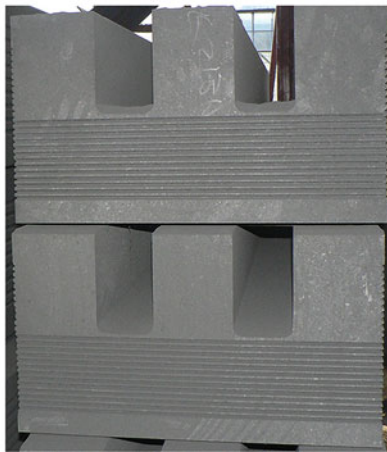
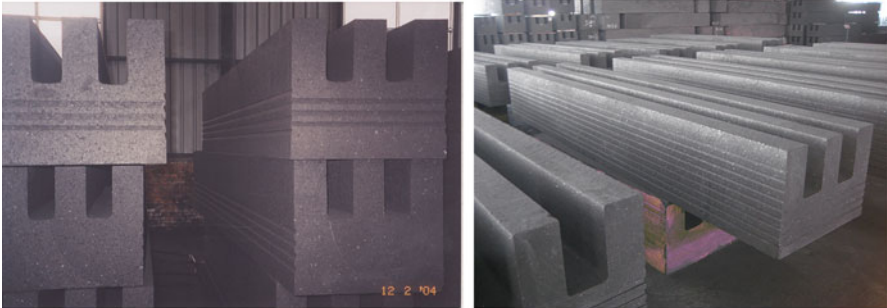


Fig. 2.18 Photos of cathode bottom

The carbon cathode bottom blocks are the most important part of the cathode construction, and this statement is not an overestimation. A single crack that reaches the surface of the block at startup may cause shutdown of the cell within the first months of service. On the other hand, the expected service life of the cell is calculated on the basis of the bottom wear. That is why the quality of carbon cathode blocks is given special attention (Fig. 2.18).

We would like to mention the idea that the materials science of carbon cathode bottom blocks is currently in development. The answers about the optimal complex of

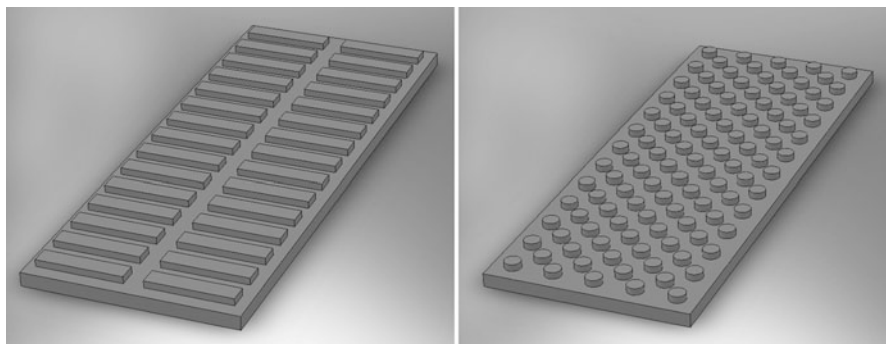


Fig. 2.19 Shaped carbon cathode blocks

properties of carbon cathode materials and the optimal structure of carbon cathode materials for the Hall–Heroult process may be given on the basis of the knowledge of interactions between carbon materials and cryolite and aluminium within 10–15 years.

One of the current tendencies in the reduction process regarding carbon cathode blocks is the possible implementation of carbon bottom blocks with a shaped (ridged) surface (Fig. 2.19). The main advantage of such shaped (ridged) blocks is the decreased turbulence of electrolyte in the cell due to magnetic forces. It is doubtful that this shape of blocks may decrease energy consumption, but it may increase the current efficiency. However, the most problematic part of such a decision is the wear resistance of the material of the parts that stick out above the surface.

The materials science approach to carbon cathode blocks is almost the same as the approach to the carbon ramming mix. There are no particular questions—after the preheating, the ramming mix should have the properties of the carbon cathode material or close to them. Here are the specific aspects of application:

- After the preheating and during startup, the ramming mix should neither exfoliate nor shrink, giving not even minor gaps and cavities in the joints.
- The porosity of the carbon mix after the preheating is always higher than the material of the carbon cathode block.
- The pore size distribution in the carbon mix after the preheating always differs from the pore size distribution of carbon cathode blocks.
- The ramming mix in the peripheral seams to some extent compensates for the linear thermal expansion of cathode carbon blocks (until it becomes nondeformable due to the carbonization).

2.3.2 *Elements of Technology, Raw Materials, and Processing*

Within the last 30–40 years, the processing of carbon cathode blocks has become more complex and sophisticated. Many types of cathode carbon blocks have appeared, and it is not easy to understand the different changing properties of carbon materials.

Initially, carbon cathode blocks were made from anthracite; after some time, synthetic graphite was added to anthracite to achieve better electrical conductivity and have fewer problems with sodium swelling. Today, between 20 and 80 % of synthetic graphite is added in the raw mixture for cathode blocks to calcined anthracite. This line may be extended to 100 % of synthetic graphite, when graphite and coal pitch are used for the green mixture, yet the temperature of the heat treatment is around 1,200 °C, so in this type of material, the grains of synthetic graphite are surrounded by grains of coke (the coke appears because of the carbonization of the pitch).

Although within the age of trials there have been tests with graphite contents of 15 %, 20 %, 50 %, 80 %, and 100 %, currently there are three more or less standard compositions: 30 % graphite, 80 % graphite, and 100 % graphite (graphitic blocks). All these compositions are obtained by mixing raw materials (calcined anthracite and synthetic graphite) with coal pitch, shaping, and firing in a reduction atmosphere at 1,200 °C.

The cathode blocks are shaped by extrusion and by vibro pressing (vacuum pumping out is applied to both processes sometime). Extrusion gives more productivity, but vibro pressing gives the ability to obtain shapes with a lower porosity and higher apparent density. Another advantage of vibro pressing is a lower amount of pitch (organic binder for shaping). Extrusion requires 20–25 % of pitch, while vibro pressing require 15–20 %. During heat treatment, the pitch converts to coke, and in vibropressed blocks, there is 6–8 % coke, while in extruded blocks, there is 11–13 % coke. It is necessary to mention that although there are some advantages in vibro pressing compared to extrusion, it is possible to obtain good cathode blocks by both processes.

The quality and grain size composition of synthetic graphite have a big influence on quality. In semigraphitic blocks (30 % of graphite), the grains of graphite don't form a continuous matrix. In blocks with 60 %, 80 %, or 100 % graphite, they form a matrix, and its quality is significant. The balance between the grain size composition of graphite and anthracite is a question to be resolved, because it is possible to use only big grains of graphite, or only medium and fine fractions. It is possible to vary the real density, ash content, and electrical conductivity of graphite and anthracite within certain limits.

There are several grades of carbon cathode bottom blocks with different characteristics (Table 2.3). All producers of carbon cathode blocks have standard grades, yet there are minor differences in properties among the grades of various producers:

with 30 % synthetic graphite;	}anthracitic graphitic
with 50 % synthetic graphite;	
with 70–80 % synthetic graphite;	

- graphitic (with 100 % graphite, heat treatment at $\sim 1,200$ °C);
- graphitized;
- graphitized and impregnated.

Anthracitic blocks without the addition of graphite are either no longer used or used rarely. For super-powerful reduction cells, graphitic and graphitized carbon cathode blocks are increasingly being used (although there are constructions of cells with 30–50 % graphite in the blocks). We can suppose that for cells with current below 250 kA, and even below 300 kA, the semigraphitic cathode blocks will be used for a long time.

The source of synthetic graphite for anthracitic *graphitic* and graphitic blocks may be unconditioned graphitized electrodes for the ferrous industry, specially graphitized shapes (that should be crashed and grinded), and scrap material from the mechanical grinding and surfacing of electrodes and graphitized cathode blocks. Usually, there are wastes of green shapes (before the baking furnaces) and unconditioned baked shapes. Producers try to minimize waste and try to use them as raw materials. From a technological point of view, these wastes are normal raw materials, containing carbon in the form of graphite and anthracite, yet special operations are required to implement these wastes in the production cycle. In any case, the ratio of these wastes and normal raw material should be strictly controlled. The problems may appear in the utilizing the wastes from the mechanical surfacing of graphite electrodes, because problems may occur in mixing with pitch (leading to the possible cavities in the finished product). Usually, graphite with a grain size below 1 mm is either strictly limited or even forbidden for production.

The temporary binder for the carbon blocks is coke pitch (Table 2.4). Its coking value is about 50 %, which means that if 20 % of pitch were added to the green mixture of graphite and anthracite, about 10 % of coke will be in the baked cathode block. It is believed that high-temperature pitch (with a high content of hinoline) increases wear resistance; however, it requires a higher temperature of mixing.

The leading producers of carbon cathodes pay significant attention to the preparation of raw materials (sewing, weighing), to mixing (the homogeneity of mixing, the temperature control), and to shaping (extrusion or vibro pressing), where potential defects of blocks may be introduced (cavities, cracks, unconsolidated areas). During the heat treatment (baking), these defects may only then be revealed. Process control should be performed at each stage. The density of the green-shaped block may already be the control parameter. Usually, after the shaping, each block should have its own identification number.

The next grade of carbon cathode blocks is graphitized carbon blocks. They are used (together with graphitic) for super-powerful reduction cells. The petroleum coke is mixed with coal pitch and the green shapes are installed in the graphitization furnaces with a temperature between 2,500 and 3,000 °C with ensuing mechanical grinding. Graphitized blocks are more porous than semigraphitic blocks. The true density of graphite is superior to the true density of semigraphitic blocks. The true density of graphite is superior to the true density of coke and anthracite; during graphitization, the transformation of the inner structure is fuller, which is the reason

for the bigger true density. However, in the case of a constant volume, the porosity of the carbon material increases. In order to decrease the porosity and increase the wear resistance, there is a process of impregnation of graphitized blocks by pitch with subsequent calcining. The advantage of graphitized blocks is their low electrical resistivity (which means lower power consumption) and low sodium swelling (to be described later). However, their disadvantages are higher price and low wear resistance.

The next step in this continuation to increase properties (mainly electrical conductivity and sodium swelling) is the application of graphite blocks. Mixtures from petroleum coke are mixed with coal tar pitch, shaped, baked in a reduction atmosphere at 1,200 °C, and then placed in graphitization furnaces at temperatures between 2,400 and 2,800 °C. At such temperatures, coke transforms into graphite. As the process of transformation goes with a negative volume effect, graphite blocks are more porous than anthracitic graphitic. Sometimes the customers at smelters install graphite blocks in the cells, impregnated by pitch, and baked one more time. The porosity of such blocks is lower than that of graphite blocks without impregnation. The typical properties of carbon cathode blocks appear in Table 2.2. The principal processing schemes of anthracitic, anthracitic graphitic, graphitic, and graphitized blocks appear in Figs. 2.20 and 2.21.

Raw Materials

Anthracite is a fossil carbonaceous material containing minor amounts of inorganic salts—sodium oxide, potassium oxide, calcium carbonate (carbon specialists call it “ash”), and organic compounds (called volatiles).

The deposits of anthracite around the world differ, and not all anthracite materials may be used for the production of cathode blocks. The mineralogy of anthracite is not easy, and specialists in carbon define fusenite, inererite, micrinite, and liptinite structures, all differing in the morphology of their structure. After the calcination, the influence of these structures in raw anthracite on properties is not great, so for an aluminium producer, the structures of raw anthracite are interesting only from an educational point of view (Fig. 2.22).

The main aim of calcination is to remove the volatile resin, such as organic compounds (10–15 %). Not all antracites may be used after calcination for the production of carbon cathode blocks, and not all antracites may be calcined in a similar manner.

However, the quality of anthracite in the deposit influences the density and ash content of calcined anthracite, so aluminium producers should at least be aware of the deposit of anthracite that is used for the production of carbon cathode blocks (Fig. 2.22). Sometimes the deposits of anthracite may coexist with calcite. The contaminations of calcite in carbon cathode blocks (usually, it is small white spots) are considered to be very harmful for the service life, because calcite may react with electrolyte, leaving cavities, but it may also absorb moisture from air at storage. The

Table 2.2 Typical properties of carbon cathode blocks

Composition	Semigraphitic (gas-calcined anthracite + 30 % graphite)	Semigraphitic (electrically calcined anthracite + 30 % graphite)	Semigraphitic (electrically calcined anthracite + 50 % graphite)	Graphitic (100 % graphite baked at 1,200 °C)	Graphitized	Graphitized impregnated
Properties						
Real density, g/sm ³	1.94–1.97	1.94–2	2.01–2.03	2.09–2.16	2.21–2.24	2.19–2.24
Apparent density, g/sm ³	1.59–1.62	1.54–1.63	1.56–1.63	1.59–1.64	1.62–1.63	1.72–1.73
Open porosity, %	14–19	15–19	16–20	18–22	21–23	13–17
Total porosity, %	18–22	20–23	20–23	24–25	26–28	20–22
Electrical resistivity, m Ω ·m, in normal to direc- tion of pressing at 20 °C	56/43	30/40	25/32	18/25	11/13	10/12.5
Electrical resistivity, m Ω ·m, in normal to direc- tion of pressing at 1,000 °C	–	22/30	18/26	16/20	10/12	10/12
Thermal conductivity, Wt·m/K in normal to direc- tion of pressing at 20 °C	8/6	14/10	19/14	30/22	125/100	125/100
Thermal conductivity, Wt·m/K, in normal to direction of pressing at 1,000 °C	–	13/12	14/13	22/18	50/40	50/40

Cold crushing strength, MPa, normal to direction of pressing	24/22	28/28	27/27	26/25	20/26	30/35
Flexural strength, MPa, normal to direction of pressing	9/6	12/9	12/9	12/9	13/10	17/14
Elastic modulus, GPa, normal to direction of pressing	11	10/7	9/7	8/6	7/5	9.5/8
Sodium swelling (ISO/WD 15379-1), %	0.7-0.9	0.4	0.35	0.25	0.1	0.1
Thermal coefficient of liner expansion (10^{-6} , $\Gamma_{pa}\Delta^{-6}$), 20-520 °C, normal to direction of pressing	2.1/2.8	2.9/3.5	3/3.5	2.9/3.4	2.9/3	2.9/3.4
Ash, not more than %	3	2	1.6	1.2	0.9	0.8

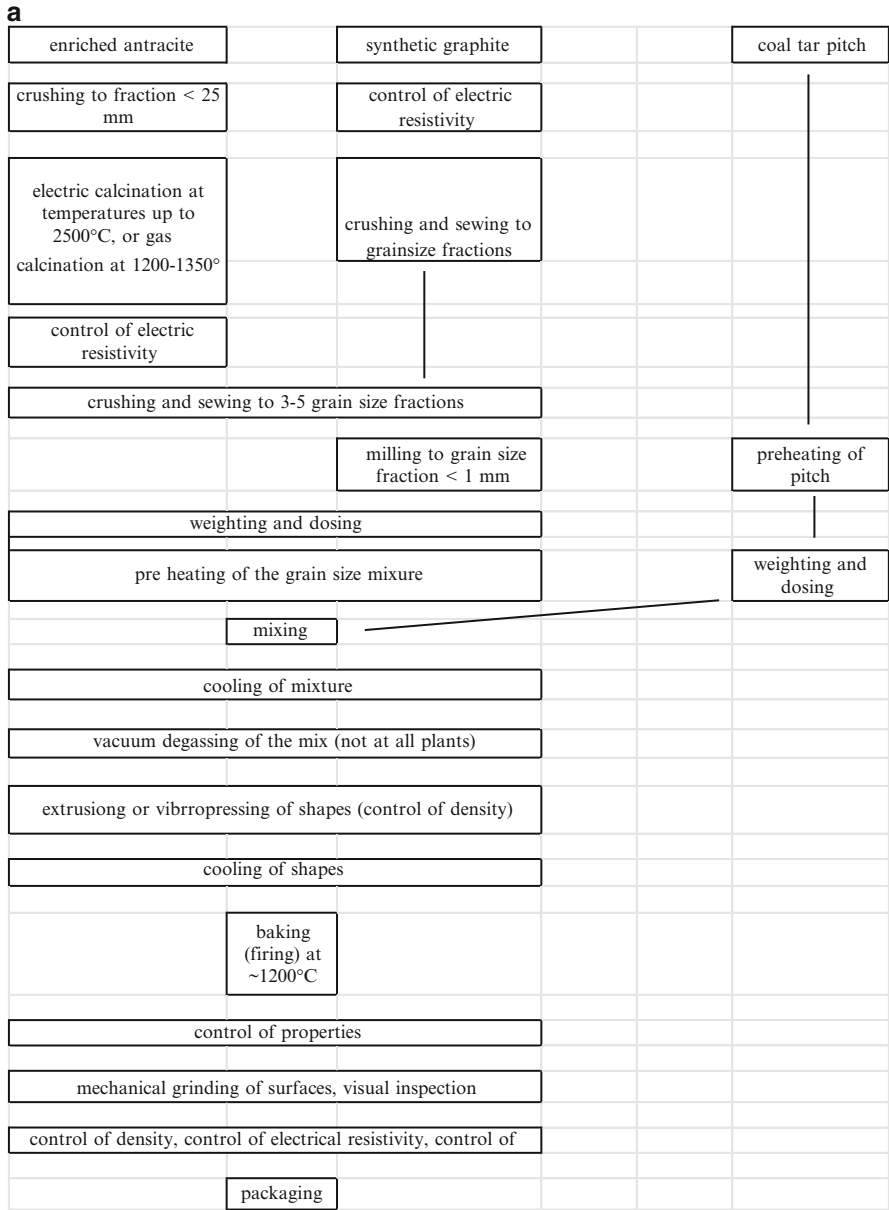


Fig. 2.20 The principal processing scheme of anthracitic graphitic and graphitic carbon cathode bottom blocks

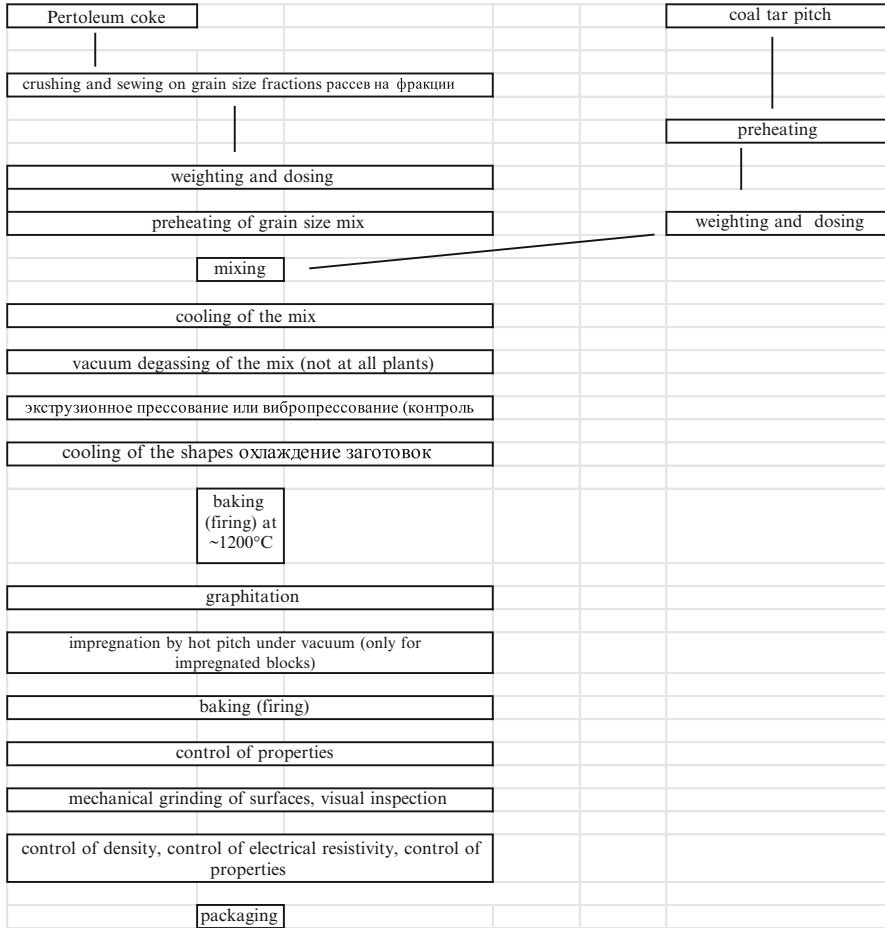


Fig. 2.21 The principal processing scheme of graphitized cathode bottom blocks

reaction of calcite with water moisture coincides with a considerable volume effect, resulting in strains and crater-like cracking of carbon blocks. Anthracite may be contaminated by iron oxide (Fig. 2.23). Ash content may influence the electrical conductivity.

Anthracite may be calcined in gas calcining furnaces (Fig. 2.24) and electrically calcining furnaces (Fig. 2.25). The calcining of anthracite in rotating gas calcining furnaces at 1,200–1,350 °C gives uniform calcination. In electric calciners, the temperature in the arch is 2,000–2,500 °C. Electric calcination gives less uniformity in properties, but a considerable part of anthracite is subjected to temperatures sufficiently higher than 1,200 °C, which leads to greater changes in the structure of anthracite, and some part (7–15 % to 10–25 %, depending on adjusted parameters of calciners) transforms into graphite. The electrically calcined anthracite has a



Fig. 2.22 Raw anthracite grains



Fig. 2.23 Raw anthracite grains with contaminations

lower electrical resistivity and a higher true density compared to gas-calcined anthracite (Table 2.3).

Electrically calcined anthracite is considered to be a more advanced raw material for semigraphitic blocks compared with gas-calcined anthracite, because it gives a lower electrical resistivity of carbon cathode blocks and a very small (but detected)

Fig. 2.24 Gas calcination furnace

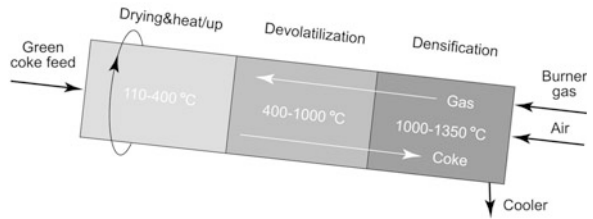
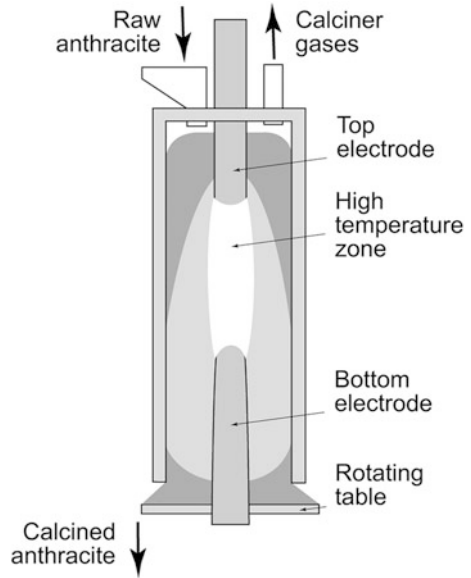


Fig. 2.25 Electric calcination furnace



decrease in sodium swelling. The reason for this is higher temperatures of thermal treatment during the electro calcination process. Gas-calcined anthracite is still rather widely used in the world for specific types of bottom blocks, side-wall carbon blocks, and carbon ramming paste. Big pores and cracks shouldn't appear during calcination. Carbon cathode blocks, made with gas-calcined anthracite, have higher strength properties (which is not considered to be an advantage).

Natural flake graphite is not used for the production of carbon cathode blocks, mainly because of economics, but also probably because the addition of flake graphite doesn't considerably increase the properties of carbon cathode blocks (as it takes place with the addition of flake graphite for refractories for ferrous metallurgy).

The raw materials for synthetic graphite are petroleum coke and coal tar pitch. The formed shapes from petroleum coke and pitch are fired in baking furnaces at 1,200 °C, and then they are installed in graphitization furnaces (direct or indirect

Table 2.3 Typical properties of raw materials for carbon cathode blocks

	True density, g/sm ³	Electrical resistivity, mkΩ · m	Ash, %
Electrically calcined anthracite	1.8–1.86	500–650	3–5
Gas-calcined anthracite	1.7–1.75	1,000–1,100	3–5
Synthetic graphite	2.15–2.25	80–180	0.3–0.5

Table 2.4 Typical properties of coal tar pitch for the production of carbon cathode blocks

Property	Unit	High temperature	Medium temperature
Softening point (ring and the rod)	°C	85–90	72–76
Softening point (ring and the ball)		–	90–98
Volatiles	%	53–58	<59
Insoluble in toluene	%	<31	26–31
Insoluble in Quinolone	%	<12	<10
Ash	%	<0.3	0.3
Water content	%	–	<4.0
Coking value	%	<55	<50
Sulphur	%	<0.5	<0.5
Na ₂ O	%	<0.018	<0.018
Viscosity at 155 °C	sPz	1,500–4,500	400–1,500
Viscosity at 185 °C	sPz	300–500	100–300

graphitization) with a temperature of 2,500–2,800 °C. It is necessary to remember that to receive the raw graphite materials for semigraphitic blocks, it is possible to use either specially prepared shapes or the scrap material from the production of graphitic cathodes or electrodes.

Synthetic graphite is produced in graphitization furnaces. The green shapes, consisting of calcined petroleum coke and pitch, are baked (fired) in baking furnaces at 1,200 °C and placed in graphitization furnaces (direct or indirect graphitization). During this process, the shapes from petroleum coke at temperatures of 2,500–3,000 °C become graphitized. The shapes from coke may be specially prepared for the following crushing but also may be the wastes and unconditioned materials from the production of graphitized electrodes for ferrous metallurgy. The properties of synthetic graphite appear in Table 2.3; they may vary depending on the chemical composition of the coke and the temperature of the graphitization process. Graphitized shapes are crushed, milled, and sewed for grain size fractions.

The properties of coal tar pitch are listed in Table 2.4. The pitch with a higher softening point is considered preferable for the production of carbon cathode blocks because in the high-temperature pitch, the coking value is bigger and there are fewer volatiles. Yet the pitch with a higher softening point requires higher temperatures for preheating and mixing with powdered mix.

The grain size fractions are preheated in the mixers (with electric or steam heating) to 95–105 °C, the weight amount of preheated to 140–150 °C pitch is poured in the mixer, the mixing process is continued for 10–15 min (for the temperature homogenization up to 135–145 °C), and then the mix is transported to the press (in vessel or by vibro conveyer). The pressing mix is cooled to 100–110 °C and is ready for extrusion or vibro pressing. In intensive mixers, the process of preheating the grain size composition and cooling the mix is sufficiently quicker.

Occasionally, possible defects originating from raw materials arise in carbon cathode blocks. Of course, there may be problems with coal tar pitch, but pitch itself is not the source of defects if the mixing and shaping were performed correctly. The synthetic graphite varies in ash content and in the degree of graphitization, which finally reveals a different electrical conductivity (which may be adjusted by various technological means). Impurities are rare in graphite (if a magnetic separator is installed). Impurities are possible in calcined anthracite, and they have two origins: natural calcite inclusions or ferrous inclusions due to calcination (which should be removed by a magnetic separator). Usually, there are wastes from the shaping process (extrusion or vibro pressing), which actually may be normal materials and that are usually implemented in the process one more time. The amount of such wastes should be limited, and they should be carefully preheated and mixed; otherwise, they also may become the source of deviations in properties and in density (possible source of cracks).

The shaping of carbon cathode blocks may be performed by extrusion and by vibro pressing. Both processes have advantages and disadvantages. The possible defects in cathode blocks after extrusion and after vibro pressing also differ.

Usually, the extrusion press has a force (effort) of 3,500–6,300 ton. The pressing mix is cooled to 100–110 °C and then loaded in the drum (container) of the press, which is heated to 110 °C and is pre-pressed at pressure 150–180 atm to eliminate cavities and holes. On some extrusion presses, the degassing (vacuuming) is made after prepressing, and then the closing mechanism of the die-hole (nozzle) is opened and the shaping process (at pressure 50–60 atm) begins. After each 3–5-m-long shape passes through the nozzle, the knife cuts off the shape and the closing mechanism closes. The nozzle of the extrusion press is preheated to 110–190 °C, and the temperature in different parts of the nozzle is controlled by thermocouples. After the pressing, the shapes are cooled by water and after some aging are transported to the baking furnaces.

A vibro press can produce shapes of carbon cathode blocks having a length up to 4.1 m and width up to 0.75 m at an effort of 120–240 t. The mold of the vibro press is preheated to 100–120 °C, the temperature of the pressing mix is 120–140 °C, and vacuuming is not done on every press. The pressure of the process is 5–7 MPa, the amplitude of vibration is 2–4 mm, the frequency is about 25 Hz, and the duration of the pressing cycle is 5–8 min, which allows 3–4 shapes to be made per hour. Frequently, producers apply vibration without applying pressure, and then the prepressing with pressure takes place, and only then does the final pressing occur.

Fig. 2.26 A stamp on extruded green shape



Usually, vibro-pressed blocks have an advantage in porosity in comparison with extruded blocks; the difference might be up to 5–7 %. Usually, the vacuuming decreases the porosity by up to 2–3 %.

Conventionally, each block is measured in the air and in water and the density determined (Archimedes' method). This value is a good technological parameter for control of the green shape. Usually, each block is stamped (Fig. 2.26), and the number is used for the records.

High-quality carbon cathode blocks may be produced by extrusion and by vibro pressing. The productivity of the extrusion process is a little bit better than that of vibro pressing. Defect-free blocks may be achieved by both methods, though the extrusion process is more sensitive to inhomogeneities in the density of the pressing mix. Yet big cavities in carbon cathode blocks are very rare, which cannot be said about pre cracks (which are not seen by the naked eye even after baking or graphitisation and mechanical finishing, but may open during preheating of the reduction cell and during service). As mentioned, extruded blocks have a bigger porosity, but a good pore size distribution may be achieved in both processes, so this small difference in porosity may not be considered an advantage (in case of good pore size distribution).

Firing

Carbon cathode blocks are fired (baked) in a chamber ring furnaces, where the hor zone is moving along the chambers of the furnace while the shapes are located in the chambers, which is not quite conventional in today's refractory industry.

The chamber ring furnaces are used for firing of carbon cathode blocks for the following reasons:

- the necessity of a long and finely adjusted temperature regime in the reduction atmosphere;

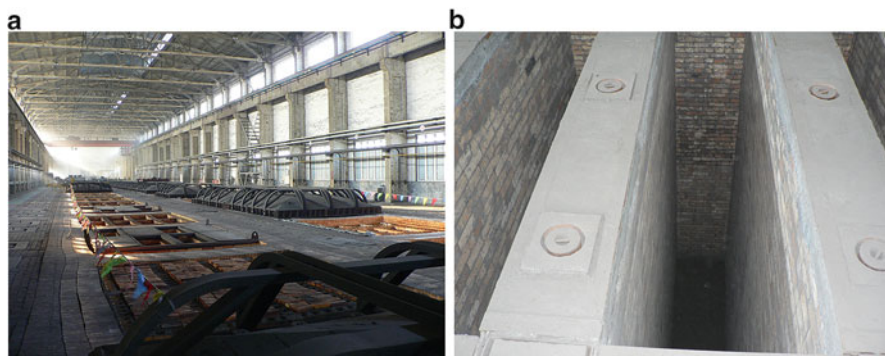


Fig. 2.27 Baking furnace: (a) general view and (b) the chamber

- the necessity of using the filling (which gives a reduction atmosphere, but also prevents the deformation of cathode blocks under gravity forces).

The baking furnaces are operated on natural gas, diesel oil, or generator gas that burns in flues, and the heat is transferred through refractory lining (indirect heating). All zones (preheating, heating, and cooling) move accordingly. The material in the chamber is subjected to all stages of the cycle: loading of shapes, loading of coal filling, preheating, heating, cooling, unloading of filling, unloading of shapes. Actually, the ring-baking furnace is a counter-flow reactor (green shapes are heated by gases, appearing due to the burning of the fuel material and the volatiles, emerging in the hot zone).

There are open (without cups) and closed (with cups) ring-baking furnaces (both variants are good). Each chamber consists of five to eight cassettes. A cassette is a rectangular box, having a height between 4.5–7 m, a length of 3–6 m, and a width of 0.5–1 m (Fig. 2.27). The shapes are placed in the cassettes (both vertical and horizontal loading is accepted), and the coal filling is loaded in the cassettes. The thermocouples may be placed in the top of the chambers, in the flue wall (sometimes the initial part of firing is controlled according to the thermocouples in the flue walls, and the final part of firing takes place according to the thermocouple above the upper part of fired cathodes). The variant of the temperature firing regime appears in Fig. 2.28 (the thermocouple is above the fired cathodes).

Usually, the temperature of the fired cathodes is around 1,200 °C. A very important characteristic of the ring furnace is the temperature gradient along the height. In good variants, the temperature gradient is within 20°, and this is achieved by perfect thermal insulation of walls and correct thermal balance. A low-temperature rise increases the firing time and the energy consumption; too fast a temperature increase may cause cracking of cathode shapes. The most critical (for cracking) is a temperature interval of 200–600 °C (when the evaporation of volatiles is intensive). It is felt that the rate of temperature increase there should be below 10 °C per hour [95]. After 600 °C, the rate of the temperature increase may be 15–20 °C per hour.

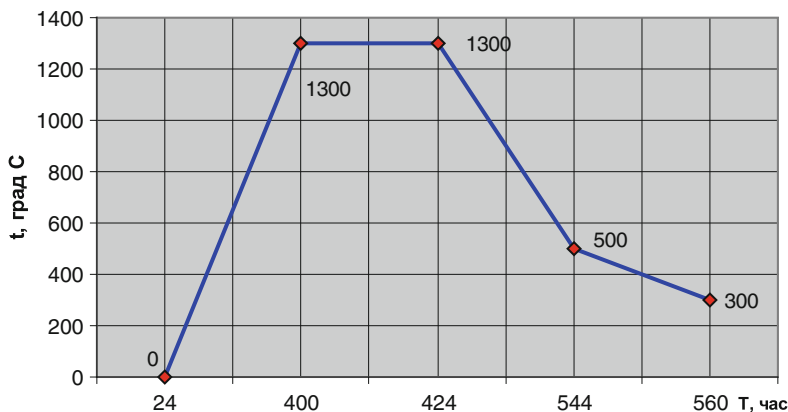


Fig. 2.28 The temperature firing regime of cathode anthracitic graphitic blocks

The inhomogeneities of density in the green shapes may be revealed as cracks and pre cracks during firing, which is why the attention given to the temperature regime should always be painstaking. Another possible defect of baking (that may happen in furnaces with temperature gradients) is insufficient firing of part of the block (in case of vertical loading) or the surface of the block (in case of horizontal loading). In service, it may cause the exfoliation of the surface layers of the blocks due to sodium swelling.

Graphitization

Fired shapes are loaded in graphitization furnaces. In the Acheson process (indirect graphitization), the electroconductive media is carbon filler, and the shapes are heated due to the electroresistivity of the filler. In direct graphitization, the filler is used only to make the reduction atmosphere and to prevent heat losses. The electroconductive media are the shapes of carbon cathode blocks. They are placed lengthwise to the current leads and the movable transformer is switched to the leads, so the hot zone of the furnace is also moving (Fig. 2.29).

In both processes, the percentage of unconditioned shapes due to cracking is considerable (many cracks are revealed after surface finishing of blocks). These unconditioned blocks are used for the production of anthracitic graphitic blocks. In both processes, it is possible to produce good production, but direct graphitization is less costly.

So-called isotropic coke and anisotropic coke were used for the production of graphitized carbon blocks. The blocks from isotropic coke have a higher strength and wear resistance, while the blocks from anisotropic coke have a higher coefficient of expansion. Depending on the shaping method (extrusion or vibro pressing), the orientation of the grains from anisotropic coke may differ. The blocks from isotropic coke are more popular.

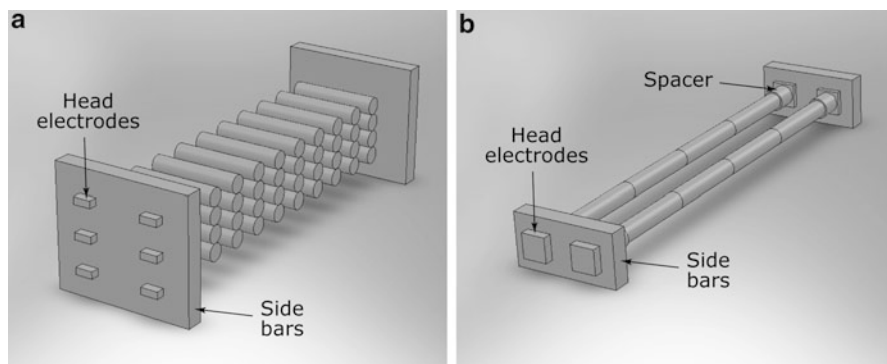


Fig. 2.29 Schematic drawings of (a) indirect (Acheson) and (b) direct graphitization processes

In order to reduce the porosity of graphitized blocks, it is possible to impregnate it with coal tar pitch and its compositions. After the graphitization process, the carbon shapes are cooled down and placed in special vessels with vacuum and controlled temperature. After the air is pumped out, the coal tar pitch compositions fill in the vessel and infiltrate the carbon shapes. Different organic substances are added to the pitch to reduce the viscosity. The impregnated carbon shapes are dried and fired in previously described baking furnaces, and the pitch in the pores carburizes and transforms into coke. One impregnation with the following firing diminishes the porosity to 7–8 %, which is a considerable value. The trials on double impregnation showed a sufficient cost increase of a rather costly production.

Mechanical Milling (Finishing)

Modern blocks are mechanically grinded from all surfaces (including the inner slot surface). The grinding reveals inner defects and gives strict tolerances in dimensions. The quality of mechanical grinding depends not only on the type of equipment, but also on the type of the instrument. A diamond instrument is more expensive, but its service time is longer.

The requirements of aluminium producers for tolerances are rather strict – ± 10 mm in length and ± 3 mm in width and height. The same may be said about the tolerances in normality of the surfaces and cavities. Mechanical grinding is done by a carbide hard alloy instrument, but a diamond instrument may also be used. Depending on the philosophy of surface finishing, mechanical grinding may be done by a special multiposition milling machine or on a series of machines, beginning with a diamond saw and including a bed-type milling machine, planer-type millers, and so forth.

Mechanical grinding is done in a mechanical shop. It is usually accompanied by visual inspection (because after surface finishing, many defects, such as small cracks and metal of mineral inclusions are easily seen in good light), by control

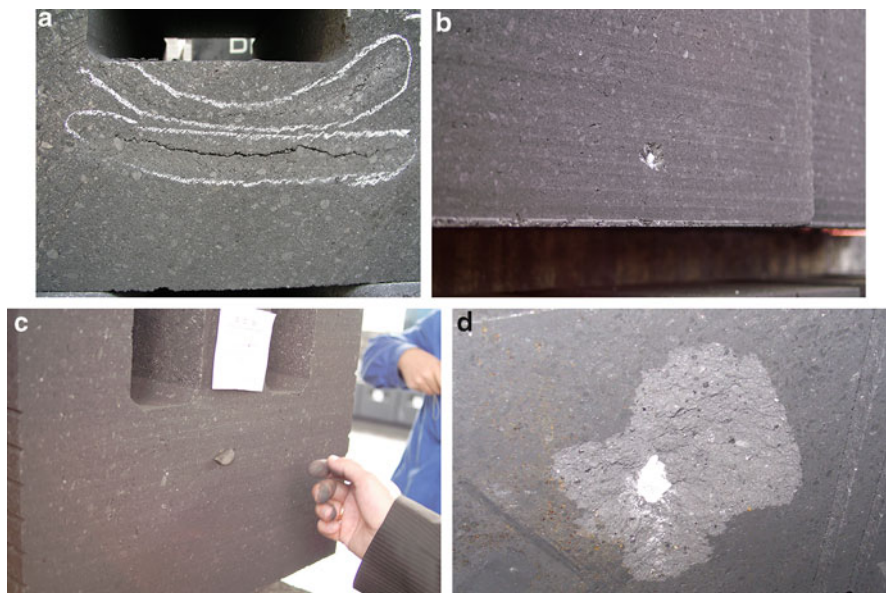


Fig. 2.30 Inner defects in carbon cathode blocks that may be revealed at cutting: (a) inner crack; (b) calcite grain; (c) ferrous contamination (it is almost undetectable visually, but magnet sticks to it); (d) calcite contamination

of electrical resistivity, sometimes by some nondestructive control for internal defects (sonic, ultrasonic, electro-impulse, X-ray, etc.). Then the blocks are packed.

2.3.3 Defects in Carbon Cathode Blocks

Carbon cathode bottom blocks have big dimensions. Unfortunately, during the fabrication process—during pressing or during baking—defects may appear in carbon cathode blocks—cracks, cavities, impurities, and inclusions (Fig. 2.30). If cracks or cavities are on the surface of blocks, they are more or less clearly seen, and during the visual inspection at the producer's or customer's plant in the Al industry, blocks with defects are rejected as defective and sorted out. They may be crushed and then the crushed material reused for production. The same may be said about metallic or calcite inclusions.

The problem is that not all defects may be seen on the surface. Only one crack in the bottom block—that is, inside the block, not seen on the surface—might be the cause of the sudden shutdown of the cell during startup or during early service. Unfortunately, such internal defects are not rare, and they may occasionally appear. One example of the appearance of such an internal defect may be when graphite

Fig. 2.31 Picture of two surface cracks: one inside the block, another reaching with one edge the surface of the block



grains were not wetted properly by high-temperature pitch, and in the mixer some inhomogeneity appeared in the mix of graphite and pitch—the major part was wetted properly, but probably one tenth of the mix in the mixer was not wetted by pitch to the same condition. Once this ready mix of graphite and pitch was placed in the mold of the extrusion press or vibro press, the pressure (and probably the vacuumation of the mix in the mold was done before the application of pressure) was applied, the pressing in the mold became a solid body, but at unloading, during the elastic relaxation (recovery) of the pressing, the parts of that poorly wetted mix moved slightly in a different way than the rest of the pressing. The strain between the portion of poorly wetted mix and the portion of properly wetted mix revealed the microcrack during baking (firing). This possible microcrack, which has a very complex surface, might have dimensions up to 300 mm × 400 mm but still remain undetectable. Even if this microcrack reaches the surface of the block, it will still be almost undetectable (Fig. 2.31), because the distances between the surfaces of this crack are 100–300 μm and are not seen visually. This crack may or may not open during the preheating of the cell or startup if tensions in the temperature appear.

The most dangerous technological defects are

- Internal cracks that didn't reach the surface of the block (strain concentrators for the growth of crack), and internal cavities, which may be filled in with bath and which are also strain concentrators (the bath may crystallize in such cavities, while the volume effect of the crystallization is positive).
- Poorly premixed parts of blocks, where the porosity may be 1.5–2 times higher than normal. Usually, the dimensions of pores in such parts may exceed the average dimensions of pores by a factor of hundreds. This defect may appear if the pressed shape was considered to be a defect. This pressed shape is typically crushed' the crushed material is considered to be a common raw material and is added to the mixer. During mixing, this crushed material may become part of the mix or may retain its own structure.

- Poorly premixed parts of blocks (e.g., due to insufficient preheating of grain composition or the pitch or because of insufficient premixing of green scrap) might give other, almost undetectable defects in carbon cathode blocks. Parts with a different density in the green state may form parts with mechanical strains in the fired state, which are pre-cracks. During preheating of the cell, the carbon bottom blocks withstand bending tensions, and these pre-cracks might start growing. Of course, the edges of these pre-cracks are inside the blocks and have a very small width, but due to bending tensions, the width of the cracks that reach the surface might be sufficient for infiltration of electrolyte and even aluminium. Thin cracks that reach the surface of the block are almost undetectable.
- Insufficient firing of carbon cathode blocks may lead to exfoliation (shipping, spalling) of the upper part of blocks due to excessive sodium swelling (compared with other parts of the blocks). Usually, it is almost unrealistic for the producer of carbon cathode blocks to deliver production that is not fired according to the temperature regime. However, it is necessary to remember that the depth of the chambers in the baking furnaces may reach 7 m, and temperature gradients are inevitable. Currently, in the best constructions, the temperature drop along the height is 50° , but the temperature drop might be sufficiently bigger. The variation depends on in what way the green carbon cathode blocks are placed in the chambers and how the chambers are filled. For the open type of carbon baking furnaces, the amount of carbon filler above the green carbon blocks during firing also might be critical. This is essential even for graphitic carbon blocks (which usually demonstrate low sodium swelling); however, the grains of coke between the graphite grains might also be subjected to excessive sodium swelling.

Another reason for exfoliation might be insufficient calcination of anthracite.

- Inclusions may have considerable dimensions. The source of the metallic inclusions are mechanical parts of equipment (including calcinators and crushers and disintegrators). Mineral inclusions are quite rare in graphitic and graphitized blocks. The source of mineral inclusions is usually calcite layers in anthracite deposits. During purification, some parts of calcite may remain in the anthracite. Calcite inclusions in carbon cathode blocks are rapidly dissolved by cryolite and the cavities filled by bath; they appear in the block (Fig. 2.30b).
- Traces of oil (which might appear on the surface of blocks during mechanical grinding and finishing) are also not desirable. The spots of oil are seen on the surface, but oil might also penetrate inside the block, and during preheating this oil will evaporate and may start burning (Fig. 2.32).

Cracks and chips on the edges and corners of cathode blocks and other geometrical deviations are less dangerous, but are still not desirable. They are due to the following causes:

- Cracks and chips may appear due to an excessive speed of the grinding instrument during the surface finishing of blocks.



Fig. 2.32 Examples of the internal cracks inside the carbon cathode blocks that are not seen on the surface but are seen on cross section after cutting

- Large grains of graphite and anthracite (imperfect sewing) and big pieces of baked shapes and green shapes, considered to be defects, are implemented in the process as raw materials.
- Geometrical deviations in normality (orthogonality) and parallel alignment appeared during the mechanical finishing.

Attempts to implement nondestructive quality control for carbon cathode blocks and to reveal internal defects has a 40+-year history, and we cannot say that these attempts have stopped. Typically, the next attempt to implement another nondestructive method of quality control starts after a series of unexpected shutdowns. These attempts are initiated by customers, but producers also carry out research in this direction. Another question to discuss is where should the nondestructive control device be placed: near the producer's storage house or at the customer's quality control?

The simplest method is sound propagation in the block, where the sound appears from the knock of the hammer in the hands of the worker. Sometimes an experienced worker can recognize internal cavities or cracks based on the hammer's sound.

Some producers and customers apply ultrasonic devices, sometimes with good results. However, there has been information that these ultrasonic detectors do not give a 100 % guarantee of revealing internal defects.

Some R&D has been done on the application of the electro-impulse resonance method for the detection of internal defects.

Probably the most advanced nondestructive method of defect visualization in the cathode blocks might be the X-ray scanning and visualization technique. The apparatus is complex and expensive; it is sensitive to dust and should be situated in a special room. Yet it doesn't guarantee 100 % detection of internal defects (Fig. 2.33).

However, the philosophy of continuous permanent processing and technology giving homogeneous mixing, homogeneous structure, and permanent control of the process and properties are probably dominant in industry today.

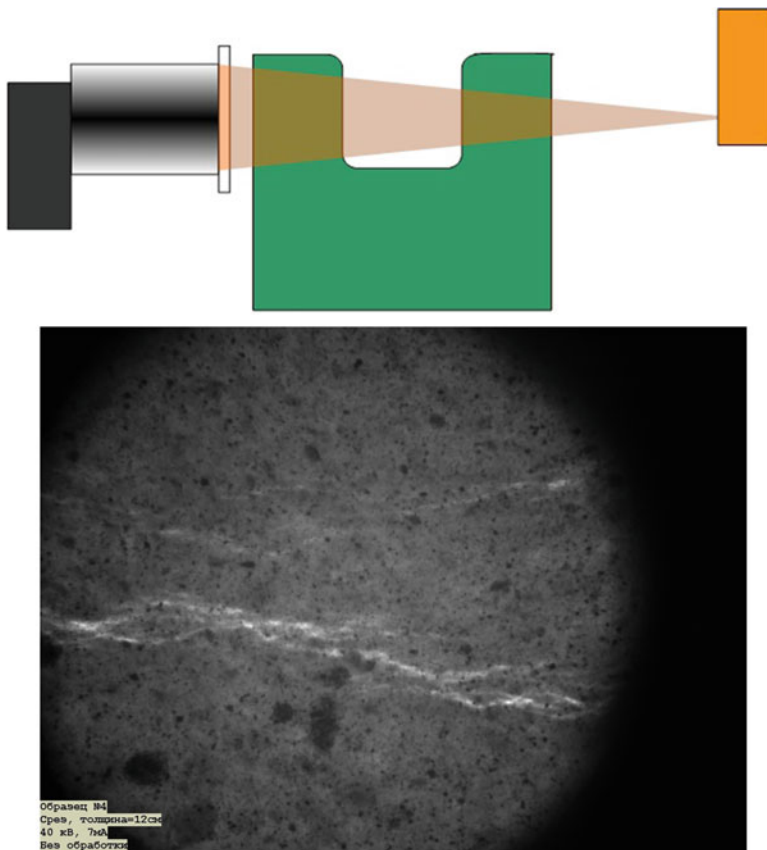


Fig. 2.33 X-ray detection of cracks in carbon cathode blocks

Permanent visual inspection of the surface defects, performed by both the producer and the customer, also gives positive results. Brightly illuminating the inspection area and vacuum cleaning all surfaces of cathode blocks prior to inspection are also useful.

2.3.4 Testing and Characterization

The properties of refractory materials are described in Chap. 1 as an overview of these properties and variations in their values. Because carbon cathode blocks are not usual refractories, we will give more attention to their properties. Carbon cathode blocks are manufactured according to the specification of properties (Table 2.3). Professor Øye, along with coworkers, made a profound generalization

Table 2.5 Temperature dependencies of electrical resistivity and thermal conductivity in different grades of carbon cathode blocks according to [17, 18]

Grade of carbon cathode block	Temperature, °C	0	200	400	600	800	1,000
Anthracitic graphitic (30 % graphite)	Electrical resistivity, $\mu\Omega \cdot \text{m}$	43	41	39	37	36	36
	Thermal conductivity, $\text{W/m} \cdot \text{K}$	6	7	8	8	8	8
Graphitic (100 % graphite)	Electrical resistivity, $\mu\Omega \cdot \text{m}$	20	18	18	18	18	18
	Thermal conductivity, $\text{W/m} \cdot \text{K}$	30	29	27	24	23	22
Graphitized	Electrical resistivity, $\mu\Omega \cdot \text{m}$	10	10	10	10	10	10
	Thermal conductivity, $\text{W/m} \cdot \text{K}$	125	90	75	60	55	50

Table 2.6 The change in electrical resistivity of carbon cathode blocks with time (lab tests during electrolysis) [17, 18])

Grade of the carbon cathode block	Time, min	0	20	40	60	80	100	120
Anthracitic graphitic (30 % graphite)	Electrical resistivity, $\mu\Omega \cdot \text{m}$	35	31	27	25	25	25	25
Graphitic (100 % graphite)	Electrical resistivity, $\mu\Omega \cdot \text{m}$	22	20	19	18	18	18	18
Graphitized	Electrical resistivity, $\mu\Omega \cdot \text{m}$	10	10	10	10	10	10	10

on the standardization of the properties of carbon cathode blocks [16, 17]. Probably the most important properties are electrical conductivity and sodium swelling. These properties make carbon cathode blocks different from all other refractories.

The electrical conductivity of carbon cathode blocks is a function of temperature (Table 2.3) and it changes during the service life (Tables 2.4, 2.5, and 2.6, Fig. 2.34) [17–19].

The voltage drop in cathode carbon blocks depends on the electric resistance and the current density [19]:

$$\Delta U = RI(2.5 + 0.92H - 1.1h + 132/b), \quad (2.15)$$

where R is the electrical resistivity, in $\Omega \cdot \text{sm}$; I is the current density, in A/sm^2 ; H is the height of the block, in sm ; and b , h are the width and height, respectively, of the slot, in sm .

In general, it is possible to say that an electrical resistance of 30–40 $\text{mk}\Omega \cdot \text{sm}$ (typical for anthracitic graphitic blocks with 30 % graphite) corresponds to a power consumption of 230–262 kWh/t ., an electrical resistance of 20 $\text{mk}\Omega \cdot \text{sm}$ (typical for

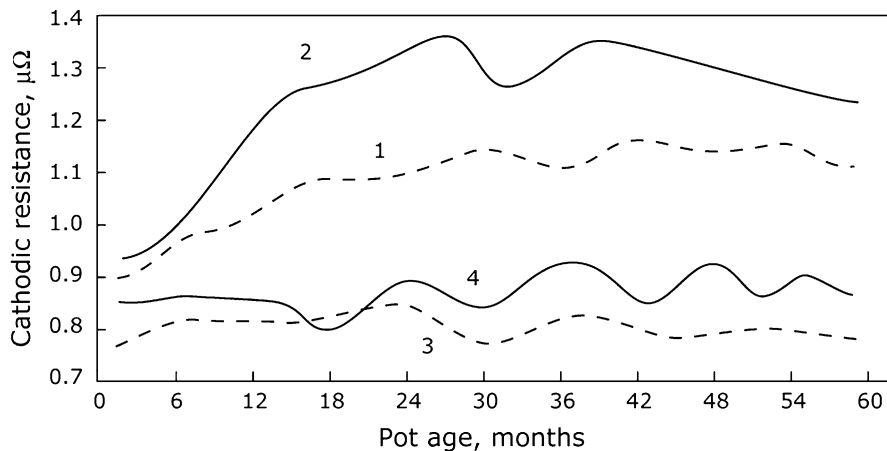


Fig. 2.34 The time dependencies of electrical resistivity of different grades of carbon cathode blocks during the service in reduction cells according to [20]

graphitic blocks) corresponds to a power consumption of 130 kWh/t, and an electrical resistance of $10 \text{ m}\Omega \cdot \text{sm}$ (typical for graphitized blocks) corresponds to a power consumption of 65 kWh/t (Fig. 2.34).

According to ISO 11713-2000 [21] and ASTM C611 [22], the electrical resistivity is measured on samples cut off from the carbon block in a parallel direction and in a normal direction. Also, the electrical resistance is measured on blocks by the contact method on every block at checkout control before storage.

The thermal conductivity of graphite decreases with temperature growth, and the temperature dependence of an anthracite block is low (Table 2.4). Graphitization leads to an increase of the thermal conductivity. Yet all these dependencies have more academic interest, because when infiltrated with bath, anthracitic graphitic and graphitized materials have a thermal conductivity that is increased several times.

A sodium expansion test is a method of determining the linear expansion of carbon from the intercalation of sodium atoms in the crystal lattice of carbon at reduction. The radius of a sodium atom is sufficiently bigger than the distance between the interlayers of carbon atoms, and this causes an expansion on both micro and macro scales. Sodium swelling is a phenomenological characteristic. It is comparative. But it is a starting point for engineering calculations. The sodium swelling test lasts 1.5 h. During the test, fluorine salts totally impregnate the carbon sample; the intercalation of sodium is probably also finished in the entire volume of material. In reduction cells, fluorine salts may reach the lower edge of the bottom block within 1–2 weeks, but they also may reach it within several months. We do not have extensive, verified data on the kinetics of intercalation at service.

In anthracitic graphitic carbon blocks with 30 % graphite, linear expansion due to sodium swelling may be up to 0.7 %, which corresponds to 3 sm for a block 3.5 m

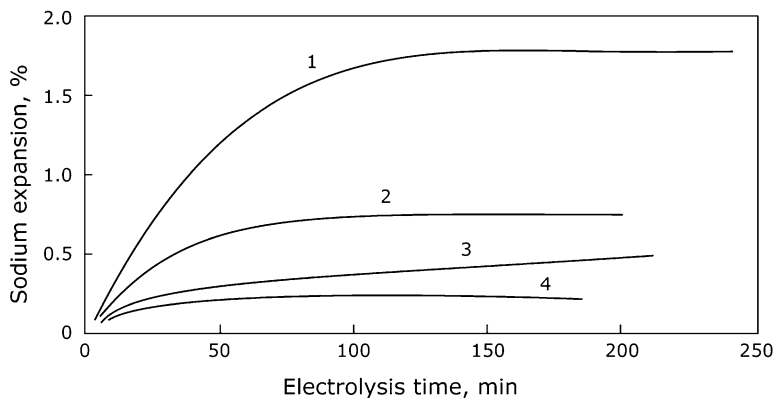


Fig. 2.35 Sodium swelling test: (1)—anthracitic graphitic; (2)—graphitic; (3, 4)—graphitized according to [25]

in length. The strains and micro cracking may take place due to this expansion, and the bending of the block may also take place. This may lead to the appearance of cracks, through which cryolite (and then Al) penetrates to the bottom of the cathode.

There are two modifications of the sodium swelling test ISO/WD 15379-1.2) [23, 24]: with and without pressure. In both variants, negative potential is applied to the test sample of the cathode carbon block that is dipped in cryolite and aluminium in the vessel while the vessel is in the furnace.

The test sample is a cathode in this electrolytic cell. In the variant of testing without pressure, the change of the dimensions of the test sample is recorded (Fig. 2.35), beginning from the start of the electrolysis process in this cell. In the variant with pressure, the change of dimensions is recorded on the compressed test sample. The differences in the values of sodium swelling with and without pressure are considerable: There is no direct correlation between the values of swelling with and without pressure; the average difference in values is about 0.1–0.15 %.

Additional research on the kinetics of sodium intercalation in a carbon lattice together with information on the rate of capillary movement of the melt in permeable pores in carbon will likely give information about the interaction of carbon with cryolite, and these tests will be improved. Sodium swelling depends on the cryolite ratio as well as on the direction of pressing of blocks, but the most important thing for the producer of carbon blocks (that doesn't depend on producer) is that sodium swelling strongly depends on the material of the block—it is low for graphitized blocks and considerably higher for anthracitic graphitic blocks (Fig. 2.35).

Mechanical properties of carbon cathode blocks are the crushing strength (CCS) [26, 27], bending or flexural strength according to ISO 12986-1, ISO 12986-2, ASTM C651, DIN 51944-1999, and DIN 51902-1997 [28–32], and elastic modulus according to ASTM C747, ASTM C1025, and DIN 51915-97 [33–35].

The strength properties are determined at ambient temperature, but the samples are taken in directions normal and parallel to the directions of pressing at fabrication.

Strength characteristics of carbon materials almost do not depend on temperature—at least at temperatures of Al reduction, so the temperature dependence of strength for carbon cathode materials more likely has academic interest. It is well known that the static elastic modulus (determined at mechanical testing) is sufficiently lower compared with values obtained via ultrasonic methods.

Producers of carbon cathode blocks try to lower the compression strength, bending strength, and elastic modulus in order not to overtemper the material, knowing that overtempering may lead to cracking. From the view point of thermal shock resistance, the elastic modulus (as well as linear expansion) should be low, while the thermal conductivity should be high. Currently, customers require many mechanical properties of carbon cathode blocks, while most of them are found empirically.

Carbon cathode blocks are brittle (although from an academic point of view, carbon cathode blocks demonstrate an elastoplastic behavior [36]). According to Panov [36], the fracture toughness of carbon cathode blocks is only $0.15 \text{ MPa} \cdot \text{m}^{1.5}$. Allard [37] gives values of $0.3\text{--}1 \text{ MPa} \cdot \text{m}^{1.5}$ for anthracitic graphitic blocks, with a tendency to decrease in the case of graphitic materials. The critical crack initiation stress and critical crack propagation stress are not determined, causing customers and producers to base specifications on empirical knowledge. It is likely in the future that it will be useful to include the fracture toughness K_{1C} Eq. (1.19) in the specifications. For research purposes, the energy of crack initiation and the energy of the crack propagation might be useful, while forecasting the service life of the cell and the slow crack growth might be essential.

On the contrary, there is almost no degradation in strength characteristics at high temperatures [17], and the strength itself is not a limiting property at service; usually, cathode blocks disintegrate due to the appearance of cracks. However, we feel dubious declaring that an optimal complex of thermomechanical properties for carbon cathode blocks—leading to estimation and direct calculation of service life—is known.

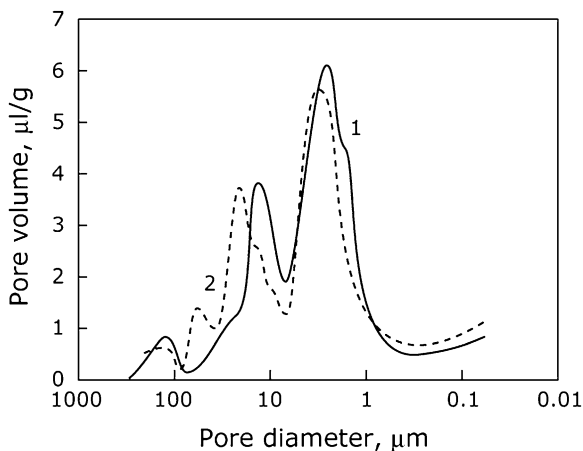
Although there is no direct proportionality, the thermal conductivity for carbon cathode blocks follows electrical conductivity, which has a priority. For design purposes, the high thermal conductivity of a carbon cathode block may be compensated by the low thermal conductivity of heat insulation materials.

As the thermal conductivity of carbon is high, it is difficult or impossible to measure it by static methods, so the comparative ISO 12987-2003 [38] dynamic method is used (measurement in normal and in parallel directions). The knowledge of thermal conductivity temperature dependence is of limited value, because the change in thermal conductivity due to infiltration by electrolyte is sufficiently bigger.

The linear expansion is measured according to DIN 51909-2009 [39] (measurement in normal and parallel directions) and ISO 14420 [40].

The porosity of carbon cathode blocks should be low, the pore size distribution should be uniform, and the percentage of permeable porosity (which is calculated upon permeability) should be low. These requirements are based on the necessity to

Fig. 2.36 Pore size distributions in carbon cathode antracitic graphitic (30 % graphite) blocks of different producers, having open porosity below 20 %



diminish the bath penetration through the cathode block to the refractory level. Figure 2.36 gives an example of different pore size distributions in the carbon cathode blocks of different producers. The open porosity in all these blocks was in the range of 20 %.

There has been information [41] that the considerable number of shutdowns of cells may be connected with the large number of big pores and cavities in the rammed peripheral seam through which a considerable amount of the liquid bath penetrated during the startup period.

It is considered that pores of 1–10 μm are in the nature of carbon materials, while pores of 15–100 μm are due to the peculiarities of technology. Big pores greatly increase the value of the gas permeability, and a large gas permeability is typical for the materials with an irregular pore size distribution. The total porosity and open porosity for carbon blocks of two different producers may be similar, but the values of the gas permeability may differ by a factor as large as 10. In the best samples of the blocks, the porosity is monomodal, though a bimodal pore size distribution is more typical (Fig. 1.5). Sometimes it is possible to see an irregular pore size distribution with pore sizes ranging from 5 μm up to 100–130 μm . In the future, the average pore size in carbon cathode blocks should probably be limited to 10–15 μm , while the permeability should be limited to 0.3–0.4 μm^2 (3–4 nPm or 3–4 μdarcy).

The apparent density gives information on the ratio of the space occupied by pores and not directly points on the graphite content (for a certain porosity), while the true density gives information on the level of the calcination of anthracite and the graphitization in graphitic materials. Some producers of carbon cathode blocks use the apparent density as an industrial parameter; it is determined by weighing after baking (not waiting for mechanical grinding and sampling for lab testing procedure before storage). The apparent density is determined according to ISO 12985-1,2 [42, 43], DIN 51918-1999 [44], and ASTM C559 [45], the porosity is determined according to ISO 12985-2 [43], ASTM C1039 [46], and DIN 51913-2001 [47], while the true density is determined according to ISO 9088-1997 [48],

Table 2.7 Information on grades of carbon cathode blocks from different papers and books

Grade of carbon cathode material	Resistivity, $\mu\Omega \cdot m$	Sodium expansion, %	Wear resistance	Strength	Comments on transformations during service
Anthracitic graphitic (30 % graphite)	30–40	0.7	High	CCS 30–45 MPa, moderate fracture toughness	Anthracite partially transforms into graphite, porosity increases
Anthracitic graphitic (75–80 % graphite)	25	0.4–0.5	Relatively high	CCS 25–35 Mpa	
Graphitic (100 % graphite, coke binder)	18–25	0.25	Moderate	CCS 20–25 MPa	
Graphitized	11–13	0.1	Low	CCS 20–25 MPa, fracture toughness very low	Electrical resistivity slightly decrease
Graphitized impregnated	10–12	0.1	Rather low	CCS 30–35 MPa, fracture toughness low	

ISO 21687 [49], and DIN 51913-2001 [47]. The standards for determining the gas (air) permeability (ISO 15906 [50]) and pore size distribution are valid for carbon and refractory materials and are described in Sect. 1.2.

The ash content shows the amount of admixtures in carbon materials. For carbon materials, ash is oxides of sodium, potassium, calcium, and iron. For specialists in refractory materials, it is strange to unite these oxides in one group and call it one word—ash. Still, if the ash content is within certain limits, it influences only the thermal and electrical conductivities. The ash content is determined according to DIN 51903 [51] and ISO 8005 [52].

2.3.5 Some Words on Grades of Carbon Cathode Blocks

The question of which grade of carbon cathode blocks to use when designing a reduction cell does not involve making just one decision. There are many pro and cons; there are many properties that change during the service life that are necessary to take into account. The general tendency is to install graphitic or graphitized carbon cathode blocks.

Professor Øye [17] gives the data from Wilkening [53], Table 2.7, with two main characteristics that strongly depend on the grade of the carbon block: sodium

swelling and electrical resistivity. An additional characteristic that it is probably necessary to include is wear resistance.

It is necessary to remember that sodium swelling is an irreversible process that takes place at the beginning of startup and service life without any continuation (if not to mention mechanical tensions), and the electrical resistivity changes during the service life, but it is not only the electrical resistivity's influence on cathode drop that finally influences the energy consumption of the reduction cell at service.

On the contrary, sodium swelling locks all gaps, cavities, and poor joints in the lining, preventing leakage of electrolyte in the lining. Sometimes on smelters after retrofit and changing the cathode carbon blocks for a higher grade, problems with leakage appear.

An uninvestigated problem of the graphitization of anthracite in blocks at service in the presence of sodium (which we will discuss later) has two practical consequences:

- The graphitization promotes stable electrical characteristics of semigraphitic blocks at service (due to the possible increase in electrical conductivity).
- The transformation of anthracite to graphite goes with a negative volume effect, increasing the porosity and possibly increasing the dimensions of permeable pores and the capillary flow of electrolyte to the refractory lining.

There is information that the service life of cells with graphitized cathode bottom blocks decreases by 15–20 %, and there are no proven data on the increase or decrease of the service life of cells with impregnated graphitized blocks.

As we recall, the cathode voltage drop depends not only on the electrical resistivity of the carbon block, but also on the cathode—collector steel bar connection.

The question of how to choose the grade of carbon cathode blocks depends on the forecasted power losses due to the voltage drop, the local economic situation, and the price of electricity.

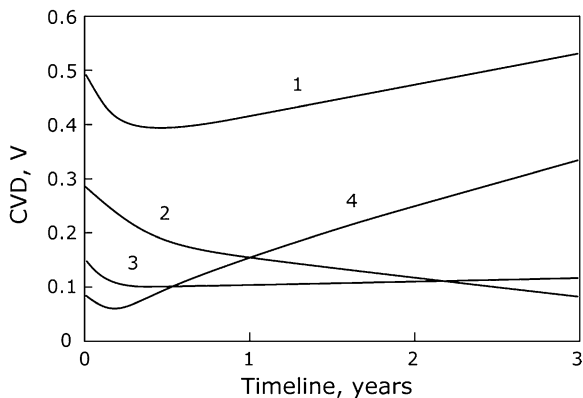
In [54], the cathode voltage drop at 350-kA cells at graphitized blocks is 220 mV, while the blocks with 75 % graphite provide 284 mV.

As we've mentioned already, there is no single technical decision on the best variant of grades of carbon cathode blocks; when working out the design of the cell, it is necessary to find an optimal compromise of properties, taking into account not only the permanently changing technical parameters, but also the economic situation and the prices for electricity in the region. However, it is necessary to consider that the energy consumption of the cell would increase not only due to the voltage cathode drop, but also due to the voltage drop in the connection “block—steel collector bar” [55] (Fig. 2.37).

According to Panov [36], the voltage drop in the joint “carbon cathode block—steel collector bar” for a cast-iron connection is 10–15 times lower compared with the cathode voltage drop in a rammed or sealed connection.

Usually when there is demand to increase the production of Al, the standard decision is to increase the current of the cells, which requires changing anthracitic

Fig. 2.37 Components of cathode voltage drop, changing with service time according to [55]



graphitic blocks for graphitic or graphitized and modernizing the cell construction, including the lining.

We won't go into details, but we can say that the grade of the carbon cathode blocks doesn't influence the current efficiency of the reduction process, but it seriously influences the energy consumption and may have an influence on the service life.

2.3.6 Some Words on the Structure of Carbon Cathode Blocks in Connection with Grain Size Composition, Sintering, and Pore Size Structure

The grain size composition of the mix is coarse. The typical grain size composition of raw materials for the production of carbon cathode blocks (calcined anthracite, graphite, or coke) consists of three (and rarely four) grain fractions. The coarse fraction is 10–5 mm, the fine fraction is less than 0.075 mm, and the medium fraction is 5–0.5 mm.

For a long time, the standard problem for the specialist in the technology of refractory materials was to obtain the minimum possible porosity of the green shape, which opened the possibility to obtain the minimum possible porosity in fired refractory material.

Well-known equations of optimal amounts of grain size fractions [56–60] are a help for the specialist to obtain the desired low porosity:

$$Q_i = (d_i/d_{\max})^n \times 100, \quad (2.16)$$

$$Q_i = (d_i^n - d_{\min}^n) / (d_{\max}^n - d_{\min}^n) \times 100, \quad (2.17)$$

$$Q_i = [\alpha + (1 - \alpha) (d_i/d_{\max}^n)] \times 100, \quad (2.18)$$

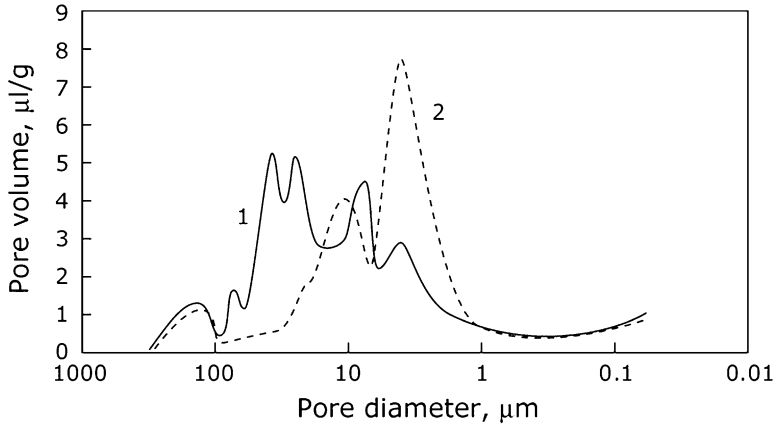


Fig. 2.38 Pore size distributions in carbon cathode blocks, produced on one and the same carbon plant with a 1-year time shift

where Q_i is the amount of a certain grain fraction, d_i is the volume-weighted diameter of the grain fraction, d_{\max} and d_{\min} are the maximum and minimum grain size dimensions, respectively, n is the coefficient of shape (0.3–0.6), and α is a coefficient that accounts for additional quantities of fine fractions.

These equations do not take into account the size of pores, and a direct aim to diminish the open porosity below the requirements of the customer from an aluminium smelter may lead to a large variety in pore size distributions (Fig. 2.38). The gas permeability of these blocks may also vary considerably.

Later we will discuss the influence of the pore size of permeable pores in cathode blocks on infiltration. Here we will say only that today the specialist in refractory technology usually solves not only the problem of how to diminish the porosity, but rather frequently also that of how to diminish the pore size of permeable pores.

In conventional refractory materials, the porosity of the green shape diminishes during firing in the course of the sintering process. In coarse-grained carbon materials, during the firing process the grain structure remains almost unchanged. The only exception is that during carburization the pitch transforms into coke. About 20 % of the pitch in the pressing mix transforms into approximately 10 % coke in the fired material, with particles of coke being below 0.075 mm. The porosity of the green shape during firing is slightly increased. Thus, in large part, the porosity size of fired carbon material is governed by the porosity size distribution of the green shape.

The porosity size distribution of the green shape is formed by the shape of grains; between the big grains are the pores of large sizes. Between the small grains are the pores of small sizes. Hence, to obtain a pore size structure with a more or less narrow and small size distribution, it necessary for the grains of small sizes to form a continuous matrix.

Now we present the results of some trials.

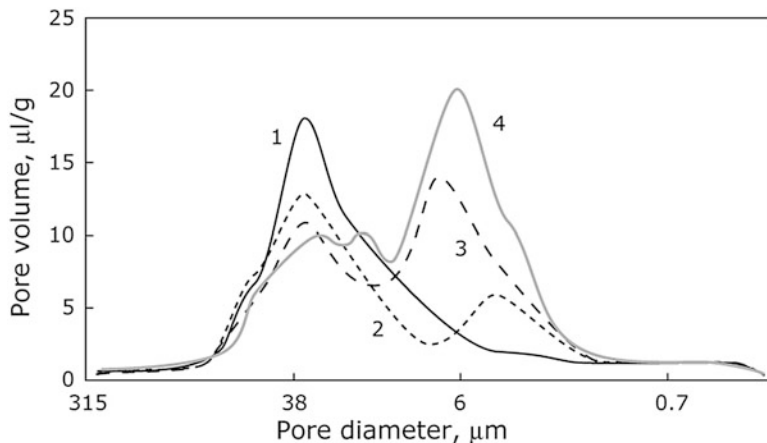


Fig. 2.39 Pore size distribution in carbon materials with changing amount of fine (<0.075-mm) fraction: (1) 15 %; (2) 30 %; (3) 40 %; (4) 60 % [61]

Three grades of grain size compositions with sizes 5–10 mm, 0.5–5 mm, and below 0.5 mm (80 % were below 0.075 mm) were investigated, and the only variable was a changing amount of fine fraction [61]. It was considered that the coarse fractions form the frame of the structure, while the fine fraction fills in the cavities in the frame. On filling in the cavities in the frame, it was possible to follow the change of the frame structure to a matrix structure when the coarse particles do not contact each other but only fine particles have contact. The amounts of the fine-grained fraction were 15 %, 30 %, 40 %, and 60 % in the trials.

The properties of fired material correspond either to properties of the frame or to properties of the matrix. With a fine fraction of 15 %, all pores were larger than 25 μm ; the same result (not shown) was seen at two grain size compositions without a fine fraction. The addition of a 30 % fine fraction leads to the appearance of pores with dimension 3–5 μm . However, the considerable decrease in pores above 25 μm and the increase in fine pores of 3–5 μm take place only upon the addition of 40 % and 60 % fine fraction of carbon material (Fig. 2.39). The properties of the material also change (Table 2.8).

The matrix structure gives an increase in electrical as well as thermal conductivity. We would like to note that upon addition of 60 % fine fraction, the porosity of the fired material increased by 5 %, so from the viewpoint of minimal porosity, the grain size composition is not optimal. Note also that this was a result of laboratory research. An excessive amount of fines creates considerable problems with the mixing of grain size composition with pitch and gives other technological problems. The implementation of such laboratory studies also creates some problems, though solvable.

The pore structure of the industrial grain size composition was bimodal: There were pores with average dimension 5 μm and 100 μm . After the fine fraction was increased to 40 %, the total and open porosities remained approximately the same,

Table 2.8 Influence of fine fraction (<0.075 mm) on properties of carbon materials [61]

Amount of fraction <0.075 mm, %	Specific surface area, sm^2/g	CCS, MPa	Apparent density, of green shapes, g/sm^3	Apparent density of fired materials, g/sm^3	Electrical resistivity, $\text{mk}\Omega \cdot \text{m}$	Thermal conductivity, $\text{W}/\text{m} \cdot \text{K}$	Shrinkage at firing, %	Total porosity, %
15	473	5.7	1.38	1.27	266.4	0.44	0.14	27.4
30	844	24.2	1.46	1.38	100.2	0.97	0.13	21.1
40	1092	33.3	1.51	1.39	78.3	2.09	0.20	20.6
60	1590	31.3	1.55	1.31	74.8	1.25	0.27	25.1

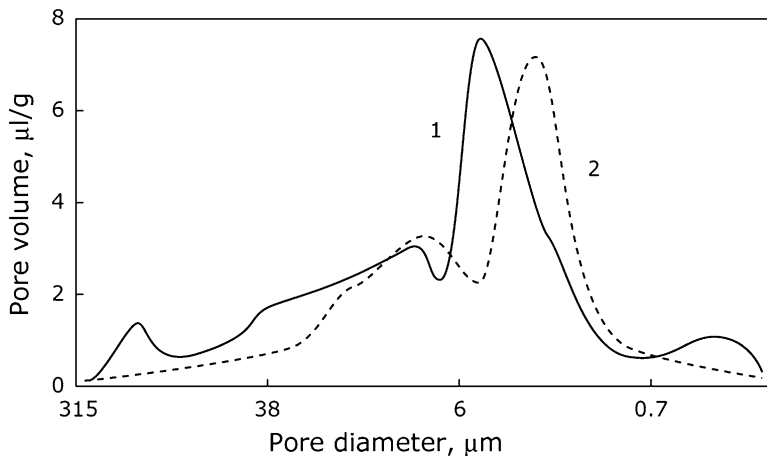


Fig. 2.40 Pore size distribution in industrial carbon materials (1) before and (2) after fines are increased to 40 % [61]

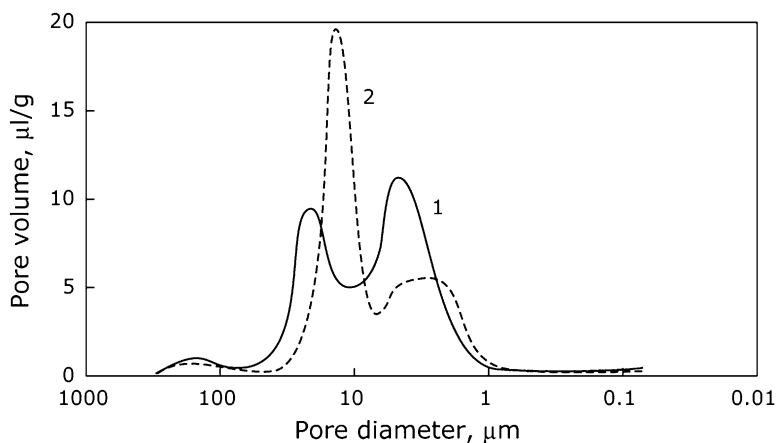


Fig. 2.41 Pore size distributions in carbon compositions: 5–10 mm—40 %, 0.5–5 mm—20 %, <0.075 mm—40 %, having amount of pitch (2)—18 %; (1)—24 %. [61–63]

but the 100- μm pores were eliminated (some changes in the form and shape of other pores were also seen) (Fig. 2.40).

The amount of binder (pitch) may also influence the pore size distribution. A large amount of pitch promotes better filling of cavities in the frame by fine particles, but at the same time the volume of carburizing gases increases, giving a larger amount of relatively big pores (Fig. 2.41).



Fig. 2.42 Cracking of the carbon cathode block in the angles of the slot

2.3.7 Interaction of Carbon Cathode Blocks with the Steel Shell and the Collector Bars. Cracks Induced by Thermal Strains and Thermal Shock

The shape of the slots in the carbon cathode blocks may differ (Figs. 2.17 and 2.19); a two-slot design of the blocks (Fig. 2.17b) is typical for high-capacity cells. The rectangular collector bars are adjusted in the *slots*. These collector bars are the conductors for the negative electric potential on the blocks. The collector bars are adjusted in the slots by cast iron, contact carbon pastes, or carbon glues. All methods of *adjustment* of collector bars in carbon blocks have advantages and disadvantages, and currently there is no strict preference among aluminium producers. Casting gives proof of contact between collector bars and carbon, but there is a risk of cracking in the angles of the slot (Fig. 2.42) due to thermal shock. Special furnaces for the preheating of the block and the collector bars before casting diminish the possibility of cracking.

There is no cracking with carbon glues and contact carbon pastes, but such contacts give a voltage drop that will increase with time.

Cracking in carbon cathode blocks may take place during preheating and startup, but more frequently, cracks in carbon blocks reach the surface at service. The main reason for cracks appearing in carbon cathode blocks is mechanical tensions due to interaction with the shell (via siding and peripheral seam) and with refractory layers, but, of course, inner defects, such as cavities and inner cracks, may dramatically enhance the appearance of cracks on the surface. Cracks reaching the service of cathode blocks within the first 3 years of service are mostly disliked at smelters, because they cause the service life at the smelter in general to diminish considerably. However, during the service life, a sort of a balance exists between the tensions in the blocks and mechanical strains between the shell and the blocks, and there are many thin cracks in the blocks that are not filled by bath or aluminium (Fig. 2.43).

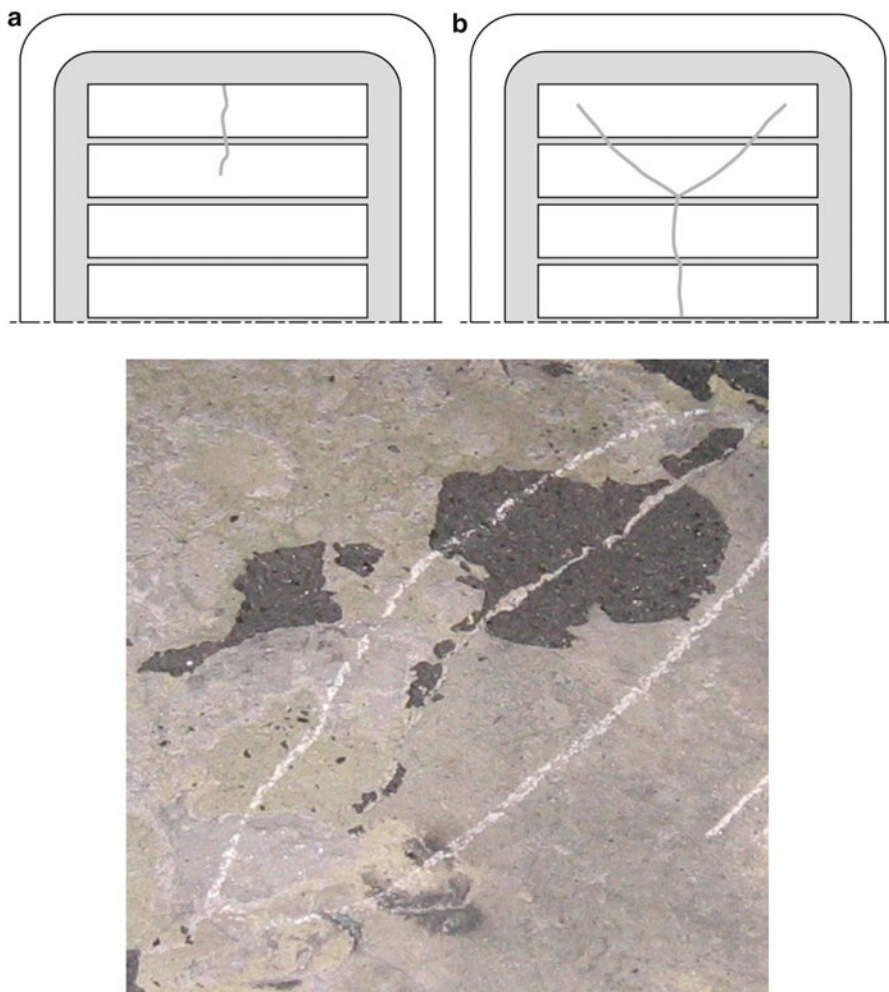


Fig. 2.43 Cracks in the carbon blocks in the end of the cell

Computer simulations of the mechanical behavior of carbon cathode blocks and the mechanical interaction between the carbon blocks and the shell and lining have not been completed. The design of a cathode for the Hall–Heroult process is still in development, and new cell designs will most likely appear within the next 10–20 years. Although not frequent, the sudden shutdowns of cells still take place, and so analytical and research efforts are still required in this direction (Fig. 2.44).

Cracks induced by thermal strains and thermal shock.

As we recall, the temperature gradients in carbon cathode blocks at preheating and in the moment of pouring electrolyte may reach $300\text{--}1,100^\circ/\text{m}$ at the surface of cathode blocks and up to $1,500^\circ/\text{m}$ in the direction from the surface to the refractory layer. Estimations show (Table 2.9)

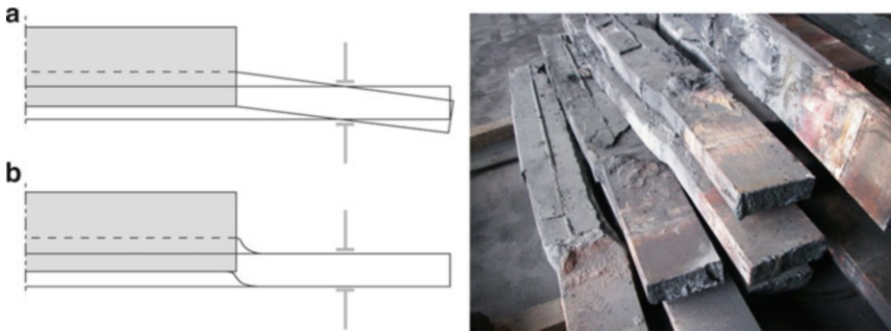


Fig. 2.44 Bus bar with slope

$$\sigma = \alpha E \Delta T / (1 - \mu), \tag{2.19}$$

where σ is the strain, E is the elastic modulus, ΔT is the temperature gradient, and μ is Poisson's ratio.

The possible stresses in cathode blocks due to thermal gradients may be comparable with the bending strength of the blocks.

The first Hasselman criterion [65],

$$R = \sigma E / \mu \Delta T, \tag{2.20}$$

has a physical meaning of maximum temperature gradient per meter, giving the possibility for the crack not to appear. The values of the calculated criterion are close to the values estimated above: 300–1,100°/m at the surface of cathode blocks and up to 1,500°/m in the direction from the surface to the refractory layer, which gives additional evidence that the thermal strains at preheating and startup may be responsible for the initiation of cracks in carbon cathode blocks. Durand [66] gives the value for the first criterion of thermal shock resistance, 1,290°/m.

Usually, there are no visual cracks in cathode blocks at startup. But this doesn't mean that these cracks (pre cracks) are not formed inside the blocks. The strains are quite sufficient for the formation of pre cracks of subcritical dimensions. According to the slow crack growth model [67], the strains for the slow propagation of cracks are lower than strains for initiating the cracks. Usually, thermal strain cracks reach the surface of cathode blocks, and the distance between them is 80–100 sm (Fig. 2.45). Normally, they are parallel to each other and normal to the surface of the cathode. However, it is necessary to remember that these cracks reach the surface after 6–36 months although it is most likely that they appear during preheating and startup.

In service, the carbon cathode blocks are in a stress–strain state. From the viewpoint of fracture mechanics, overheating by 50° or increasing the current

Table 2.9 Properties, thermomechanical strains at preheating and startup, and calculated values of first Hasselman criterion of thermal shock resistance in carbon cathode blocks of different producers [63, 64]

Plant	Bending strength, MPa	Cold crushing strength, MPa	Elastic modulus (static), GPa	Elastic modulus (dynamic), GPa	Thermal coefficient of linear expansion $\times 10^{-6}$, degree ⁻¹	Thermomechanical strains, MPa	R' , degree
1	13.5	45	3.8	12	3.1	11.0	922
2	13.5	39	3	10	3.9	10.9	750
3	12.2	34	2.6	8.5	2.6	6.3	1,150
4	11	35	3.3	10	2.9	8.9	905
5	10	33.5	2	7.6	3.1	5.8	1,086
6	11	39.8	2.7	8.2	3.2	8.1	1,128
7	10	33.2	2.4	8	3.4	7.6	864
8	13.4	39.5	2.7	8	3.6	9.1	1,032

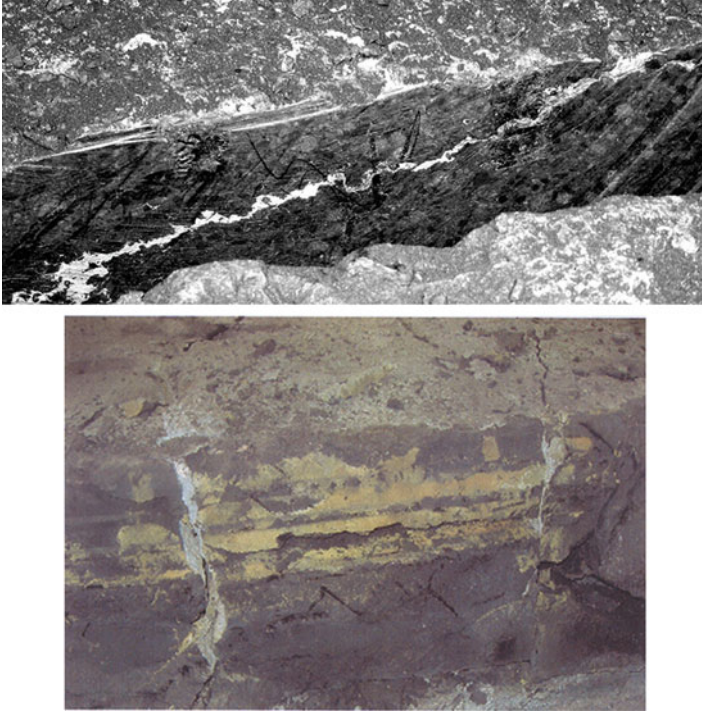


Fig. 2.45 Cracks in cathode blocks

density by 0.1 A/sm^2 shouldn't be critical for the start of the crack. Additional stress upon overheating 50° is sufficiently lower compared with strain, causing fracture. However, this overheating may be critical for the following:

- stress of crack propagation;
- slow crack growth rate, especially in a nonequilibrium stress–strain state.

This assumption may be proved by industrial experience [62] showing that the temperature changes of electrolyte at the startup period, fluctuations in the cryolite ratio and in the level of metal and electrolyte, and all uncontrolled deviations of processing negatively affect the service life (Fig. 2.45, 2.46).

Returning back to thermal shock resistance, it is possible to state [63, 64] that anthracitic graphitic carbon blocks with electrically calcined anthracite have larger values of Hasselman criteria compared with carbon blocks from gas-calcined anthracite. This has some connection with the percentage of shutdowns of the cells. The reason for this is in the looser structure of electrically calcined anthracite, resulting in a lower strength and a lower value of elastic modulus of cathode blocks. Such materials may absorb strains and restrain the crack development, which plays a positive role in thermal shock resistance (Fig. 2.46).

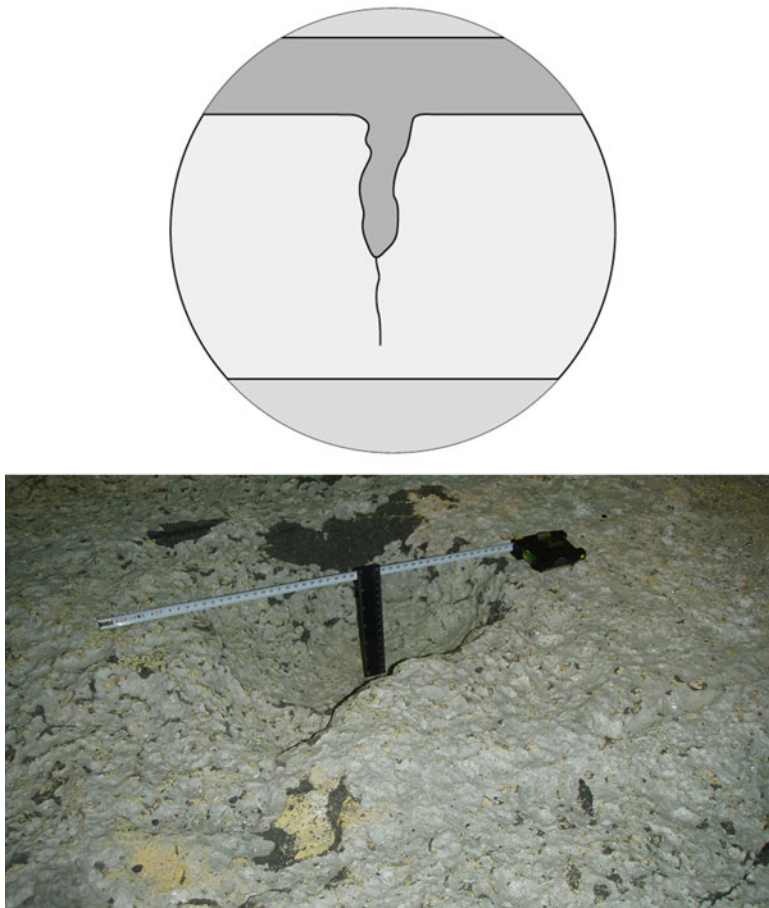


Fig. 2.46 Cavities in blocks, probably originating from small cracks

2.3.8 Interaction of Carbon Cathode Blocks with Electrolyte During Startup and in Service: Wear. Infiltration

There are two main variants for sodium to reach the barrier refractory layer of the reduction cell:

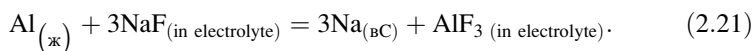
- sodium diffusion in the carbon lattice;
- capillary flow of electrolyte through permeable pores of carbon cathode blocks and rammed carbon of ramming paste.

It appears that one of the consequences of both processes is the graphitization of anthracite (and coke) in anthracitic graphitic blocks.

Table 2.10 Sodium saturation level in carbon cathode materials according to [73]

Grade of carbon cathode material	Na saturation, wt. %	Na saturation, kg/m ³
Gas-calcined anthracite	4	60–70
Electrically calcined anthracite	4	60–70
Graphitic	2	30–35
Graphitized (at 2,300 °C)	1	15–20

The initial reaction that leads to the appearance of sodium in carbon cathode blocks is



Sodium may exit the carbon lattice in the form of intercalation compounds, such as NaC₆₄ [68, 69].

The main mechanism of the propagation of sodium in carbon is thought to be the diffusion in the carbon lattice [70, 71] although there has been a suggestion it's the propagation of sodium in the lattice in vapor state [72]. The reported values of diffusion coefficients [73] currently are more likely to have academic interest, and the reported values differ, more likely due to different conditions, current, cryolite ratio, and other factors.

The levels of sodium saturation are reported in [73] and give a good understanding of the amount of sodium in carbon cathode blocks at service (Table 2.10).

Sodium diffusion after saturation should be permanent and may stop at the leveling of sodium concentrations in the upper and lower surfaces of carbon block, which appears to be some sort of barrier (or probably would not in case of activation by current). Of course, the sodium penetration should depend on the CR and current density.

Reaction (2.16) may proceed not only on the upper surface of blocks, but also on the surfaces of pores inside the block. Other reactions [17] of sodium-containing substances with carbon may take place, resulting in the formation of sodium aluminates, aluminium carbide, aluminium nitride, and sodium cyanide in the volume of carbon cathode blocks.

The “dry” penetration of sodium to the refractory layers due to the diffusion of sodium through carbon cathode blocks really should be taken into account. The consequence of such diffusion is the appearance of free silicon in the form of balls of ore drops or globules, having a diameter from 1 to 4 sm, which appear due to the reaction of sodium with silica or silica-containing compounds. However, the “dry” penetration of sodium doesn't seriously deteriorate the refractory lining, which cannot be said about “wet” penetration or the capillary flow of electrolyte through permeable pores of carbon cathode blocks and rammed carbon of ramming paste.

The Transformations in Carbon Cathode Blocks During the Service Life

Liquid electrolyte penetrates the carbon cathode blocks through permeable pores, sodium intercalates in the lattice of carbon, and amorphous carbon undergoes graphitization. All these processes increase the electrical and thermal conductivities.

The details of the graphitization process are unknown. One belief is that sodium itself cannot be a catalyst of graphitization at temperatures below 1,000 °C, and the graphitization proceeds via the formation of carbides with their subsequent decomposition [17, 74]. According to [75], the anthracitic carbon block after 1 year of service contained 25 % graphite. After 2 years of service, the rate of graphitization becomes stabilized [76] or diminishes [77]. The density of graphite is 2.15–2.25 g/sm³, while the density of anthracite is at the level of 1.7–1.86 g/sm³. The volume effect of graphitization in negative and equals

$$\Delta V/V = 77-83\%. \quad (2.22)$$

So the graphitization of anthracitic or semigraphitic blocks is followed by the increase in the pore volume, whereas the pores are filled in with bath. The process of graphitization may also be followed by the fracture of coke bridges between the grains of graphite and anthracite, which in a pessimistic variant may cause cracking.

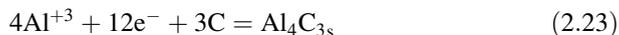
After several years of service, the anthracitic block has an electrical conductivity similar to the electrical conductivity of a semigraphitic block with 30–50 % graphite, yet it will never have the electrical conductivity of a graphitic block [78–80]. According to lab tests, there is no degradation of the electrical conductivity of graphitized blocks, while the degradation of semigraphitic blocks is lower compared with graphitic blocks (Table 2.5).

Formation of Aluminium Carbide. Chemical Erosion Mechanism of the Wear of Cathode Blocks. Wear and Erosion Tests

The hardness of graphitized and graphitic materials is sufficiently lower compared with anthracitic graphitic materials; consequently, the wear resistance of graphitic materials is also sufficiently lower. The wear resistance of anthracitic graphitic blocks under the influence of abrasive and erosion wear by alumina particles in the electrolyte is not critical or almost not critical for the service life of cells, while the wear resistance of graphitic and graphitized blocks is critical. Wear resistance testing of carbon cathode blocks became essential. There were several approaches to erosion testing of carbon cathode blocks, beginning with early investigations of the wear resistance of carbon cathode material in a water slurry of alumina [81].

According to Prof. Øye [17], the current understanding is that the wear of carbon cathode blocks is mainly the process of the formation of aluminium carbide,

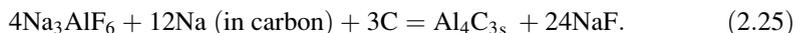
The reaction between aluminium and carbon is possible from the viewpoint of thermodynamics within all ranges of temperatures in the cell [17]:



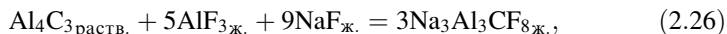
and



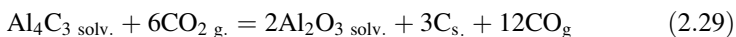
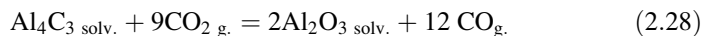
Also, the formation of aluminium carbide due to reaction (2.17) may be shown as



The formation of aluminium carbide does not lead to the degradation of carbon materials. The light yellow film of aluminium carbide is formed on the surface of the cathode, reaches a certain thickness, and starts acting as a barrier. However, the solubility of aluminium carbide in aluminium is several orders of magnitude lower compared with the solubility of aluminium carbide in electrolyte [17]. The cryolite film and alumina act together and dissolve the protective film of aluminium carbide. Aluminium carbide dissolves in the electrolyte,



and is oxidized at the anode:



Sort of a chain reaction takes place, while the reaction products are moved away from the reaction zone due to the circulation of the bath and aluminium in the cell.

According to [17], this chemical process, for one thing, is almost independent of the quality of carbon material, but, for another, the value of aluminium carbide formation in wear is much stronger than physical wear.

The reactions of the formation of aluminium carbide may take place on the surface and at the internal surface of pores inside the cathode block. The reaction takes place with positive volume effect, so the formation of aluminium carbide in the pores may follow the mechanical tensions and even cracking due to these tensions. The probability of the reaction increases as the level of graphitization decreases.



Fig. 2.47 Aluminium carbide in the crack in carbon cathode block

Lab investigations have shown [17] the following:

- The wear rate by electrolysis increases with as the current density increases, but levels off at current densities above 0.8 A/cm^2 .
- Electrochemical wear is much higher than physical wear and is the same for graphitic and anthracitic materials.
- The presence of alumina slurry suppresses the electrochemical wear.
- The physical wear rate increases strongly with velocity and increased concentration of an alumina slurry.
- The physical wear rate of graphite is about five times the physical wear rate of anthracitic carbon.
- The physical wear ratio graphite/anthracite is about the same in room-temperature abrasion tests and in cryolitic melts.
- The mechanisms of wear in industrial cells are a combination of physical and chemical wear in spite of the fact that the physical wear is much smaller.

Industrial investigations, initiated by industrial experience on the implementation on graphitic and graphitized carbon blocks, have revealed several dependencies.

Industrial practice gives wear values of about 2.3–3.3 sm/year for graphitized blocks, 1.2–1.7 sm/year for graphitic blocks, and 0.8–2.2 sm/year for anthracitic graphitic blocks (70–85 % graphite) [81, 82]. Probably the best proof for the fact that anthracite-based materials are less subjected to wear is well known to industrial specialists: the profiles of the cathode bottom of graphitized or graphitic blocks with anthracite-based ramming paste (Fig. 2.48). Other publications contain other values of wear [83], which is quite obvious because the wear rate depends on several factors (current, current density, type of a cell, CR, etc.), which are impossible to keep on one level in industrial calls of different constructions.

There is a direct proportionality between the wear rate in industrial conditions and the cathode current density, which may reach 70–80 mm/year [84]. A larger open porosity of graphitized carbon cathode blocks promotes increased wear rates due to the increased formation of aluminium carbide, shown in the lab and at industrial scale [85, 86].

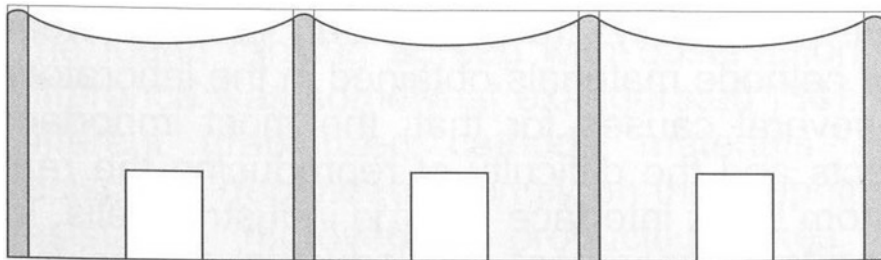


Fig. 2.48 Profile of cathode bottom: graphitic blocks with anthracite-based ramming paste

Erosion increases the wear, and the combined mechanism of chemical wear takes place. Once at the smelter, there is a decision to modernize and to install graphitic or graphitized blocks instead of semigraphitic, and the increased wear takes place. Anthracite is sufficiently harder than graphite. Yet there is no direct proportionality between the wear rates and the graphite content in the blocks [87].

The problem of wear is serious. The profile of cathode wear having a W shape is well known to industrial specialists (Fig. 2.49). Of course, this leads to shortening of the service life.

Special studies aimed at increasing the wear resistance of graphitized and graphitic cathode blocks have begun. Special research was designed to form a gradient structure with different electrical resistivity along the length of the block. Another approach is increasing the resistance to wear. Impregnated graphitized blocks demonstrate higher wear resistance. There have been attempts to increase the wear resistance of graphitized blocks, impregnating the blocks with phenolic resin with additions of zirconium and titanium oxides. On the contrary, a sufficient increase in wear resistance may be achieved on anthracitic graphitic blocks with 80–85 % graphite.

In the publications [87, 88], lab tests give reasonable values of wear of different grades of carbon blocks, which give a more or less similar rating of wear during industrial electrolysis. Lab wear tests are a good instrument for R&D practice of carbon cathode blocks with respect to the reduction process. There is a dependence of wear during lab tests on CR as well as on the cathode density [90, 91]. According to lab testing [17], graphitized cathode blocks demonstrate a wear resistance that is 7–10 times lower compared to anthracitic grades.

A variation of the cathode test with vibration (which imitates the movement of the metal) is combined with lab electrolysis. In Thornstad's variation [92], both electrochemical and abrasion resistance are taken into account. This variant of testing is very complex. The test sample under negative potential is in the alumina crucible with aluminium and the bath with 8 % alumina. The crucible is in the lab furnace, the temperature is increased up to 960 °C, the anode is from tin oxide, and the rotor is from boron nitride. The time of testing is 6 h. The registered parameters are voltage and the CO/CO₂ concentration. After the testing, a visual inspection is carried out, but the wear forecast is made based on the volume of CO/CO₂ output.

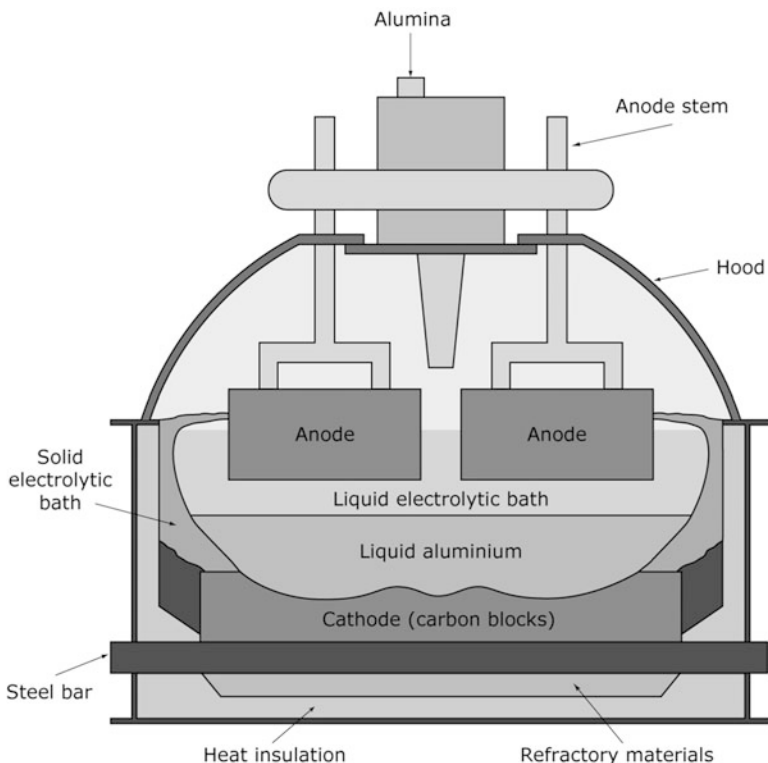


Fig. 2.49 W-shaped profile of cathode bottom from graphitic or graphitized blocks after 3–4 years of service

According to [92], there was a good agreement between the forecasted wear and actual wear in the cells.

The research on increasing the wear resistance required special lab testing that was invented at SINTEF [89, 90]. The test, based on a concept of wear by the electrochemical formation of aluminium carbide, is performed in a lab reduction cell at 980 °C, CR of 2.2, current density of 0.75 A/sm², and rotating speed of 0.6 m/s.

Coatings of carbon cathode blocks may significantly diminish the wear of carbon cathode blocks. The most promising material for coatings is titanium boride although there are other variants.

Infiltration of Electrolyte in the Permeable Pores of Carbon Cathode Blocks

The open porosity of carbon cathode blocks is 14–22 % (in graphitized up to 28 %), and the permeability of carbon cathode blocks is 0.15–0.65 μm². Almost all pores are permeable; some small amount of closed pores may be in anthracite grains

(if anthracite is used for the production), and so open porosity is very close to true porosity—this is the peculiarity of carbon materials.

According to an estimation of Prof. Øye [17], the permeability $0.4 \mu\text{m}^2$ corresponds to an infiltration rate of 3.2 sm/h for a liquid with viscosity 0.1 Pa/s. According to the experiments of Brilloit et al. [93], bath penetrated around 18 mm for 1.5 h at 1,010 °C, CR = 2.25, CD = 0.75 A/cm². Other estimations are in the papers [94–96]. According to Feng [96], electrolyte penetrated from 0.4 to 15 mm for different carbon materials over 1.5 h at 1,000 °C, at the same CR and current density.

Industrial experience gives evidence that sometimes the melt of electrolyte reaches the lower surface of carbon cathode blocks within half a year, but sometimes it reaches the refractory layer within 1–2 weeks. The value of irreversibly spent cryolite at startup for the cell with square about 30 m² is up to 15 t. It looks like there may be constant electrolyte flow through the pores of cathode blocks if some barrier is not formed.

There are several reasons for contradictory data about what time the electrolyte reaches the refractory level [17, 61–64]:

1. Depending on the method of shaping (extrusion or vibro pressing), the raw materials, and the peculiarities of the processing, the porosity of carbon cathode blocks and the pore size distribution may vary.
2. There is always a temperature gradient of 150–400 °C at the surface of the cathode block at the moment of pouring the electrolyte (e.g., 900 °C in the middle and 600 °C at the periphery).
3. The designs of the cells differ, the methods of preheating and the startup differ, and consequently the temperature gradients between the upper and lower surfaces of cathode blocks differ.
4. At different smelters, the CR during startup may be from 2.3 to 4; consequently, the viscosity of electrolyte also differs.

In pores having a small diameter, the interactions between the walls of pores and the liquid are considerable, and the fluid spreads [61]. The main constituents are capillary forces:

$$P_k = \frac{-2\sigma_{El} \cdot \cos \theta}{r_k}, \quad (2.30)$$

where P_k is the capillary pressure, σ_{El} is the surface tension of electrolyte, and θ is the contact wetting angle of carbon by electrolyte.

Capillary pressure is inversely proportional to the pore radius, and the flow of electrolyte in porous media may be considered the flow of viscous liquid in the channels with a small radius. Laminar flow takes place [62], and rate of flow is directly proportional to the square root of time.

Another type of flow is in the pores when the surface of pores is wetted by liquid. According to [62, 63], the viscous friction of liquid influences the type of flow. The flow rate is proportional to time in the power of 0.2–0.3.

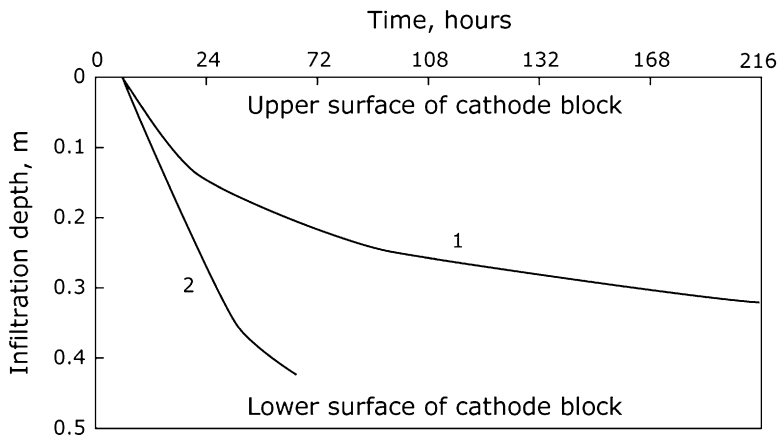


Fig. 2.50 Isothermal regime of electrolyte flow in the porous carbon cathode blocks: 1—flow in permeable pores, with dimension below critical radius (25 μm); 2—flow in permeable pores with dimensions above critical diameter of pores

The existence of the first or second type of flow depends on the balance between capillary forces and external pressure. In porous materials with a bimodal structure, two types of flow may coexist. According to [63], the critical radius of permeable pores, at which one type of flow changes to another, is

$$r_k = \frac{-2\sigma_{EI} \cdot \cos \theta}{g(\rho_{Al} \cdot h_{Al} + \rho_{EI} \cdot h_{EI})}. \quad (2.31)$$

The laminar flow of electrolyte will be in carbon cathode materials with pores greater than 25–30 μm .

Computer simulations [61, 62] have shown two types of flow in the porous structure of carbon blocks in isothermal conditions. Electrolyte will flow in the laminar regime in big pores and cracks with above-critical dimensions down the lower surface of cathode blocks at a speed of 5–7 mm/h. The infiltration of carbon cathode blocks with porosity below the critical diameter proceeds at a speed of 2–2.4 mm/h (Fig. 2.50).

However, at startup, the temperature field in carbon cathode blocks is far from isothermal [62, 63] (Fig. 2.50). The movement of the “crystallization point” of electrolyte at startup takes place at a speed of 4.3–4.6 mm/h (of course, this speed may depend on the type of preheating, startup, CR, and so forth).

The comparison of movements of “point of crystallization” of electrolyte and the speed of penetration of electrolyte show that the latter may be sufficiently faster for pores above the critical diameter (Fig. 2.49). It means that in such a case in nonisothermal conditions (startup), the movement of penetration of electrolyte in big pores will be determined by the movement of the crystallization point. In carbon cathode blocks with pores below the critical dimension, the movement of

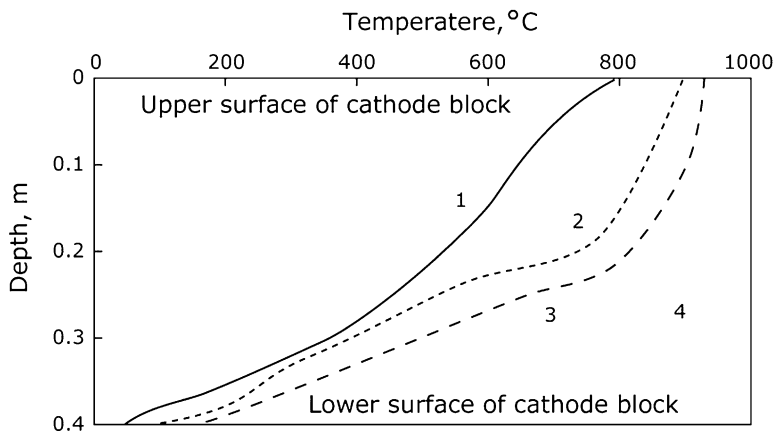


Fig. 2.51 Temperature gradients between the upper and lower surfaces of carbon cathode blocks at startup of reduction cells according to Panov [36]: 1—before pouring electrolyte; 2—after 23 h; 3—after 7-h; 4—after 3 months of operation

electrolyte through pores will be sufficiently slower compared with the movement of the crystallization point. It means that electrolyte may reach the refractory barrier layer though the pores of carbon cathode blocks within several days.

That is probably the answer for various industrial experiences, where sometimes the melt of electrolyte reaches the lower surface of carbon cathode blocks within half a year, but sometimes it reaches the refractory layer within 1–2 weeks.

The calculations showed two types of behavior of electrolyte flow through porous carbon cathode blocks [61–64] at startup:

- In carbon cathode blocks with pores below the critical dimension ($25 \pm 5 \mu\text{m}$), the velocity of filtration of electrolyte in a flow-spreading regime will be 2–2.4 mm/h, which is lower than the velocity of the crystallization point movement (4.3–4.8 mm/h). Due to the increase in the thermal conductivity of carbon block and increased heat flow, the crystallization point after a certain period (7–8 days) will go up to the upper surface of the cathode and will block the penetration of liquid electrolyte (Figs. 2.51 and 2.52). The interaction of electrolyte and the refractory layer will start after many months, because electrolyte will crystallize in the pores of the carbon cathode block, not reaching the refractory layer.
- In carbon cathode blocks with pores above the critical dimension, the velocity of filtration of electrolyte in a laminar regime will be 5–7 mm/h; it will be bigger than the velocity of the crystallization point movement (4.3–4.8 mm/h). The penetration of electrolyte will be governed by the movement of point of crystallization (Fig. 2.51); after 96–110 h, the interaction of electrolyte and refractories will start up, resulting in the formation of “lenses” (to be described later).

Selected industrial trials show [41, 61, 64] that electrolyte may reach the refractory barrier layer within 4–6 days. That was shown of a set of experimental cells with thermocouples under the carbon blocks and in refractory layers. It was

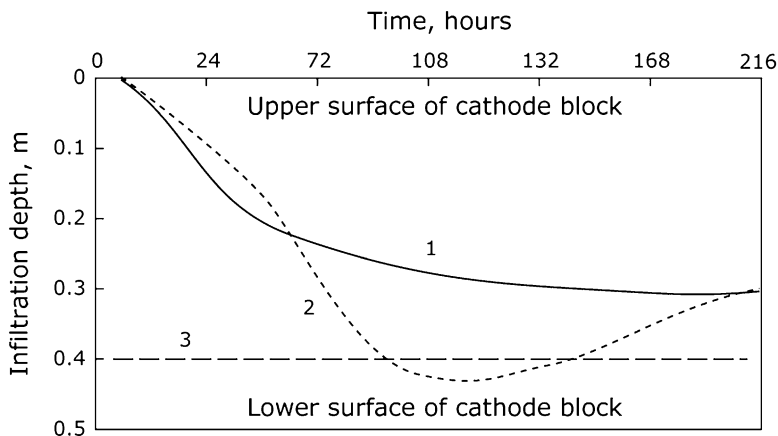


Fig. 2.52 Nonisothermal flow (at startup) of electrolyte through the porous media of carbon cathode blocks: 1—through permeable pores below critical radius ($25\ \mu\text{m}$); 2 – through permeable pores above critical radius; 3—movement of crystallization point of electrolyte [63, 64]

considered that electrolyte has reached the thermocouple (in alumina cover) when the thermocouple stops indicating the temperature.

2.3.9 Carbon Ramming Paste

From a materials science point of view, carbon ramming paste between the carbon cathode blocks and in the seam lining is the same carbon cathode material. The finished properties of baked ramming paste are the same, and the testing is almost the same. Yet it is an unfinished product that will receive the properties only after preheating and startup.

The decision to use carbon ramming paste between the carbon cathode blocks and in the peripheral seam sometimes is met with some puzzlement among the refractory producers, who know that in ferrous metallurgy, this technical decision was ended many years ago. Yet this decision has served aluminium producers for many years, and it doesn't seem they are going to introduce something new.

Raw materials for carbon ramming paste are the same: gas-calcined or electrically calcined anthracite (described in Sect. 2.3), sometimes a small amount of grained graphite, and silicon carbide grain. The raw materials for binders should provide the possibility of installation, while the temperature of the ramming paste is about $30\text{--}40\ \text{°C}$. In order to provide good rammability at ambient temperature, usually the producers add some organic substances to coal tar pitch or use synthetic organic binders.

Initially, hot ramming pastes were used in repair shops of the smelter, but cold ramming pastes give fewer problems due to ecological issues. Certain effects are made to reduce the polyaromatic hydrocarbons in the binders in order to avoid fumes at preheating.

The processing of ramming paste is very much like the preparation of anthracite graphite carbon cathode blocks—only without shaping and baking parts (Fig. 2.19). The raw materials are preheated and mixed in the mixers with pitch-based preheated binders and then packed into packs or barrels.

When considering the final properties the ramming material receives during preheating of the cell and startup, it is necessary to remember that the temperature of carburization goes from the surface of the rammed material to the lower end of the shaft or seam, and the process takes a rather long time.

The Testing

According to a generalization on testing of cathode materials [98], the ramming pastes before installation are tested for rammability [99], apparent density [100], dilatation (expansion–shrinkage curve during baking) [101], and baking loss and loss of volatiles [102].

Also, the determination of organic binder content might be useful [103]. Green apparent density is measured on rammed samples, while the rammability is measured using a Fisher sand ramming machine (Fig. 2.53). The density is measured as a function of the number of strokes.

Ramming paste has numerous key properties, one of which is the expansion–shrinkage dilatation curve and its mismatch, the expansion curve of the cathode block. During preheating, the organic binder of ramming paste carbonizes, and the volatiles fly away. At the moment of carbonization of the binder, some shrinkage is inevitable; however, the carbon block expands, and the question is whether, in the course of preheating, no gaps would appear between the paste and the blocks (Fig. 2.54).

After baking, the ramming paste is tested for apparent density [42–44], open porosity [46, 47], cold crushing strength [26, 27], thermal conductivity [38], and electrical resistivity [21, 22]. Also, it is possible to measure the ash content [51, 52] (Table 2.11).

Currently, the most popular are gas-fired preheating and resistance preheating of reduction cells. During the preheating, the cathode bottom becomes a unit, and the organic binder of ramming paste in the shafts and seams loses volatile matter and becomes hard. Of course, the surface and subsurface layers of the ramming paste gain the service temperature sufficiently quicker than the bottom layers. The pore structure of the ramming paste is formed during baking. Even if the grain size composition of the ramming paste is chosen properly, the pore size distribution in the baked ramming paste may differ, depending on the preheating regime. Generally speaking, the pore size distribution of a ramming paste, installed in the peripheral seam as well as in the shafts between the blocks, may have different values because the temperature

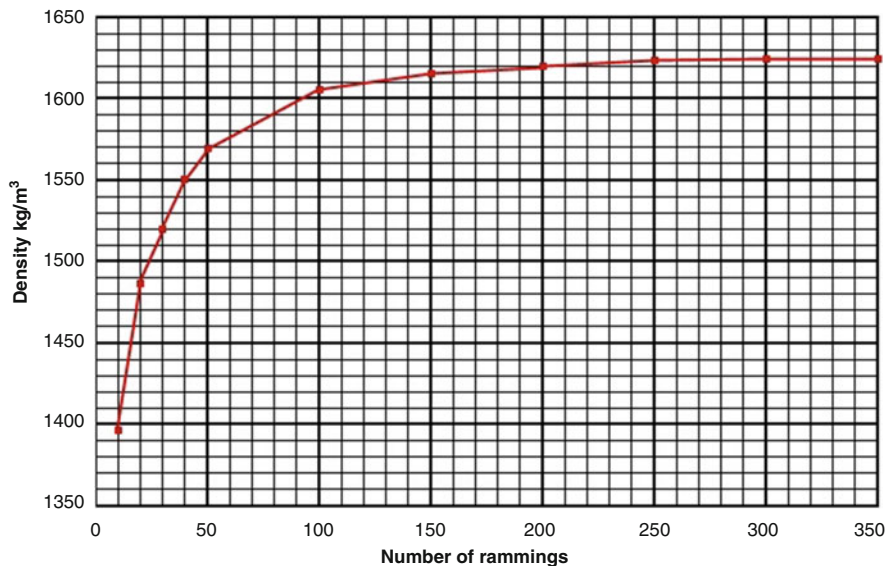


Fig. 2.53 Results of rammability test on Fischer sandrammer

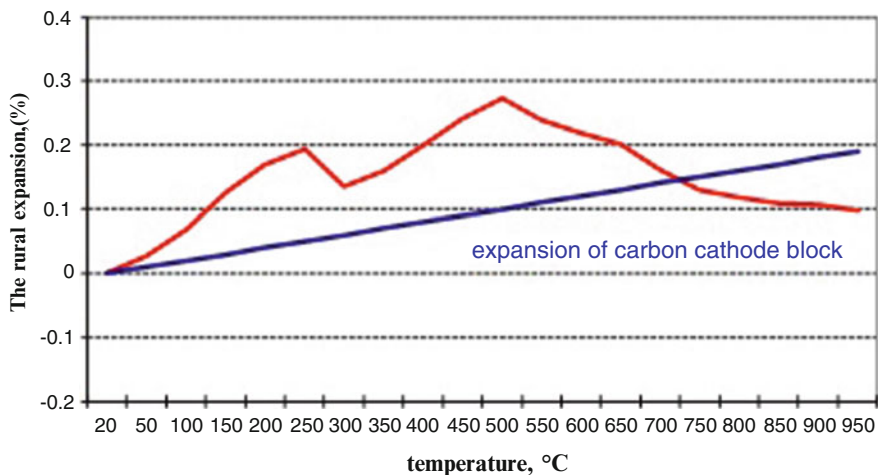


Fig. 2.54 Expansion/shrinkage/dilatation curves of ramming paste in comparison with expansion of carbon cathode block

increase in these different places will differ. Figures 2.55 and 2.56 demonstrate the difference in pore size distribution of the ramming paste in the peripheral seam and in the shafts between the blocks.

The ratio of the surface of shafts between the blocks, filled in with ramming paste, to the surface of the cathode is usually 0.6–0.9 %. However, we recall that

Table 2.11 Properties of ramming paste

Property	Value
Apparent density, g/sm ³	
Green	1.5–1.62
Baked	1.34–1.48
Cold crushing strength, MPa	16–26
Open porosity, %	18–27
Electrical resistivity, mkΩ · m	65–110
Volume expansion, %	0–2.5
Relative shrinkage, %	<0.15–0.3
Thermal conductivity < W/m · K	5–7
Baking loss, %	9–10
Thermal coefficient of expansion, K ⁻¹ × 10 ⁻⁶	4
Ash, %	<5–7

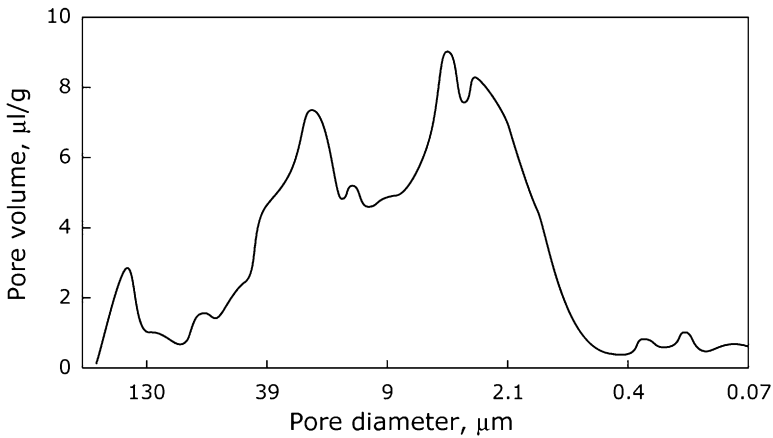


Fig. 2.55 Pore size distribution in baked (without infiltration of electrolyte) ramming material from the shaft between the carbon blocks. Porosity is 18 %

local infiltrations of electrolyte may cause local overheatings, so pore size control of the ramming paste is also desirable.

The ratio of the surface of a peripheral seam, filled in with ramming paste, to the surface of the cathode (if combiblocks are not the part of the construction) is 1.5–2.5 %. At startup, usually the temperature of the peripheral seam is low and sufficiently lower than the freezing point of electrolyte. Even in normal operation, the temperature of the peripheral seam is not high, and usually it is covered against penetration of electrolyte with a side ledge. However, sometimes [41] during dry autopsies, the peripheral seams are fully infiltrated with electrolyte, and so it is worth controlling the pore size distribution.

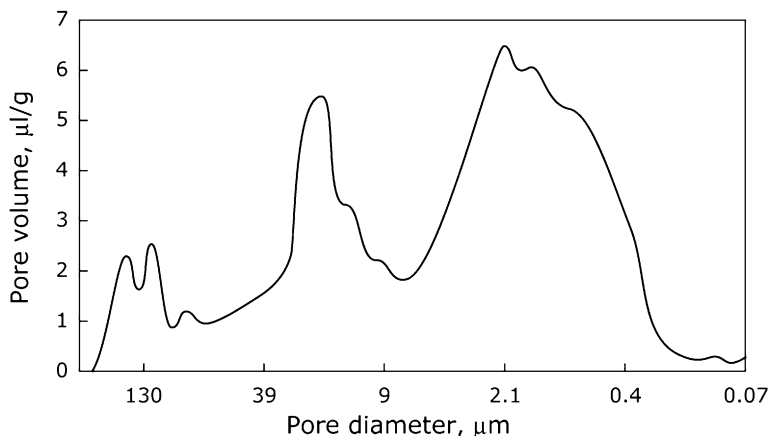


Fig. 2.56 Pore size distribution of baked (without infiltration of electrolyte) rammed material from peripheral seam. Porosity is 21.2 %

Installation of the Ramming Paste

The ramming paste installation is done by machine (Fig. 2.57) or hand rammers (Fig. 2.58). Ramming paste preheated to 30–50 °C (in the repair shop) is poured in the shafts at a certain height and rammed. Usually, the brick layers make five to seven ramming cycles, which means that each portion of ramming paste is rammed in the shaft, and then the next portion is poured. It is necessary to obtain a good and permanent densification during ramming. Before the installation, it is necessary to check the green apparent density in rammed state. At installation, the simplest way to check on the proper achieved density is the use of an impact penetrometer. The depth of penetration gives an idea of the rammed density. Overcompaction is also undesirable, because it may lead to stratification at preheating and startup. Poor compaction leads to big porosity and the appearance of big pores—channels for penetration of electrolyte.

The preparation of the ramming paste remains state-of-the-art; the same may be said about the installation, even with the help of ramming machines (Fig. 2.57).

During preheating and startup, the ramming paste is considered to absorb the thermal tensions and sodium swelling. Usually, baked ramming paste is more porous than carbon cathode blocks and less strong; however, the hardness of ramming paste is superior to the hardness of graphitic and graphitized cathode blocks because of the hardness of anthracite, which is the main constituent (Fig. 2.58).

It is not easy to separate the deviations of the properties and the defects of installation of the ramming paste, which finishes with shutdowns of the cells.

Usually, the stratification (Figs. 2.59 and 2.60) of the rammed paste is caused either with overcompaction or with some problems with a binder (which may be



Fig. 2.57 Machined ramming of peripheral seam

caused by too low a ramming paste temperature). Also, it might be caused by preheating of the cell.

The gaps between the rammed paste and the cathode blocks appear due to problems with the binder (which may be caused by too low a temperature of the ramming paste or cathode blocks). More rarely, it is caused from problems with the grain size composition. Also, it might be caused by preheating and problems in a mismatch of the thermal expansion of the ramming paste and the cathode blocks. It is likely the most serious defect, which causes immediate leakage of the electrolyte in the refractory layer.

Fig. 2.58 Hand ramming of the peripheral seam

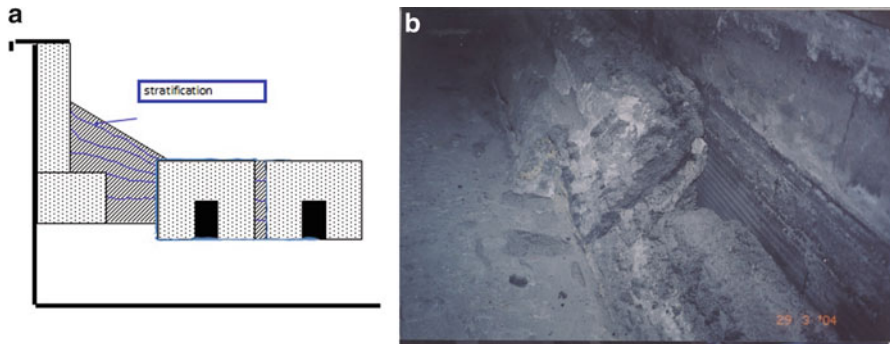
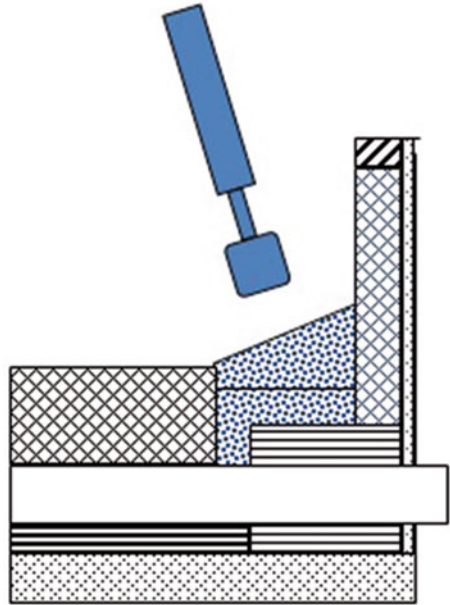


Fig. 2.59 (a, b) Possible stratification of the ramming paste at preheating of the cell in the shafts between the blocks and in the peripheral seam (strongly undesirable)

2.4 Coatings of Carbon Cathode Blocks and New Cathode Materials. Drained Cathode

Carbon cannot be considered optimal cathode material for Hall-Heroult reduction cells. The optimal cathode material should have [105]

- high electric conductivity,
- high thermal shock resistance,
- low porosity,

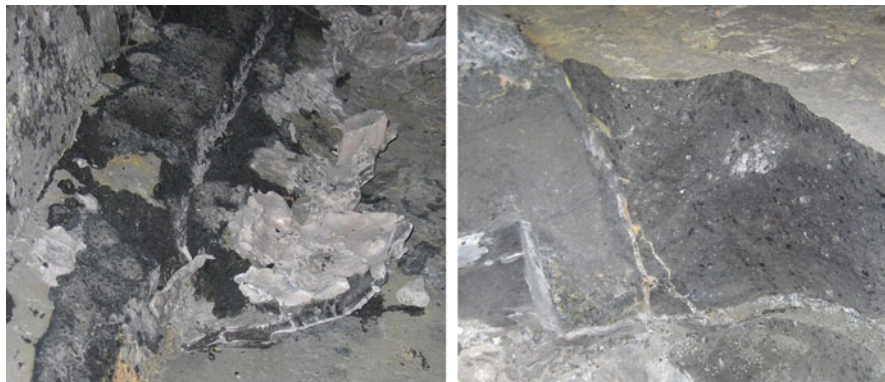


Fig. 2.60 The gap between the ramming paste and the cathode block after preheating and startup (strongly undesirable)

- good wettability by the molten Al,
- high wear resistance,
- small rate of electrolyte flow in capillary permeable pores,
- good contact with current conductors,
- high chemical inertness,
- high resistance to sodium intercalation and to the movement of sodium to refractory.

There is no known carbon material that would fit all these requirements. A deep body of research on noncarbon cathode materials for the Hall-Heroult process was carried out, beginning in the 1980s [106]. At that time, it was believed that the implementation of noncarbon cathode materials would give a longer service life and considerable energy savings due to decreasing the anode–cathode distance (CAD) and the cathode voltage [107–110]; some improvements were expected in increasing the current efficiency.

Yet it is necessary to remember that the expectations on energy savings could be fully realized with the implementation of a drained cathode construction. In a drained cathode, Al will flow to some vessel due to the slopes of the cathode; the Al film will be very thin. This design really gives the ability to decrease energy consumption due to of the decrease in voltage drop. It has been reported that the wetted surface of a traditional reduction cell permitted a 1–2 % increase in the current efficiency and an improved cathode current distribution [111] (Fig. 2.61).

More close to the above-stated requirements are some carbides, borides, and nitrides of refractory metals and their compositions. The chemical requirements for such materials are

- no interactions with Al,
- no interactions with electrolyte,
- no solubility of these materials in the molten Al.

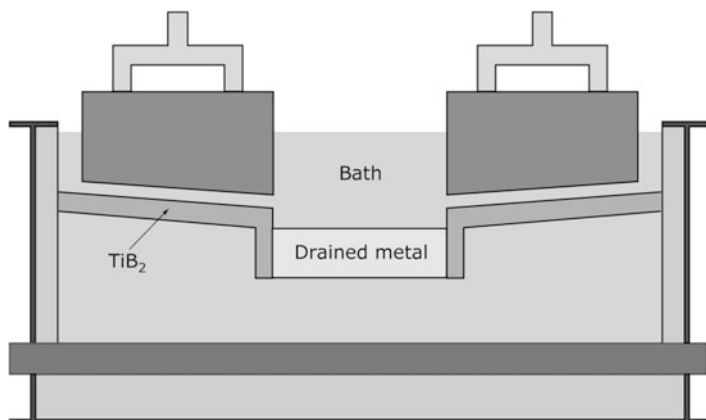


Fig. 2.61 Schematic view of drained cathode

Thermodynamically, there are many compounds that wouldn't interact with molten Al. However, it is necessary to take into account that in a Hall-Heroult process on the surface of the cathode, there is always a thin film of electrolyte, so it is necessary to consider the possible interaction of the material with electrolyte (in the absence of oxygen). The third requirement is a low solubility in the molten Al.

We will not pursue a full theoretical analysis on the fulfillment of the above-mentioned nonoxygen high-temperature materials to these three (no interaction with aluminium and electrolyte, no solubility in aluminium) requirements. Thermodynamically [106, 112, 113], the Gibbs energy of interaction of the compounds with the components of alumina-electrolyte melts at 1,100 °C (which is partly the theoretical analysis) is increasing in the scheme



The possibility of carbides interacting with aluminium is increasing in the scheme



Nitrides of refractory metals interact with aluminium, giving aluminium nitride [114]. The absence of interaction of borides and carbides, which are on the left side of the schemes, was proved experimentally [115].

Thermodynamical analysis of interaction at 1,230 K or 957 °C of borides, carbides, and nitrides with electrolyte, containing 10 % alumina, gives the following rows of resistivity:





Hence, the closest to the above-stated conditions (no interactions with Al, no interactions with electrolyte, no solubility of these materials in the molten Al) are titanium boride and titanium carbide.

There is information on industrial trials of wetted cathodes, made from TiB_2 -TiC and TiB_2 -C; probably good results might be with the compositions TiB_2 -ZrB₂, TiB_2 -TiN, TiB_2 -MoSi₂ [116, 117], and TiB_2 -WSi₂ [118]

It is necessary to remember that titanium boride is soluble in aluminium [106]. The reported solubility of titanium boride [119] is $(\text{ppm Ti}) \times (\text{ppm B})^2 = 1.21 \times 10^4$ at 960 °C, and typical wear due to solubility is 0.98 kg/m² [120]. The consequence is that even if one doesn't take into account abrasion wear and the solubility of binders for titanium boride grains, the coatings should be thick; the thickness should be some millimeters.

From a materials science point of view, the requirements are the minimum possible porosity and the absence of the additives that can promote corrosion. Such materials—dense titanium boride—based compositions—were made in the 1980s and 1990s. They were compositions with a titanium boride matrix (usually 70–80 % TiB_2 , with admixtures of carbon, carbides, borides, and ferrous and nickel alloys), with good electrical conductivity and relatively high corrosion resistance, produced by hot pressing, self-propagating high-temperature synthesis (SHS), or sintering, in the form of plates with a thickness of 10–20 mm. The main barriers for the implementation of such plates in the reduction cells of existing constructions were high cost and absence of glues for gluing or adjusting of these plates to the current conductors. The problem of implementing titanium boride plates may arise as a part of the project on drained cathodes and inert anodes.

The main advantage of titanium boride-based coatings is that the application of coatings doesn't require changing the design of the cell and is not costly. Another advantage is that the depth of the coating is millimeters, and again it is not costly.

There are many papers on titanium boride coatings of carbon materials by plasma spray method, electrochemical deposition, and slurry methods. Usually, researchers started their investigation trying to make a dense coating. Making a dense titanium boride coating on a carbon by a more or less industrial technique is not an easy job, and the continuation of these research projects tended to technologies of porous titanium boride coatings. The follow-up papers considered whether porous titanium boride coatings might enhance the wetting of the cathode by aluminium, might enhance the erosion resistance, and to some extent might be a barrier for the penetration of sodium and electrolyte in the cathode.

The investigations on applications of wetting coatings on the bottom cathode of reduction cells may be divided into investigations on application of coatings on carbon blocks at the plant-producer of the blocks and investigations on application of coatings on the carbon cathode in the readily constructed cell. In the first variant, there are no limitations on the temperature of the process, while in the second variant, the temperature of the process should be limited to 900–1,000 °C.

Plasma spray of titanium boride requires special equipment, preheating of carbon blocks, probably a protective atmosphere, and likely intermediate coatings to achieve good adhesion and a rather long time period [121, 122]. In plasma, the particles have a temperature of several thousand degrees, and it is possible to make dense titanium diboride coatings. However, such temperatures require protection of the surface of coated material from oxidation and from cracking due to a mismatch in thermal expansion coefficients. The thermal spray-coating process usually takes place at 1,200–1,300 °C, and the attempts to make titanium boride coatings by thermal spray didn't give dense coatings.

For starters, we have plasma spray devices, which allow us to apply coatings on large objects, so there is theoretically a possibility of performing the plasma spray process in a cell. Additionally, it looks more attractive to make such coatings at the plant, producing the cathode blocks, to make the bottom cathode lining from such blocks, and to cover the surface of the gaps between the blocks and peripheral seams by titanium boride slurry.

It is possible to make electroolithically deposited coatings in special cells and in the cells under operation [123, 124]. Thermodynamically, it is possible to receive the deposited coatings, combining the addition of titanium compounds in electrolyte, and boron oxides to the carbon anode material. Metal oxides dissolve in electrolyte; the ions of metals discharge at the cathode and deposit on the cathode as titanium boride and titanium carbide. The problem involves the poor controllability of the process and the need to fulfill the required purity of aluminium (in titanium and boron content). Once small amounts of boron oxide and titanium (in the form of oxide of salt) are added, it is possible to obtain the metal of required purity and quality, but the coating process lasts for a long time and is poorly controlled.

Some papers describe the process of fabrication of pitch or resin based composite coating [125], it has high coking value and good adhesion to carbon cathode blocks. The filler is titanium boride. Sometimes the fillers are not only titanium boride but also carbon fibers [126–128]. At preheating of the cell, the pitch carbonizes, giving a coke (carbon) matrix. Although there were the statements of thermodynamic calculations and the stated possibility of the appearance of titanium carbide, it doesn't look probable that the reaction of carbon with titanium will proceed at a considerable rate at 900–1,000 °C.

A series of publications was devoted to the implementation of titanium boride coatings having an oxide binder [129–131]. A slurry of alumina sol with titanium boride filler is applied on the surface of the carbon cathode bottom by spraying or with a brush. The coating is dried, so the water evaporates, and then during the preheating, alumina sol transforms into alumina, which becomes the binder for titanium boride filler. In formed coatings, the content of titanium boride particles is 70–80 %, so they form a continuous matrix, which makes the coating electroconductive. It has been said that the alumina that appears is in α -modification, which is less soluble in cryolite. The advantages of this method are that the shafts and seams are coated in the same way as the carbon blocks. Another advantage is that the material becomes hard at relatively low temperatures. The application of alumina sol is a typical nano method. In this particular case, it

allows us to make a relatively dense coating at a relatively low temperature (conventional sintering of alumina particles requires temperatures of 1,200–1,500 °C). The thickness of these coatings is up to 2–3 mm.

The alumina binder of the coatings slowly dissolves in cryolite, and within 2–3 years, the surface of the cathode becomes free of this coating. The advantages of such a coating may be the decrease of cryolite penetration in the cathode during startup and the possible prolongation of the service life due to the existence of the coating on the surface for a certain period. There is information on another mechanism of exfoliation of such coatings [132]. One mechanism is dissolution of alumina binder in cryolite; another variant is the formation of aluminium carbide under the coating, which results in mechanical tensions between the surface of the cathode and the coating and subsequent cleavage.

It is probably necessary to keep in mind that the general feature for all research devoted to the technology of titanium boride coatings in the constructed cell is that at temperatures below 1,000 °C (it is very difficult to achieve higher temperatures at an aluminium smelter), the coatings will be porous, and the porosity will be relatively high. The binder in pitch titanium boride compositions is about 30 %; the pitch transforms coke with a negative volume effect (the coking value of pitch is about 50 %). The pores should appear in such coatings. The same situation occurs with alumina sol binder. The alumina particles that appear occupy about 30–40 % compared to the volume of alumina sol binder of the initial mixture.

Another approach is the technology of “gradient” coating on carbon cathode blocks. It is applied in the shop of a carbon-producing plant. After preshaping of the green mixture of graphite and anthracite in the mold of a vibro press, a thin layer of titanium boride particle is placed on the upper surface, and the entire pressing is performed, so that the layer of titanium boride particles with a binder is pressed in the green shape. The following procedures are conventional: The green shape is placed in the baking furnace, and the coating of titanium boride (composition of coke with titanium boride) appears on the surface. This layer is about 10 mm thick, is porous, cannot protect the carbon part of the block from cryolite penetration, and, of course, should improve the wear resistance. There has been no research information devoted to decreasing the cathode–anode distance in the cells with such a cathode bottom [133].

The cost of dense titanium boride plates (porosity below 5 %) is 10–20 times higher than the cost of the cathode carbon materials, even if we are speaking about the most costly graphitized impregnated blocks. Dense titanium boride materials have excellent strength, wear, corrosion resistance, and wettability, yet their application may be economically efficient to implement the construction of the reduction cell with inert anode and wettable cathode.

The idea of porous titanium boride coatings, which to some extent increase wear resistance and improve the wettability of the cathode by molten Al, might be efficient for graphitized blocks [133, 134]. This research will require not only a good coating with good permanent adhesion, but some research on the construction and reduction technology as well.

2.5 Side Lining

The side lining of Al reduction cells is a part of the construction. It cannot influence current efficiency; if everything is good with the cell design and technology of reduction, the service life is usually not limited by the side lining. The energy consumption might be influenced a little by the construction of the side lining, but the problem is not easy.

2.5.1 Side Lining Materials

The side-wall lining of reduction cells should withstand the following:

- chemical interaction with electrolyte (described in Sect. 2.3);
- erosion interaction of circulating metal (due to the Lorentz forces) and the bath with particles of alumina;
- oxidation of the upper part of the side wall (above the bath) in complex oxidative-reduction atmosphere of CO/CO₂ and vapors of fluorine and sodium compounds;
- oxidation of the back side (contacting the steel shell) if there are gaps between the shell and the side lining or air leakage in the collector bar windows.

The side lining materials of reduction cells are carbon blocks and silicon carbide blocks. Anthracite-based carbon side blocks were used for many years. As a continuation of R&D in the application of carbon side blocks, many approaches were offered (Table 2.12):

- anthracitic graphitic side blocks (with synthetic graphite);
- with the addition of silicon carbide;
- with impregnation of the surface with molten and gaseous silicon;
- with impregnation by salts of boric acid;
- graphite-based blocks with increased oxidation resistance.

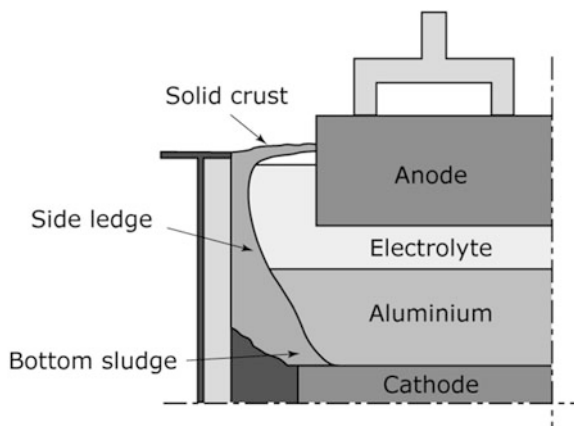
The trials with the implementation of silicon carbide (SiC) side-wall blocks started in the 1980s, and now it is a proven lining element for cells with high current. Anthracitic graphitic side-wall blocks are still used in cells with low current, and they will probably be changed for SiC blocks if the design of these cells is not changed. For Soderberg technology reduction cells, the application of SiC is not effective (or should be accompanied by a complex work on design and thermal balance).

The technology of carbon side-wall blocks is very similar to the technology of anthracitic graphitic cathode bottom blocks (Figs. 2.20 and 2.21). The requirements for carbon side-wall blocks are similar to the requirements for bottom blocks but easier: moderate strength, moderate sodium swelling, relatively high resistance to oxidation and to corrosion by bath and by aluminium.

Table 2.12 Properties of carbon side lining materials

Material	Anthracitic	Anthracite + graphite	Anthracitic, with increased oxidation resistance	Anthracitic, with increased oxidation and erosion resistance	Graphitic, with increased oxidation resistance	Graphitic, with increased oxidation resistance
Properties						
Density, g/sm ³	1.83	1.94	1.82	1.88	2.07	2.13
Apparent density, g/sm ³	1.52	1.54	1.49	1.54	1.56	1.63
Porosity, %	17	20.5	18	18	25	23.5
Thermal conductivity < W/m · K at 20 °C	9	13	8	9	28	32
Cold crushing strength, MPa	26	25	30	33	23	34
Bending strength, MPa	9	9	13	13	12	15
Sodium swelling (Rapoport test), %	0.7–0.8	0.7	0.7–0.8	0.7–0.8	–	–
Oxidation resistance, %	2.9	2.8	0.9	0.9	0.5	0.7
Ash, %	2.9	2.8	0.9	0.9	3.5	9

Fig. 2.62 Side ledge in reduction cell



The main advantages of SiC side lining compared with carbon side lining are higher corrosion resistance to electrolyte and aluminium, higher oxidation resistance, and higher thermal conductivity. Higher electrical resistivity is also an advantage.

The thickness of carbon blocks is 150–200 mm. The higher corrosion resistance of SiC permits one to use side-wall blocks with a thickness of 50–100 mm (more frequently, 65–70 mm) (Fig. 2.62).

It is necessary to emphasize that according to the principles of reduction cell design, the side lining should be covered by a 30–50-mm side ledge, which is the side lining's main protection from corrosion. So due to the proper thermal balance, the guaranteed frozen side ledge has a priority in design.

2.5.2 Carbon Side Lining; Causes for Decay

The side lining of the cell withstands

- the chemical action of the electrolyte [135],
- erosion by bath with the alumina particles and aluminium circulating due to the Lorentz force and due to the movement of the gas bubbles that appear during the reduction,
- oxidation by oxygen from air in the redox atmosphere and the vapors of fluorine and sodium compounds in the upper part of the lining (above the melt),
- oxidation near the shell (in case of oxygen flow because of poor airtight seal of the bus bar windows).

According to the Hall-Heroult reduction cell heat balance [136, 137], approximately 35 % of heat is transferred away through the sides (Fig. 2.6).

Consequently, the requirements for the side lining materials of a reduction cell are

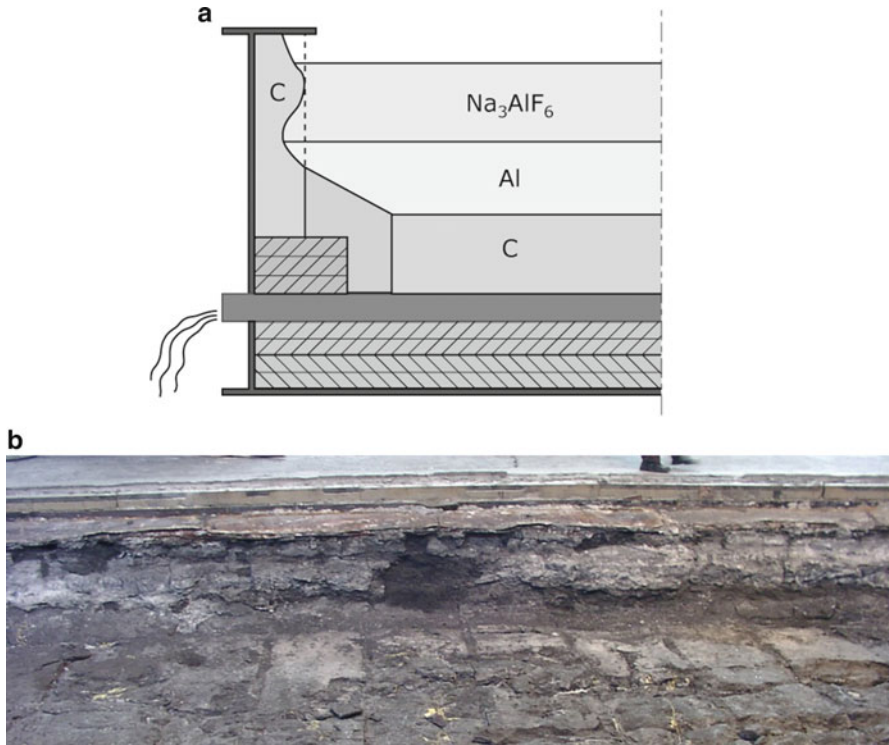


Fig. 2.63 (a, b) Schematic degradation of carbon side-wall block and the photo of ruined carbon side lining in the cell

- high thermal conductivity,
- high corrosion and erosion resistance to the bath and aluminium melts,
- high oxidation resistance.

Carbon anthracite side-wall blocks were used for a long time. The reaction between air oxygen and the carbon starts beginning at 400–500 °C; at 900 °C, the reaction rate is considerable. Additives to the material of carbon side-wall blocks make oxidation slower. The carbon side lining deteriorates due to oxygen in the upper part (Fig. 2.63) or in the lower part from the side of the shell (in case of air leakage through busbar windows).

Bath and aluminium circulation enhance the wear of carbon side-wall blocks due to erosion, so the combination of chemical attack and erosion takes place. The biggest wear is at the border of bath and aluminium, as the formation of aluminium carbide is enhanced in the presence of cryolite, which acts as a solvent for oxide layers and aluminium. Chain reactions (2.27, 2.28, 2.29 and 2.30) are in Sect. 2.3.

The producers of carbon materials offered several decisions to increase the properties of carbon side lining (Table 2.12). There were variants of anthracite-

based carbon side lining materials with increased thermal conductivity and corrosion resistance:

- with graphite;
- with boric acid salt impregnation;
- with addition of SiC;
- with Si-impregnated working surface.

There were no significant results in the application of carbon side-wall materials with enhanced characteristics in the reduction cells, and the current technical decision is silicon carbide side lining. Yet it is necessary to mention that a carbon side lining is in use in low-current cells, especially in Soderberg technology.

2.5.3 Silicon Carbide Side Lining

Attempts to use silicon carbide as a side lining material started in the 1980s when the problems with carbon side lining began at the reduction cells with increased current. The technical solution was the application of nitride-bonded silicon carbide. Within the next 20 years, several variants of SiC side lining designs were tested (Fig. 2.64a–f):

- SiC block 20–30 mm thick, preventing the carbon block from contact with the bath and aluminium (2.64a);
- SiC block 20–30 mm thick in contact with steel shell, preventing leakage of the melt in case of carbon lining damage (2.64b);
- SiC “ring,” promoting increased heat transfer in the upper part of the side lining (2.64c);
- SiC block 20–30 mm thick, with a 10–20-mm heat insulation layer for decreasing heat transfer (2.64d);
- SiC block 60–100 mm thick, in contact with steel shell, with carbon artificial side ledge, preventing SiC block from contact with the bath and aluminium (2.64e);
- SiC block 60–100 mm thick, in contact with steel shell, with carbon side-wall block, preventing SiC block from contact with the bath and aluminium (2.64f). This design was named “combiblock.”

In the course of the trials, designers came to the variant of SiC block that is 60–100 mm thick without heat insulation with a carbon artificial side ledge, preventing the middle and lower parts of the SiC block from contact with the bath and aluminium. The upper part of the carbon artificial side ledge was slightly above the border “cryolyte–aluminium.” This is the typical construction (2.64e). The continuation of this design with an artificial side ledge was the “combiblock” (2.64f).

As we know, carbon side-wall blocks are installed “side to side.” The thickness of carbon side-wall blocks is 150–200 mm, while the thickness of SiC blocks is sufficiently smaller. There were trials of installing SiC side-wall blocks having a

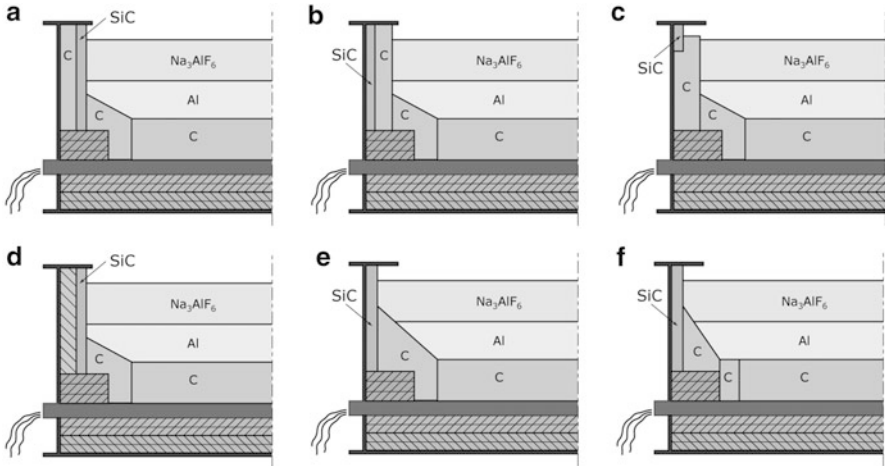


Fig. 2.64 The tested SiC side lining variants

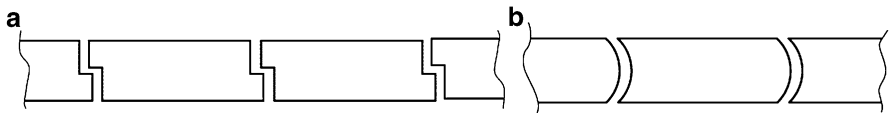


Fig. 2.65 The tested variants of joining side-wall SiC blocks: (a) step; (b) rounded and curved side surface

step (Fig. 2.65a) or a rounded and curved side surface (Fig. 2.65b) in order to prevent electrolyte leakage through the shaft. The trials showed that the “flat side to flat side” variant with mortar between the blocks, covered by a side ledge, provides normal operation of the cell.

Combiblocks have strong and weak features. For instance, the application of combiblocks helps to diminish the “human factor” in the construction (homogeneities of the ramming paste at production and ramming, the problems of pore size distribution, lamination of ramming paste, problems of heating at startup of the cell). Combiblocks are more reliable in achieving the desired properties, which is important for the heat balance.

Additionally, the weight of the combiblock is sufficiently higher, which presents some problems during construction. Another problem is the minimization of the shafts. Usually, the thickness of SiC side-wall blocks is 65–70 mm. There was a tendency to increase the thickness of side walls to 100 mm for installation in the 350–400-kA reduction cells; however, the trials showed that the proper thermal balance of cell protects the side wall better than increasing the thickness of silicon carbide.

Initially, the corner side-wall lining in the corners of the reduction cells was performed with straight blocks with inclinations (Fig. 2.66a), but a more accepted

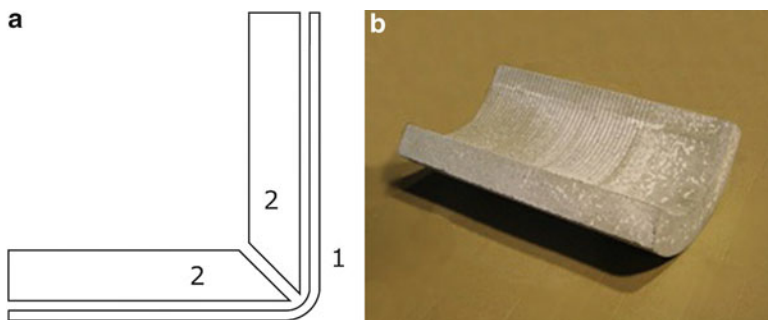


Fig. 2.66 The shape of SiC side lining of the corners: (a) 1—steel shell; 2—SiC corner blocks; (b) rounded corner block

variant now is a rounded corner block (Fig. 2.66b). There still exist variants of installing carbon corner blocks (while the sides are lined with SiC) or simply filling the corners with carbon ramming paste.

2.5.4 Variants of Silicon Carbide Materials (and Others) as a Side Lining

Nitride-bonded silicon carbide (silicon nitride–silicon carbide material) is not the only variant for application as a side lining material. Here is a list of variants:

1. Oxide-bonded (aluminosilicate), sintered, porosity about 15 %
2. Oxide-bonded, sintered, porosity 5–6 %
3. Nitride-bonded SiC (bonded with silicon nitride)
4. SiAlON-bonded SiC (comments ahead)
5. Self-bonded SiC—Si-SiC
6. Self-bonded SiC—SiC-SiC
7. Recrystallized SiC
8. Aluminium nitride
9. SiC-TiB₂
10. Oxide materials

As shown in laboratory experiments, nitride-bonded SiC is sufficiently more corrosive-resistant, comparing with aluminosilicate-bonded SiC (sintered in air). Currently, nitride-bonded silicon carbide is the main and only material for SiC side lining.

Nitride-Bonded Silicon Carbide: Elements of Technology

Conventional refractories shrink during thermal treatment and sintering. Shrinkage is about 10–20 %; due to the sintering process, refractories becoming stronger and

less porous. The process for the formation of nitride-bonded silicon carbide is “reaction sintering.” During reaction sintering, the porosity decreases and the strength increases, but the shrinkage is less than 1 %. The melting point of SiC [138] and the energy barrier for the dislocation’s movement (Nabarro–Peierls barrier) are very high, so the sintering of SiC takes place at 2,100–2,300 °C. Reaction sintering gives a chance of diminishing the temperature. During reaction, sintering in the green shape silicon reacts with nitrogen (in nitrogen atmosphere), and silicon nitride appears according to the reaction



Silicon nitride occupies some part of the space between the grains of SiC. To determine the volume of silicon atoms, we divide the atomic weight of silicon by its real density:

$$\text{the atomic volume of silicon is } \frac{28}{2.3} = 12.17, \quad (2.33)$$

$$\text{the atomic volume of } \text{Si}_3\text{N}_4 \text{ is } \frac{140}{3.19} = 43.89. \quad (2.34)$$

One of the reagents (N) comes to the reaction zone outside; hence, the mol volume of reactant (Si_3N_4) is bigger than the initial atomic volume of reagent (Si), and the volume change is 120 %:

$$\Delta V/V = V \text{ Si}_3\text{N}_4 / 3V \text{ Si} = 43.89 / (3 * 12.17) = 43.89 / 36.51 = 1.2. \quad (2.35)$$

Thus, in the process of reaction sintering, the porosity diminishes because the volume of the reagent (Si_3N_4) appearing in the pores is bigger than the volume of the initial silicon grains. The theoretical decrease of porosity in nitride-bonded SiC is easily calculated, taking into account the porosity of the green shape and the amount of silicon in the green mixture.

The weight of Si_3N_4 is bigger than the weight of Si in the green shape:

$$\Delta m/m = m \text{ Si}_3\text{N}_4 / 3m \text{ Si} = 140/84 = 1.67. \quad (2.36)$$

The theoretical weight increase of the green shape in the process of sintering of nitride-bonded SiC is easily calculated, taking into account the amount of silicon in the green mixture.

Yet it is necessary to take into account that in industrial furnaces, the real weight increase is 60–80 % of the theoretical. The ratio of the real weight increase to theoretical weight increase may be a good estimate of the completion of the nitridation process.

Nitride-bonded silicon nitride is a material with porosity 14–19 %; the structure of the material is represented by big grains of silicon carbide, surrounded by fine grains of silicon nitride (Figs. 2.67 and 2.68).

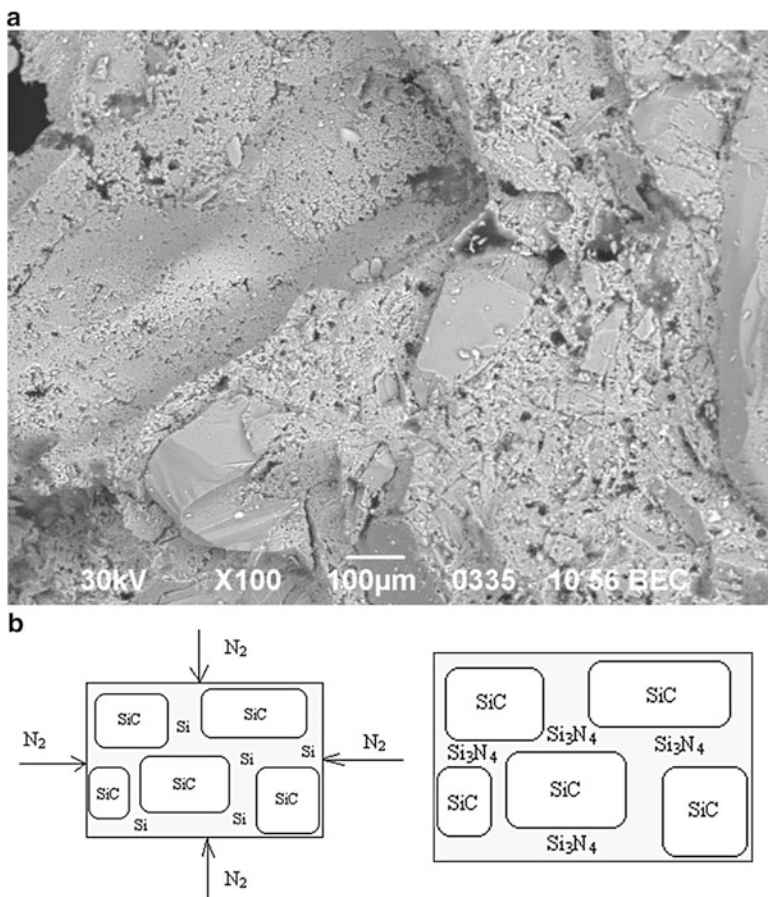


Fig. 2.67 (a) The structure and (b) principal scheme of formation of N-SiC

Usually, N-SiC producers finish the process of thermal treatment above the melting point of silicon, which is 1,410 °C. In the green shape, the silicon is in the form of fine grains, and the surface of the reaction is rather high. If the green shape is fired at an increased velocity, silicon might melt, and the surface of the reaction will diminish several times; as a consequence, the full nitridization will not take place.

According to [139], the reaction between silicon and gaseous nitrogen is started beginning at 1,100–1,200 °C. The reaction may take place with solid silicon and in gaseous phase due to evaporation of silicon. At a certain temperature, the pressure of silicon becomes sufficient, and the vapors of silicon will react with nitrogen. The silicon nitride that appears will condense on the surface. The limiting phase for the reaction between the gaseous nitrogen and solid silicon will be the diffusion of nitrogen atoms to silicon through the layer of silicon nitride. According to [140], on the surface of silicon appear the areas of silicon nitride and the areas of nonreactive silicon, and through those, the evaporation of silicon takes place.

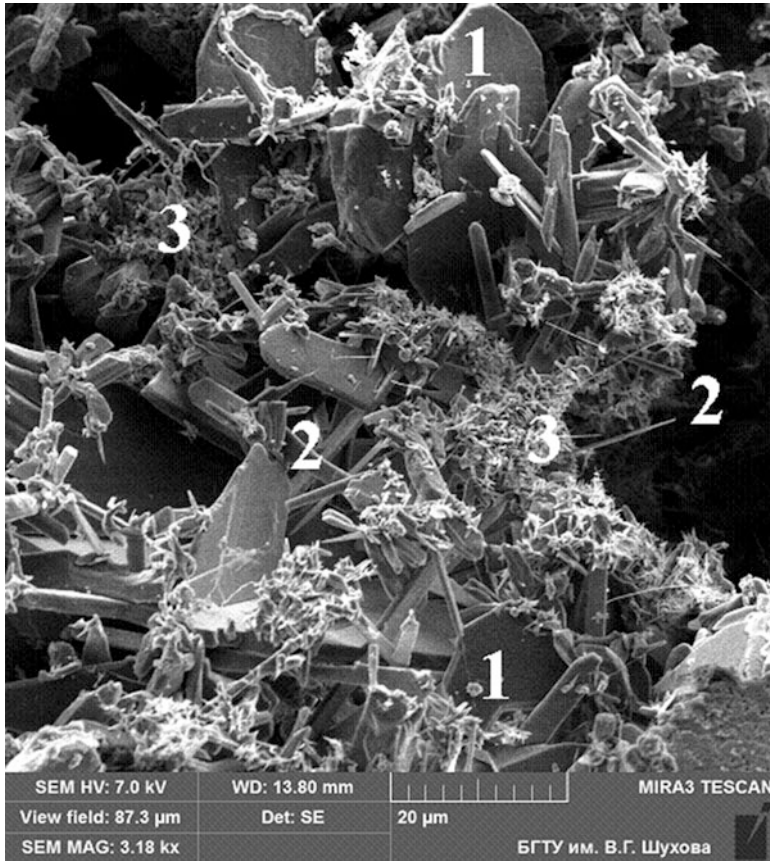


Fig. 2.68 The structure of nitride-bonded silicon carbide. 1—coarse SiC grain; 2—needlelike α -Si₃N₄; 3— β -Si₃N₄

The reaction of silicon and nitrogen is strongly exothermic, ΔQ (1,400 °C) = 720 kJ/mol [141]; the material is heated additionally due to heat going out, and the final stages of N-SiC formation are poorly controlled. In the final stages of nitridization, the temperature of the process is higher than silicon's melting point, and presumably at least some part of free silicon is in the gaseous phase. The difference between the temperature in the middle of the shapes and near the edge might be critical from the viewpoint of final properties.

In refractories, there are usually no gradients of porosity and density, while in N-SiC, gradients of porosity and density always exist [142, 143]. Sometimes the gradients of porosity are 1–2 %, but sometimes they may reach 5–7 % (Fig. 2.69). The reason for this is the overheating of the middle of the shapes due to the exothermic reaction of silicon nitridization. Volatile silicon tends to move in places with a lower temperature; presumably the reaction of silicon and nitrogen

Fig. 2.69 Porosity gradients in different 70-mm-thick N-SiC blocks according to [143]

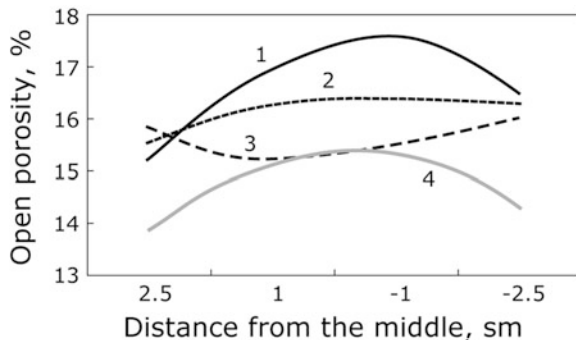


Table 2.13 Porosity and composition of N-SiC near the surface and in the middle (the porosity of the green shape is 17–19 %, and the width of the green shape is 70 mm) [143]

	Near surface	Middle
SiC, %	76.8	78.8
Si ₃ N ₄ , %	24.4	22.7
$\alpha/(\alpha + \beta)$	0.49	0.46
α , %	12.0	10.4
β , %	12.4	12.3
Si free, %	0.2	0.1
SiO ₂	–	–
(Al ₂ O ₃ + Fe ₂ O ₃ + CaO), %	1.3	1.28
Fe ₂ O ₃ , %	0.94	1.0
Porosity, %	16.6	16.2

predominantly takes place near the edges of the shape. This is the cause for the different color of the finished product at its cross section.

It is believed that the reaction of nitrogen and solid silicon gives predominantly β -silicon nitride, while the reaction of nitrogen with volatile silicon gives α -silicon nitride. Cubic γ -modification of silicon nitride may be synthesized only at high pressures. The parameters of α - and β -modifications of silicon nitride are quite similar Table 2.14).

In N-SiC refractory product, the silicon nitride phase is normally a mixture of α - and β -modifications, but the α/β ratio may differ considerably. In some N-SiC refractories, α -Si₃N₄ is predominant, while in others, β -Si₃N₄ is predominant. Usually, there is no commercial N-SiC with 100 % α - or β -Si₃N₄ (Table 2.14).

Usually, there are always some minor leakages of air in industrial processes. Another source of oxygen may be the organic binders, which decompose at relatively low temperatures and might become the constituent of a nitrogen atmosphere. It is quite common for silicon oxynitride to appear in the final composition. Later we will discuss the benefits of silicon oxynitride in corrosion and oxidation resistance.

Table 2.14 Lattice parameters of α - and β -modifications of silicon nitride [138]

Modification	Lattice parameters, pm:		Volume of elementary lattice, nm ³	Length of Si–N bond, pm	ρ , g/sm ³	Number of formula units in the lattice	Tetrahedron edge distance, pm
	a	c/a					
α	781.8	559.1	0.7151	171.5–175.9	3.148	4	271.2–291.3
β	759.5	290.23	0.3821	170.4–170.7	3.211	2	277.4–290.2



Fig. 2.70 Combiblocks

Combiblocks

As we stated previously, there are currently two variants in the side linings of reduction cells: an N-SiC side lining with rammed carbon paste, and a combiblock (Fig. 2.70)—N-SiC block with glued carbon block (or artificial side ledge).

An N-SiC lining is the same as described previously. As for the carbon part of combiblocks, depending on the design of the cell, it may be anthracitic graphitic (usually with 0 % graphite) or graphitic (specifications for the carbon part of combiblocks appear in Table 2.15).

Usually, the glues are carbon-containing phenolic or nonphenolic thermal setting or air setting resins.

There are advantages and disadvantages in the application of combiblocks. Silicon carbide blocks weigh on average 30–45 kg and are relatively easy to install by hand. Combiblocks weigh from 60 kg to 80–85 kg and require some mechanization in installation. Problems with gaps appear in the installation of combiblocks (if the steel shell is in use for 2 or 3 cycles). The gaps between combiblocks are strongly undesirable, but it is not easy to solve this problem when the width of a combiblock is 300–400 mm. So some smelters buy SiC blocks from one producer, the carbon part of combiblocks from another producer, and first install the SiC lining, then the carbon part of the combiblock, and then make the ramming of the peripheral seam (but with combiblocks, the peripheral seam is not wide).

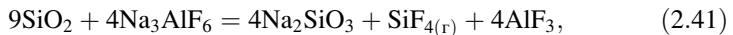
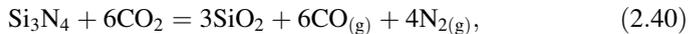
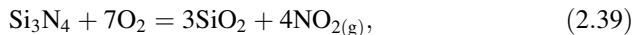
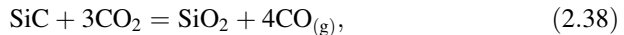
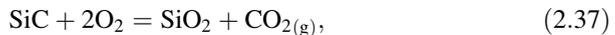
Table 2.15 Properties of carbon part of combiblocks

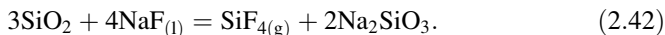
	Unit		Value	
Graphite content	%		~30	100
Real density	g/sm ³	ISO 9088	≥1.89	2.0–2.2
Apparent density	g/sm ³	ISO 5017	≥1.55	1.58–1.65
		ISO 12895-1		
Porosity	%	ISO 12895-1	≤22.0	≤19
Thermal conductivity	W/m · K	DIN 51908	≥10	≥30
		ASTM C767		
		ISO 12987		
Cold crushing strength	MPa	ISO 10059-1	≥30	26–30
Flexural strength	MPa	ISO 12986-1	≥10	≥10
Elastic modulus	GPa	ASTM C747	>10	>10
Thermal expansion coefficient (25–525 °C)	10 ⁻⁶ K ⁻¹	DIN 51909	≤3.0	2.4–3.0
Ash	%	ISO 8007	<3	≤1
Electric resistivity (20 °C)	μΩ/m	ISO 11713-2000	30–40	15–20

Changes in SiC Lining in Service and the Mechanisms of Decay

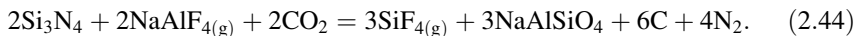
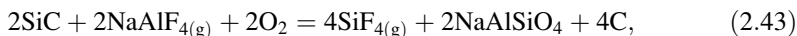
Changes in N-SiC side lining occur from the first hour of baking and the startup and do not finish until the final hours of service [142–145]. Yet in the properly designed cell (from the point of baking, startup, reduction technology), shutdown of the cell due to the side lining does not take place.

More likely, the entire degradation mechanism of SiC-Si₃Ni₄ side lining is oxidation [146–149] according to reactions (2.37, 2.38, 2.39 and 2.40), with following reactions of silicon oxide with salts (2.41, 2.42, 2.43 and 2.44). It is necessary to mention that temperatures of 800–900 °C are not critical for the oxidation of SiC and Si₃N₄. Yet in the presence of sodium and fluorine compounds, the reactions proceed more rapidly. Volume effects of SiC and Si₃Ni₄ oxidation are described in Sect. 1.7:

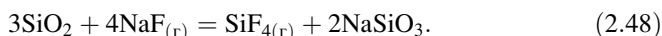
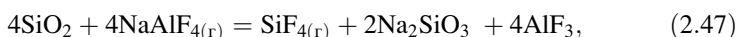
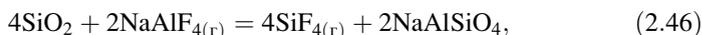
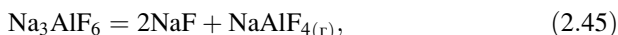




In the presence of CO_2 , SiC and Si_3Ni_4 may react directly:



The oxidation of the upper part of the SiC lining probably proceeds according to these reactions:



According to [144, 145], the degradation mechanism of the SiC side lining is equal for all service conditions and has three stages of aging. In the first stage, the oxidation is rather rapid and the decay of the thermal conductivity is rather low, so that the second phase takes place (when the silicon oxide layer is formed). In the second phase, the rate of oxidation is permanent, and the second phase lasts for a long period—a number of years. Then (when the silicon oxide content reaches 15–20 %) the third phase takes place—relatively rapid growth of silicon oxide content. At the end of the third phase, the silicon oxide content reaches 28–39 %, while the thermal conductivity drops to 5–7 $\text{W/m} \cdot \text{K}$. The aim is to slow down the arrival of the third phase, when the thermal conductivity drops because of the increased silicon oxide content (Fig. 2.71).

Lowering the porosity during service may have a positive effect (diminishing the oxidation surface). However, it is necessary to keep in mind that the oxidation reactions have a positive volume change, which may lead to the cracking of the refractories (Fig. 2.72).

Sulfur from the anode may be a catalyst for the oxidation of SiC and Si_3Ni_4 .

Shutdowns of reduction cells due to failures of SiC side-wall blocks are not common (Fig. 2.71). Once again, in normal operation, an SiC side lining is covered by a side ledge. The exceptions are startup, periods of overheating due to operation decay and possible magnetic instability, and increased velocities of electrolyte. Due to the increased velocity of electrolyte in the cell, there may be no side ledge at least on some parts of blocks or at some blocks. Cracking of SiC side lining (at Fig. 2.72b) is exotic (which may be influenced by overheating of the deck plate—for example, using under the deck plate fireclay castable with thermal conductivity 1–2 $\text{W/m} \cdot \text{K}$ instead of SiC castable with 5–9 $\text{W/m} \cdot \text{K}$). Overheatings of electrolyte for a long time with reduction technology decays will promote the dissolution of the side ledge and slow corrosion of SiC blocks. Reduction specialists know that even in properly designed reduction shops, there are local places with uncompensated

Fig. 2.71 Eroded SiC block

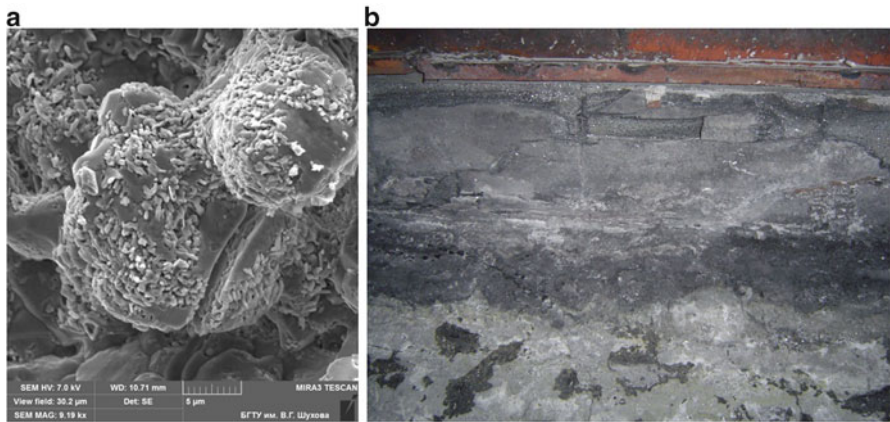


Fig. 2.72 Microstructure of oxidized N-SiC (a) and silicon carbide lining, broken in the upper part (b)

magnetic fields (especially near studs in the outermost cells in a row), which are risky for an SiC lining.

Oxidation due to an overheated upper part of SiC blocks usually may be seen as white layers on SiC blocks, which may become cracked in the future.

If a steel shell is overheated, the oxidation of the steel shell may give an iron oxide layer up to 30 mm thick [150] that may become an additional thermal barrier, but it also may give additional strain to the SiC block.

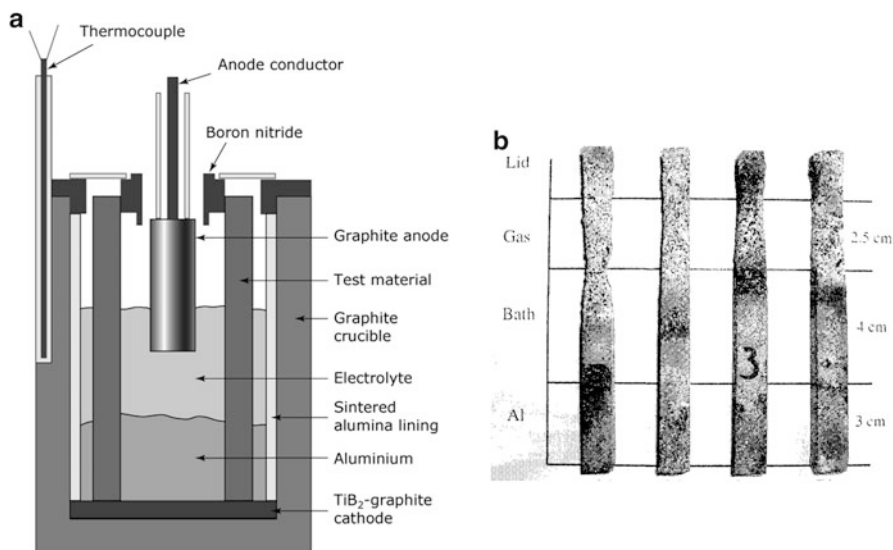


Fig. 2.73 (a) Laboratory reduction cell for the SINTEF corrosion resistance test to bath and aluminium and the samples (b) after testing [150]

Corrosion Resistance Tests for Bath and Molten Aluminium

The rod test is accepted for laboratory corrosion testing. All rod tests may be considered to be dynamic, because in all tests the corrosive liquid moves near the tested samples either due to the electrolysis process or because of rotation or lifting and dipping.

The rods are $10 \times 10 \times (100-130)$ mm, in the melt of the bath and aluminium. The existing variants of the rod test imitate the service of the SiC side lining in slightly different ways, giving a different corrosion resistance for the materials of different producers.

There is a variant of testing with the preoxidation of samples at $900\text{ }^{\circ}\text{C}$ in moisture for 100 h. The cryolite resistance is determined by volume change after 22 exposures to bath without voltage. This kind of testing may be considered as static although it is a tough variant of testing.

The world-accepted test for corrosion resistance is the SINTEF test (Fig. 2.73a). A lab reduction cell [151–154] comprises graphite crucible. On the bottom of the crucible there is a TiB_2 -coated cathode, the anode is in the upper part, and the tested SiC rods, dipped into the melts of aluminium and bath, are exposed to the bath, aluminium, and oxygen in the presence of vapors. The lab reduction cell is in the furnace. The corrosion resistance is determined by the volume change (Fig. 2.73b). The inventors [151] made a corrosion resistance scale, determined by the volume loss of the samples (Tables 2.16).

Table 2.16 The scale used to characterize the degree of corrosion based on volume loss [151–153]

Volume loss (%)	Degree of corrosion
<0.1	0
0.11–1.00	1
1.01–2.00	2
2.01–3.00	3
3.01–4.00	4
4.01–5.00	5
5.01–6.00	6
6.01–7.00	7
7.01–8.00	8
8.01–9.00	9
>9.00	10

Actually, in the test [144, 145] the corrosion resistance at the second stage of service [144, 145] is determined, while during the test of nonoxidized samples [151–154], the corrosion resistance at the first phase is calculated.

There are variants of the corrosion test with a supply of CO₂ to the bath with simulation of the reduction atmosphere to the upper part of the blocks and some other modifications [155–159].

Usually, the side-wall lining does not fail; more frequently, the shutdown of the cell takes place due to the bottom cathode block. However, sometimes there are shutdowns of cells due to the side-wall lining. Most problems with the side lining occur with problems with the design of the pots or in case of deviations of reduction technology (overheating, etc.).

In the first case, the side ledge is removed due to increased bath circulation, and in the second case, it dissolves due to increased temperature. In both cases, the side-wall lining is exposed to the direct action of the molten electrolyte and aluminium, which might be the reason for the side lining failure.

Existing corrosion tests do not reflect all causes of side-wall lining failure, so the possibilities for the enhanced development of the corrosion test do exist.

There is a variant of testing [159] that involves rotating SiC rods in the melt and periodically dipping and removing [160] the tested samples. Of course, these methods give slightly different corrosion resistance values.

Some authors wrote [161–163] that Si₃Ni₄ is less corrosion-resistant than SiC. Yet we didn't manage to find numerous experiments proving this. Probably the reason for such a statement is that in N-SiC refractory, the grains of SiC are coarse (up to 2–3 mm), while Si₃Ni₄ grains are fine (below 10 μm), so a kinetic factor of reaction plays a role.

There are opinions that β-Si₃Ni₄ is superior to α-Si₃Ni₄ in corrosion resistance to cryolite. We didn't manage to find evidence of this statement. The grains of β-Si₃Ni₄ tend to have an isomorphic shape (sometimes a short prismatic shape) with length/diameter from 1 to 2–2.5. It is likely that the suggestions on the superior corrosion

resistance of β - Si_3N_4 come from the fact that the reaction surface of α - Si_3N_4 is higher because the grains of α - Si_3N_4 are elongated, tending to a needlelike and whiskers shape with $l/d > 5$ due to the deposition of α -modification after the reaction of gaseous N and volatile Si.

Speaking about testing for corrosion resistance to cryolite and aluminium, it is possible to say that all existing methods give the idea of corrosion resistance and are a good tool for sorting and rejecting materials. Yet probably these methods are rather far from real quantitative estimation for forecast. However, it is difficult to say if these methods might be quantitative even after serious adjustments. Also, it is worthwhile to remember that corrosion by molten cryolite is not the only way for SiC material to change its properties. At some smelters in specifications the test for oxidation resistance in steam according to ASTM 863 recently appeared [164]. According to this test, the samples are subjected to oxidation in a steam for 500 h. The volume expansion of trial samples is a criterion of resistance to oxidation. Such testing is probably a good addition, estimating the oxidation resistance of the upper part of SiC blocks near the deck plate.

Silicon Carbide—Based (and Non-SiC-Based) Side-Wall Materials and the Application Possibilities of Other Materials

Self-bonded SiC, sintered SiC, aluminium nitride (AlN), SiAlON-bonded SiC, titanium boride—SiC composition, oxide materials were considered to be promising for application as a side lining of the reduction cell.

The initial laboratory tests on the application of SiC began from oxide-bonded SiC. Lab tests showed that N-SiC is as corrosive-resistant as O-SiC. There was a hope that SiAlON*-bonded SiC would be more resistant [165], but the experiments proved opposite. In experiments, also AlN (sintered and reaction-sintered), SiC with TiO_2 addition, aluminium titanate, Al-Mg, and Al-Ni spinels were tested [166–168].

Aluminium nitride might be the ideal material for side lining because it cannot give any impurities to the Al melt, while the thermal conductivity of AlN is close to the thermal conductivity of metals. In reality, AlN is not resistant to oxidation in the presence of fluorine vapors above the bath level. The vapors of fluorine compounds penetrate the grain boundaries and cause intensive oxidation. According to the lab corrosion tests, sintered SiC and recrystallized SiC are superior to N-SiC in corrosion resistance, yet they are sufficiently more expensive. The attempts to diminish the sintering temperature (and the cost) by the addition of titanium diboride resulted in deterioration of corrosion and oxidation resistance [35]. Silicon-self-bonded SiC showed good corrosion resistance in the lab; however, it is necessary to remember that Si-SiC contains up to 10 % free Si, which may be the impurity in Al. Even more resistant to corrosion in the lab was SiC material with oxide additives and porosity below 5 %. The SiAlONs are a class of compounds found in the 1970s [166, 167]. The name of the compounds is the abbreviation of the elements forming the compound—Si, Al, O, and N. Probably the more

“scientific” name for these compounds might be aluminium silicon oxynitrides. SiAlON is a compound, or continuous solid solutions with a very large homogeneity range (the solubility of AlO in Si₃N₄ lattice is up to 67 %) and general formula



while z may vary from 0 to 4.2. In initial trials [147], a z -value of 3 was used, but low z -values might be of interest.

There are certain possibilities for the optimization of the structure, yet it seems less likely that some new materials might be applied instead of N-SiC. The changes might be a drained cathode and inert anode application.

Corrosion tests have shown that self-bonded SiC material has superior corrosion resistance [161]. The barrier for the application of SiC-SiC materials is their high cost (compared to N-SiC). The service records of 300-kA cells showed that side lining is not the limiting factor of the service life of high-amperage cells. The applications of new materials that differ from N-SiC seems unlikely. Yet there are possibilities of R&D in the direction of increasing the oxidation of N-SiC and decreasing the gas permeability (N-SiC material has certain potentials for improving these characteristics).

Currently, N-SiC refractory, for one thing, is a material that satisfies the requirements of the Hall–Heroult process on corrosion resistance and thermal conductivity; additionally, it is considered to be cost-effective although it is not an optimal material for side lining of the Hall–Heroult process from a materials science viewpoint.

Increased energy costs compel Al producers to reduce energy consumption. It is worthwhile remembering that in Hall–Heroult reduction cells, 30–40 % of the heat is dissipated through the upper part of the side lining (Fig. 2.6a). Recent designs (Fig. 2.6b) have accounted for the latest trends, and the lower part of the side lining has changed into constructions with less heat flow.

Yet there is a serious doubt that even if the ideal material (or combination of materials), resistant to electrolyte and aluminium without side ledge, is found (tin oxide, ferric nickel spinel in combination with titanium boride, etc.), it would be possible to make a side lining of a reduction cell as a lining of a classical metallurgical device with proper heat insulation, which might decrease the heat flow by a factor of 10. The idea of suitable material might be realized using a construction made from a combination of two or three different materials (e.g., from tin oxide or nickel ferrite, resistant to electrolyte, and from titanium boride, resistant to molten aluminium), even in spite of the fact that in the existing process, the level of the border of electrolyte and aluminium moves along the height of the cell.

However, the heat of reaction of the reduction of Al (2.1, 2.2, 2.3, 2.4, 2.5, 2.6, 2.7 and 2.8) should dissipate; a total of up to 50 % of the heat should either be utilized or dissipate. Otherwise, problems with overheating of the electrolyte will occur, and maintaining the required temperature would require increasing the

Fig. 2.74 The inner side of the steel shell with leveling mix that filled in some dents and cavities



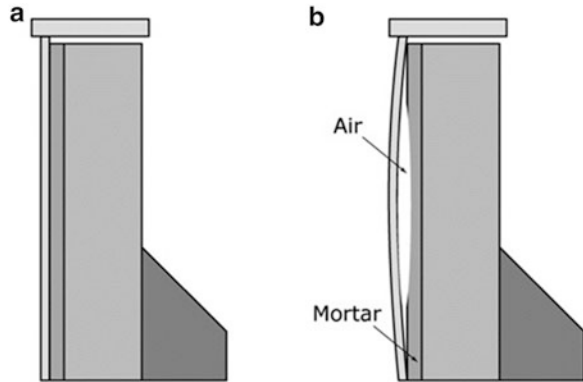
surface of the cathode, where reactions (2.1, 2.2, 2.3, 2.4, 2.5, 2.6, 2.7 and 2.8) take place, and decreasing the cathode current density.

2.5.5 Silicon Carbide Mortars, Ramming Mixes and Castables for Installation of SiC Side Lining

According to today's concept of reduction cell construction, SiC blocks are "glued" to the steel shell. Silicon carbide-based mortars (cements) are used as a glue. Usually, there is no problem to "glue" an SiC block to the new steel shell (of the first campaign); it is flat and smooth. However, the shells of the second and third campaigns have dents, cavities, and hollow imprints, and these should be filled in to avoid hollows filled in with air (which are very good barriers for heat transfer). These gaps, dents, and hollow imprints are filled in with SiC "leveling mixes" (Fig. 2.74).

The SiC lining should be installed in the steel shell of a reduction cell on a peripheral brick lining attached tightly to the steel shell. Usually, SiC ramming mix is poured and leveled on the peripheral brick lining, and an SiC block is installed on

Fig. 2.75 Air gap between SiC side lining and the steel shell



this layer, strictly normal to the surface. Silicon carbide-based mortar is uniformly placed on the back side of the SiC block to create a tight and smooth joint between SiC and steel. After SiC blocks are installed and the deck plate is welded, the gap between the deck plate and the upper part of SiC blocks is filled in with SiC-based ramming mix. The thermal conductivity of air is extremely low, and where there are air gaps, there will be local overheatings, which will cause the side ledge, protecting the SiC lining, to dissolve (Fig. 2.75).

If there are cavities or misprints, first it is necessary to trowel the cavities with an SiC castable, do the leveling, and then give it the chance to dry. After that, the SiC mortar should be applied and the SiC lining installed (Fig. 2.76, Table 2.18).

Silicon carbide mortars are high-quality cements consisting of 75–85 % fine silicon carbide. Small amounts of organics are added to the compositions for plasticity, and the addition of alumina cements, high-quality clay, fine silica, or solid/liquid sodium silicate gives the compositions binding properties (Table 2.9). The mortars are prepared in mixers with water. They are applied on standard cement technology—in plastic states they are placed and leveled on the torque and the main surface of the block. Then the block is installed on the side line to the shell and is knocked accurately by rubber hammer. During installation, it is necessary to avoid air gaps (Table 2.19).

The difference between the mortar and the leveling mix or ramming mix is the grain size composition. Fine SiC powders are used for the mortars, while for the leveling mix and ramming paste (some producers reach required properties of leveling mix and ramming paste in one composition SiC castable of concrete), producers typically use three grades of grain size composition, whereas the coarsest grain size may reach 2 mm. The binders for SiC castables (concretes) are either alumina cements or sodium silicate (castables on alumina cements have a limited storage time). Sodium silicate may be added to the dry mix in dry form, but also the mix with liquid sodium silicate may be prepared right before the installation of the SiC side lining. Some smelters agree with additional labor efforts. The difference between the leveling mix and the ramming paste is plasticity and adhesion ability;



Fig. 2.76 Installation of the corner SiC block

Table 2.18 Properties of SiC castables—leveling mix and ramming mix

Properties	Unit	Castable for leveling	Silicon carbide ramming mix
		Value	
SiC, min	%	84	85
Bulk density, min	g/cm ³	2.3	2.5
Thermal conductivity at 1,000 °C, min	W/m · K	7	~6.5
Adhesive strength after heating to 110 °C within 24 h, min*	MPa	1.8	
Adhesive strength after heating to 1,000 °C within 3 h, min*		3.5	20
Cold crushing strength, min	MPa		
110 °C × 24 h		35	50
1,000 °C × 3 h		80	90
Modulus of rupture, min	MPa		
110 °C × 24 h			20
1,000 °C × 3 h			25
Linear change, max	%	-0.1	
110 °C × 24 h		-0.3	
1,000 °C × 3 h			
Storage life, max	Month	12	12
	mec.		

Table 2.19 The properties of SiC mortars

Properties	Unit	Value
Bulk density, min	g/cm ³	2.5
SiC, min	%	85
Adhesive strength after heating to 110 °C within 24 h, min*	MPa	3.5
Adhesive strength after heating to 1,000 °C within 3 h, min	MPa	5
Thermal conductivity at 1,000 °C, min	W/m · K	5

the leveling mix should be able to fill in and adhere to a gap of 500 × 500 mm with a thickness up to 50 mm, and the bond should be rather firm.

The adherence ability of the mortars for gluing of SiC block to the shell is measured according to ISO 13655-4:2004 [169].

Sometimes misunderstandings occur between the bricklayers and the producers of SiC-based castables. In the language of refractory producers, a castable that should be installed in the cavity of a steel shell is called a troweling mix, but bricklayers at smelters continue to call it a ramming mix. This latter term is more likely for the composition that is filled in between the deck plate and the upper part of an SiC block (Fig. 2.76).

In the fabrication of combiblocks, high-quality organic resin glues are used to glue an SiC block to the carbon part. Likely the only requirement for this glue is high adherence in order to install the combiblock in the cell.

The corrosion resistance of SiC mortar to cryolite in the cup test is below 1 sm², which is 5–6 times lower than common fireclay bricks (Table 2.20), yet modern LCCs demonstrate even more corrosion resistance. The adherence of such mortars is not high, which presents certain problems during construction of cells, and there might be other variants of materials (e.g., phosphate-bonded) for installation of SiC side lining. However, the described technical decisions described earlier in this chapter provide working constructions. In well-designed reduction cells, there are no shutdowns due to the leakages of electrolyte of molten Al in the gaps between SiC blocks. In well-designed cells, there are no air gaps between the shell and SiC side lining that cause overheating and oxidation or dissolution of SiC block.

Sometimes on smelters SiC mortars are used as brick mortar at brick laying of fireclay bricks of the refractory layer below cathode blocks. In some smelters SiC castables are installed in plastic state as a layer below carbon cathode blocks above the refractory layer. In both cases, the goal is to prevent electrolyte penetration in the refractory layer.

Table 2.20 Chemical composition and properties of refractory barrier materials, according to [176–181]

	Composition, %										Apparent density, g/sm ³	Thermal conductivity, W/m · K (300 °C)	Thermal conductivity, W/m · K (900 °C)	Porosity, %	Permeability, μm ²	CCS, Mpa	Corrosion resistance (cup test), sm ²
	Al ₂ O ₃	SiO ₂	MgO	CaO	Fe ₂ O ₃	Na ₂ O	TiO ₂										
Bricks																	
Alumina silica 1	26	68	–	–	<3	–	–	2.15	1.23	1.5	14	0.05–0.1	80	3.5–4.5			
Alumina silica 2	35	60	–	–	<3	–	–	2.25	1.24	1.5	13	–	50	<5			
Alumina silica 3	30	48	–	15	1	3	–	2.1	–	–	14	–	–	–			
Alumina silica 4	22	70	–	–	–	–	–	2.1	–	–	14	0.1	45	3.7			
Alumina silica 5	23–27	60–65	–	–	–	–	–	2.13–2.26	1	1.4	11–17	–	55–97	–			
Alumina silica 6	43–46	54–57	–	–	–	–	–	2.26–2.31	1.24	1.34	15–17.5	–	28–52	–			
Fireclay 1	30	50–65	–	–	–	–	–	2.1	1.5	–	22–24	0.2–0.4	25–30	6–6.5			
Fireclay 2	28	50–65	–	–	–	–	–	2.2–2.3	1.5	–	20–21	0.2–0.4	20–24	5			
Dry barrier mixtures																	
Fireclay compositions	40–45	50–55	0.2–0.4	0.2–0.4	0.7–2.9	–	1–2	–	0.34	–	21.5	–	–	–			
	26–32	60–65	0.5–1	0.5–1	5–7	–	1–2	1.925	0.43	–	20–25	–	–	–			

Anortite compositions	3	48	-	15	1	3	-	2.1	-	0.4	-	-	-	-
Olivinite compositions	12	44	37	-	5	-	-	2.3	-	1.2	-	-	-	-
	4	44	42	-	7	-	-	2.3	-	0.8	-	-	-	-
Low-cement castable	8-22	70-85	-	1.5	-	-	-	2.5-2.8	2-3	-	13-15	0.05	80-90	0.5-0.8
SiC mortar	SiC 70-85	5-10	-	-	-	0.6-1.7	-	2	5-10	-	22-25	-	4-5	0.8-1

2.6 Refractory Barrier Materials of the Cell Lining. Dry Barrier Mixes and Bricks. Properties and Chemical Resistance. The Processes During Service. Interactions with Infiltrated Electrolyte. Change of Properties. Lenses

2.6.1 Bricks and Dry Barrier Mixtures

Carbon cathode blocks with collector bars are installed on a refractory layer that is made from fireclay bricks or dry barrier mixtures (DBMs). In Al reduction cells, this refractory layer is usually called a “barrier refractory layer” because the temperature under the cathode blocks is relatively small if we think in refractory terms. The main purpose of the refractory barrier layer is to stop infiltration of electrolyte—in other words, to be the barrier for the infiltration of electrolyte.

The infiltration of electrolyte in refractory (and then in the heat insulation) layers has two negative consequences:

1. The thermal conductivity of refractories infiltrated by electrolyte may change by a factor of 3–5, while the thermal conductivity of heat insulation materials may change by a factor of 10–50 [170–174]. The heat flow through the bottom increases, the thermal balance of the reduction cell changes, electrolyte (with alumina) starts to crystallize on the surface of cathode blocks, forming a bottom sludge and decreasing the surface of cathode, and there might be changes with the current distributions, the current efficiency, and the energy consumption.
2. Depending on the circumstances, the “lens of products” of reactions of infiltrated electrolyte and the refractory barrier layer, having a thickness up to 40–70 μm , may press the carbon cathode blocks from inside the reduction cell, causing bending strains and cracking. Such a phenomenon happens—and not rarely—if the pores in the carbon cathode blocks are above 25–30 μm (this is described in Sect. 2.3) (Fig. 2.77).

Fireclay bricks (alumina silica bricks, alumina calcium oxide silica bricks, and other silicate bricks) are not optimal barrier materials for Al reduction cells. As we have mentioned, cryolite-based electrolyte for Al reduction is a substance that dissolves alumina better than anything else. Certainly, it will dissolve all alumina-based refractory compositions and almost all other oxides similar in chemical structure to alumina. From a chemical point of view, the effective refractory barriers against the penetration of cryolite might be tin oxide, nickel oxide, compounds of nickel oxide, iron oxide, or zinc oxide (such as spinel Fe NiO_3). These oxides almost do not react with NaF and aluminium fluoride [175]. Yet the cost of these materials, which is 50–100 times higher than that of firebrick, provides the impetus to find less costly variants of alumina silica materials.

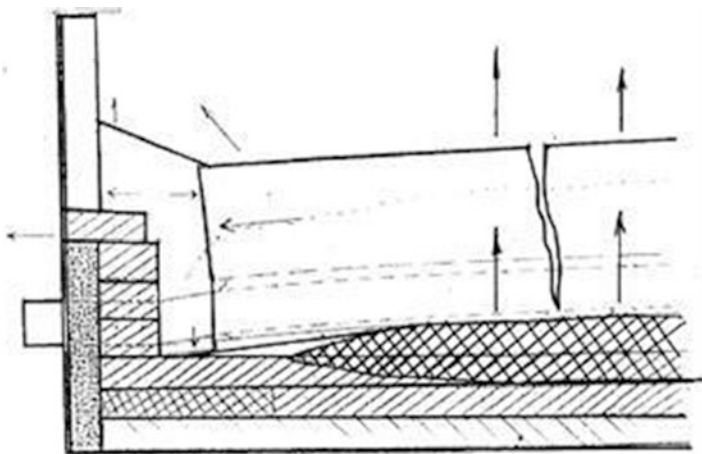


Fig. 2.77 The “lens” of interaction of infiltrated electrolyte and refractories

There were attempts to make barriers between the carbon blocks and refractory layer from electrolyte penetration, using steel plates and plates of window glass. These barriers didn't find industrial application. We will discuss other barriers later.

Alumina Silica Refractory Barriers

Long ago, the refractory layer was made from powdered alumina that was poured on a layer of heat insulation. After shutdown of the cell, the alumina, infiltrated by electrolyte, was used for the production of alumina. The main disadvantages of such a variant are high thermal conductivity and low resistance to electrolyte. This type of refractory lining is not used today.

The properties and compositions of refractory barrier materials used in reduction cells (including corrosion resistance according to cup test) appear in the Table 2.20.

Fireclay-type bricks with a porosity of 13–15 % are preferred over fireclay bricks with a porosity of 22–25 %, although they are more expensive. Some researchers consider a slightly lower alumina content of bricks to be an advantage. Of course, the geometrical tolerances of bricks should be rather strict and should not exceed $\pm 1\text{--}2$ mm, because with these tolerances, the brick lining from one side of the brick and from another side of the next brick may double. The current tendency is to make brick lining from small blocks that are 250 mm \times 250 mm \times 65 mm by 320 mm \times 250 mm \times 65 mm (and to avoid using bricks of standard sizes, 230 mm \times 114 mm \times 65 mm) in order to decrease the number and total length of the shafts between bricks.

There have been nonexclusive points of view on the optimum chemical composition of refractory barrier bricks. According to [176], the upper layer (contacting

the cathode bottom blocks) should be made from high-silica fireclay bricks, while the lower layer should be made from fireclay bricks containing more alumina. According to the other point of view [177], the upper layer should be made from high-silica fireclay bricks for a reduction pot with graphitic or graphitized carbon cathode blocks and from fireclay bricks containing more alumina for a reduction pot with semigraphitic blocks (30–50 % carbon).

It seems obvious that fireclay bricks with a porosity of 13–15 % and a permeability of 0.05–0.1 μm^2 is preferable to a 22–25 % porosity fireclay brick, because the corrosion resistance (cup test) of a low-porosity brick is 1.5–2 times higher. This has also been confirmed in industrial testing. There is no doubt that strict dimensional tolerances and minimization of shafts in fireclay bricks are preferable.

There is a belief that the question on the optimal silica/alumina ratio in fireclay brick for reduction cells will not be resolved with a strict proportion. Indirect evidence for this belief are numerous industrial trials of using silica bricks, powdered silica sand, all variants of fireclay brick, powdered fireclay, mullite bricks, alumina bricks, powdered alumina, and red constructional bricks as a refractory barrier layer.

Dry Barrier Mixtures

Dry barrier mixtures are used instead of refractory (fireclay) barrier bricks and as a powdered dumping for installation of carbon cathode blocks, and sometimes as a dumping between barrier bricks and heat insulation. These refractory compositions are used without water and should withstand the penetration of cryolite to heat insulation. The active use of DBMs in the lining of reduction cells started in the 1980s. There have been no strict preferences or negative considerations on using DBMs and their advantages over brick linings. Undoubtedly, DBMs are preferable to fireclay brick, having a porosity of 22–25 % and dimensional tolerances of ± 3 mm.

There are several compositions of DBMs, as seen in Table 2.20.

Dry barrier mixtures are applied instead of barrier refractory bricks. There are variants of refractory lining only from DBMs (instead of a layer made entirely of refractory brick) or a partial change of one or two layers of bricks to DBMs.

The certain advantage of DBM application is time. The lining by DBM (using flat vibrator) takes sufficiently less time compared to a brick lining. The disadvantage is the dust during installation and vibro compaction. Another advantage is the lack of shafts through which cryolite may penetrate to the heat insulation layer.

The thermal conductivity of a DBM is a little lower than that of fireclay brick (at least at preheating and startup). Usually, at retrofit of reduction cells, designers prefer not to change anything, so the heat flow through the bottom in such cells may decrease in the beginning of the operation.

Publications [179, 180] describe that cryolite reacts with grains of alumina silicates, forming a viscous layer on the surface. According to [179, 180], this viscous layer prevents the penetration of cryolite to the refractory and heat insulation lining. This layer doesn't crystallize or solidify and remain viscous—it doesn't crack.

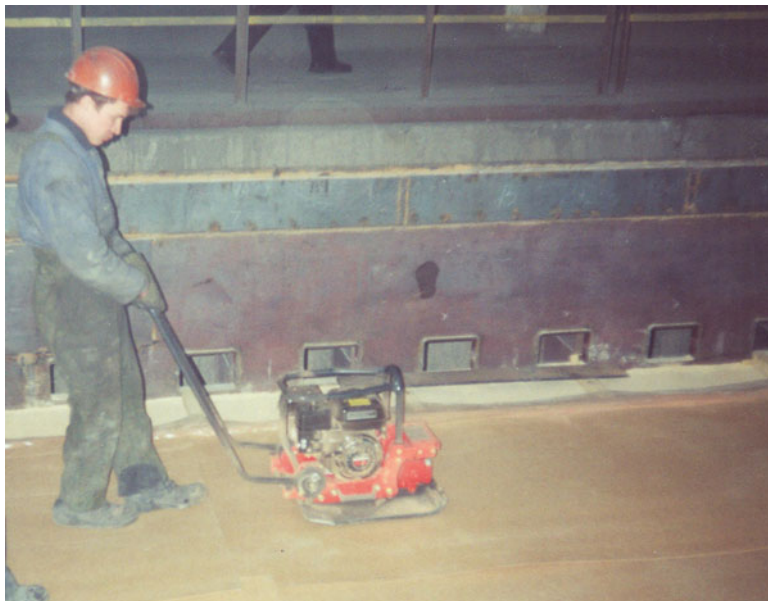


Fig. 2.78 Vibration of dry barrier mix during installation in the cell

This mechanism may take place, but not on the entire surface of the cell and not anytime. In reality, even within a surface of 5 sm^2 there may be two types of interactions—that described above and the penetration of cryolite melt in the depth of DBM without forming a viscous layer. In the latter case, there is no protection against cryolite penetration, and the cryolite melt will freeze, only reaching the place with the freezing point.

2.6.2 Corrosion Resistance Testing

The approved method of testing of fireclay brick for corrosion resistance to electrolyte is the standard ISO 20292 [182]. The hole is drilled in the brick, or it is preformed in a castable, then the electrolyte is poured in the hole, and the brick is placed in the furnace. After the exposure, the brick is cut, so that the change to the square of the hole may be measured. The degree of corrosion is calculated in the surface of corrosion. The lower the square of corrosion is, the more corrosion-resistant the material will be (Fig. 2.78).

The variation of the cup corrosion test is [183] in using the graphite crucible for electrolyte. The porosity of the graphite crucible may vary. The graphite crucible is placed on a refractory layer. In this type of test, the sodium vapor is taken into account. If the porosity of the graphite crucible is 12–14 %, the result depicts the interaction of refractory with sodium, which moves in graphite. If the porosity of graphite is 28 %, the result depicts the interaction due to the capillary movement of



Fig. 2.79 The results of cup test for cryolite resistance of fireclay brick and low-cement castable (concrete)

electrolyte through pores of carbon [184–186]. Experiments have shown that in case of testing the refractory in three variants, there will be different results on corrosion resistance, which points out the complex character of interaction.

Siljan [187] has found a good correlation between the corrosion resistance in a cup cryolite corrosion test and the depth of cryolite infiltration. A 220-kA reduction cell was lined with eight different alumina silica refractory materials and switched off for investigation of refractory conditions after 500 days. The results proved the good correlation. However, it appears that it is not a strict correlation from a physicochemical point of view between the interaction during hours and the kinetics of penetration of the melt within many months.

It has been stated [187] that there is a good agreement between the corrosion resistance (cup cryolite resistance test, 24 h, 950 °C) and the silica content in alumina silica refractory. In the beginning of the process, a silica-rich layer appears that plays the role of a protective layer. Rather often the segregation of the melt on the silica reach and fluoride reach parts takes place (Fig. 2.79). Usually, the cup cryolite resistance of refractories increases as the porosity decreases.

2.6.3 Chemical Interaction of Sodium Fluoride Salts with Alumina Silica Refractories

There are many possible chemical reactions among cryolite, sodium fluoride, alumina, silica, and mullite [181, 188–193]. Classical considerations on the corrosion resistance of refractories have limited significance for the problem of corrosion resistance to cryolite and are good from an educational and informational point of view due to the extra low viscosity of cryolite melt and unique corrosion ability of

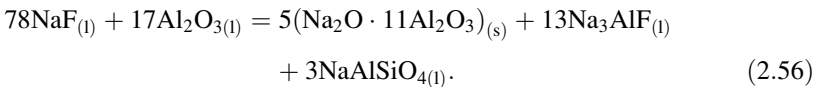
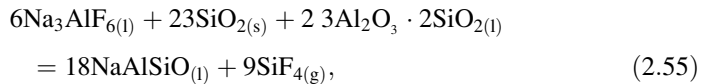
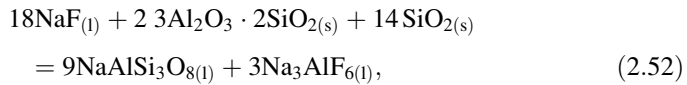
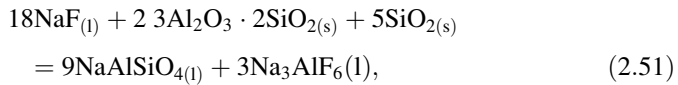
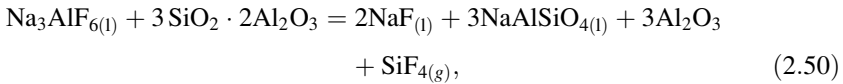
cryolite melt to alumina and alumina-containing compounds. The multifactorial behavior of electrolyte, multicomponent refractory lining, multivariability of chemical reactions, and limited knowledge on the mechanisms of sodium penetration to the refractory lining make the physical modeling almost impossible. We can discuss only approaches that could lead to partial encapsulation of the refractory and heat insulation lining.

Many chemical reactions are possible thermodynamically between the components of electrolyte and the components of refractory lining. The interaction may be described as a reaction between solid and liquid reagents on the border of solid reagent in case of no mixing and in case of permanent feeding with one component. However, the dissolution limit of alumina and silica in cryolite is about 10 % at 950–960 °C [185], and the penetrated electrolyte will relatively rapidly reach the saturation limit, become viscous, and stop dissolving the refractory. The temperature of the melt should be close to the crystallization point.

Mullite, $3\text{Al}_2\text{O}_3 \cdot 2\text{SiO}_2$, may interact with sodium fluoride (NaF), giving cryolite and nepheline, 3NaAlSiO_4 :



The possibility of the reaction of cryolite with mullite, giving gaseous silicon fluoride, has been confirmed experimentally:



The alumina component of refractory may react with sodium fluoride, giving sodium aluminates and cryolite:

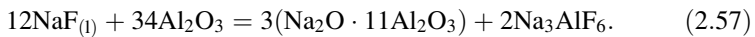




Fig. 2.80 The cell with bottom heaving before dry autopsy

The products of the reactions of cryolite components with alumina silica refractories are albite (sodium feldspar) and nepheline, which may coexist with cryolite. The solubility of alumina and silica in cryolite and sodium fluoride lowers as the acidity of the system decreases, and the freezing point of the system decreases as the silica content increases (from nepheline to albite).

There were certain hopes on calcium and magnesium alumina silicate as possible barrier layers, preventing interactions of refractories with electrolyte [194–197]. These minerals are a little more expensive than alumina silica refractories, but the cost is not sufficiently bigger. The basis for these hopes was the fact that the products of interactions of anortite ($\text{CaAl}_2\text{SiO}_8$), forsterite (MgSiO_4), and olivinite with sodium fluoride will have the freezing points above 900°C , and the melts will crystallize [194, 195].

The volume effects for the reactions were calculated [198], taking into account that one constituent comes from outer space:

- for reaction (2.49): 1.21;
- for reaction (2.50): 1.34;
- for reaction (2.51): 1.78;
- for reaction (2.52): 1.93;
- for reaction (2.53): 1.31;
- for reaction (2.54): 1.13.

It is almost impossible to estimate the real value of each reaction. However, the calculation of the volume effect gives the real cause of heaving (Fig. 2.80) of the cathode bottom due to interaction of infiltrated electrolyte with refractories and formation of the lenses that press on carbon cathode blocks and cause cracking (Fig. 2.81).

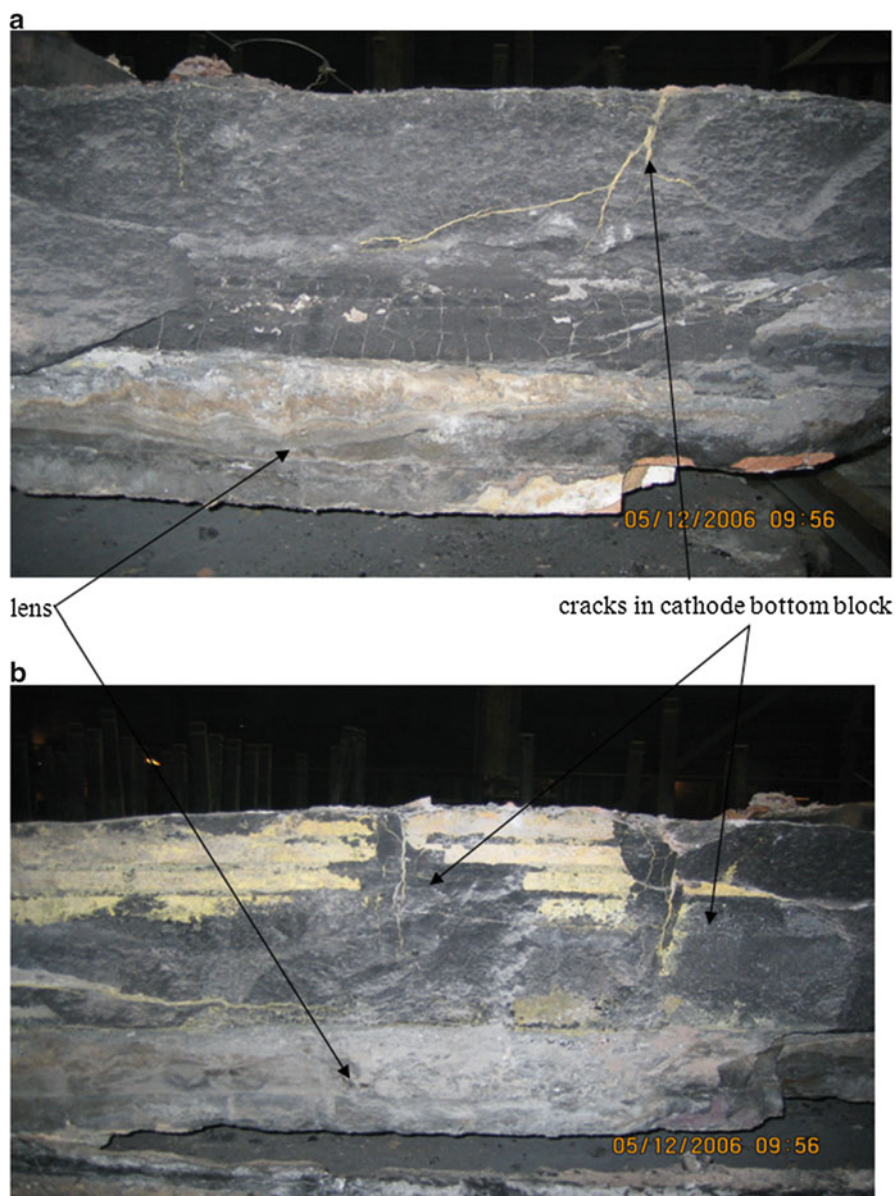


Fig. 2.81 (a, b) Cross section of cells lining, showing lenses of interaction of electrolyte with refractories instead of the refractory layer. It is possible to see the flow of aluminium in the cracks of cathode blocks

The lenses were 250–300 mm high and 1.5–2.5 m in length, and the heaving in the center was up to 100 mm.

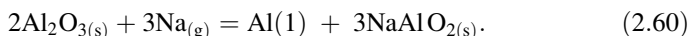
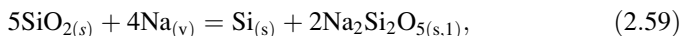
The upper part of the lens (50–70 mm below the carbon block) is formed by albite, nepheline, cryolite, and sodium fluoride [199]. The middle part of the lens (100–150 mm below the cathode block) consists of a mix of albite, nepheline, cryolite, sodium fluoride, quartz, and mullite. In the lower part of the lens (200–250 mm below the cathode block) the part of unreacted fireclay was 30–50 %, which depicts the kinetics of interaction, followed by infiltration of electrolyte.

Sodium Vapor Degradation

It has been considered [200, 201] that the major part of sodium formed according to the reaction



dissolves in the electrolyte and oxidizes near the anode, yet some sodium is transported through the carbon cathode block downward to the lower surface of the cathode block. It has been reported that the sodium pressure might be up to 0.02–0.03 atm:

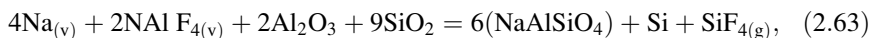


The reaction of sodium with refractory compounds gives metallic Al and Si, but it has been reported that the direct transformation of fireclay shamotte compositions is possible with nepheline and albite.

Sodium also reduces albite and can react with nepheline:



Sodium may interact with SiF_4 and NaAlF_4 in gaseous state [202]:



Direct evidence of silicon balls and drops to some extent proves this concept. From Prof. Øye's viewpoint, the mechanism opens the way for the transport of electrolyte through permeable pores due to the capillary forces [181].

2.6.4 *The Influence of Porosity and Permeability on Corrosion Resistance of Refractories*

According to Poiseuille's law, the velocity of liquid in a capillary is

$$dh/dt = (d^2 * \Delta p) / (32 * \eta * h), \quad (2.65)$$

where d is the diameter of a capillary, Δp is the difference in pressure, η is the viscosity of the liquid, h is the depth of infiltration, and t is time.

The capillary pressure of the liquid is

$$\Delta p = (4\sigma \cos \Theta) / 4\eta, \quad (2.66)$$

where σ is surface tension and Θ is the wetting angle. Combining Eqs. (2.65) and (2.66) gives

$$h = (d * \sigma \cos \Theta) / 4\eta. \quad (2.67)$$

According to Eq. (2.65) (not taking into account the temperature gradient and possible chemical interaction of the melt with the surface of a capillary), the depth of infiltration is directly dependent on the diameter of the capillary, surface tension, and wetting angle and is inversely proportional to the viscosity.

The viscosity is strictly dependent on temperature; it is strongly recommended to keep (at least in the design of the cell) the isotherm of the freezing point of electrolyte near the lower edge of the carbon cathode blocks. Generally speaking, the surface tension is dependent on the composition of the melt in the capillary (taking into account the interactions with the walls), but in practice the wetting angle of alumina silicate refractory by cryolite melt is close to zero.

However, Eq. (2.65) states that the diameter of the permeable pores (and, consequently, the permeability) should be minimal, but the value of porosity doesn't affect the corrosion by cryolite melt. A reasonable limitation for the pore diameter in the refractory might be 3–5 μm .

A zero contact angle of wetting gives optimal physical contact between the melt and the refractory for the beginning of chemical reactions. An absence of chemical interactions or a low rate of the reactions gives the melt the ability to penetrate. Within some time, the viscous albite melt will appear on the surface of permeable pores, limiting the next penetration.

The viscosity of the melt in the system NaF-AlF₃ follows the Arrhenius equation:

$$\eta = A \exp[B(1/T - 1/T_m)R]. \quad (2.68)$$

The solute in the melt alumina increases the viscosity. On the contrary to the freezing points, the viscosity of the melt strongly depends on the alumina/silica ratio in the reaction products. There is information that the solubility of albite in

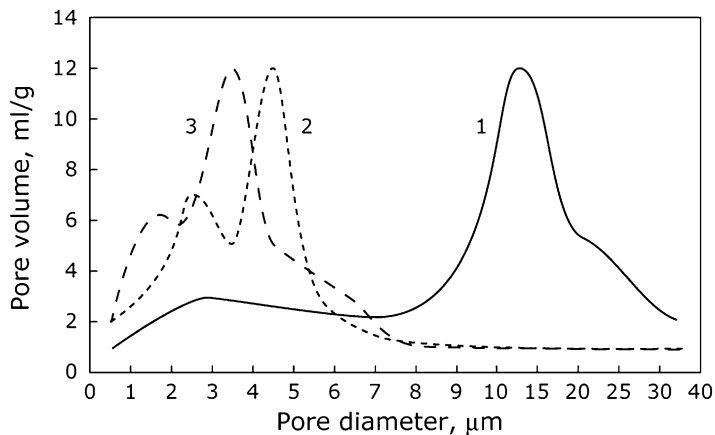


Fig. 2.82 Pore size distributions in fireclay brick (1) and in two low cement castables LCCs (2, 3)

cryolite is rather high. In lab tests, it has been shown that with big concentrations of silica in the melt, there may be segregation of the melt: low-viscous melt with an increased concentration of fluorides, and high-viscous melt with a high concentration of silica. According to [189], the viscosity of nepheline reach melt may be several orders lower compared to the viscosity of albite reach melt.

Hence, for the formation of viscous albite reach, cryolite melt, which could be the barrier for the penetration of sodium compounds inside the refractory lining, is a problem of conditions for the segregation of the melt into low-viscous melt with increased alumina content and high-viscous melt with increased silica content.

However, it looks like this question can be solved by changing the composition of the refractory. It is likely that the conditions for the formation of a viscous albite layer are in controlled input of sodium compounds. Formally, this condition is realized with excess sodium fluoride and excess reactant—a refractory with silica content above 60 % [190] when there's a rapid reaction of base melt with reactant with a high specific area (low-grained component of DBMs).

At a low rate of infiltration and low reactivity of the refractory, or, on the contrary, at rapid penetration of cryolite through the gaps, the low-viscous melt will appear in the lining, which will become low-viscous only in the case of real barriers. This is realized with application of the bricks with small-dimension pores, and the chemical composition doesn't play a significant role.

It is more likely that the structural factors (pore size distribution and consequent permeability) have more influence on corrosion resistance (according to cup test) than chemical composition [203, 204] (Fig. 2.82) (Table 2.21).

Table 2.21 Properties and cup corrosion resistance to cryolite of fireclay bricks and LCC castables [200–203]

Properties	LCC material		Fireclay material		
	A	B	A	B	C
Open porosity, %	17.1	17.8	22	21.8	21.8
Permeability, μm^2	0.02	0.01	0.45	0.08	0.19
CCS, MPa	93	91	30	35.3	42.2
Al_2O_3 , %	20.7	72.4	>30	>28	>28
SiO_2 , %	65.3	22.3	~60	~65	~65
CaO, %	1.4	1.5			
Corrosion resistance, %	12	5	42	48	45

2.6.5 *Some More Words on Barriers for Electrolyte Penetration*

- An alumina silica refractory is far from being the optimal material for a refractory barrier. Although some theoretical considerations on the silica/alumina ratio may exist, other variants should be found.
- There is a long history of trials with different barrier materials: silica block, silica powder, alumina brick, alumina powder, red constructional brick, mullite brick, various combinations of mullite brick or fireclay brick in the upper and lower layers.
- Chemical considerations suggest that tin oxide, ferric nickel spinel, zinc oxide, and their variations might be good barrier materials; however, these compounds don't meet economic considerations. Also, these compounds are not stable to sodium vapor.
- SiC-based refractories look (in the form of preshaped or not previously shaped castables or mortars) like more probable barrier materials.
- Structural considerations suggest limiting the pore size in the refractory material and decreasing the length of the shafts between the refractory barrier bricks.
- The advantage of DBM is the absence of shafts although the limitation of the pore size in a DBM is impossible.
- The cryolite resistance of LCCs is superior (according to cup test) to medium-cement SiC castables.
- Alumina silica DBMs and refractory bricks of relatively big shapes, with low permeability and low pore size, more or less successfully provide the service life of reduction cells within 6–7 years, and some cells reach service over 10 years.
- But probably the best barrier is the accurate temperature control of the freezing point isotherm in carbon cathode block and the limitation of electrolyte flow through the pores and consequent limitation of the pore size in carbon cathode blocks.

2.7 Heat Refractory Insulation Materials for the Lining of Reduction Cells

Although in refractory practice there are hundreds of heat insulation materials, the list of heat insulation materials for the lining of reduction cells is rather limited. For one thing, economic considerations add some limitations, but for another, the heat insulation materials in reduction cells should withstand mechanical compression loads without deformation at temperatures up to 900 °C for a long time, and numerous inexpensive fiber heat insulation materials don't correspond to this requirement. In the Hall–Heroult reduction cell, the heat insulation materials should withstand the pressure of the layer of the electrolyte, the layer of molten aluminium, cathode carbon blocks (taking into account collector bars), and the refractory layer. Currently, only four or five heat insulation materials are used in the lining of reduction cells: diatomaceous (moler) and perlite bricks, vermiculite and calcium silicate blocks (slabs), and sometimes lightweight fireclay bricks (but their thermal conductivity is relatively big, while the cost is not small) and fiber fireclay bricks.

2.7.1 *Diatomaceous (Moler) Heat Insulation Materials*

Diatomaceous earth is a silica rich porous fossil rock refuse of light gray, light yellow, and light pink color, formed by shells of diatomaceous weed. The shells were deposited on the bottom of water reservoirs, and mud clay between these shells cements the deposits. Diatomaceous ore exists on all continents; probably the most famous is in Denmark (Fig. 2.83).

In good diatomaceous ore, there is more than 70 % silica. Due to the small pore dimensions (pore diameter 5–100 µm), diatomaceous materials have low thermal conductivity.

Clay minerals, which are part of diatomaceous ores, determine the plasticity at shaping, the sintering process, and the service temperature. Probably the three main variables in diatomaceous ores are the nature (and dimensions) of diatomaceous shells, the nature of clay minerals, and the ratio of diatomaceous shells to clay minerals [205, 206]. These variables vary from deposit to deposit, so the properties of diatomaceous bricks from different deposits differ.

The shaping of diatomaceous bricks may be performed by pressing, by extrusion with subsequent cutting, and by slurry technology (pouring in the molds followed by drying). Sometimes in order to increase the porosity, wooden chips and sawdust are added to the mix or to the slurry. The firing is performed at a temperature of 800–900 °C in the tunnel kilns. The standard technological procedure is cutting in order to have strict dimensional tolerances.

The possible defects are only dimensional tolerances and cavities (in case of slurry processing), but it is necessary to keep in mind the safe service temperature (Fig. 2.88). In large part the safe service temperature is determined by the clay

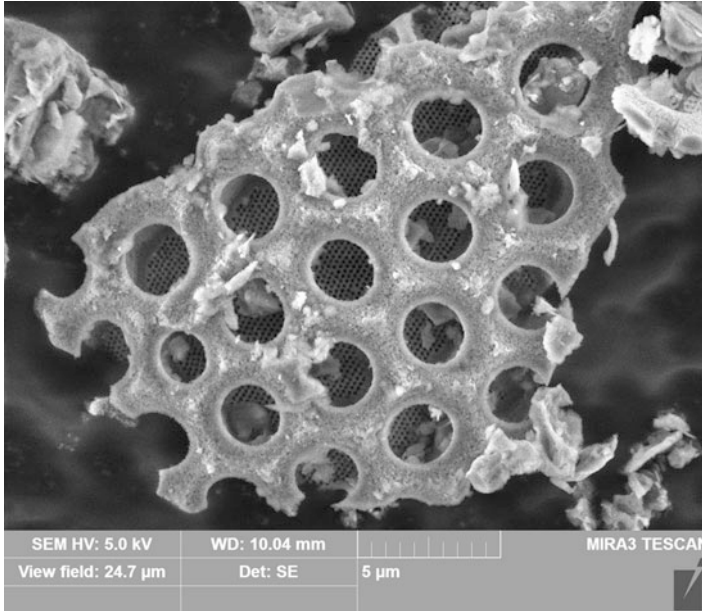


Fig. 2.83 Diatomaceous shells at multiplication

binder of the deposit. Figure 2.88 shows the linear change dependencies of two diatomaceous bricks, made from materials from different deposits.

2.7.2 *Perlite-Based Heat Insulation Materials*

Perlite is a high-silica glassy acidic volcanic rock mineral, whose chemical composition is close to granite, and contains about 15 % of chemically bonded water. At heating, due to evaporation of this water, perlite blows up with considerable volume effect, forming light porous material. The number of blowups (showing the number of times the volume increased at heating) of the best perlites is about 20. It is possible to obtain materials with round isolated pores at rapid heating at 800–900 °C.

Perlite heat insulation materials may be made cement-bonded (without firing) and fired clay-bonded. The service temperature of good perlite-based heat insulation materials may be up to 1,200 °C and is determined by the binder.

The possible defects are only dimensional tolerances and cavities.

2.7.3 Vermiculite-Based Heat Insulation Materials

Vermiculite ore is a result of the erosion and disintegration of black mica and the subsequent geological hydrothermal interaction. Probably the best-known deposit of vermiculite ore is in South Africa. Vermiculite is magnesium potassium hydro alumino silicate, with approximate formula $(\text{Mg}^{+2}, \text{Fe}^{+2}, \text{Fe}^{+3})_3 [(\text{AlSi})_4\text{O}_{10}] \cdot (\text{OH})_2 \cdot 4\text{H}_2\text{O}$, a type of hydrated biotite mica. Vermiculite expands at heating to 650–1,000 °C up to 18–25 times. Before expansion, the density is 2.4–2.7 g/sm³; after expansion, the density is 0.15–0.3 g/sm³. The blowup (thermal expansion) of vermiculite is usually performed in fluidized bed furnaces. The expanded vermiculite has a low thermal conductivity and is a good heat insulation material.

Vermiculite-based heat insulation materials may be made with firing and without firing. The first step in processing is refining and expansion (blowup). In fired processing, the expanded vermiculite is mixed with clay and shaped in blocks by pressing and then fired in a tunnel kiln up to 900–1,000 °C. Fired materials do not contain water and do not absorb water from the atmosphere; the safe service temperature of fired vermiculite blocks is superior to the safe service temperature of unfired ones.

At processing of unfired vermiculite heat insulation materials, expanded grained vermiculite is mixed with small amounts of aqueous solution sodium or potassium (ore mixed of sodium and potassium) liquid glass. The mix is pressed and the blocks are heated at 250–300 °C. Unfired vermiculite materials are cheaper, but the final properties of the material are reached after the installation of the materials in the reduction cells, preheating, and startup. At preheating, a considerable amount of water escapes from the liquid glass binder, and it is necessary to take this into account at preheating. Unfired vermiculite heat insulation materials may additionally absorb up to 3–4 % water from the atmosphere at storage (in addition to 5–6 % of the existing water in liquid glass binder). During preheating of the reduction cell, this water should evaporate, and that is a little bit less convenient compared with fired materials.

The safe service temperature of unfired vermiculite heat insulation materials is determined by the binder and may vary considerably, depending on processing and the sodium/potassium ratio (Fig. 2.90). The materials with sodium liquid glass binder have a lower safe service temperature than materials with potassium liquid glass binder, because of different high-temperature deformations (Fig. 2.84).

Other than safe service temperature, usually in vermiculite-based materials there are no defects, and the dimensional tolerances at pressed materials are perfect (Fig. 2.84). If something is not going steadily in the fluidized furnaces, the density of grained vermiculite might increase, which leads directly to an increase in the thermal conductivity of materials. On the contrary, if some problems appear with temperature in a fluidized bed furnace and vermiculite doesn't exfoliate properly, it might start exfoliating during the service, which is not desirable.



Fig. 2.84 Lining of the reduction cell: installation of heat insulation vermiculite blocks

Beginning from 1,000 °C, the slow transformation of vermiculite to clinoenstatite occurs, which may lead to cavities and decay of the thermal conductivity properties. That is why although the melting point of vermiculite is 1,350 °C, even for fired materials, the safe service temperature should be considered as 1,000–1,100 °C. For unfired vermiculite-based materials, the question about safe service temperature is sufficiently trickier.

2.7.4 Calcium Silicate Heat Insulation Materials

Calcium silicate heat insulation material is a synthetic material produced from silica (refined diatomaceous ore or milled silica sand) and of calcium oxide (high-quality calcium carbonate chalk or lime) with the addition of organic fibers (in order to keep shape after pressing). Pulp slurry from the mixer is squeezed out, pressed, and after exposure at air placed in the autoclave with steam pressure about 10 atm and temperature 120–130 °C. The synthesis of xonolite [207] mineral takes place at the above-mentioned conditions, and actually it is the end of the technological process. The dimensions of calcium silicate boards may be up to 2,500 mm × 1,500 mm.

At preheating and during startup of the reduction cell, calcium silicate boards lose physical water and chemically bonded water (in total, up to 10 %), and the burning out and degradation of organic fibers take place.

Usually in calcium silicate slabs, there are no geometrical defects (the torque sides of blocks may be grinded); however, the technology of the material is complex and needs accurate processing: There are no problems in the service stability of calcium silicate at high temperatures if there are no problems with

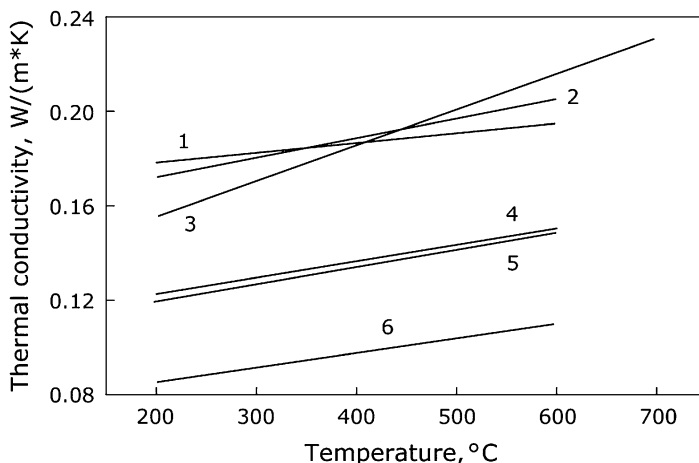


Fig. 2.85 Thermal conductivity of heat insulation materials: 1, 2—diatomaceous bricks; 3—lightweight fireclay brick; 4—diatomaceous brick; 5—vermiculite slab; 6—calcium silicate slab

processing. However, transformation of xonolite into tobermorite leads to shrinkage and the loss of insulation properties (Fig. 2.91).

Thermal Conductivity of Heat Insulation Refractory Materials for Reduction Cells

In Chap. 1, we showed that the temperature dependence of refractory and heat insulation materials usually is a complex function. Yet for diatomaceous, vermiculite, lightweight fireclay, and calcium silicate materials in temperature intervals, the temperature dependence is linear (Fig. 2.91). The linear character of the temperature dependence of thermal conductivity reveals the peculiarities of heat transfer in lightweight refractory materials [206] (Fig. 2.85).

Lightweight fireclay (density: 400–500 kg/m³) and some kinds of diatomaceous materials have the largest thermal conductivity values. The processing of lightweight fireclay materials includes relatively high-temperature firing (giving good contacts between the grains), while the pores are big (up to millimeters). This is the reason for the relatively large thermal conductivity of lightweight fireclay compared to materials with similar density.

The thermal conductivity of diatomaceous and vermiculite heat insulation materials is similar. Diatomaceous materials have a very fine pore structure; in such materials, the radiation effect on the thermal conductivity is low. An interesting dependence of thermal conductivity vs. temperature appears in Fig. 2.86—diatomaceous bricks with density 400, 500, and 600 kg/m³ have different values of thermal conductivity at 200 °C, but rather similar values at the temperature of service—400–600 °C. At such temperatures, the thermal conductivity of materials

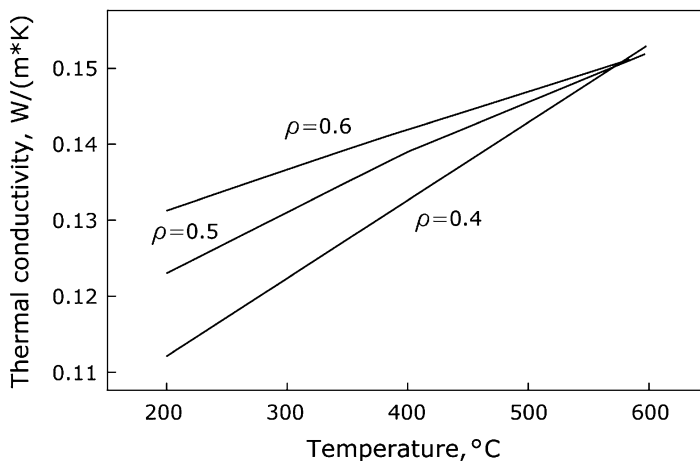


Fig. 2.86 Thermal conductivity of diatomaceous bricks with different densities

with different densities is equal (this is the evidence of the effect of small pores on the thermal conductivity value). From a practical point of view, it means that the heat flow through the bottom of the cell will be similar for diatomaceous materials with different densities, but with infiltration by electrolyte, denser materials are preferred.

In vermiculite materials, the radiation effect on thermal conductivity is low, because the mica sheets are the barriers for the radiation thermal conductivity.

Calcium silicate materials have the finest structure; the thermal conductivity of calcium silicate is approximately 1.5 times lower compared to diatomaceous and vermiculite thermal insulation. The inner surface temperature of calcium silicate materials is ~ 80 m²/g, and the particles have dimensions of 0.05–0.1 μm . Such a structure gives a very high thermal resistance of pores and intergrain contacts, which is the reason for such a small conductivity of calcium silicates.

The constancy of thermal conductivity is guaranteed by the constancy in processing and raw materials. It is strongly recommended to make control check tests of the thermal conductivity when changing suppliers, because the reference data on thermal conductivity may vary and change, depending on raw materials, processing, and the method of testing (see Sect. 1.6).

2.7.5 Thermal Aging of Heat Insulation Materials at Service and Thermal Conductivity of Infiltrated Heat Insulation Materials

During service at elevated temperatures, there is a thermal process called “thermal aging.” Thermal aging of heat-insulating materials takes place even in the absence of chemical reagents. At elevated temperatures and permanent pressure, there is a



Fig. 2.87 Picture of dry autopsy: due to pressure and the formation of the lens, the height of the heat insulation layer decreased

partial sintering process at the contacts of the grains, and these contacts become stronger, which increases the conductive constituent of thermal conductivity. According to records of industrial research obtained in the course of dry autopsy [207–211], the increase in the thermal conductivity of diatomaceous materials in the absence of infiltration is 10–15 % after 60–65 months, while the increase in the thermal conductivity of calcium silicate after the same period is 3–5 %.

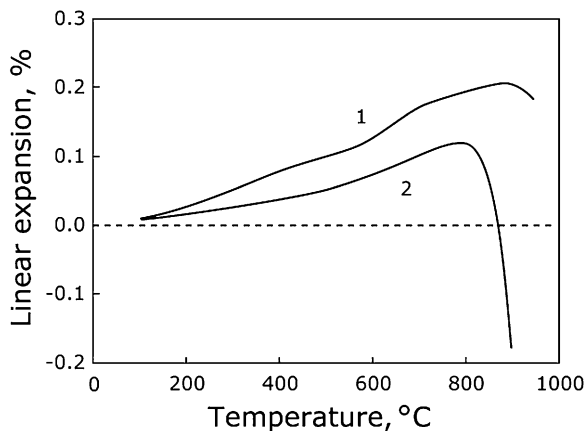
The increase in the thermal conductivity of heat insulation materials due to infiltration by electrolyte is sufficiently higher.

High-porous heat insulation materials cannot be resistant to the aggressive melts of fluoride salts. During conventional service of the reduction cells, the heat insulation materials are protected from infiltration by electrolyte by the barrier refractory layer. However, in reality, there is a slow infiltration through the gaps between the bricks, infiltration through big pores and holes in DBMs, and possible sudden penetrations through cracks. According to the data of dry autopsies [207–211], the infiltrated diatomaceous and vermiculite materials contain up to 15 % cryolite, up to 29 % sodium fluoride, and up to 6 % calcium fluoride. The thermal conductivity of infiltrated heat insulation materials increases dramatically, giving values of 5–21 W/m·K, so the increase in thermal conductivity may be up to 25–70 times!

Infiltrated heat insulation materials deform under compression sufficiently easier, so that their thickness may decrease by a factor of 2–4 (Fig. 2.87).

For the producer of aluminium, it means that the heat flow through the bottom increases, and to prevent the occlusion of the bottom by sludge, he or she should increase the voltage of the cell, which may result in an increase in the temperature of the electrolyte, the dissolution of the side ledge, and power consumption losses.

Fig. 2.88 Linear change at heating for diatomaceous materials from different deposits



Safe Temperature of Service for Heat Insulation Materials in Reduction Cells

According to standards ASTM 155 [212] and ISO-2245 [213], heat insulation materials are divided into groups corresponding to certain classification temperatures. The classification temperature corresponds to reheat change 2 %.

The classification temperature is a guide mark for the use of heat insulation materials in the lining of the reduction cell, but it does not correspond to safe service temperature of the material.

Heat insulation materials may undergo some sintering and, as a consequence, additional shrinkage at temperatures close to the temperature limit of safe service and at permanent pressure.

Figure 2.88 contains the dilatation curves of two different diatomaceous heat insulation materials. The process of additional sintering starts in material 1 at 830–840 °C, so the service temperature for this material shouldn't exceed 800 °C. This assumption is confirmed by creep testing at 900 °C (Fig. 2.89), where the time dependence for diatomaceous material never reaches the plateau within 24 h, and reheat change (shrinkage) is more than 3 %.

According to ISO 2245, unfired vermiculite heat insulation materials are in group 100. The dilatation curves of vermiculite materials show a large variety of behaviors at increasing temperature. It looks like materials 1, 2, and 3 were not blown up (expanded) up to certain degree, and at increasing temperatures, the materials expand additionally. This process cannot be considered desirable during preheating and startup in the reduction cell. Also, the softening points of these materials are too low. The behavior of materials 4 and 5 fits the standards; however, the softening point of material 4 is approximately 50° lower than the softening point of material 5. According to the classification of ISO 2245 [213], both materials are in group 100, corresponding to reheat change below 2 %, when tested at 1,000 °C.

Fig. 2.89 Creep dependence of heat insulation materials at 900 °C: 1—diatomaceous material 1; 2—diatomaceous material 2; 3—vermiculite material 1; 4—calcium silicate material 1

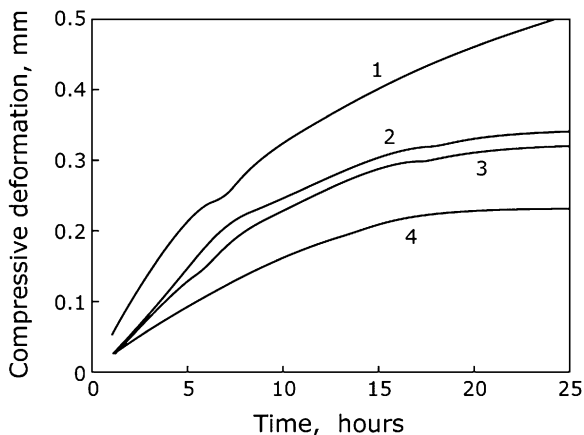
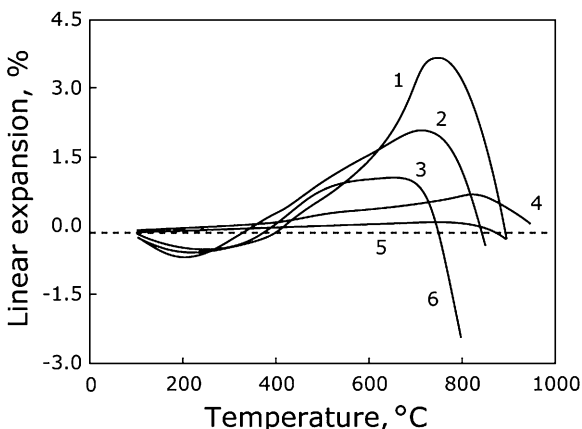


Fig. 2.90 Linear change at heating for different unfired vermiculite heat insulation materials

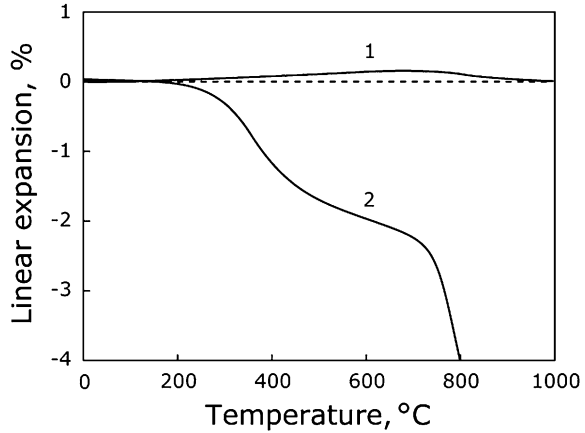


The dilatation curves of calcium silicate materials (Fig. 2.91) are only an illustration that materials that look normal at visual observation may demonstrate a different behavior at heating.

In ASTM-155 [212], one recommendation is to use the material at least at a temperature 30° lower than the classification temperature. The best variant is to have information on the softening point of the dilatation curve and the temperature load deformation behavior, because heat insulation material may demonstrate high shrinkage after the softening point (materials 1 and 3 in Fig. 2.90) and rather steep behavior (Fig. 1.15 in Sect. 1.4) (Fig. 2.91).

It should be noted that for short periods, heat insulation materials may sometimes withstand temperatures near the softening point without shrinkage [214]. Yet at preheating and startup of the cells, when the carbonization process in the rammed parts is not finished and the cathode bottom might shift even one millimeter down, that might be enough for the appearance of a thin gap between the carbon block and the rammed material, through which electrolyte might start to penetrate in the refractory lining.

Fig. 2.91 Linear change at heating for calcium silicate materials



References

Reduction of Aluminium. Elements of Reduction Technology. The Main Controlled Parameters of Reduction (Electrolysis). Elements of Energy Balance and Heat Balance of Reduction Cell. Reduction Shop. Types of Reduction Cells

1. Thonstad J, Fellner P, Haarberg G, et al. Aluminium electrolysis. Fundamentals of the Hall-Heroult process. Dusseldorf: Aluminium Verlag; 2001. 359 p.
2. Grjothheim K, Welch BW. Aluminium smelter technology. 2nd ed. Dusseldorf: Aluminium-Verlag; 1988. 328 p.
3. Borisoglebsky Y, Galevsky G, Kulagin N. The metallurgy of aluminium (in Russian). Novosibirsk: Nauka; 1999. 437 p.
4. Sørli M, Øye H. Cathodes in aluminium electrolysis. 3rd ed. Dusseldorf: Aluminium-Verlag; 2010. 662 p.
5. Martin O, Jolas JM, Benkahla B, et al. The next step to the AP3X-Hale technology: higher amperage, lower energy and economical performances. Light Met. 2006;135:249–54.
6. Martin O, Allano B, Barrioz E, et al. Low energy cell development on AP technology. Light Met. 2012;141:569–74.
7. Fengqin L, Songqing G. Review on the energy saving technologies applied in Chinese aluminum reduction industry. Light Met. 2012;141:575–9.
8. Dongfang Z, Xiaodong Y, Wei L. Development and application of SAMI's low voltage energy-saving technology. Light Met. 2012;141:607–12.
9. Bastaki M, Zarouni A, Jonqua B, et al. DUBAL cell voltage drop initiatives towards low energy high amperage cells. Light Met. 2014;143:451–5.

Lining of Reduction Cells. The Preheating, Startup, and Operation. Retrofit of Cells and Tendencies. The Main Causes of Failures. Dry Autopsies

10. Sørli M, Øye H. Cathodes in aluminium electrolysis. 3rd ed. Aluminium-Verlag; 2010. 662 p.
11. Panov E, Diachenko S, Danilenko S, et al. Heat processes in reduction cells and holding furnaces of aluminium production (in Russian). Moscow: Ruda i Metally; 1998. 256 p.
12. Gromov B, Panov E, Bojenko M, et al. Pre heating and start up of aluminium reduction cells (in Russian). Moscow: Ruda I Metally; 2001. 336 p.
13. Thonstad J, Fellner P, Haarberg G, et al. Aluminium electrolysis. Fundamentals of the Hall-Heroult process. Aluminium Verlag; 2001. 359 p.
14. Grjothheim K, Welch BW. Aluminium Smelter Technology. 2nd ed. Dusseldorf: Aluminium-Verlag; 1988. 328 p.
15. Borisoglebsky Y, Galevsky G, Kulagin N. The metallurgy of aluminium (in Russian). Novosibirsk: Nauka; 1999. 437 p.

Carbon Cathode Bottom Blocks

16. Øye H. ISO standards for testing of cathode materials. Light Met. 2008;137:937–42.
17. Sørli M, Øye H. Cathodes in aluminium electrolysis. 3rd ed. Aluminium-Verlag; 2010. 662 p.
18. Allard B, Dreyfus JM, Lenclud M. Evolution of thermal, electrical and mechanical properties of graphitised cathode blocks for aluminium electrolysis cells with temperature. Light Met. 2004;133:641–5.
19. Borisoglebsky Y, Galevsky G, Kulagin N. The metallurgy of aluminium (in Russian). Novosibirsk: Nauka; 1999. 437 p.
20. Lombard D, Behergaray T, Feve B, Jolas JN. Aluminium P echiney experience with graphitized carbon blocks. Light Met. 1998;127:653–8.
21. ISO 11713:2000. Carbonaceous materials used in the production of aluminium – cathode blocks and baked anodes – determination of electrical resistivity at ambient temperature.
22. ASTM C611-98(2010). Standard test method for electrical resistivity of manufactured carbon and graphite articles at room temperature.
23. ISO/WD 15379-2. Carbonaceous materials for the production of aluminium – cathode block materials – part 2 – determination of the expansion due to the sodium penetration without application of pressure.
24. ISO/WD 15379-1. Carbonaceous materials for the production of aluminium – cathode block materials – part 1: determination of the expansion due to the sodium penetration with application of pressure.
25. Brisson P, Soucy G, Fafard G, Darmstadt H, Servant G. Revising sodium and bath penetration in the carbon lining of aluminium electrolysis cell. Light Met. 2005;134:727–32.
26. ISO 18515. Carbonaceous materials for the production of aluminium – cathode blocks and baked anodes – determination of compressive strength.
27. DIN 51910-1997. Testing of carbon materials – determination of compressive strength.
28. ISO 12986-1:2000. Carbonaceous materials used in the production of aluminium – prebaked anodes and cathode blocks – part 1: determination of bending/shear strength by a three-point method.

29. ISO 12986-2. Carbonaceous materials used in the production of aluminium – prebaked anodes and cathode blocks – part 2: determination of flexural strength by the four-point method.
30. ASTM C651. Test method for flexural strength of manufactured carbon and graphite articles using four-point loading at room temperature.
31. DIN 51944-1999. Testing of carbonaceous materials – determination of flexural strength by four-point method – solid materials.
32. DIN 51902-1997. Testing of carbonaceous materials – determination of flexural strength by three-point method – solid materials.
33. ASTM C747. Test method for moduli of elasticity and fundamental frequencies of carbon and graphite materials by sonic resonance.
34. ASTM C1025. Test method for modulus of rupture in bending of electrode graphite.
35. DIN 51915-97. Testing of carbon materials – determination of dynamic modulus of elasticity by the resonance method – solid materials.
36. Panov E, Diachenko S, Danilenko S, et al. Heat processes in reduction cells and holding furnaces of aluminium production. Moscow: Ruda i Metally; 1998. 256 p.
37. Allard B, Roughby D, Fantozzi G, Dumas D, Lacroix P. Fracture behavior of carbon materials. Carbon. 1991;29(3):457–98.
38. ISO 12987-2003. Carbonaceous materials for the production of aluminium – anodes, cathodes blocks, sidewall blocks and baked ramming pastes – determination of the thermal conductivity using a comparative method.
39. DIN 51909-2009. Testing of carbon materials – determination of coefficient of linear thermal expansion–solid materials.
40. ISO 14420:2005. Carbonaceous products for the production of aluminium – baked anodes and shaped carbon products – determination of the coefficient of linear thermal expansion.
41. Borisov V, Hramenko S. Investigation of bottom materials of shut down reduction cells. Alum Sib. 1995;10:145–51.
42. ISO 12985-1:2000. Carbonaceous materials used in the production of aluminium – baked anodes and cathode blocks – Part 1: determination of apparent density using a dimensions method.
43. ISO 12985-2:2000. Carbonaceous materials used in the production of aluminium – baked anodes and cathode blocks – Part 2: determination of apparent density and of open porosity using a hydrostatic method.
44. DIN 51918-1999. Testing of carbonaceous materials – determination of bulk density by buoyancy method and the apparent porosity by impregnation with water.
45. ASTM C559. Test method for bulk density by physical measurements of manufactured carbon and graphite articles.
46. ASTM C1039. Test methods for apparent porosity, apparent specific gravity, and bulk density of graphite electrodes.
47. DIN 51913-2001. Testing of carbonaceous materials – determination of density by gas pycnometer (volumetric) using helium as a measuring gas.
48. ISO 9088-1997. Carbonaceous materials used for the production of aluminium – cathode blocks and prebaked anodes – determination of the density in xylene by a pycnometric method.
49. ISO 21687:2007. Carbonaceous materials used in the production of aluminium – determination of density by gas pycnometry (volumetric) using helium as the analysis gas – solid materials.
50. ISO 15906:2007. Carbonaceous materials for the production of aluminium – baked anodes – determination of the air permeability.
51. DIN 51903. Testing of carbon materials; determination of ash value; solid matters.
52. ISO 8005. Carbonaceous materials used in the production of aluminium – green and calcined coke – determination of ash content.

53. Wilkening S. Untersuchungen über Kathodeblöcke für die Aluminium-Elektrolyse. *Erzmetall*. 1977;30:232.
54. Shi Z, Xu J, Ren B, Ban Y, Wang Z. Tests of various graphitic cathode blocks materials for 300 kA aluminium reduction cells. *Light Met*. 2007;136:849–52.
55. Haupin W. Cathode voltage loss in aluminum smelting cell. *Light Met*. 1975;104:339.
56. Dinger DR, Funk JE. Particle packing I – fundamentals of particle packing: monodisperse. *Spheres Interceram*. 1992;41(1):10–4.
57. Dinger DR, Funk JE. Particle packing II-Review of packing of polydisperse particle systems. *Interceram* 1992;41(2):41–6.
58. Dinger DR, Funk JE. Particle packing III – Discrete versus continuous particle size. *Interceram* 1992;41(5):41–6.
59. Dinger DR, Funk JE. Particle packing IV – computer modelling of particle packing phenomena. *Interceram*. 1993;42(3):150–2.
60. Dinger DR, Funk JE. Particle size control for high-solids castable refractories. *Am Ceram Soc Bull*. 1994;73(10):66–9.
61. Yurkov AL, Hramenko SA, Borisov VI. The influence of the structure and the properties of carbon cathode blocks on shut downs of reduction cells (in Russian). *Novye Ogneup*. 2008;4:3–12.
62. Khramenko SA, Polyakov PV, Rozin AV, Skibin AP. Effect of porosity structure on penetration and performance of lining materials. *Light Met*. 2005;134:795–804.
63. Yurkov AL, Hramenko SA, Mosin YM. Grain structures and the porosity variations in carbon cathode blocks for the reduction cells (in Russian). *Novye Ogneup*. 2010;5:26–30.
64. Yurkov AL, Hramenko SA, Borisov VI. The influence of the structure and the properties of carbon cathode blocks in early shut downs of the reduction cells. *Alum Sib (Krasnoyarsk)*. 2007;13:236–239
65. Hasselman DPH. Unified theory of thermal shock fracture initiation and crack propagation in brittle ceramics. *J Am Ceram Soc*. 1969;52:600–4.
66. Durand F, Rouby D, Fantozzi G, Allard B, Dumas D. Characterization of the high-temperature mechanical behavior of carbon materials. *Carbon*. 1994;32(3):857–65.
67. Evans AG, Farber KT. Crack growth resistance of microcracking brittle materials. *J Am Ceram Soc*. 1984;67:255–60.
68. Brisson PI, Soucy G, Fafard M, Dionne M. The effect of sodium on the carbon lining of the aluminum electrolysis cell – A review. *Can Metall Q*. 2005;44(2):265–80.
69. Wang Z, Ratvik AP, Skybakmoen E, Grande T. Interaction of sodium vapor and graphite, studied by thermogravimetric analysis. *Light Met*. 2014;143:1239–44.
70. Dewing EW. The reaction of sodium with non-graphite carbon: reactions occurring in the linings of aluminium reduction cells. *Trans Met Soc AIME*. 1963;227:1328.
71. Krohn C, Sorlie M, Øye H. Penetration of sodium and bath constituents into cathode carbon materials used in industrial cells. *Light Met*. 1982;111:311.
72. Ratvik AP, et al. The effect of current density on cathode expansion during start-up. *Light Met*. 2008;137:973–8.
73. Lossius LR, Øye H. Melt penetration and chemical reactions in industrial aluminum carbon cathodes. *Metall Mater Trans B*. 2000;31B:1213–24.
74. Dreyfus JM, Rivoaland L, Lacroix S. Variable resistivity cathode against graphite erosion. *Light Met*. 2004;133:603–8.
75. Øye H, Thonstad J, Dahlqvist K, Handa S, de Nora V. Reduction of sodium-induced stresses in Hall-Heroult cells. *Aluminium*. 1996;72:918–24.
76. Rafieli F, Hiltman F, Hyland M, Welch B. Sub-surface carbide formation contributing to pitting and accelerated cathode wear. *Light Met*. 2001;130:747–52.
77. Murchi A, Chen W, Tremblay M. Comparative characterization of graphitized and graphitic cathode blocks. *Light Met*. 2003;132:617–24.

78. Houston GJ, Welch B, Young D. Uptake of electrochemically generated forms of sodium by various carbons. *Light Met.* 1981;110:529–40.
79. Dell M. Percolation of Hall bath through carbon potlining and insulation. *J Met.* 1971;23(6):18.
80. Dewing EW. The reaction of sodium with non-graphitic carbon: Reactions occurring in the linings of aluminium reduction cells. *Trans Metall Soc AIME.* 1963;227:1328–34.
81. Wilkening S, Reny P. Erosion rate testing of graphite cathode materials. *Light Met.* 2004;133:597–602.
82. Taberaux A, Brown JH, Eidridge IG, Alcom TR. Erosion of cathode blocks in 180 kA prebaked cells. *Light Met.* 1999;128:187.
83. Toda S, Wakasa T. Improvement of abrasion resistance of graphitized cathode block for aluminium reduction cells. *Light Met.* 2003;132:647–53.
84. Schnittker A, Nawrocki H. Performance of graphitized carbon cathode blocks. *Light Met.* 2003;132:641–5.
85. Patel P, Hyland M, Hiltman F. Influence of internal cathode structure on behavior during electrolysis, part 2: Porosity and wear mechanisms in graphitized cathode material. *Light Met.* 2005;135:757–62.
86. Patel P, Hyland M, Hiltman F. Influence of internal cathode structure on behavior during electrolysis, part 3: Wear behavior in graphitic materials. *Light Met.* 2006;136:633–8.
87. Dreyfus JM, Joncourt J. Erosion mechanisms in smelters equipped with graphite blocks: A mathematical modeling approach. *Light Met.* 1999;128:199–206.
88. Liao X, Øye H. Physical and chemical wear of carbon cathode materials. *Carbon* 1996;649–61.
89. Vasshaug K, Foosnaes T, Haarberg G, Ratvik A, Skybakmoen E. Wear of carbon cathodes in cryolite-alumina melts. *Light Met.* 2007;136:821–6.
90. Skybakmoen E, Ratvik A, Solheim A, Rolseth S, Gundbransen H. Laboratory test methods for determining the cathode wear mechanism in aluminium cells. *Light Met.* 2007;136:815–20.
91. Tschöpe K, Store A, Solheim A, Skybakmoen E, Grande T, Ratvik A. Electrochemical wear of carbon cathodes in electrowinning of aluminium. *J Metals.* 2013;65:1403–10.
92. Hiltman F, Gudbransen Y, Rolseth S, Thornstad J. Laboratory test method for measuring wear rates of carbon cathode materials. *Light Met.* 2003;132:655–9.
93. Brillouit P, Lossius LP, Øye H. Penetration and chemical reactions in carbon cathodes during aluminum electrolysis: part I. Laboratory experiments. *Metall Trans B.* 1993;24B:75–89.
94. Krohn C, Sorlie M, Øye H. Penetration of sodium and bath constituents into cathode carbon materials used in industrial cells. *Light Met.* 1982;111:311–24.
95. Zolochovsky A, Hop JG, Foosngs T, Øye H. Rapoport-Samoilenko test for cathode carbon materials I. Experimental results and constitutive modelling. *Carbon.* 2003;41:497–505.
96. Feng N, Kvande H, Øye H. Penetration of sodium and molten bath into high pressure baked cathode blocks. *Aluminium.* 1997;73:265–70.
97. Øye H. ISO standards for testing of cathode materials. *Light Met.* 2008;137:937–42.
98. ISO 17544 ISO 17544:2004. Carbonaceous materials used in the production of aluminium – cold and tepid ramming pastes – determination of rammability of unbaked pastes.
99. ISO 14427 ISO 14427:2004. Carbonaceous materials used in the production of aluminium – cold and tepid ramming pastes – preparation of unbaked test specimens and determination of apparent density after compaction).
100. ISO 14428 ISO 14428:2005. Carbonaceous materials for the production of aluminium – cold and tepid ramming pastes – expansion/shrinkage during baking.
101. ISO 20202 ISO 20202:2004. Carbonaceous materials used in the production of aluminium – cold and tepid ramming pastes – preparation of baked test pieces and determination of loss on baking.
102. ISO 14425:2004. Cold ramming pastes – determination of volatile matter content of unbaked pastes.

103. ISO/TS 14425:2004. Cold ramming pastes – determination of effective binder content and aggregate content by extraction with quinolone, and determination of effective grain size distribution.
104. ISO 20202: ISO 5017 ISO 5017:2013–01. (E) Dense shaped refractory products – determination of bulk density, apparent porosity and true porosity.

Coatings of Carbon Cathode Blocks and New Cathode Materials. Drained Cathode

105. Zhang H, de Nora V, Sekhar JA. Materials used in Hall-Heroult cells for aluminum production. Warrendale, Pa: Minerals, Metals & Materials Society. 1994.
106. Sørliie M, Øye H. Cathodes in aluminium electrolysis. 3rd ed. Aluminium-Verlag; 2010. 662 p.
107. Billehaug K, Øye H. Inert Cathodes for Aluminium Electrolysis in Hall Heroult Cells. (II). Aluminium 1980;56:642–648, 713–17.
108. Sierre R, Pawlek P. Cathodes Wettable by Molten Aluminium for Electrolysis Cells. Aluminium 1990;66:573–82.
109. Liao X, Lin Y. TiB₂coatings on Carbon Cathode Blocks. Light Met. 1990;409–12.
110. Alcorn TR, Stewart DV, Taberaux AT. Recent Advances in wetttable Cathodes for Aluminium Smelting. Light Met. 1990, TMS, 413–8.
111. Brown GD, Hardie GJ, Shaw RP, Taylor MP. Proceedings of 6th Australian Al Smelter Workshop, 1998, p. 499.
112. Borisoglebsky Y, Galevsky G, Kulagin N. The metallurgy of aluminium (in Russian). Novosibirsk: Nauka; 1999. 437 p.
113. Yasanskaya G. Investigation of interactions of molten metals with refractory compounds. Kiev: Naukova Dumka; 1964. 18 p.
114. Yasanskaya G. Properties, processing and application of refractory compounds, Reference book. Moscow, Metallurgiya; 1986. 893 p.
115. Wendt H, Dermietiek S. Erosion of sintered titanium diboride cathodes during cathodic aluminium deposition from lithium chloride/aluminium chloride melts. J Appl Electrochem. 1990;20(3):438–41.
116. Wrei X, Runchi L, Xingwei Z, Xu S, Meiqiu L. Titanium diboride-carbon composite as inert cathode materials in Hall-Heroult cells for aluminium electrolysis. Rare Met. 1992;11(4):260–4.
117. Lu H, Jia W, Ma R. Titanium diboride and molybdenum silicide composite coating on cathode carbon blocks in aluminium electrolysis cells by atmospheric plasma spraying. Light Met. 2005;134:785–8.
118. Huimin L. Titanium diboride and wolfram silicide composite, used as aluminium electrolysis inert cathode materials. Light Met. 2006;135:687–90.
119. Finch NJ. The mutual solubilities of titanium and boron in pure aluminium. Metall Trans. 1992;3:2709.
120. Øye H, de Nora V, Duruz JJ, Jhonson G. Aluminum reduction cell and system for energy. TiB₂ coating on cathode carbon materials. Light Met. 1997;126:279–86.
121. Seitz K, Hiltmann F. Titanium diboride plasma coating of carbon cathode materials, part 1, coating process and microstructure. Light Met. 1998;127:379–83.
122. Hiltmann F, Seitz K. Titanium diboride plasma coating of carbon cathode materials, part 2, characterization. Light Met. 1998;127:385–90.
123. Duan S, Shi Q, Wang Z. Electrode processes in the electrochemical synthesis of TiB₂ in molten fluorides. Proc Electrochem Soc. 1994;94–13:539–47.

124. Devyatkin SV, et al. Electrochemical synthesis of titanium diboride coatings from cryolite melts. *Molten Salt Forum* 1998;5–6 (*Molten Salt Chemistry and Technology* 5): 331–34.
125. Ibrahim MO, Foosnæs T, Øye H. Stability of TiB₂-C composite coatings. *Light Met.* 2006;135:691–5.
126. Liao X, et al. Potline scale application of TiB₂-coating in Hefei Aluminium and Carbon Plant. *Light Met.* 1998;127:685–8.
127. Parker DM. New cathode material may bring revolution. *Am Met Mark.* 1996;104(40):8–9.
128. Sekhar JA, et al. A critical analysis of sodium membranes to prevent carbon cathode damage in the Hall-Heroult cell. *Light Met.* 1996;125:271–8.
129. Sekhar JA, De Nora V, Liu J. A porous titanium diboride composite cathode coating for the Hall-Heroult cell. *Metall Mater Trans B.* 1998;29B:59–69.
130. Sekhar JA, et al. TiB₂/colloidal alumina carbon cathode coatings in the Hall-Heroult and drained cells. *Light Met.* 1998;127:605–15.
131. Wang X, et al. Evaluation of colloidal alumina bonded TiB₂ coatings for improving the carbon cathode performance in Hall-Heroult cells. *Molten Salt Forum.* 1998;5–6:319–26.
132. Liu F, Yang H. Production technology development of carbon materials for aluminium electrolysis in China. *Light Met.* 2003;32:575–9.
133. Welch B. Aluminium production paths in the new millennium. *J Metals.* 1991;51:24–8.
134. Welch B, Hyland M, James BJ. Future materials requirements for the high-energy-intensity production of aluminium. *J Metals.* 2001;N2:13–8.

Side Lining

135. Sørli M, Øye H. Cathodes in aluminium electrolysis. 3rd ed. Aluminium-Verlag; 2010. 662 p.
136. Jarret N. Cathode design, p. 60–85. In: Burkin AR, editors. *Production of aluminium and alumina.* Wiley; 1987. 238 p.
137. Grjothheim K, Welch B. *Aluminium smelter technology.* 2nd ed. Dusseldorf: Aluminium-Verlag; 1988. 328 p.
138. Kosolapova TY (ed). *Properties, application and application of heat prof compounds, Reference book (in Russian).* M Metall 1986. 928 p.
139. Moulson F. Review reaction-bonded silicon nitride: its formation and properties. *J Mater Sci.* 1979;14(5):1617–51.
140. Mangels JA. Effect of rate-controlled nitriding and nitriding atmospheres on the formation of reaction-bonded Si₃N₄. *Am Ceram Soc Bull.* 1981;60:613–7.
141. Riley F. *Structural ceramics. Fundamentals and case studies.* Cambridge University Press; 2009. 405 p.
142. Yurkov A, Danilova O, Dovgal A. Nitride bonded silicon carbide refractories: structure variations and corrosion resistance, 13th Biennial Worldwide Congress on Refractories UNITECR 2013, the Unified International Conference on Refractories, 10–13 Sept. 2013, Victoria, p. 991–6.
143. Yurkov A, Danilova O, Dovgal A. N-SiC side lining – variations of materials structure. *Light Met.* 2014;143:1245–9.
144. Jorge E, Marguin O. Si₃N₄ bonded SiC refractories for higher aluminium cell performance. *Aluminium times.* Sept 2004;47–50.
145. Jorge E, Marguin O, Temme P. The usage of N-SiC refractories for the increasing of productivity of aluminium reduction cells. *Alum Sib.* 2003;9:203–8. Krasnoyarsk.
146. Etzion R, Metson J, Depree N. Wear mechanism of silicon nitride bonded silicon carbide refractory materials. *Light Met.* 2008;137:955–9.
147. Zhao J, Dong J, Wang W, Cheng Z, Zhang Z. Comparison of cryolite resistance of silicon carbide materials. *Light Met.* 2000;123:443–8.

148. Wang Z, Skybakmoen E. Tor Grande chemical degradation of Si_3N_4 -bonded SiC sideling materials in aluminium electrolysis cells. *J Am Ceram Soc.* 2009;92:1296–302.
149. Xue J, Wu L, Liu Q, et al. Sidewall materials for the Hall-Heroult process. *Light Met.* 2007;139:883–7.
150. Proshkin AV, Pingin VV, Polyakov PV, et al. Analysis of decay of side lining in cathodes for aluminium reduction cells. *J Sib Fed Univ Eng Technol.* 2013;3:276–84.
151. Skybakmoen E, Stoen L, Kvello J, Darrel O. Quality evaluation of nitride bonded silicon carbide sideling materials. *Light Met.* 2005;134:773–8.
152. Skybakmoen E, Gudbransen H, Stoen LI. Chemical resistance of sideling materials based on SiC and carbon in cryolitic melts – a laboratory study. *Light Met.* 1999;128:215–22.
153. Skybakmoen E, Kvello J, Darrel O, Gudbransen H. Test and analysis of nitride bonded SiC sideling materials: typical properties analysed 1997–2007. *Light Met.* 2008;137:943–8.
154. Xiaozhou C, Bingliang G, Zhaowen W, Xiamwey H, Zhuxian Q. A new test method for evaluating Si_3N_4 -SiC brick's corrosion resistance to aluminium electrolyte and oxygen. *Light Met.* 2006;135:659–61.
155. Zhao J, Zhang Z, Wang W, Liu G. Test method for resistance of SiC material to cryolite. *Light Met.* 663–6.
156. Liu C, Huang Z, Liu G, Zhang Z. Excellent cryolite resistance and high thermal conductivity SiC sidewall material for high amperage aluminium reduction cells. *Light Met.* 2010;139:889–94.
157. Cao C, Gao B, Wang Z, Hu X, Qui Z. A new test method for evaluating Si_3N_4 -SiC bricks corrosion resistance to aluminium electrolyte and oxygen. *Light Met.* 2006;135:659–61.
158. Zhao J, Zhang Z, Wang W, Liu G. Test method for resistance of SiC material to cryolite. *Light Met.* 2006;135:663–6.
159. Mikhalev Y, Proshkin A, Isaeva L, Polyakov P, Filonenko A. Modification of a method for testing of SiC blocks, proceedings 31st international conference ICSOBA and 19th International Conference Aluminum of Siberia, Krasnoyarsk, 2013, p. 693–7.
160. Pawlek R. SiC in aluminium electrolysis cells. *Light Met.* 1995;124:527–33.
161. Gao B, Wang Z, Qiu Z. Corrosion tests and electrical resistivity measurement of SiC- Si_3N_4 refractory materials. *Light Met.* 2004;133:419–24.
162. Etzion R, Metson JB. Factors affecting corrosion resistance of silicon nitride bonded silicon carbide refractory blocks. *J Am Ceram Soc.* 2012;95:410–5.
163. ASTM C863-00(2010) Standard test method for evaluating oxidation resistance of silicon carbide refractories at elevated temperatures.
164. John D, Maurage R. Sialon bonded silicon carbide sidewall pieces for the aluminium reduction cell. *Ceram Ind Int.* 1992;182:42.
165. Jack KH. Sialons and related nitrogen ceramics. *J Mater Sci.* 1976;11:1135–58.
166. Gauckler LJ. Contribution to the phase diagram Si_3N_4 -AlN- Al_2O_3 - SiO_2 . *J Am Ceram Soc.* 1975;58:346–7.
167. Yan XY, Mikhlis RZ, Rhamdhani MA, Brooks GA. Aluminate spinels as sidewall lining for aluminium smelters. *Light Met.* 2011;140:1085–90.
168. Flickel AF, Volker M. On the technological potential of SiC-TiB₂- Si_3N_4 compounds in Al-electrolysis cells. *Light Met.* 1994;123:493–9.

Silicon Carbide Mortars, Ramming Mixes, and Castables for Installation of SiC Side Lining

169. ISO 13765-4:2004. Refractory mortars – Part 4: Determination of flexural bonding strength.

Refractory Barrier Materials of the Cell Lining. Dry Barrier Mixes and Bricks. Properties and Chemical Resistance. The Processes During Service. Interactions with Infiltrated Electrolyte. Change of Properties. Lenses

170. Arhipov G. Physico-chemical and thermo mechanical processes in the lining of aluminium reduction cells. News of RUSAL (in Russian) 2002;(1):37–45.
171. Yakimov I, Arhipov G, Pogodaev A, Shimansky A. Physico-chemical investigations of parts of the cathode lining of aluminium reduction cells. Alum Sib. 2003;9:209–13.
172. Arhipov G. Physico-chemical and thermo mechanical processes in the lining of aluminium reduction cells. News of RUSAL (in Russian), 2003;(4):9–18.
173. Arhipov G, Borisov V, Ivanova A. The changes of materials properties in the lining of aluminium reduction cells. News of RUSAL (in Russian), 2004;(8):23–8.
174. Arhipov A, Borisov V, Ivanova A. The properties of the lining of aluminium reduction cells. Novye orneupory (in Russian), 2004;(6):39–45.
175. Ivanovsky L, Lebedev V, Nekrasov V. Anode processes in molten halogenides. M Nauka 1983. 268 p.
176. Schoning C, Grande T, Silian O-J. Cathode refractory materials for the aluminium reduction cells. Light Met. 1999;128:231–8.
177. Sturm E, Prepeneit J, Sahling M. Economic aspects of an effective diffusion barrier. Light Met. 2002;131:433–9.
178. Pelletier R, Allaire C. Corrosion in potlining refractories: Effect of cathode material interpreted using a unified approach. J Met. 2003;55:59–62.
179. Siljan OJ, Junge O, Swendsen T, Thovsen K. Experiences with dry barrier powder materials in aluminium electrolysis cells. Light Met. 1988;117:573–81.
180. Melas J. Chemobar, a dry barrier material for aluminium reduction cells. Light Met Age. 1994;53(1–2):62.
181. Sørli M, Øye H. Cathodes in aluminium electrolysis. 3rd ed. Aluminium-Verlag; 2010. 662 p.
182. ISO 20292:2009. Materials for the production of primary aluminium – dense refractory bricks – determination of cryolite resistance.
183. Tabereaux AT. Reviewing advances in cathode refractory materials. J Met. 1992;20–6.
184. Allaire C. Electrolysis bath testing of refractories at Alcan. J Can Ceram Soc. 1991;60(2):47–52.
185. Allaire C, Pelletier R, Siljan OJ, Tabereaux A. An improved corrosion test for potlining refractories. Light Met. 2001;130:245–9.
186. Simakov D, Proshkin A. Tests for cryolite resistance of refractory materials. News of RUSAL (in Russian). 2004;8:34–41.
187. Siljan OJ, Grande T, Schoning C. Refractories for aluminium electrolysis cells. Part 4: Comparison of laboratory investigations and autopsies of pot linings. Aluminium. 2001;77:809–14.
188. Thonstad J, Fellner P, Haarberg G, et al. Aluminium electrolysis. Fundamentals of the Hall-Heroult process. Aluminium Verlag; 2001. 359 p.
189. Harris D, Oprea G. Cryolyte penetration studies on barrier refractories for aluminum electrolytic cells. Light Met. 2000;129:419–27.
190. Rutlin J, Grande T. Fluoride attack on aluminosilicate refractories in aluminium reduction cells. Light Met. 1997;127:295–301.
191. Grande T, Rutlin J. Viscosity of oxyfluoride melts relevant to the deterioration of refractory linings in aluminium reduction cells. Light Met. 1999;138:295–301.
192. Oprea G. Corrosion tests on refractories for aluminium electrolytic cells, Proceedings of the 9th symposium on refractories for the aluminum industry, 1999, p. 189–205.

193. Guangchun Y, Wangxi Z, Zhuxian Q, et al. On the MgO-C composite refractory diffusion barriers in alumina reduction cell cathodes. *Light Met.* 1993;122:349–51.
194. Siljan OJ, Slagnes S, Sekkingstad A, Aaram S. Olivin-based refractories in potlinings of aluminium electrolysis cells. *Light Met.* 2004;133:405–11.
195. Grande T, Rutlin J. Viscosity of oxyfluoride melts relevant to the deterioration of refractory linings in aluminium reduction cells. *Light Met.* 1999;138:431–436.
196. Siljan OJ. Studies of the refractory –melt interface in aluminium reduction cells, refractories for the next millennium, Proceedings of the 9th Symposium Refractories for the Aluminum Industry, 1999.
197. Schoning C, Grande T, Siljan OJ. Cathode refractory materials for aluminium reduction cells. *Light Met.* 1999;155–76.
198. Yurkov A, Hramenko S, Mosin Y. Grain structures and the porosity variations in carbon cathode blocks for the reduction cells (in Russian). *Novye Ogneup.* 2010;5:26–30.
199. Yurkov A, Hramenko S, Borisov V. The influence of the structure and the properties of carbon cathode blocks in early shut downs of the reduction cells. *Alum Sib* 2007;13.
200. Solheim A, Schoning C. Sodium vapor degradation of refractories used in aluminium cells. *Light Met.* 2008;137:967–72.
201. Grande T, Schoning C, Siljan OJ. Cathode refractory materials for aluminium reduction cells. *Light Met.* 1999;128:231–7.
202. Proshkin A, Pogodaev A. Property change of dry barrier mixes in a cathode of aluminium reduction cells. *Light Met.* 2007;137:833–8.
203. Yurkov A, Akselrod L, Kvyatkovsky O. The corrosion resistance to cryolite of new and traditional refractories. *News of RUSAL (in Russian).* 2003;4:53–6.
204. Allaire C. Refractory lining for electrolytic cells. *J Am Ceram Soc.* 1992;75:2308–11.

Heat Refractory Insulation Materials for the Lining of the Reduction Cells

205. Weibel R, Juhl LF, Nielsen B, et al. Aging of cathode refractory materials in aluminium reduction cells. *Light Met.* 2002;131:425–33.
206. Kaplan F, Akselrod L, Puchkelevich Y, Yurkov A. Heat insulation materials for aluminium reduction cells. *Novye Ogneup (in Russian).* 2002;10:9–18.
207. Arhipov G. Physico-chemical and thermo mechanical processes in the lining of aluminium reduction cells. *News of RUSAL (in Russian),* 2002;(1):37–45.
208. Yakimov I, Arhipov G, Pogodaev A, Shimansky A. Physico-chemical investigations of parts of the cathode lining of aluminium reduction cells. *Alum Sib.* 2003;9:209–13. Krasnoyarsk.
209. Arhipov G. Physico-chemical and thermo mechanical processes in the lining of aluminium reduction cells. *News of RUSAL (in Russian),* 2003;(4):9–18.
210. Arhipov G, Borisov V, Ivanova A. The changes of materials properties in the lining of aluminium reduction cells. *News of RUSAL (in Russian),* 2004;(8):23–8.
211. Arhipov G, Borisov V, Ivanova A. The properties of the lining of aluminium reduction cells. *Novye Ogneup (in Russian),* 2004;(6):39–45.
212. ASTM C-155-97 (2002). Standard classification of insulating firebrick.
213. ISO 2245-1990. Shaped insulating refractory products: classification.
214. Refractory engineering: Materials – design – construction. 2nd ed. Essen, Vulkan-Verl.; 1996. 355 p.

Chapter 3

Refractories and Heat Insulation Materials for the Cast House

3.1 Cast House

Aluminium alloys are cast in the cast houses of aluminium smelters and at the cast houses of the plants for the secondary aluminium. At smelters, the raw liquid aluminium is transported from the reduction shop in the ladles. Primary aluminium ingots are shipped to the cast house of the secondary aluminium plant from the aluminium smelter. The organization of the cast house at the smelter and of that at the secondary aluminium plant has some differences.

The reduction of alumina-electrolyte melts gives metal, containing 99.8–99.85 % Al. The conventional raw aluminium is 99.5–99.7% Al. Raw Al from reduction cells contains admixtures, and it is refined before pouring. After treatment with flux, raking of the slag, adjustment of temperature, and chemical analysis, the molten Al is considered to be ready for pouring.

Usually at the smelters, the production of the cast house includes small and large ingots, extrusion billets, rolling ingots (slabs), T-ingots, and sometimes Al wire. Raw Al from the reduction shop is poured in the holding furnace, and it is used for primary Al ingots or for alloys in the form of extrusion billets, rolling ingots (slabs), and T-ingots. In the holding furnaces, the raw Al is kept for a certain time for degassing, for the addition of the master alloys and admixtures for the preparation of alloys, and for the addition of fluxes for the removal of admixtures.

There are three groups of admixtures in raw Al: nonmetallic, metallic, and gaseous. Nonmetallic admixtures are electrolyte, alumina, aluminium carbide, carbon particles, and oxide spots. They are taken from the reduction cell at tapping. Metallic admixtures are iron, silicon, titanium, sodium, and calcium. They come from raw materials. The gaseous admixture in raw Al is mostly hydrogen.

For primary Al, the molten metal of a slightly different composition from different cells is mixed in the holding furnace. The mixing (together with purification and degassing) is done in certain proportions in order to obtain metal of a



Fig. 3.1 The ladle

certain quality, corresponding to a certain grade. It is poured from the tap hole through the launder to the ingot casting machine.

To receive alloys, there are additional purification and alloying procedures. Raw Al is purified from metallic and gaseous admixtures and from sodium and calcium by a gas purging technique. Aluminium goes through the launders to the degassing unit and then to the direct chill mold.

The metallurgical equipment of cast houses at smelters includes ladles for transporting raw Al from the reduction shop to the cast house (Fig. 3.1), stationary or tilting holding furnaces, degassing units, induction furnaces for remelting of disposal or wastes and preparation of alloys, and gas-fired furnaces for remelting of disposal and wastes.

The typical metallurgical device on the secondary Al plants is a combined melting and holding furnace. Metal is loaded in the melting furnace either through the side windows or from above (if the roof is removable); it is melted in the melting furnace and then goes through the launder to the holding furnace. The metal arrives at the secondary Al plant already purified of gas and some admixtures. There are no other principal differences.

The metallurgical equipment of cast houses at secondary Al plants is melting furnaces, stationary or tilting holding furnaces, degassing units, crucible- or channel-type induction furnaces for remelting of disposal or wastes and preparation of alloys, and gas-fired furnaces for remelting of disposal and wastes.

Usually in the cast houses of smelters, primary Al (Table 3.1) ingots and low-alloyed extrusion billets, rolling ingots (slabs), and T-ingots are cast. The cast house of the secondary Al plants produces highly alloyed extrusion billets and rolling ingots (Table 3.1).

Table 3.1 Classification of aluminium alloys

Alloy group	Mechanical forming group	Casting group
Primary	1XXX	1XXXXO
Al-Cu	2XXX	2XXXXO
Al-Mn	3XXX	
Al-Si	4XXX	4XXXXO
Al-Mg	5XXX	5XXXXO
Al-Mg-Si	6XXX	6XXXXO
Al-Zn	7XXX	7XXXXO
Al-Li, other	8XXX	

3.2 Physical and Chemical Interaction of Refractories with Aluminium and Aluminium Alloys

The melting point of Al is only 660 °C, and the temperature of the molten Al in holding furnaces is in the range of 700–750 °C, so for a long time it was considered that in an Al cast house it is possible to use the refractories for ferrous metallurgy. Initially, the fireclay brick was a main refractory in the Al cast house. Later, some alumina silica refractories and alumina refractories appeared. The trend of refractories for the Al cast house started to appear around the mid-1980s.

In comparison with other metals (ferrous industry), Al

- has a very low viscosity (at 700–800 °C, the viscosity of Al is close to the viscosity of water),
- has a high wetting ability,
- oxidizes at the temperature of processing.

The refractories should withstand high chemical corrosion (which increases at alloying), erosion, thermal shock, and mechanical loads. The action of fluxes is not as severe as in ferrous metal

3.2.1 *Chemical Interaction of Aluminium and Aluminium-Based Alloys with Components of Refractories*

Table 3.2 [1] gives the first assumption of interactions of Al and Al-based alloys with oxides, which are the base of refractories. Silicon oxide, iron oxide, titanium oxide, and sodium oxide can be deoxidized by Al:



In the presence of magnesium (the most common component of aluminium alloys), spinel may be the product of the reaction:

Table 3.2 Gibbs energy of reactions of aluminium and magnesium with oxides at 1,000 °C [1]

							<i>G</i> (kJ/mol)
Al	+	¼SiO ₂	→	½Al ₂ O ₃	+	¾Si	−138.3
Al	+	½FeO	→	½Al ₂ O ₃	+	½Fe	−374.2
Al	+	½Na ₂ O	→	½Al ₂ O ₃	+	Na	−289.9
Al	+	¼TiO ₂	→	½Al ₂ O ₃	+	¾Ti	−110.2
Mg	+	½SiO ₂	→	MgO	+	½Si	−97.2
Mg	+	FeO	→	MgO	+	Fe	−134.1
Mg	+	Na ₂ O	→	MgO	+	Na	−205.3
Mg	+	½TiO ₂	→	MgO	+	2Ti	−123.2
Mg	+	½Al ₂ O ₃	→	MgO	+	¾Al	−39
Mg	+	Al ₂ O ₃	→	MgAl ₂ O ₄	+		−33.5
Mg	+	⅔Al ₂ O ₃	→	MgAl ₂ O ₄	+	¾Al	−72.5



According to the main laws of thermodynamics, the value of Gibbs energy ΔG shows the route of the reaction. The reaction proceeds if ΔG is below zero, and arrows in Table 3.2 show the route.

The values in Table 3.2 do not show the following circumstances:

- In the melt of Al, there are always impurities (sodium, potassium, and gases) and admixtures (magnesium, strontium, zirconium, etc.). These impurities and admixtures are, for one thing, the corrosive agents, but additionally, due to their activity, they increase the corrosive action of Al.
- Oxides in compounds (silicon oxide in calcium silicate, magnesium silicate, and aluminium silicate) are less active and less reactant.
- As is always recommended for the analysis of thermodynamic data, it is necessary to take into account not only the thermodynamic probability, but also the kinetic factor and the properties of materials as well: bonding phase, porosity, and type and shape of pores, and so on.

In fireclay and other alumina silica refractories, the interaction with Al proceeds from the first hours of the service. The practical proof for this is the increased silicon content in Al during the first 2–3 days [2, 3] if the metallurgical service is lined with fireclay or alumina silica refractories. After that, a layer of so-called corundum – a mixture of partly oxidized aluminium and partly reduced silicon – covers the lining and prevents Al melt from contamination by silicon (but doesn't stop the infiltration of Al inside the refractory).

Thermodynamically, reaction (3.1) is possible at all temperatures of service. Aluminium wets the refractory, which opens the possibility for a phase-to-phase reaction. Aluminium melt infiltrates through the open pores. The pore dimensions, through which the melt cannot penetrate due to the capillary effects, vary depending on the temperature, structure, and composition of refractories, as well as on the type of Al alloy.

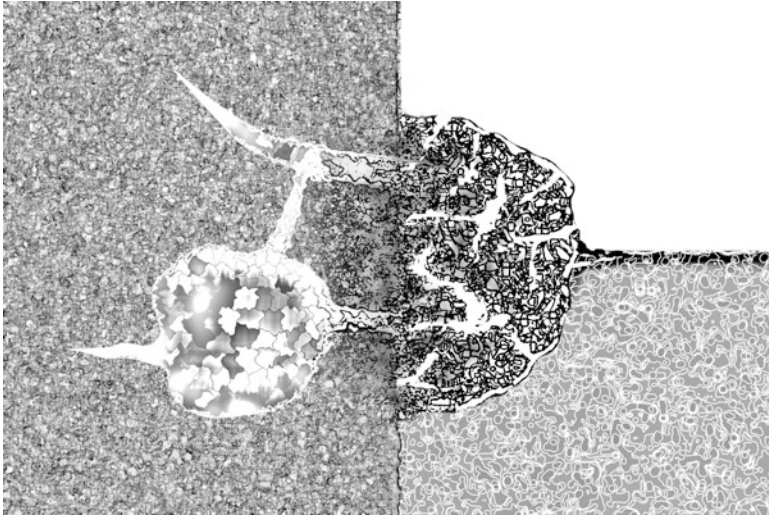


Fig. 3.2 Corundum growth at the border of metal and refractory

For a general understanding, the following is list of comparative data:

- The critical pore dimension (through which the melt cannot penetrate due to the capillary effect) for molten steel – about 30 μm ;
- for molten cast iron – 5 μm ;
- for Al melt – 0.5 μm .

Due to the appearance of silicon on the surface of capillary pores according to reaction (3.1), the infiltration of molten Al increases. In an Al holding furnace, fireclay brick is metallized (infiltrated) after 2–3 years, and mullite brick is after 3–4 years. In the course of these interactions, the refractory gains weight, and the weight increase of fireclay brick is up to 3 kg (starting weight about 4.5 kg), while the weight increase for alumina brick is 1 kg (starting weight about 6.5 kg) [2, 3].

Generally, the decay of alumina silica refractories in the presence of molten Al is described in the literature [3] as

On the triple border “refractory–air–molten Al” (Fig. 3.2), molten Al interacts with oxygen from the air, giving “corundum” (here the term “corundum” is for the mix of alumina with alumina, partly reduced by aluminium). This process is activated by magnesium and other metals. As a result, the outgrowth appears on the walls, which decreases the volume of the furnace. These outgrowths are removed mechanically, but as its strength is big, as well as the adhesion, cracks appear in the lining. These cracks allow the infiltration of Al.

Aluminium penetrates the lining through pores; in the pores, Al may react with silicon oxide, titanium oxide, and iron oxide. This process is accompanied by an increase in thermal conductivity.

Table 3.3 Gibbs energy for reactions of aluminium and magnesium with oxides, $T = 1,000$ K (according to [1-4])

Reaction	ΔG (kJ/mol)
$4Al + 3SiO_2 = 2Al_2O_3 + 3Si$	-528.25
$8Al + 3 \times 3Al_2O_3 \cdot 2SiO_2 = 13Al_2O_3 + 6Si$	-1,101.80
$4Al + 3TiO_2 = 2Al_2O_3 + 3Ti$	-432.05
$2Al + Cr_2O_3 = Al_2O_3 + 2Cr$	-483.35
$2Al + 3ZnO = Al_2O_3 + 3Zn$	-618.40
$2Al + 3FeO = Al_2O_3 + 3Fe$	-374.20
$2Al + 3Na_2O = Al_2O_3 + 6Na$	-289.90
$2Mg + SiO_2 = 2MgO + Si$	-97.20
$Mg + FeO = MgO + Fe$	-134.10
$Mg + Na_2O = MgO + 2Na$	-205.30
$2Mg + TiO_2 = 2MgO + Ti$	-123.20
$3Mg + Al_2O_3 = 3MgO + 2Al$	-39.00
$Mg + 2Al + 2SiO_2 = MgO \cdot Al_2O_3 + 2Si$	-72.50
$Mg + 0.5O_2 + Al_2O_3 = MgO \cdot Al_2O_3$	-33.50
$2Al + Y_2O_3 = Al_2O_3 + 2Y$	+254.70
$2Al + 3CaO = Al_2O_3 + 3Ca$	+232.10
$4Al + 3CaO \cdot SiO_2 = 2Al_2O_3 + 3CaO + 3Si$	-178.50
$2Al + 3 MgO = Al_2O_3 + 3Mg$	+116.90
$4Al + 3 MgO \cdot SiO_2 = 2Al_2O_3 + 3MgO + 3Si$	-98.30
$4Al + 3ZrO_2 = 2Al_2O_3 + 3Zr$	+4.15
$4Al + 3ZrO_2 \cdot SiO_2 = 2Al_2O_3 + 3Si + 3ZrO_2$	-527.60
$4Al + 3 MgO \cdot SiO_2 = 2Al_2O_3 + 3MgO + 3Si$	-98.30
$2Mg + SiO_2 = 2MgO + Si$	-97.20
$Mg + FeO = MgO + Fe$	-134.10
$Mg + Na_2O = MgO + 2Na$	-205.30
$2Mg + TiO_2 = 2MgO + Ti$	-123.20
$3Mg + Al_2O_3 = 3MgO + 2Al$	-39.00
$Mg + 2Al + 2SiO_2 = MgO \cdot Al_2O_3 + 2Si$	-72.50
$Mg + 0.5O_2 + Al_2O_3 = MgO \cdot Al_2O_3$	-33.50

The process should be passivated (stoped) by the films of alumina on the surface, but the presence of alcalies together with fluorine and chlorine from fluxes (in the gaseous phase) prevents the appearance of dense films.

Molten Al cannot interact with aluminium oxide, magnesium oxide, barium oxide, or calcium oxide. In the 1960s, magnesia bricks were used for the lining of furnaces. At that time, this decision was not accepted in industry due to the low thermal shock resistance of magnesia bricks (in melting furnaces, this factor is essential). The previously mentioned refractory materials are sufficiently more expensive compared with alumina silica refractories. Generally speaking, there are other compounds (yttrium oxide and zirconium oxide) that also may be resistant to molten Al, as Table 3.3 shows.

Compounds containing magnesium, barium, calcium, and aluminium are the main antiwetting agents for the refractories for Al; it is to some extent the consequence from the data appearing in Table 3.3.

Another consequence from Table 3.3 is that silicates of magnesium, calcium, and zirconium (which are more available based on cost considerations) can interact with aluminium.

The same cost considerations promote research activities in refractories for molten Al in the direction of the enhancement and advancement of the structure and properties of alumina silica refractories, which are not optimal materials for contact with molten Al.

3.2.2 *Antiwetting Admixtures to Alumina Silica Refractories*

There are several publications [4–16] on admixtures of barium sulfate, aluminium fluoride, aluminium borate, aluminium titanate, calcium silicate (wollastonite), aluminium nitride, and silicon carbide and its combinations in alumina silica refractories for decreasing the wetting ability of Al in these refractories.

Barium sulfate, BaSO₄, is introduced in amounts up to 5–10% in concrete compositions (if calculating barium oxide) and up to 5% in the green mixtures of bricks. It is considered to have a good antiwetting effect. Above 1,000–1,100 °C, BaSO₄ slowly decomposes, giving barium oxide and gaseous sulfur oxides. This reaction (3.3) is accompanied by a negative volume effect and the appearance of cavities:

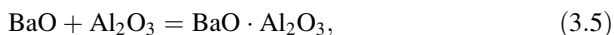


According to [8, 9], the antiwetting effect of barium sulfate decreases above 1,050 °C. This probably takes place due to the transformation of barium sulfate into celsian BaAl₂Si₂O₈:

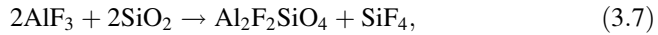


Barium alumina silicate celsian also may be an antiwetting agent, although is a lower degree than barium sulfate. Barium sulfate transforms into celsian in service in concretes and in phosphate-bonded bricks as well. Celsian is stable until 1,500 °C.

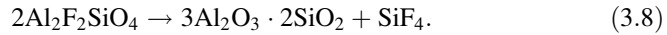
Barium oxide also may interact with alumina, giving barium aluminium spinel or barium hexaaluminate BaO · 6Al₂O₃:



Aluminium fluoride and calcium fluoride (fluorite) also are introduced in a green mixture of refractories up to 5–7 %. The mechanism of their antiwetting action is probably similar. They are not stable in an oxidizing atmosphere and slowly oxidize, yet their transformations differ. Aluminium fluoride interacts with silica [6–8]:



which slowly decomposes into mullite and silicon tetrafluoride:



Aluminium fluoride may interact with calcium oxide, giving calcium fluoride [8, 9]:



In the beginning, the antiwetting action is probably due to anions of fluorine, and after the transformation of anorthite ($\text{CaAl}_2\text{Si}_2\text{O}_8$), it is due to the calcium atom in anorthite.

The temperature of the transformation of calcium and aluminium fluorides is 1,200–1,250 °C, which means that the temperature interval of their application is a little higher than that of barium sulfate.

One point of view is that the antiwetting action is due to the cation part, and one may suppose that the antiwetting action would increase with the increasing ionic radius in the range aluminium, calcium, magnesium, barium.

Another point of view is that the antiwetting action is due to the anionic part [13]; barium sulfate in the presence of oxygen may react with molten aluminium, and the antiwetting action takes place due to the occupation of permeable pores with the products of reaction:



Antiwetting additives increase the wetting angle up to 105–125°; consequently, the infiltration will depend on the hydrostatic pressure of the layer of Al. Barium sulfate transforms into celsian, barium spinel, and barium hexaaluminate, and the antiwetting action decreases, and consequently, the wetting angle increases, and the wetting ability of Al increases. In service, these processes take 2–4 years.

There have been publications [14] on the antiwetting additive wollastonite (calcium silicate, CaSiO_3). Wollastonite is not wetted by Al and might be a good refractory for Al. Unfortunately, at 1125 °C, β -wollastonite transforms into α -wollastonite with a big volume effect. The temperature of the phase transformation is a temperature of safe application as a refractory material. It is too low for using wollastonite-based material for furnaces; however, it is used in the runners, where the temperature cannot be too high. As a compound of refractory mixes, it transforms into anorthite.

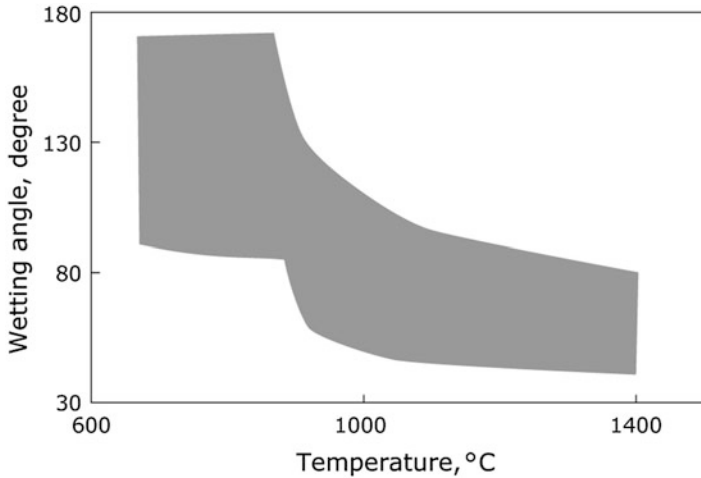


Fig. 3.3 Summarized data on wetting of alumina silica materials by molten Al [16]

It is considered [8] worth adding together admixtures of barium sulfate and calcium fluoride. The decrease in the antiwetting ability of refractory after 1,000 °C will not be sharp.

3.2.3 *Wetting of Alumina Silica Refractories by Molten Aluminium and Aluminium Alloys*

The wetting behavior depends on several factors. In an oxidizing atmosphere, there is always reaction wetting, which means that molten Al reacts with oxygen, giving oxide films. This process is intensified near a refractory that is on the border “gas–liquid–solid.” There is a lot of data on the wetting of oxides with molten Al in vacuum, which has limited significance for the metallurgy of Al [17–25]. The surface of real refractories is rough, which increases wetting. Fluxes give potassium and sodium chlorides; sodium and aluminium fluorides come with electrolyte and also influence the wetting ability. These are all reasons why the values of the wetting angle of Al differ. Figure 3.2 depicts data gathered by [17] from many references [18–25]. The wetting angle varies from 90 to 160° near the melting point of Al, whereas at 900–1,000 °C it varies from 30 to 80° (Fig. 3.3).

In papers devoted to the wetting of real refractories [20–24], the measured wetting angle differs from 80 to 140°. It decreases with increased temperature. In industrial furnaces, there are always elements of wetting. Without antiwetting additives, the wetting angle is 80–140° at 700 °C, and at 900 °C, it varies from 80 to 110°. If the wetting angle is more than 90°, the hydrostatic pressure of Al at a depth of 50–300 mm will be from $1,13 \times 10^3$ Pa (at depth 50 mm) to 6×10^3 Pa (at depth 300 mm).

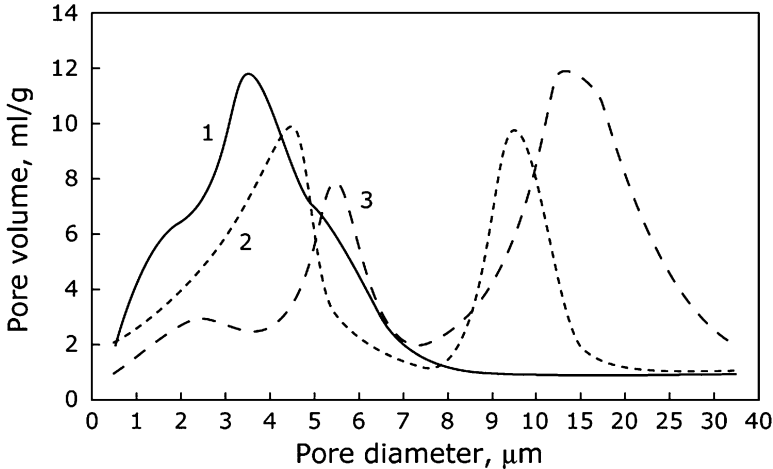


Fig. 3.4 The pore size distribution of low cement castables (1, 2) and mullite brick (3)

$$P_h = \rho_{Al} g h_{Al}, \quad (3.11)$$

where P_h is the hydrostatic pressure, ρ_{Al} is the density of molten Al, h_{Al} is the height of the Al layer, and g is the gravitational acceleration

from $1,13 \times 10^3$ Pa (at depth 50 mm) to 6×10^3 Pa (at depth 300 mm).

The capillary pressure in the pores is

$$P_k = \frac{-2\sigma_{Al} \cdot \cos \theta}{r_k}, \quad (3.12)$$

where P_k is the capillary pressure, σ_{Al} is the surface tension of molten Al, θ is the wetting angle; the infiltration of Al in the pores of the refractory will depend on the dimension of permeable pores.

So for the refractories without anti-wetting additives (considering the angle of wetting 100°) the critical pore radius at the depth of 100 mm will be $10 \mu\text{m}$. If the angle of wetting will be 120° , the critical pore radius at 300 mm will be $30 \mu\text{m}$ [26]. Generally speaking, the critical pore radius is $10\text{--}20 \mu\text{m}$ for refractories without antiwetting additives. In general, antiwetting additives increase the wetting angle to $105\text{--}125^\circ$, so the critical pore radius will be bigger. As antiwetting additives decompose, the wetting angle increases, and the critical pore radius increases at service in 2–4 years.

3.2.4 Some Words on Corrosion Mechanism

Aluminium can react with oxides on the surface of the refractory and in the pores. If Al reacts on the surface, the liquid product of reaction (silicon) will dissolve in Al and will be taken away. It should not be calculated as a product in a calculation of

Table 3.4 Capillary pressure of molten aluminium ($\text{Pa} \times 10^3$) in pores of different dimensions for different wetting angles

Wetting angle ($^\circ$)	<i>r</i> of pore (μm)						
	5	10	15	20	25	30	40
95	0.30	1.50	1.00	0.75	0.60	0.50	0.37
100	0.60	3.00	2.00	1.50	1.20	1.00	0.75
110	1.17	5.85	3.90	2.92	2.34	1.95	1.46
120	1.72	8.61	5.74	4.31	3.44	2.87	2.15
130	2.20	11.02	7.35	5.51	4.41	3.67	2.75
140	2.61	13.09	8.72	6.54	5.23	4.36	3.27

Table 3.5 Volume effects of reactions of aluminium with oxides [26–28]

No.	Reaction	ΔG (kJ/mol)	$\Delta V/V$ (% volume effect)	
			On the surface	In pores
4.1	$4\text{Al} + 3\text{SiO}_2 = 2\text{Al}_2\text{O}_3 + 3\text{Si}$	-528.25	-47.25	-81.10
4.2	$8\text{Al} + 3 \times \text{Al}_2\text{O}_3 \cdot 2\text{SiO}_2 = 13\text{Al}_2\text{O}_3 + 6\text{Si}$	-110.80	-66.20	-80.4
4.3	$2\text{Mg} + \text{SiO}_2 = 2\text{MgO} + \text{Si}$	-97.20	-44.30	-68.05
4.4	$3\text{Mg} + \text{Al}_2\text{O}_3 = 3\text{MgO} + 2\text{Al}$	-39.00	-49.70	-49.70
4.5	$\text{Mg} + 2\text{Al} + 2\text{SiO}_2 = \text{MgO} \cdot \text{Al}_2\text{O}_3 + 2\text{Si}$	-72.50	-49.88	-80.20
4.6	$\text{Mg} + 0.5\text{O}_2 + \text{Al}_2\text{O}_3 = \text{MgO} \cdot \text{Al}_2\text{O}_3$	-33.50	-99.00	-99.00
4.7	$\text{Mg} + 2\text{O}_2 + 2\text{Al} = \text{MgO} \cdot \text{Al}_2\text{O}_3$	-65.80	116.40	116.40
4.8	$3\text{Mg} + 3\text{Al}_2\text{O}_3 \cdot 2\text{SiO}_2 = 3\text{MgO} + 2\text{Si} + 3\text{Al}_2\text{O}_3$	-72.50	-77.80	-94.70
4.9	$3\text{Mg} + 3\text{Al}_2\text{O}_3 \cdot 2\text{SiO}_2 = 3\text{MgO} \cdot \text{Al}_2\text{O}_3 + 2\text{Si}$	-82.50	-83.50	100.30

the volume effect. The volume effect of the reactions on the surface of the refractory is negative, which means that there will be no continuous film. If Al reacts with oxide in the pore, the liquid product of the reaction (silicon) will crystallize in the pore because the melting point of silicon is $1,410^\circ\text{C}$, while the temperature of the melt is below 800°C . In this case, the product of the reaction should be taken into account when one calculates the volume effect. Thus, there are two values of volume effects of reactions – on the surface of refractories and in the pores (Table 3.4).

The volume effect of reactions on the surface is negative; the reaction products occupy less space than reactants do, meaning there will be no continuous film, and Al will continue to penetrate inside the refractory. The silicon that appears in the pores (especially in dead-end pores) will crystallize, and the volume effect of some reactions is positive, which means that the products of reactions might incline the pores, causing spalling and cracking [15, 16] (Table 3.5).

The porous film of the aluminium oxide that appears is not a barrier for the reactions of Al with constituents of the refractory. Molten aluminium and magnesium will continue to penetrate inside the refractory through pores (which will not

Fig. 3.5 Corroded by infiltrated aluminium refractory grain

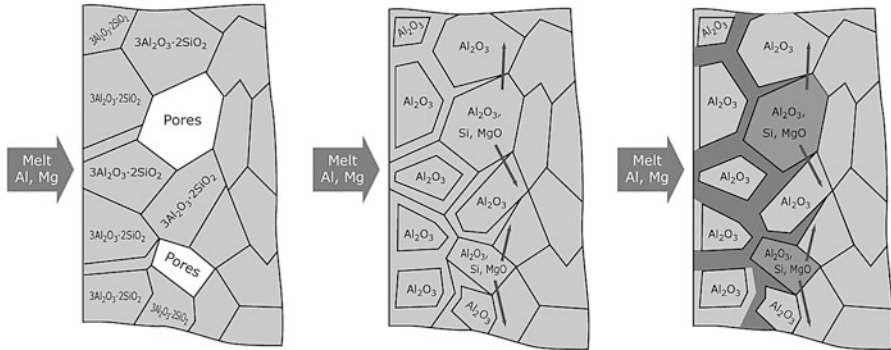
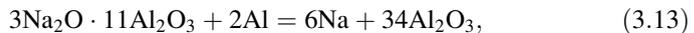


Fig. 3.6 The mechanism of degradation of refractory due to the negative volume effect of reactions of Al with refractories

be closed by the products of reactions and through cavities that appear due to the reactions with a negative volume effect). Alumina silica compounds will continue to interact, the cavities will be filled by aluminium, and so the metallization of refractory will take place. This phenomenon is well known among engineers who work with melting and holding aluminium furnaces (Figs. 3.5–3.7).

Sodium on the surface of molten aluminium may also add its input in the corrosion of refractories. Reactions (3.13) and (3.14) proceed with a negative volume effect, which also doesn't promote the formation of continuous alumina film:



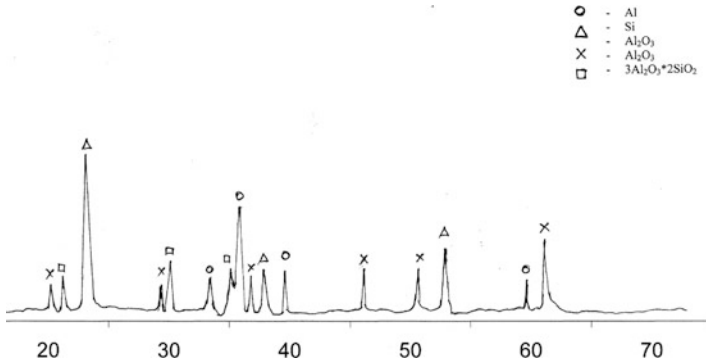
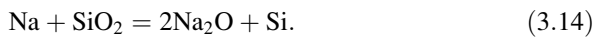
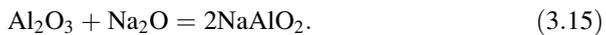


Fig. 3.7 X-ray diffractogram of Al-corroded alumina silica refractory



The same may be said about the formation of sodium aluminate: The density of alumina is 3.96 g/sm³, while the density of sodium aluminate is 2.69 g/sm³:



In industry, there is a belief [2, 3] that the corrosion of refractories by molten Al is inversely proportional to the alumina content in the refractories. This point of view is not quite correct, because alumina can react with magnesium, giving alumina magnesia spinel. The reaction (Table 3.4) proceeds with a positive volume effect, which may cause spalling and cracking.

As we mentioned earlier in this chapter, fireclay, mullite, and alumina refractories have been used for the layer that is in contact with molten Al. There were trials of magnesia, zirconium, aluminium titanate, and silicon carbide refractories. The results of these trials cannot be called unsuccessful. Most likely, these trials were sustainable for the entire range of actions necessary at implementation of a new material. In a limited amount, these materials are used today (crucibles for secondary Al for low-pressure dye casting, runners between melting and holding furnaces for special alloys, burner blocks, tap hole blocks). Yet the existing technical decision is to use alumina silica refractories with a relatively sophisticated structure and antiwetting additives.

As mentioned earlier, alumina silica refractories are far from being ideal materials for contact with Al. Yet modified alumina silica structures (Fig. 3.4) provide a service life up to 10–15 years, which is comparable with the time of technical obsolescence. It is achieved via three approaches: antiwetting additives, increasing alumina content, and modifying the structure. It is worth to mentioning that the single approach for the formation of refractories that are more or less resistant to molten Al doesn't give the desired result: Adding antiwetting additives to fireclay

material with relatively big pores and low alumina content doesn't provide the result; dense low-cement castables without antiwetting additives slowly corrode, and corundum appears on the walls at the level of the metal. To achieve a considerable service life, it is necessary to implement all three approaches.

The alloys of the fourth, fifth, and seventh series (Table 3.1), which are those with silicon, magnesium, and zinc, are the most corrosive to refractories. In the furnaces for master alloys for the preparation of conventional aluminium alloys, the temperatures are higher, and the antiwetting additives decompose relatively fast (which promotes additional porosity in the structure of refractories). Usually, refractories without antiwetting additives are used in the furnaces for the preparation of master alloys.

3.2.5 Tests for Corrosion Resistance

Traditionally, the corrosion resistance of refractories to molten Al was checked by cup test [29, 30]. It is a widely used, simple, and cheap technique. Aluminium is poured or placed in pieces in a "cup" that was drilled in the brick or in a previously formed "cup" in the concrete. Usually, the dimension of the cup is 40×40 mm. The brick or prepared sample of concrete with aluminium is placed in a furnace for a certain period of time (the most common time is 72 h; however, experiments may last from 12 h to weeks). The temperature may vary from 730 to 1,200 °C [14–16, 31, 32]. After cooling, the sample is cut to determine the interaction surface of the refractory with Al as well as the state of the surface. It is possible to estimate the surface of the reacted refractory; it is a static test. The molten Al is not stirred. This method can give an approximate estimation (Fig. 3.8).

There are modifications to the corrosion test. In [32], rods of $25 \times 25 \times 51$ mm are immersed in the alloy with 5 % Mg, the temperature is 850 °C, the time of testing is 4 days, and magnesium is added to maintain the 5 % concentration. In order variant of testing [33] the amount of Al in the crucible is bigger, the concentration of Mg is maintained at 6 %.

Usually, testing castables for corrosion is done at temperatures of 800 °C and 1,200 °C, which reflects the service conditions of the castables in the furnace.

In test [30], samples of $2.54 \times 2.54 \times 22.86$ sm are immersed in molten Al with 5% Mg and analyzed after 4 days of exposure at 1,150 °C, mainly on the triple border "refractory–metal–air." A rod test at elevated temperatures gives more information than a cup test, but it is more time-consuming and more expensive.

There are no strict criteria when choosing refractory materials for Al melting and holding furnaces. The action of fluxes is not taken into account, but their influence on corrosion resistance in the metallurgy of Al is not much. If the material is not corrosion-resistant, it is possible to estimate the depth of penetration: The deeper the penetration, the less resistant the refractory.

Advanced refractories effectively withstand Al corrosion. Even after one or two weeks, there may be almost no interaction. In such a case, it is impossible to



Fig. 3.8 Cup corrosion test of fireclay brick and LCC. The LCC refractory is unchanged

estimate the depth of penetration in mm/h or mm/day. Qualitative estimations without certain numerical values may be used, such as whether or not cracks appear on the border with metal, adhesion of the metal to the refractory (easily removed or not), change in the color of the refractory, and so on.

3.3 Refractory Materials

Currently, conventional fireclay brick is a rarely used material for the lining of holding or melting furnaces. The alumina content of conventional refractories for molten Al is 57–85 %. The application of pure alumina refractories doesn't add sufficient service life, but it does add cost.

Castables are more convenient refractories than bricks at this time. The main principles for the structure of corrosion refractories (castables and bricks) that are resistant to Al are low porosity (<13–15%) and low gas permeability (<0.4–0.5 μm^2), while most pores are smaller than 3–4 μm .

Advanced bricks for molten Al are made from white bauxite with low iron content and a fine pore structure; they are phosphate-bonded and contain barium



Fig. 3.9 The failure of the holding furnace from bricks. Aluminium, which penetrated through the shafts between the bricks, can be clearly seen

sulfate. The filler for low-cement castables and ultra-low-cement castables are bauxite or alumina (fireclay is rare).

Usually, the service life of melting furnaces is lower than that of holding furnaces due to mechanical interactions and thermal shock. Consequently, the requirements for holding furnace materials are stricter in terms of thermal shock and strength.

Mechanical interactions are a serious factor for holding furnaces that melt ingots and billets. They may weigh up to hundreds and thousands of kilograms, and once they fall, even from a low height, the interaction is high.

At electromagnetic stirring in the holding furnaces, the refractory should withstand erosion. The erosion is not as big as in reduction cells, but it should still be taken into account.

There is almost no thermal shock in the holding furnaces [if not accounting for the material-charging doors and feeding cavity (hole)]. The refractories of the melting furnaces should withstand thermal shock at loading of the cold metal. Also, at the beginning of melting, the metal is overheated; its temperature is sufficiently higher than necessary for the holding furnace. The overheating of the metal in the beginning is inevitable, but it may cause cracking.

Castable technology is more popular for the lining of holding and melting furnaces. The shaft between the bricks is a weak point in the lining. The porosity of the mortar in the shaft may be even twice higher than in the brick, and the pore size distribution is not controlled. Also, it is necessary to take the human factor into account, such as the variations in the thickness of shafts, some remaining cavities, and so forth (Fig. 3.9).

The brick lining also has some advantages. It is less frequently subjected to mechanical interactions in holding furnaces. The shafts between the bricks are the

natural border for the crack propagation. However, Al infiltrates the shafts, and the lenses of Al in the lining change the thermal balance of the lining and of the furnace.

Low-cement castables (LCCs) and ultra-low-cement castables (ULCCs) with a high-alumina filler are more frequently used than medium-cement castables (MCCs) (Table 3.6). The advantage of the castables is the absence of shafts. The strength characteristics of LCCs and ULCCs are quite comparable with bricks and sometimes are superior to bricks. However, the shaft may have a positive role as a barrier for crack propagation. To some extent, the disadvantage of castables is the increased human factor.

It was thought that the temperature of the melt in the furnaces is in the range 750–800 °C and that under the roof is below 1,000 °C. The current tendency is the intensification of the melting processes, and sometimes in the beginning of melting, the temperature of Al in contact with the refractory may be as high as 900 °C. Antiwetting additives at such temperatures decompose, and their effectiveness thus diminishes. It is better in such cases to use bricks and castables without additives, which provides high corrosion resistance due to the low permeability and narrow pore size distribution.

The working layer of the furnaces above the level of molten metal is made from conventional alumina silica bricks and castables. The temperatures are in the range of 1,000 °C, and even under the roof it is below 1,200 °C, so the requirements for refractories are not strict.

The barrier layer should prevent the infiltration of Al in the heat insulation layer. It is necessary for a brick lining, but it is desirable for a castable lining (because there is no guarantee that the crack wouldn't propagate through the working layer of castables). The barrier layer is made from castables, and there is no need to add antiwetting additives to it (although sometimes people do add them).

Currently, furnaces do not have arched roofs; flat roofs are more conventional. The roofs may be two- or three-layer (in order to diminish the heat flow). Sometimes the roof is made from monolithic blocks, but it is covered above with heat insulation. The usual requirements for the refractories apply for the roof, including moderate thermal shock resistance (>30 thermal air cycles) and no deformation at 1,200 °C (refractoriness above 1,500 °C). Usually, the roof's material is a conventional castable with fireclay filler. The second layer is heat insulation castable, and the third layer is a fiber slab.

The feeding cavity (hole) is the most abraded part of the furnace. The material of the feeding hole should withstand thermal shocks, mechanical shocks, and abrasion. If material of the feeding hole is worn out, it is a path for the heat flow and instability in the service of the furnace. The lower part of the feeding hole is made from high-strength bricks or castables, while the upper part is made from the castables with sufficient thermal shock resistance (above 30 thermal air cycles). Sometimes metallic fiber is added to castables to increase the abrasion and thermal shock resistance.

It is possible to use various heat insulation materials for the melting and holding furnaces. Fiber materials are usually not used in the bottom, but they may be used in the walls and in the roof. Materials that may withstand relatively high pressures at relatively high temperatures (diatomaceous bricks, vermiculite slabs, calcium

Table 3.6 Refractory materials for holding and melting furnaces

Type	Composition, %		Properties				Comment
	Main component	Al ₂ O ₃	BaO, %	Density, g/sm ³	Porosity, %	Shrinkage, %, 800°C	
<i>Working layer, contacting with aluminium</i>							
Brick	Alumina	72	4.5	–	20	–	50
Brick	Boxite	78.5	4.8	3	–	–	115
Brick	Boxite	83	1.9	3	14.5	–	110
Brick	Boxite	80	–	2.96	12.5	–	210
Concrete	Boxite	80.9	–	2.88	19	–0.2	85
Concrete	Boxite	74	–	2.95	13–15	–0.2	140
Concrete	Alumina	80	6	2.93	13–15	–0.2	95
Concrete	High alumina	68	–	2.5	13–15	–0.3	80
<i>Working layer above aluminium</i>							
Brick	Fireclay	42	–	2.31	16	–	60
Concrete	Fireclay	48	–	2.3	18–22	–0.3	45
Concrete	Fireclay	46	–	2.28	18–22	–0.4	90
Concrete	Fireclay	45	–	2.1	18–22	–0.3	25
<i>Barrier layer</i>							
Concrete	Fireclay	48	1.7	1.1	20–25	–0.5	3
Concrete	Fireclay	30	–	1.87	20–25	0.6	20
Voncrete	Fireclay	49	–	1.7	20–25	–	15
<i>Roof</i>							
Brick	Fireclay	30	–	1	55	–	3
Concrete	Fireclay	48	–	2.32	18–22	–0.2	45
Concrete	–	30	–	0.8	18–22	–0.4	1.5
Concrete	Fireclay	46	–	2.28	18–22	–0.4	90

Concrete	Fireclay+ perlite	41	–	0.85	–0.5	1.5	Insulation	
Concrete	Fireclay	50	–	2.3	18–22	90	Flat roof	
Concrete	Fireclay	45	–	2.1	18–22	25	Flat roof	
Concrete	Fireclay	50	–	2.35	18–22	100	Flat roof	
Concrete	–	25	–	0.95	–	1	Insulation	
<i>Freezing hole</i>								
Brick	Boxite	80	–	2.96	12.5	210		
Concrete	Alumina	85	–	2.9	13–15	120	LCC	
Concrete	Boxite	80.9	–	2.88	19	85	LCC	
Concrete	Boxite	74	–	2.95	13–15	140	LCC	
Concrete	Andalusite	57	–	2.5	17	90	LCC	
<i>Heat insulation materials</i>								
Type	Main component	Max service temperature, °C	Thermal conductivity at 400°C, W/mK	Density, g/sm ³	Porosity, %	Shrinkage, % ,800°C	CCS, MPa (for castables – after 800°C)	Comment
Brick	Diamomite	800	0.14	0.4	85	1.5	0.8	Bottom and walls
Slab	Vermiculite	850	0.14	0.4	85	1	0.8	Bottom and walls
Brick	Fireclay	1,300	0.21	0.8	–	–0.8	10	Bottom
Slab	Fiber	1,100	0.1	0.25	–	–	–	Walls
Slab	Calcium silicate	8,000	0.08	0.25	90	–1	1	Walls
Concrete	Vermiculite	1,000	0.18	0.7	–	–	1	Bottom and walls
Concrete	Fiber	1,300	0.2	1	–	–	7	Bottom and walls
Concrete	Alumina fiber	1,300	0.25	0.9	–	–0.3	2	Bottom and walls

silicate boards) are used for the bottom. Fiber heat insulation and calcium silicate boards are the most effective thermal barriers, which allow a relatively large freedom for designers. Castables with vermiculite, fibers, and lightweight fireclay granules might also be used sometimes. The current tendency in furnace design is decreasing the thickness of the lining by using highly efficient thermal insulation.

Almost all the materials just mentioned may be used in induction furnaces, ladles, and launders.

3.4 Elements of Lining Design

The viscosity of the molten Al is close to the viscosity of water. One of the principles of protection of the lining from infiltration of Al (and Al leakages through cracks) is designing the lining in such a way so that Al will crystallize in the working layer (Al's freezing point of 660 °C should be in the working layer). It is acceptable for the freezing point to be in the barrier layer, but having the freezing point of aluminium in the heat insulation layer is unacceptable.

The calculation of the location of the freezing point in the lining is a part of the thermal balance calculation (which is a very complicated problem) and the calculation of the heat flow through the multi-layer lining (side wall or bottom). The heat flow in different parts of the furnace will differ (heat transfer from the area above the metal and from the area with metal) [34].

The total heat flow (flux) resistance of the multi-layer lining,

R_k , is the sum of the heat flow resistances of each individual layer [35]:

$$R_k = R_{\alpha i} + R_{\lambda_1} + R_{\lambda_2} + R_{\lambda_3} + R_{\alpha a}, \quad (3.16)$$

and the thermal conductivity λ is inversely proportional to the heat flow resistance:

$$\lambda = 1/R_i. \quad (3.17)$$

The total heat flow through the multi-layer lining is calculated as

$$Q = S_k(t_i - t_a), \quad (3.18)$$

and the temperature drop in any layer is

$$t_i - t_{i-1} = (t_i - t_a) R_{\alpha i}/R_k. \quad (3.19)$$

Approximately 20–30 years ago, in the mid-1980s and 1990s, it was possible to see a two-layer liming of melting and holding furnaces with a total thickness up to 1,000 mm in the bottom (mullite or fireclay brick plus diatomaceous brick or vermiculite slab), as seen in Fig. 3.10a. The paradox is that having additional heat insulation layers – whose purpose was to decrease the heat flow through the

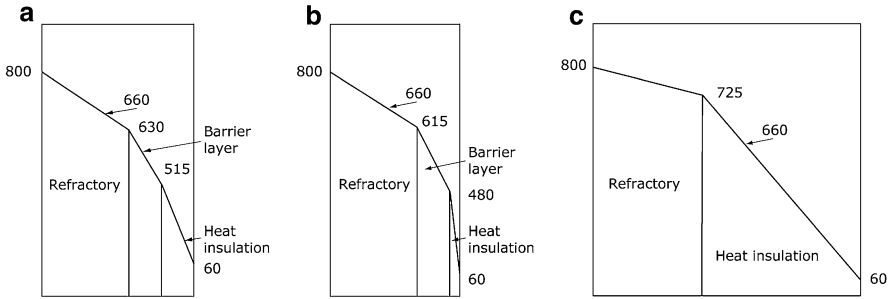


Fig. 3.10 Temperature gradients in linings. (a) three layer lining with freezing point of Al in the working layer; (b) three layer lining with freezing point of Al in the working layer; (c) two layer lining with freezing point of Al in the insulation layer

Fig. 3.11 The carts of the bottom

1	2	3
4	5	6
7	8	9
10	11	12

lining – didn't allow the heat insulation layer to realize its properties. The crystallization point of Al moved to the heat insulation layers. When liquid aluminium reached the heat insulation layers, the thermal conductivity of the lining increased dramatically. The consequence was overheating the walls.

Conventional heat insulation materials (Table 1.6) have a low thermal conductivity and can withstand large temperature gradients; this property gives new capabilities in the design of the three- to four-layer linings (Fig. 3.10b). The freezing (crystallization) point of Al usually is in the working refractory layer, while the thickness of walls is in the range of 400–500 mm (the thickness of the bottom lining is within 600 mm).

In case the heat insulation layer is made from high-porosity materials, it is necessary to provide the insulation of these materials from water in the concretes (castables) by polymer film or any other variant.

If castable technology is used to make the refractory bottom, it is necessary to use cast framework forms. The side lining can be made by casting and gunning.

The casting of the bottom is made by carts (Fig. 3.11), which are rectangular spaces, boarded by cast framework forms. The casting is made in line, leaving the neighboring carts empty (for example, the sequence of casting is 1, 3, 5, 7, 9, 11,

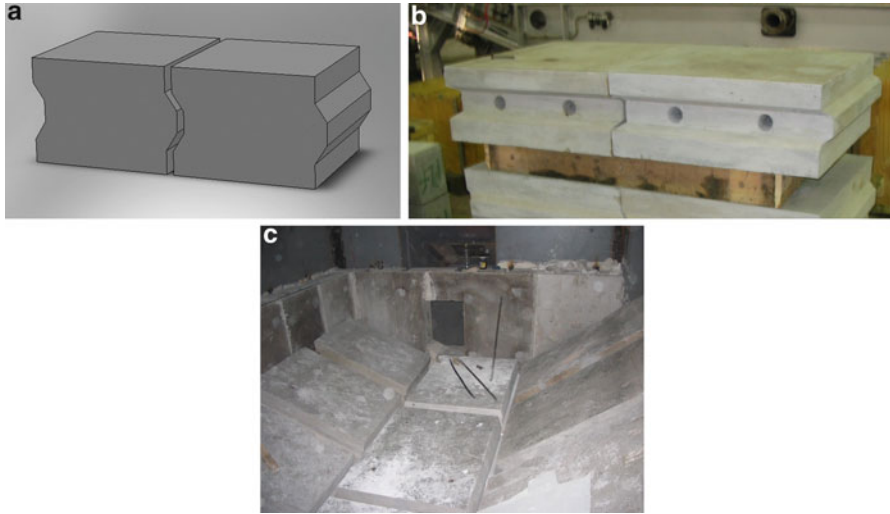


Fig. 3.12 The shape of cast (a) and precast (b) blocks in the refractory bottom (c) of the holding furnace

and then 2, 4, 6, 8, 10, 12). When a multilayer lining is made, only one layer is cast in one set. The shafts are not flat but have a special form (Fig. 3.12). The casting of the side walls is also made, leaving the neighboring carts empty.

3.4.1 Some Words on Drying and Preheating of Furnaces

Drying and preheating of furnaces are very important operations. If the furnace is lined with bricks, it is recommended to make the preheating after at least 24 h, so that the lining mortar and the plastic masses will become dry and become more or less rigid. In order to diminish the tensions, it is recommended to do a 24-h exposure at 800 °C; after that, the heating rate is determined by the thermal shock resistance of the refractory.

If the furnace is made from castable refractories, the water is in the pores (physically bonded water) and in the structure of the hydrates (chemically bonded water). Drying is the evaporation of physically bonded water through the permeable pores, which cause tensions. If these tensions are higher than the strength of the dried material, then cracks will appear in the material, sometimes a single crack, sometimes numerous cracks, sometimes shallow, sometimes cracks through the material. During the drying and preheating, the strength of the dried material diminishes and increases several times.

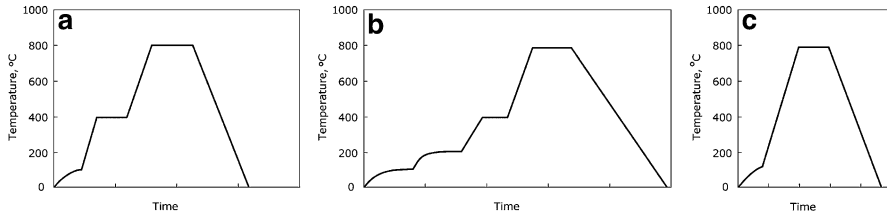


Fig. 3.13 The approximate rates of preheating of the furnaces with lining: (a) the working layer is from castables, and the heat insulation layers are from bricks or slabs; (b) the working, barrier, and heat insulation layers are from castables; (c) the lining is from bricks, slabs, or preshaped castables according to [36]

In MCCs, the first temperature interval for the decreasing of strength is 110–300 °C, when the hydrates of calcium aluminates are decomposed. The other temperature interval of decreasing strength is 700–800 °C (the exposure is recommended), and then the growth in strength takes place. In LCCs and ULCCs, the strength increases continuously as the temperature increases. In LCCs and ULCCs, the amount of alumina cements is low, and the reactive silica and alumina form gels; upon dehydration, these gels bond the grains of the filler, and the porosity is lower than that of MCCs.

The evaporation of water below 100 °C is insignificant, and it is difficult to control the rate of heating. The rate of heating for the furnace with a working layer from castables and a heat insulation layer from preliminary heat-treated boards or bricks is a little bit quicker compared with the rate of heating for the furnace with all layers made from castables, because the water should evaporate through the lining. Exposure at 400 °C is required for both linings, but with LCCs, it is not as necessary. If the furnace is stopped for some reason, preheating is possible to do at increased rates of heating, because the lining doesn't contain water (Fig. 3.13). It has been reported [36] that colloidal silica binders in castables gives the ability for a serious decrease in the dry-out and heating time of the refractory lining of holding furnaces.

Uncompensated thermal expansion of refractories in the holding or melting furnace may lead to damage to steel shells and the chipping and spalling of the refractory lining. Usually, the design of the furnaces includes temperature shafts that compensate for the thermal expansion. There are several constructions of temperature shafts. The main problem is to give the refractory the ability to expand, leaving some space for this expansion, yet eliminating leakage of the metal in this gap; that should compensate for the expansion. Thermal insulation materials are used sometimes in these gaps, but the problem is to hide these gaps, filled in with heat insulation, from the leakage of the metal.

If the width of the holding furnace is 6 m, and the bottom is made from an LCC with thermal expansion $6 \times 10^{-6} \text{ K}^{-1}$, the flat roof is made from MCC blocks with the same thermal expansion coefficient. If the temperature in the bottom and on the roof is 800 °C, the expansion of the bottom and the roof will be



Fig. 3.14 The temperature gaps between the preshaped concrete blocks

$$6 \times 10^{-6} \text{K}^{-1} \times 800 \times 6 \times 10^3 \text{mm} = 28.8 \text{mm}.$$

The calculation is made without accounting for the expansion of concrete blocks upon preheating. Only thermal expansion at increasing temperature of the fired material is calculated.

Sometimes the gaps for the compensation of the thermal expansion are made near the walls under the side lining, and the gaps are filled with ceramic fiber materials, taking into account 50 % shrinkage of this fiber material.

Another variant of compensation is the construction of a “fish tail” between the concrete blocks, where the gaps between them are filled in with ceramic paper (Fig. 3.14).

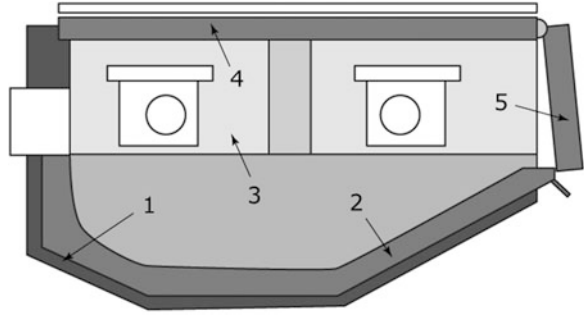
In stationary melting and holding furnaces, the distance between anchor bolts should not exceed 500 mm in the walls in the vertical direction and should not be less than 1,200 mm in the horizontal direction. In the roof, the distance between anchor bolts should be within 450 mm. For tilting furnaces, these distances should be smaller.

In the Al industry, the temperatures are not high. Steel anchor bolts can be in service up to 1,100–1,200 °C. Above these temperatures only anchor bricks should be used.

3.5 Melting and Holding Furnaces

There is almost no difference in the constructions of melting and holding furnaces. The metal may be loaded from above and sideways. The molten Al is transferred to the holding furnace through the runner or through the metal inlet well. Usually, melting furnaces are heated by natural gas, and holding furnaces are heated by natural gas or by electric heaters. Holding furnaces with electric heating are easier to operate, but it is necessary to change the heating elements periodically. The heating elements are made from nickel chromium alloys, frequently placed in a steel tube. Silicon carbide heaters are sometimes used in small melting furnaces.

Fig. 3.15 Melting furnace:
 1 – insulation, 2 – working refractory layer, 3 – refractory lining above the metal layer, 4 – roof, 5 – door



The upper and side-wall loadings of metal in the holding furnaces have advantages and disadvantages. Tilting furnaces are easier in service but have stricter requirements in terms of the design and quality of the refractory lining. The load of Al furnaces may vary from 20 to 120 t; the decision on the load is based on the capacity of the industrial line. Sometimes on small plants there are constructions combining the melting zone and the holding zone in one furnace. The depth of the molten metal is in the range of 900–950 mm, sometimes reaching 1,100 mm, and the productivity is about 30–35 t/h.

The typical flux (there are the variations) is $\text{KCl} \cdot \text{MgCl}_2$ (melting point 488 °C); it interacts with impurities and with Al as well, giving Al and sodium chlorides. At holding, these chlorides (dross) appear on the surface and are taken off. The temperature of molten aluminium alloys at casting is 690–710 °C (Fig. 3.15).

The requirements to refractories were mentioned earlier: porosity <15 %; average pore size <5 µm; and low wetting by Al.

The service life of melting furnaces is lower than that of holding furnaces because of the mechanical action of ingots at loading. Consequently, the requirements for refractories for melting furnaces are tougher.

A modern concept is lining melting and holding furnaces by castables, yet a brick lining is more resistant to thermal shock and mechanical stresses. One of the decisions is the application of preshaped blocks (Fig. 3.16). Multilayer blocks are cast and heat-treated in a refractory plant and shipped to an Al plant for installation in the steel shell.

The advantages are the homogeneity of the refractories, the decreased installation time (compared with the cast works in the steel shell, following drying), and no need to have specialized division for the cast works and the workers. The disadvantage is the gaps between preshaped blocks, which are filled in by castables and plastic mixes.

The roof in contemporary melting and holding furnaces is flat and made from preshaped castable blocks. The precast blocks consist of two or three layers with heat insulation and are hung on anchor bolts. The pads between the preshaped blocks are fiber materials. In tilting furnaces, the roofs are usually not from preshaped blocks and are made by gunning. If there is a chance that a temperature at the roof will exceed 1,200 °C, the refractory anchor bricks are used.



Fig. 3.16 Melting furnace from preshaped blocks

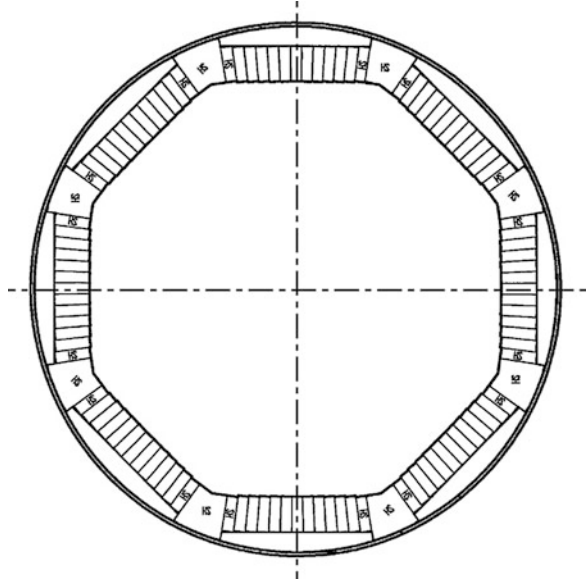
Burner blocks are made from alumina or silicon carbide. The temperature near the burner blocks of melting furnaces may exceed 1,350 °C. The tap hole blocks should withstand thermal shock and erosion. Usually, they are made from silicon carbide or zircon, but also from alumina castables.

The range of heat insulation materials is rather broad. Heat insulation materials that can withstand relatively high mechanical loads – this list includes lightweight fireclay bricks, vermiculite slabs, perlite bricks, calcium silicate boards, and diatomaceous bricks – are used for the heat insulation of the bottom. The pressure on the walls is lower, so it is possible to use fiber-based boards (in addition to the above-mentioned materials). Sometimes lightweight castables with fillers, such as lightweight fireclay, vermiculite, and fiber, are also used for heat insulation.

The temperature regime of the furnaces for the preparation of master alloys (Al-Mn, Al-Zr, Al-V, etc.) differs from the common melting furnaces; the temperature at the border of the melt may reach 900–1,050 °C, and the temperature under the roof is up to 1,200 °C. The corrosion of alloys at such temperatures is aggressive, and usually the service life of the lining is two times lower. The antiwetting additives decompose, leaving the bulky structure. Usually, a fine pore size structure with a small pore dimension is the best protection for such conditions. Phosphate-bonded bauxite bricks or LCCs with filler from bauxite are used.

Degassing units are used for the refining of Al alloys from gases, fluxes, and oxide films. The degassing unit is a vane with a depth up to 1 m and sides from 1 × 1.5 m to 1.5 × 2.5 m, where alloys are purified with gases (Ar-Cl). The gases are supplied through the hole in a stirrer. After purification, the alloys go to the foam filter in a filter box.

Fig. 3.17 Rotating furnace for the remelting of dross and wastes



The requirements for refractories for the vanes of the degassing units do not differ from the requirements for the melting and holding furnaces (Table 3.6). They are high thermal shock resistance, low wetting by Al, and high erosion resistance.

The same may be said about the refractories for the rotating furnaces for remelting of dross and wastes (Table 3.6). Such furnaces, having a diameter up to 4 m and a length of 8–10 m, are lined with bricks (in weir walls, inside the inner lining) and with LCCs (under hexagonal or octagonal inner construction) (Fig. 3.17).

The main interaction of the lining is mechanical action of the pieces of wastes and dross and chemical erosion. The service life usually doesn't exceed 1.5–2 years (Fig. 3.18).

3.6 Induction Furnaces, Ladles

Induction furnaces are used for making alloys and master alloys and for remelting of scrap and noncondition billets.

A crucible induction furnace (Fig. 3.19) consists of a refractory crucible, a water-cooled inductor around the crucible, a steel shell (which takes most of the mechanical tensions), a pouring crucible lip, and a cup.

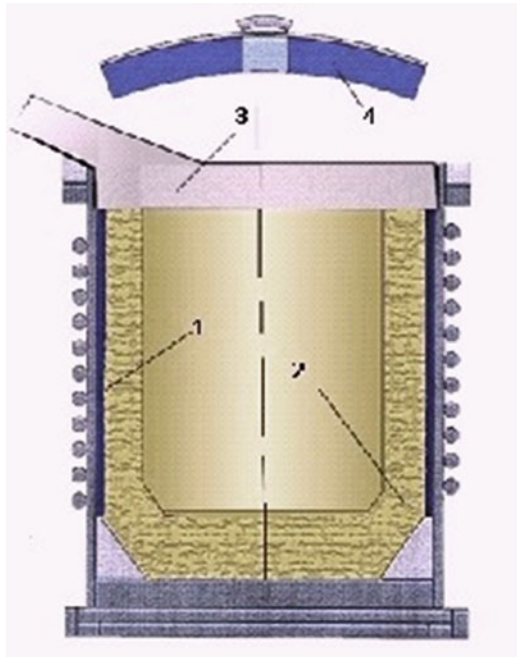
The water-cooled inductor is made from copper wire and is a source of electromagnetic field, heating the metal in the crucible.

Usually, between the inductor and the refractory layer is a barrier layer that compensates the movement of the inductor along the crucible and prevents cracks



Fig. 3.18 Holding furnace

Fig. 3.19 The lining of the crucible induction furnace:
1 – barrier insulation of inductor, 2 – working refractory layer, 3 – pouring lip, 4 – cup



from appearing in the crucible and molten metal leaking to inductor through the cracks.

In the induction furnace, the metal, which flows through cracks in the crucible to the inductor, comes to the sphere of a more intensive magnetic field, and it won't freeze. The penetration of the molten metal to the inductor leads to a short circuit. The refractory lining of an induction furnace should have no cracks.

The other peculiarity is that although the temperature of the melt won't exceed 900 °C, the temperature on the lining may be even higher due to the high concentration of heat near the walls, because of the large heat capacity of billets and ingots and the enhanced melting regimes.

The induction furnace fails due to cracks and the penetration of molten metal to the inductor. This cracking may be initiated due to the chemical corrosion. Usually, the cup doesn't interact with metal and lasts for many years.

The requirements for the refractory lining of the induction furnace are as follows [39]:

- Thermal shock resistance (at pouring of the metal) and resistance to static thermal gradients (the temperature of the metal is up to 900 °C, while the temperature of the outer wall is 100–120 °C).
- High mechanical strength (the thickness of the crucible is 90–120 mm). The walls of the crucible should withstand the load of the molten metal.
- High fracture toughness (mechanical stresses at loads of the ingots and billets, also when the walls are mechanically cleaned by scrapers).
- High resistance to chemical corrosion and to erosion (the metal is circulated under the influence of the magnetic field).
- The maximum thickness of walls for a 6-t induction furnace is considered to be 120 mm, while for the furnace with a load of 2.5 t, it should be below 90 mm (otherwise, the electrical and economical characteristics of the furnace will be diminished).
- It shouldn't be electroconductive.
- There should be low expansion at firing (otherwise, there are chances of cracking).

The lining of induction furnaces is made from ramming mixes (water content below 1%) as well as plastic mixes (water content below 6%); lining by concretes is rarely made. It is necessary to have the pattern of the crucible. Also, it is necessary to have a specialized heating element for preheating. Yet the sintering of the refractory layer takes place only in service, so it is recommended to make exposure of the furnace with metal for 3 h without electricity and then at a temperature of 750–800 °C for a day.

The normal procedure is to clean the surface of the inner walls of dross and metal with scrapers; almost all the metal is poured off. The service life of the induction furnace is 2.5–3.5 years, but sometimes emergency shutdowns take place due to the failure of the lining.

3.6.1 Ladles

In a reduction shop, liquid aluminium is taken from the reduction cells and transported to the cast house. Usually, it is weighed, held for some time, and poured in the holding furnace for the preparation of alloys.

The refractory lining of the ladles should be resistant to thermal shock, and the bottom of the ladle should be erosion-resistant. In the tapped aluminium in the ladles, there is some electrolyte, which also attacks the refractory lining of the ladles. Usually, the refractory lining is made from the same materials that are used in the cast house (Table 3.7).

3.7 Launder (Runners), Casting Equipment. Elimination of Asbestos-Containing Materials

The molten Al flows from the melting furnaces to the holding furnaces, and then from the holding furnaces it goes either to the billet casting machine or to the ingot casting machine. The length of the runner (launder) to the ingot casting machine is 1–2 m, and that to the billet casting machine may be up to 30–40 m (sometimes – two or three holding furnaces provide aluminium alloy for one casting machine). The requirements for refractory and heat insulation machines differ.

Depending on a casting machine, the runner may have a small cross section (the surface of the metal $< 100 \text{ m}^2$), medium (the surface of the metal = $100\text{--}200 \text{ m}^2$), or large cross section (the surface of the metal $> 200 \text{ m}^2$). The molten Al releases heat in the runner. It has been reported [38] that the temperature drop should not exceed $0.4^\circ/\text{m}$. The velocity of aluminium in the runner should not exceed 20 m/s , which is realized at the slope of a runner of 5–8 mm/m. If the velocity of Al there is small, the heat release will be larger. It is undesirable for the velocity of Al to have a possibility of turbulence in the flow (for the quality of the billets).

In terms of heat losses, the height of the runner should be either equal to or 1.5 times the width. In terms of turbulence, the launder should have no slopes, angles, or knobs. The shape of the launder at Fig. 3.20a is less desirable than the shapes in Fig. 3.20b, c.

Currently, there are many materials for the launders, but it is difficult to find a material that combines

- low thermal conductivity,
- high thermal shock resistance,
- high erosion resistance,
- low wetting by molten Al.

The materials used for the launders – alumina silica fiber materials with coatings, fused silica, wollastonite, LCCs and MCCs, heat insulation castables – only partly satisfy the above-listed requirements.

Table 3.7 Refractories for the lining of the induction furnace

Type	Density (g/sm ³) (1,000 °C)	Al ₂ O ₃ content (%)	BaO (or other antiwetting additives) (%)	Porosity (%) (1,000 °C)	Shrinkage after firing (%) (800 °C)	Grain size of the filler (mm)	Thermal conductivity (W/mK) (500/1,200 °C)
Ramming mix	2.45	35	9	17	-0.2	<7	0.80/1.08
Ramming mix	2.95	70	9		-0.2	<7	
Castable (for lip)	2.30	43	9	20	-0.2	<7	1.35/1.44
Castable concrete	2.20	34	1.5		-0.2	<6	0.68/0.94
Castable concrete	2.75	81	2.2		-0.1	<6	1.80/2.00
Ramming mix	3.00	92	-	20	-0.2	<7	-

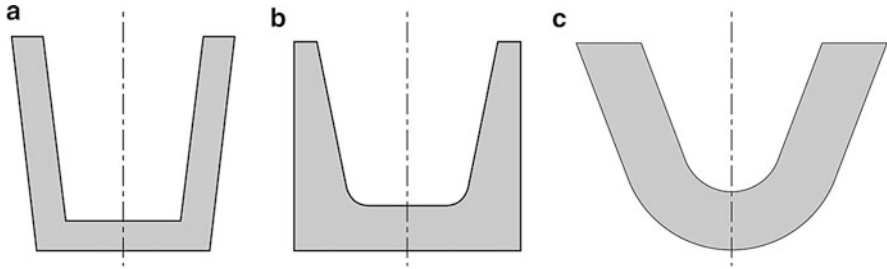


Fig. 3.20 Shapes of the runners



Fig. 3.21 Aluminium in the launders

The material for the runners to the ingot casting machine should be relatively light and resistant to erosion (Fig. 3.21).

3.7.1 Casting Equipment (Tooling)

Many articles used at casting of aluminium are called casting tooling. They are small (sometimes 1–2 kg, others are 10–20 kg), and the consumption of the cast house may be within tens to hundreds of items per year. Stoppers, glasses, sieves, siphons, plugs, funnels, terminal boxes, and the like should be thermal shock-resistant and shouldn't interact with Al. At a certain time, all these articles were made from asbestos-containing materials. Currently, they are made from wollastonite and from alumina silica fiber compositions, sometimes with impregnation.

The service life of these articles is within 1–3 months. Usually, there is no need to stop casting in case there's damage to such an article; it is possible to change it in the breaks. The income in the cost of aluminium alloys is not big, and the prolongation of the service life of casting equipment is usually not a factor to Al producers. However, the elimination of asbestos in the casting of Al still has some attention among Al producers. Discussions on the degree of how dangerous asbestos is on the human body are still ongoing [37], but the dangerous influence of asbestos has been proven.

3.7.2 *Ceramic Foam Filters*

Ceramic foam filters are widely used for the filtration of Al alloys from oxide films, and they also purify Al from gases and intermetallic inclusions due to their big surface area. Usually, they have the shape of torque bricks with a height of 50 mm and sides of 200 mm, 230 mm, 325 mm, 400 mm, 525 mm, and 585 mm, but sometimes they have a cylindrical shape. The filtration box may be with or without preheating. The main characteristic of ceramic foam filters is the number of pores per inch (ppi). Filters with 20, 30, 40, 50, and 60 ppi are used in aluminium cast houses. The most common are filters with 30 and 40 ppi. Filters with 60 ppi are used for the filtration of special alloys.

Ceramic foam filters are prepared from polymer foam (which gives the pores their structure and uniformity to the pore structure) and ceramic alumina slurry (containing borate and phosphate additives for sintering). The slurry infiltrates the polymer foam and remains on the walls of the foam. During firing, the polymer foam decomposes, but the alumina material inherits the pore structure. The cold crushing strength of such material is 1–1.5 MPa, which is enough for service.

References

Physical and Chemical Interaction of Refractories with Aluminium and Aluminium Alloys

1. Richardson FD, Jeffes JE. Standard free energy of formation of oxides as a function of temperature. *J Iron Steel Inst.* 1948;160:261.
2. Andreev D, Gogin V, Makarov G. Efficient melting of aluminium alloys (in Russian). *Metallurgy*; Moscow; 1980, 136 p.
3. Napalkov VN, Cherepok GV, Mahov SV. Continuous casting of aluminium alloys (in Russian). Moscow: Intermet Engineering; 2006. 328 p.
4. Siljan OJ, Rian G, Petterson D. Refractories for the molten aluminum contact. Part 1. Thermodynamics and kinetics. *Refractories Applications and News.* 2002;7(6):17–25.
5. Allaire C. Refractories for the lining of holding and melting furnaces. *Proceedings of the International Symposium on Advances in Production and Fabrication of Light Metal and Matrix Composites.* Edmonton, Alberta, Aug, 1992. p. 1–12.
6. Quesnel S, Allaire C, Afshar S. Corrosion of the refractories at the bellybend of aluminium holding and melting furnaces. *Proceedings of the International Symposium on Advances in Refractories for the Metallurgical Industries 2.* 35th Annual Conference of Metallurgists of CIM, Montreal; 1996. p. 321–8.
7. Quesnel S, Afshar S, Allaire C. Corrosion of the refractories at the bellybend of aluminium holding and melting furnaces. *Light Met.* 1996;125:661–7.
8. Afshar S, Allair C. Furnaces: improving low cement castables by non-wetting additives. *JOM.* 2001;53:24–7.
9. Afshar S, Gaubert C, Allair C. The effects of fumed silica and barite on the aluminium resistance of alumina castables. *JOM.* 2003;55:66–9.

10. Allaire C, Guermazi M. Protecting refractories against corundum growth in aluminium treatment furnaces. *Light Met.* 2000;129:685–91.
11. Quesnel S, Allaire C, Afshar S. Criteria for choosing refractories in aluminium holding and melting furnaces. *Light Met.* 1998;127:391–1403.
12. Innus A, Rivard P. Refractory requirements for aluminium casthouses. More Informative product datasheets for materials selections. *Light Met.* 2003;132:779–86.
13. Aguilar-Santillan J, Bradt RC. Wetting of Al_2O_3 by molten aluminum: The effects of $BaSO_4$ Additions. Proceedings of the 40th St. Louis Refractories Symposium. St. Louis; 2004. V. 40, p. 35–63 (March 31 – April 1).
14. Simmat R, Dannert C. Influence of corrosive attack of $AlMg_5$ on the hot abrasion resistance of refractory materials for the use in the secondary aluminium industry. 13th Biennial Congress on Refractories, UNITECR. 2013. p. 1201–6.
15. Ziegler FL, de Valenzuela F, Ziegler FN, Ziegler F. Nanostructured self-flow refractory castable to long life melt aluminium contact lining. 13th Biennial Congress on Refractories, UNITECR. 2013. p. 1213–16.
16. Decker J. Phosphate bonded monolithic refractory materials with improved mechanical and chemical resistance for applications in the aluminium industry. 13th Biennial Congress on Refractories, UNITECR. 2013. p. 1165–70.
17. Li JS. Wetting of ceramic materials by liquid silicon, aluminum and metallic melts. *Ceram Int.* 1994;20:391–412.
18. Brennan JJ, Pask JA. Effect of mature surfaces on wetting of sapphire by liquid aluminum. *J Amer Ceram Soc.* 1968;51(10):569–73.
19. Coudurier L, Adorian J, Pique D, Eustathopoulos N. Study of the wettability by liquid aluminum and alumina covered with a layer of a refractory compound. *Rev Int Haute Temp.* 1984;21(2):81–93.
20. Ownby PD, Li KWK, Weirauch DA. High temperature wetting of sapphire by aluminum. *J Amer Ceram Soc.* 1991;74(6):1277–81.
21. Zhou XB, De Hosson JT. Reactive wetting of liquid metals on ceramic substrates. *Acta Mater.* 1996;44(2):421–6.
22. Carnahan RD, Johnston TL, Li CH. Some observations on the wetting of Al_2O_3 by aluminum. *J Amer Ceram Soc.* 1958;44(9):347–51.
23. Rhee SK. Wetting of ceramics by liquid aluminum. *J Amer Ceram Soc.* 1976;53(7):386–9.
24. Savov L, Heller HP, Janke D. Wettability of solids by molten metals and alloys. *Metallurgy.* 1997;51(9):475–85.
25. Marumo C, Pask JA. Reactions and wetting behavior in the aluminum-fused silica system. *J Mater Sci.* 1997;12:223–33.
26. Yurkov AL, Pihutin IA. Corrosion of alumina silica refractories by molten aluminium and its alloys in furnaces. *Novye Ogneupory.* 2009;4:53–61.
27. Yurkov AL. Physical chemical approach to the lining for holding and melting aluminium furnaces. *Novye Ogneupory.* 2008;3:16–7.
28. Yurkov AL, Pihutin IA. Interaction of aluminium and aluminium based alloys with refractory materials. *Tsvetn. Met.* 2010;10:47–52.
29. DIN 51069-1972. Testing of ceramic materials; comparing test of the resistance of refractory bricks to the attack of solid and liquid materials at high temperature, crucible method.
30. DIN CEN/TS 15418:2006-09. Methods of test for dense refractory products – Guidelines for testing the corrosion of refractories caused by liquids; German version CEN/TS 15418:2006.
31. Pana RP, Padhi BP, Bal AS, et al. Processing and characterization of $MgAl_2O_4$ -calcium aluminate refractories by reaction sintering of alumina-dolomite. 13th Biennial Congress on Refractories, UNITECR. 2013;13:1153–8.
32. Hemrick J, Smith J, O'Hara K. Development and application of improved shotcrete refractory for aluminium rotary furnace applications. 13th Biennial Congress on Refractories, UNITECR. 2013;13:1171–6.
33. Hammersmith V, Delberg J. New refractory test duplicates aluminium furnace conditions. *Mod Cast.* 1990;91:29–32.

Elements of Lining Design

34. Refractory engineering. Materials – design – construction. 2nd ed. Vulkan-Verlag, Essen; 1996. 355 p.
35. Refractories handbook, The Technical Association of Refractories of Japan, June 1998. 587 p.
36. Anderson MW, Hrenak LA, Snyder DA. Advances in no cement colloidal silica bonded monolithic refractories for aluminium and magnesium applications. 13th Biennial Congress on Refractories, UNITECR. 2013;13:1177–82.

Launders (Runners), Casting Equipment. Elimination of Asbestos-Containing Materials

37. Bradt RC. Asbestos in refractories – Applications and environmental uses. Proceeding of 102 American Ceramic Society Meeting, 2000.
38. Bridgham BL, Lee JW. New high performance metal delivery systems. Molten metal processing. Aluminium International. July/August 2002. p. 55–7.

Induction Furnaces, Ladles

39. Pihutin IA, Frolov VF, Yurkov AL. Implementation of semidry ramming refractory lining of induction furnaces IAT-6 (in Russian). Tsvetn Met. 2003;1:85–8.

Chapter 4

Refractories for Anode Baking Furnaces

Carbon anodes are necessary to undertake the Hall–Héroult process with prebaked anodes (Fig. 4.1).

We discussed anode baking furnaces in Sect. 2.3 because the furnaces for baking cathodes and baking anodes are the same. They have identical construction, the same problems with refractories, and the same refractories. Probably the real differences are that the service life of a cathode block should last for 6–8 years, while the service life of an anode is 30 days; thus, the consequence is the consumption of cathodes and anodes. Another difference is that the raw materials for cathodes are relatively pure, while the butts of spent anodes are utilized in raw materials for anodes, which leads to a significant sodium content in green anodes (from electrolyte). The temperature regime (Fig. 2.28) in anode baking furnaces is more or less the same. Usually, the producer of anodes is a producer of cathodes as well; sometimes they keep the furnaces for specialized production, but not always.

4.1 Lining

The lining of anode baking furnaces is made from alumina silica refractories. This type of refractory actually determines the service life of flue walls of the anode baking furnace. The heat insulation layers may be made from lightweight fireclay brick, vermiculite slabs, fiber boards, and other materials

The main characteristic of anode baking furnaces is a service life of the flue walls and their stability. The flue walls may deform (more frequently in the lower part of the chamber), and cracks may appear in the flue walls.

In practice, there are two philosophies toward the service of anode baking furnaces. One philosophy is to run the service of the furnace with minor repairs and then, after 5–6 years, make an entire relining. This philosophy doesn't require large processes for relining and repair – only minor repairs (e.g., patching cracks in the flue walls). Another philosophy is to make repairs to the flue walls. The service



Fig. 4.1 Baked anodes

of the flue walls in different parts of the furnace differ, and the repairs may change the most problematic flue walls in the center, leaving unchanged less problematic flue walls at the periphery. In this scheme, the service life of the furnace may reach up to 20 years (but the actual service life of the flue walls will be 4–5 times shorter). This philosophy considers the qualified staff for the repair and permanent supply of the bricks for the flue walls. Table 4.1 lists the properties of the refractories for anode baking furnaces.

The staff, employees of the inner part of flue walls withstands thermal shock, abrasion of the coke, and the influence of the reduction atmosphere. A CO and CO₂ atmosphere is combined with action of volatile sodium and fluorine compounds from the carbon anode butts. The material inside the flue walls interacts only with flame gases from the burning of natural gas and heavy oil. The usual requirements to the refractories for the flue walls are thermal shock resistance, minimal shrinkage, and high temperature of the deformation under the load [3–7].

The book by Prof. Yanko [1] discusses a mechanism of degradation of the flue walls, stating that the main corrosion agents are aluminium fluoride and sodium fluoride. The temperature of evaporation of aluminium fluoride is – 950 °C, while the temperature of evaporation of sodium fluoride is – 1,050 °C. Volatile sodium and aluminium fluoride penetrate the permeable pores of refractory [1] and interact with silica, giving volatile silicon tetrafluoride, while sodium oxide is released in the pores:

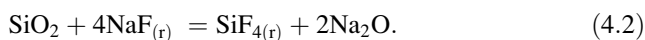
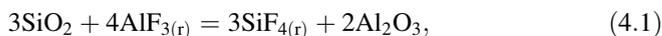


Table 4.1 Refractories for anode baking furnaces

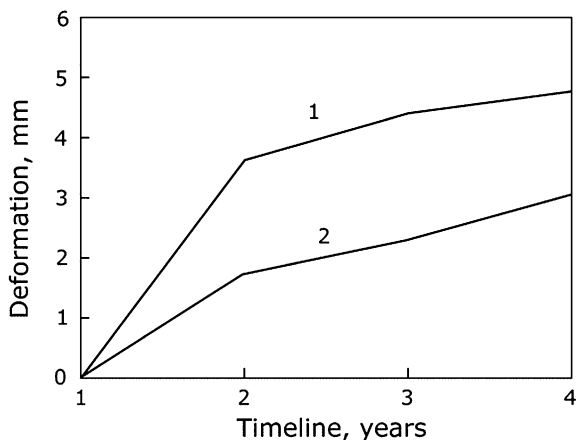
	1	2	3	4
Composition, %				
AL ₂ O ₃	62	64	47–48	46
Fe ₂ O ₃	1.5	1.4	1	1.35
CaO + MgO	–	0.8	–	0.75
Na ₂ O + K ₂ O	–	0.5	0.6	0.56
Porosity, %	24	20	14	16
Permeability, μm ²	–	–	0.3–0.6	–
MOR at 1,300°, MPa	–	–	10	–
CCS, MPa	25	37	45–70	45
Softening point, °C,	1,450	1,520	1,465	1,480
Reheat shrinkage, at	–	–		–
1,400 °C, 5 h, %	–	–	0.15	–
1,500 °C, 2 h, %	0.4	–	–	0.15
1,600 °C, 2 h, %	–	0.28		–
Thermal shock resistance (air)	–	5	15	45

**Fig. 4.2** Deformation of the flue walls

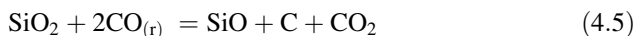
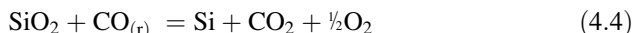
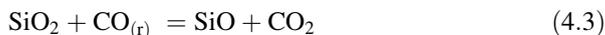
Thus, the degradation of flue walls boils down to the interaction of silica with volatile fluorides and the increase in porosity.

In industrial practice, the degradation of the flue walls is estimated on the deformations of the flue walls. If the flue wall deforms, it is difficult to load the green anodes and to unload the baked anodes. The curvature of the deformed flue wall may reach 30–50 mm within 3–5 years [2] (Fig. 4.2).

Fig. 4.3 Deformations of the flue walls during the service of materials 1 and 2



The analysis of the flue wall refractory from the furnace after 3 years of service showed three zones [2]: a zone contacting carbon; a zone near the flue wall, contacting flame; and a zone in the middle. In the zone contacting carbon, the porosity increases up to 40%, and the strength decreases, probably due to reactions (4.1), (4.2), (4.3), (4.4), and (4.5). Free silicon and sometimes free carbon are detected.



There are almost no temperature gradients in the flue walls, but sodium compounds really precipitate in the pores, sometimes in a bigger amount near the flue wall, sometimes at all cross sections, and the interaction of sodium compounds with alumina silica refractory is the main mechanism of flue wall decay. In the flue wall near contact with the flame, the amount of glassy phase is sufficiently larger than the part of the flue wall in contact with carbon.

The increase in porosity may cause cracking. The increase in the glassy phase leads to deformations at high temperature, resulting in a barrel-like shape of bricks and the flue walls itself. Both mechanisms may cause slopes and cracking. The industrial estimation based on deformation of the flue walls with time reveals the increase of the glassy phase due to the evaporation of sodium compounds (Fig. 4.3). It appears that the degree of mullitization [2] has small influence on creep, initiated by an increase in the sodium silicate glassy phase (the amount of which may reach up to 25–30%).

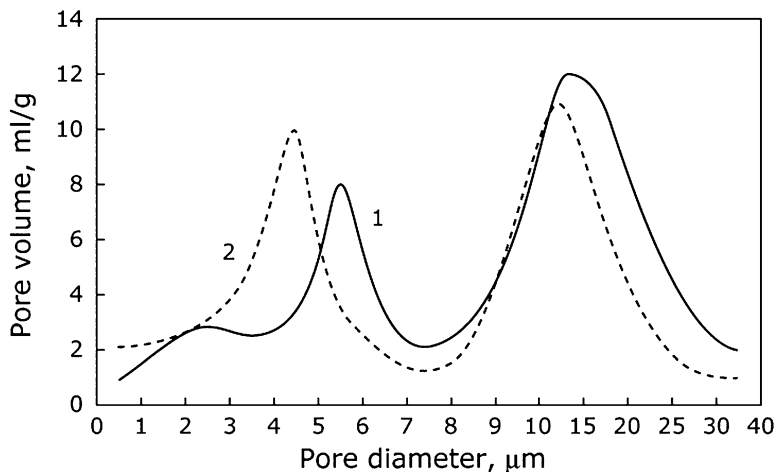


Fig. 4.4 Pore size distribution in refractories of the flue walls

Fine pores in refractories cannot be barriers for the vapors of sodium compounds. Yet the glassy-appearing sodium alumina silicate phase in the pore of 3–4 μm may close the pore, making a dead end for the subsequent penetration of sodium compounds inside the refractory. It is more problematic to create such a barrier in pores of 25 μm (Fig. 4.4).

References

1. Yanko A. Anodes for aluminium reduction, (in Russian). Moscow: Ruda I Metally; 2001. 670 p.
2. Yakovlev V, Pihutin I, Yukiev V. The results and future trends in refractories for anode baking furnaces (in Russian). VAMI. 2001;2:58–62.
3. Brunk F. Corrosion and behavior of fireclay bricks used in the flues of open anode baking furnaces. *Light Met.* 1995;124.
4. Butler J, Bongers A. Alternations of anode baking furnace bricks during operation. *Light Met.* 1995;124.
5. Perrushaud R, Meier M, Fischer W. A unique refractory solution for anode baking furnace flues. *Light Met.* 2004;133:553–7.
6. Maiwald D, Leisenberg W. Flue condition index – a new challenge to increase flue lifetime, operational safety and fuel efficiency in open pit anode baking furnaces. *Light Met.* 2006;135:625–9.
7. Franken M, Everstein S, Berkel P, Feldman R. LP bricks: a new generation of refractories that meet demands in anode baking furnaces. *Light Met.* 2005;134:709–13.

Glossary

Alumina, aluminium oxide, Al_2O_3 the main raw material for the production of aluminium; however, the main constituent of conventional refractories.

Anode baking furnace a complex construction for the temperature treatment (firing, sintering, baking) of carbon anode and cathode shapes. The green shapes are placed in (and after heat treatment taken out) the chambers while the fire is moving in the flue walls along the chambers.

Antiwetting additives admixtures of barium sulfate, aluminium fluoride, aluminium borate, aluminium titanate, calcium silicate (wollastonite), aluminium nitride, silicon carbide and its combinations to alumina silica refractories for decreasing the wetting ability of molten aluminium to these refractories. In combination with decreasing the pore dimensions, they give good results.

Bending strength, flexural strength, modulus of rupture, MOR gives the combination of compressive and tensile stresses of materials. A simple and convenient method of estimating the mechanical strength of refractories.

Bottom sludge frozen electrolyte (bath) on the cathode bottom, usually near the side walls. If it expands over the projection of anodes over the cathode bottom, it reduces the conductive surface of the cathode, where the electrochemical reaction of aluminium reduction takes place.

Carbon ramming paste a semifinished product used to fill in the gaps between the end of carbon cathode blocks and the refractory side lining. The raw materials are the same as for carbon cathode blocks, but the material receives its final properties during the preheating and startup.

Casting equipment stoppers, glasses, sieves, siphons, plugs, funnels, terminal boxes, and other small articles for the casting process of aluminium.

Cathode of the reduction cell in general, the entire reduction cell (carbon cathode blocks, sidelining, refractory barrier layer, heat insulation) is called a cathode. But sometimes the term “cathode” is used for the electroconductive surface of the carbon bottom.

Collector bar a steel bar that serves as current lead from the bus bar system to the carbon cathode blocks.

Compressive strength, compression strength, cold crushing strength, CCS a maximum compression tension that material can withstand without breaking down. A simple and convenient method of estimating the mechanical strength of refractories.

Creep a plastic deformation of refractories at high temperatures (below the melting point) under mechanical stress (below the crushing strength).

Cryolite ratio the ratio of molecules of sodium fluoride to aluminium fluoride. In pure cryolite Na_3AlF_6 ($3\text{NaF} \cdot \text{AlF}_3$), the cryolite ratio (CR) is 3. The melting point of pure cryolite is 1,010 °C, but the temperature of electrolyte may be reduced either by the additives of fluorides or by varying the ratio of sodium fluoride (NaF) to aluminium fluoride (AlF_3). Both variants — additives and variation of cryolite ratio — diminish the melting point of the bath to 930–960 °C.

Current efficiency the coefficient showing the ratio of the actual mass of aluminium, received from electrolyte by the passage of current to the theoretical mass, to the mass that should be received according to Faraday's law. One of the main controlled industrial parameters on smelters.

Drained cathode aluminium will flow to some vessel in a drained cathode. Due to the cathode's slopes, the Al film will be very thin. This will probably become the basic construction of the future.

Dry autopsy a complex set of actions to investigate the reasons for shutdown of the cell. This includes investigating the surface of the cell, cleaned of electrolyte and aluminium, digging trenches in the lining in chosen parts of the cell, and examining the condition of the lining and the lining materials.

Electrolysis of aluminium, reduction of aluminium, smelting of aluminium, electro winning of aluminium, Hall–Heroult process process of fabrication of molten primary aluminium due to high-temperature (~950–980 °C) electrochemical reaction of reduction of alumina, dissolved in electrolyte, by carbon.

Electrolyte, bath, molten bath, frozen bath a substance mainly consisting of cryolite (Na_3AlF_6), with additions of sodium fluoride, aluminium fluoride, calcium fluoride, magnesium fluoride, conducting in molten state electric current and dissolving alumina.

Energy consumption of the reduction process the amount of energy required for the fabrication of aluminium due to the electrochemical reaction. One of the main controlled industrial parameters on smelters.

Heat capacity the amount of heat necessary to increase the temperature of the unit of material 1 K.

Holding furnaces installed at the smelters and at secondary aluminium plants. In holding furnaces, aluminium from the reduction shop is purified from gaseous and solid impurities and the alloying additives are added.

Hot modulus of rupture, HMOR the high-temperature flexural strength bending strength, measured at high temperatures.

Ladle a metallurgical aggregate for the transportation of the molten aluminium tapped from the reduction cells to the cast house.

Launder, runner a metallurgical device for the transportation of the molten aluminium from the melting furnace to the holding furnace and from the holding furnace to the degassing unit, filtration box to the casting machine.

Melting furnaces installed at secondary aluminium plants for the melting of aluminium ingots and billets.

Pore size distribution the graph showing the percentage of pores of certain diameters in the material. The pore size distribution may be monomodal, bimodal (the most typical), and chaotic. Pore size distribution on materials plays a big role in the corrosion resistance of refractories.

Preheating of the reduction cell a process to achieve a temperature close to the normal operational temperature of reduction of the newly constructed (rebuilt) reduction cell. Usually, preheating may be electric or gas-fired.

Reduction cell, cell, reduction pot, electrolytic cell a metallurgical aggregate for the production of primary aluminium, having a shape of a shallow vane.

Refractoriness a property to withstand high temperatures without melting.

Reheat change of dimensions irreversible change of dimensions of refractory shape at heating. It may be negative (shrinkage) or positive (expansion).

Service life of metallurgical aggregate the time between startup and shutdown. One of the main controlled industrial parameters on smelters.

Shutdown, failure of the reduction cell (and any metallurgical aggregate as well) emergency stop of the reduction cell's operation, usually as a result of leakage of molten aluminium through the cracks in carbon cathode blocks.

Side ledge frozen electrolyte (bath) on the side-wall lining. Protects side lining from corrosion and plays a positive role in the Hall–Heroult process.

Smelter, aluminium smelter the plant producing primary aluminium according to the Hall–Heroult process. May also produce secondary aluminium.

Startup a complex sequence of actions to put the preheated reduction cell in service. These include a sequence of pouring molten electrolyte in the cell, pouring molten aluminium, and starting the feeding of alumina. In general, the startup process takes about 3 months before the cell is considered to be in normal operation.

Temperature conductivity (heat diffusivity) characterizes how fast the temperature in the material is spreading.

The lenses under the carbon cathode blocks appear due to the interaction of alumina silica refractories with electrolyte that infiltrated through the permeable pores of carbon cathode blocks. Several reactions are possible, all of which have a positive volume effect, which causes bottom “heaving.” raising of carbon cathode blocks in the middle up to 100 mm.

Thermal coefficient of linear expansion a relative increase in the linear dimension of the material as its temperature increases 1°. Thermal expansion may cause thermal strains in the material.

Thermal conductivity characterizes the amount of heat being transferred through the surface of the material.

Thermal shock resistance the ability of the material to withstand the temperature drops and rises, that is, to withstand thermal shock.

Volume effect of chemical reaction a ratio of the molecular (atomic) volume of the reaction products to the molecular volume of reactants. With a negative volume effect, the material becomes more porous and the continuous dense film of the products doesn't appear, while with a positive volume effect, the material becomes denser, but the appearing products may cause tensions and cracks in the material. If one of the reactants is gaseous and goes in the material outside, it is not taken into account in calculation of the volume effect.